

PHYSICAL ORGANIC STUDIES IN THE DESIGN AND APPLICATION OF
SUPRAMOLECULAR ANION HOSTS

by

HAZEL ANNE FARGHER

A DISSERTATION

Presented to the Department of Chemistry and Biochemistry
in the Division of Graduate Studies of the University of Oregon
in partial fulfillment of the requirements
for the degree of
Doctor of Philosophy

September 2021

DISSERTATION APPROVAL PAGE

Student: Hazel Anne Fargher

Title: Physical Organic Studies in the Design and Application of Supramolecular Anion Hosts

This dissertation has been accepted and approved in partial fulfillment of the requirements for the Doctor of Philosophy degree in the Department of Chemistry and Biochemistry by:

Dr. Victoria DeRose	Chairperson
Dr. Darren Johnson	Co-Advisor
Dr. Michael Haley	Co-Advisor
Dr. Michael Pluth	Core Member
Dr. Marian Hettiaratchi	Institutional Representative

and

Andy Karduna	Interim Vice Provost for Graduate Studies
--------------	---

Original approval signatures are on file with the University of Oregon Division of Graduate Studies.

Degree awarded September 2021.

© 2021 Hazel Anne Fargher

DISSERTATION ABSTRACT

Hazel Anne Fargher

Doctor of Philosophy

Department of Chemistry and Biochemistry

August 2021

Title: Physical Organic Studies in the Design and Application of Supramolecular Anion Hosts

Hosts for supramolecular anion binding are used for a range of applications, including real-time detection, anion transport, catalysis, extraction, and molecular machines. These applications are the result of thousands of research articles with commonly studied anions such as the halides and oxoanions. Fundamental work has allowed researchers to understand how host binding pocket geometry, non-covalent motifs, and solvophobic effects work in concert to achieve properties required in each application.

Often overlooked in anion binding research are the hydrochalcogenide anions, hydrosulfide (HS^-) and hydroselenide (HSe^-). Both anions play important roles in biological systems. At physiological pH, HS^- is favored over hydrogen sulfide (H_2S), an endogenous gasotransmitter. HSe^- is the intermediate in the metabolic pathway of selenium. The reactivity of these anions, however, has made studying their supramolecular chemistry challenging. As a result, there are only three families of hosts for HS^- , and before 2019, no reported receptors for HSe^- .

In this thesis we focus on fundamental research into anion binding of the hydrochalcogenide anions. In Chapter II we show the first receptors for HSe^- . In Chapter III we investigate the effect of changing the polarity of a C–H bond on binding with the hydrochalcogenide and halide anions. This study revealed a preference of an aryl C–H hydrogen bond donor for HS^- . To investigate this finding further, in Chapter IV we study the equilibrium isotope effect of deuteration of the C–H hydrogen bond donor on anion binding and in Chapter V we use over 423,000 C–H \cdots S contacts found in the Cambridge Structural Database to create a guide for identifying C–H \cdots S contacts in the solid state. In the final chapters of this thesis, we expand upon the scope of applications of our hosts. In Chapter VI we show that our hosts can modulate the reactivity of HS^- and in Chapter VII we use anion receptors to disrupt the Hofmeister bias in liquid-liquid extraction. Finally, in Chapter VIII we conclude with a summary of host motifs compatible with hydrochalcogenide anion binding and outline future work.

This dissertation includes published and unpublished co-authored material.

CURRICULUM VITAE

NAME OF AUTHOR: Hazel Anne Fargher

GRADUATE AND UNDERGRADUATE SCHOOLS ATTENDED:

University of Oregon, Eugene
Worcester Polytechnic Institute, Worcester

DEGREES AWARDED:

Doctor of Philosophy, Chemistry, 2021, University of Oregon
Master of Science, Chemistry, 2018, University of Oregon
Bachelor of Science, Chemistry, 2016, Worcester Polytechnic Institute

AREAS OF SPECIAL INTEREST:

Physical Organic Chemistry
Supramolecular Chemistry
Anion Binding

PROFESSIONAL EXPERIENCE:

Research Intern, for Oak Ridge National Laboratory at the University of Oregon,
2021
Graduate Research Fellow, University of Oregon, 2018 – 2021
Graduate Teaching Fellow, University of Oregon, 2016 – 2018

GRANTS, AWARDS, AND HONORS:

John Keana Graduate Fellowship, University of Oregon, 2021

Office of Science Graduate Student Research Program Award, U.S. Department
of Energy, 2021

Julie and Rocky Dixon Graduate Student Innovation Award, University of
Oregon, 2018 – 2019

Graduate Student Award for Excellence in the Teaching of Chemistry, University
of Oregon, 2017

Dean's First Year Merit Award, University of Oregon, 2016

Chemistry Student Award, Worcester Polytechnic Institute, 2016

Pi Mu Epsilon, National Mathematics Honor Society, Worcester Polytechnic Institute, 2016

PUBLICATIONS:

Fargher, H. A.; Sherbow, T. J.; Haley, M. M.; Johnson, D. W.; Pluth M. D. C–H···S Hydrogen Bonding Interactions. *Submitted*.

Fargher, H. A.; Nickels, R. A.; de Faria, T. P.; Haley, M. M.; Pluth, M. D.; Johnson, D. W. Deuterium Equilibrium Isotope Effects in a Supramolecular Receptor for the Hydrochalcogenide and Halide Anions. *RSC Adv.* **2021**, *11*, 26581–26585.

Sherbow, T. J.; Fargher, H. A.; Haley, M. M.; Pluth, M. D.; Johnson, D. W. Solvent Dependent Linear Free Energy Relationships in a Flexible Host-Guest System. *J. Org. Chem.* **2020**, *85*, 12367–12373.

Fargher, H. A.; Lau, N.; Richardson, H. C.; Cheong, P. H.-Y.; Haley, M. M.; Pluth, M. D.; Johnson, D. W. Tuning Supramolecular Selectivity for Hydrosulfide: Linear Free Energy Relationships Reveal Preferential C–H Hydrogen Bond Interactions. *J. Am. Chem. Soc.* **2020**, *142*, 8243–8251.

Eytel, L. M.; Fargher, H. A.; Haley, M. M.; Johnson, D. W. The road to aryl CH···anion binding was paved with good intentions: fundamental studies, host design, and historical perspectives in CH hydrogen bonding. *Chem. Commun.* **2019**, *55*, 5195–5206.

Fargher, H. A.; Lau, N.; Zakharov, L. N.; Haley, M. M.; Johnson D. W.; Pluth, M. D. Expanding Reversible Chalcogenide Binding: Supramolecular Receptors for the Hydroselenide (HSe⁻) Anion. *Chem. Sci.* **2019**, *10*, 67–72.

ACKNOWLEDGEMENTS

There are so many people I need to thank for their scientific and social support throughout my career as a chemist. I'd like to start with my advisors, Mike Haley and Darren Johnson. Your creativity, knowledge, and hard work made my thesis possible. You made my experience in graduate school overwhelmingly positive and kept my love of research alive. I'd like to thank Mike Pluth who acted as another advisor, helping to create and guide my thesis projects. Thank you to Bruce Moyer who made an internship with ORNL possible. Thank you to my other committee members Vicky DeRose, Jeff McKnight, and Marian Hettiaratchi. Thank you to the CAMCOR staff and the front office staff, especially Janet, Christi, Kathy, and Jim. And thank you to the NIH and the Keana Fellowship for funding.

I also want to thank the people who got me to graduate school, Marion Emmert and Ijaz Ahmed. Marion, I got my PhD because I wanted to know as much chemistry as you. Ijaz, your patience and guidance gave me confidence in the lab and helped me find where I was supposed to be. Thank you to my graduate school mentors, Justin Barry, Susan Cooper, Lisa Eytel, and Jess Lohrman. You helped me find my way when I felt lost. Lisa, thank you for encouraging me to try things outside of research. Jess, thank you for teaching me everything you know about chemistry, pangolins, and piracy.

A big thank you to all my experimental collaborators. Thank you, Nathan Lau, for your guidance as I was embarking on these projects. Toby Sherbow, thank you for always answering my questions and your constant encouragement. And to Russell Nickels and Faith Longnight, thank you for making mentoring fun. I couldn't have asked for better people to work with and I know you both will go on to do amazing things.

Thank you to my friends and labmates in the DWJ, Haley, and Pluth labs. Sean, Jess, Chun-lin, Nathan, Yu, Toby, Susan, Brandon, Brantly, Meredith, Lizzy, Lisa, Conerd, Justin, Dan, Andrea, Carrie, Matt, Ngoc-Minh, Jordan, Trevor, Josh, Jeremy, Sarah, Thaís, Hannah, Annie, Turner, Grace, Gabby, Bella, Nolan, Efrain, Jacob, Henry, Kaylin, Arman, Willow, Luca, Kyra, Alex, Olivia, Andy, Haley, Mark, Russell, Scout, and Faith, thank you for the overwhelming support, especially in these last few weeks. Together, all of you have made a community that I am sad to leave. Jeremy, Ngoc-Minh, Jordan, Josh, and Trevor, it was so much better going through the program with you five, and I am so proud of where you are today. Thaís and Hannah, you make every day in lab so much more fun, and I am so lucky to have met you two.

Thank you to new friends, Tawney, Amber, Laken, and Nic. Tawney, whether it's hiking or watching tv, it's better with you. And thank you to Amber, Laken, and Nic for hosting and celebrating holidays with me. You created a home-away-from-home, especially during the pandemic. Thank you to old friends, Emilee and Danielle for keeping me grounded and giving me glimpses of life beyond chemistry.

Thank you to my partner and best friend, Jeremy Bard, the most supportive person I know. I have had so much fun with you these past few years and I look forward to our future adventures. Thank you to my parents, Anne and Hugh Fargher. Thank you for always believing in me and encouraging me in everything that I do. I would not have gone very far without your constant love and support. Thank you to my brother, Jamie Fargher. I am in awe of your sense of adventure and work ethic and aspire to them every day. And finally, thank you to my aquatic friends, Morgan and Nero, for giving me something to worry about that wasn't work.

To Mum and Dad –

for teaching me to love science and the importance of communication in any language.

TABLE OF CONTENTS

Chapter	Page
I. INTRODUCTION	1
II. EXPANDING REVERSIBLE CHALCOGENIDE BINDING: SUPRAMOLECULAR RECEPTORS FOR THE HYDROSELENIDE (HSe ⁻) ANION	7
2.1 Introduction	7
2.2 Results and Discussion	11
2.2.1 Synthesis of tetrabutylammonium hydroselenide (NBu ₄ SeH) ...	11
2.2.2 Binding experiments of 2.1 ^{tBu} and 2.2 ^{CF₃} with HSe ⁻	12
2.2.3 Binding experiments of 2.1 ^{tBu} and 2.2 ^{CF₃} with other anions	15
2.3 Conclusions	18
III. TUNING SUPRAMOLECULAR SELECTIVITY FOR HYDROSULFIDE: LINEAR FREE ENERGY RELATIONSHIPS REVEAL PREFERENTIAL C–H HYDROGEN BOND INTERACTIONS	20
3.1 Introduction	20
3.2 Results and Discussion	23
3.2.1 Synthesis and characterization	23
3.2.2 ¹ H NMR spectroscopy titrations	26
3.2.3 LFERs reveal anion-dependent ΔG _{binding} trends	28
3.2.4 Hammett plots reveal anion-dependent substituent effects	31
3.2.5 Field/inductive vs. resonance substituent effects on anion binding	33
3.2.6 Estimation of aryl C–H···A ⁻ strength through LFERs	35
3.3 Conclusions	38

Chapter	Page
IV. DEUTERIUM EQUILIBRIUM ISOTOPE EFFECTS IN A SUPRAMOLECULAR RECEPTOR FOR THE HYDROCHALCOGENIDE AND HALIDE ANIONS	41
4.1 Introduction	41
4.2 Methods	44
4.3 Results and Discussion	47
4.4 Conclusion	50
V. C–H··S HYDROGEN BONDING INTERACTIONS	52
5.1 Introduction	52
5.1.1 C–H hydrogen bond donors	54
5.1.2 C–H··S hydrogen bonding	55
5.1.3 Scope of review	60
5.2 Results and Discussion	61
5.2.1 Organic molecules with sulfur hydrogen bond acceptors	61
5.2.1.1 S HB acceptors with traditional HB donors	64
5.2.1.2 Comparing hydrogen bond acceptors	65
5.2.1.3 S-character affects preferred hydrogen bonding angles	71
5.2.1.3.1 S oxidation state	71
5.2.1.3.2 S Coordination number	72
5.2.1.4 Alkyl vs. aryl based C–H donors	74
5.2.1.5 Hydrogen bond acceptor directionality	76
5.2.2 Sulfur hydrogen bonding interaction in metal sulfur ligated complexes	78

Chapter	Page
5.2.2.1 Structures exhibiting short C–H···S–M contacts	84
5.3 Conclusions	88
VI. CONTROLLING THE REACTIVITY OF HYDROSULFIDE WITH A SUPRAMOLECULAR HOST	90
6.1 Introduction	90
6.2 Methods	93
6.3 Results and Discussion	94
6.4 Conclusion and Future Outlook	97
VII. ARYLETHYNYL UREA ANION RECEPTORS FOR DISRUPTION OF THE HOFMEISTER BIAS IN TETRABUTYLPHOSPHONIUM SALT LIQUID-LIQUID EXTRACTION	99
7.1 Introduction	99
7.2 Methods	100
7.2.1 Liquid-liquid extraction experiments	101
7.3 Results and Discussion	102
7.3.1 Calculating energy of partitioning for TBP ⁺	102
7.3.2. Host-mediated extraction by 7.1	104
7.3.3 Host-mediated extraction by 7.2	108
7.4 Conclusion	109
VIII. CONCLUSIONS AND FUTURE OUTLOOK	111
APPENDICES	115
A. SUPPLEMENTARY CONTENT FOR CHAPTER II	115
B. SUPPLEMENTARY CONTENT FOR CHAPTER III	135

Chapter	Page
C. SUPPLEMENTARY CONTENT FOR CHAPTER IV	178
D. SUPPLEMENTARY CONTENT FOR CHAPTER V	194
E. SUPPLEMENTARY CONTENT FOR CHAPTER VI	204
F. SUPPLEMENTARY CONTENT FOR CHAPTER VII	221
REFERENCES CITED	232

LIST OF FIGURES

Figure	Page
1. Figure 1.1. a) The first examples of supramolecular hosts for anion binding from our labs. b) The generalized arylethynyl bisurea scaffold that is well-studied as a supramolecular host for anion-binding in our labs.	4
2. Figure 2.1. Summary of selenium metabolism in the human body.	9
3. Figure 2.2. The two families of receptors used for binding HS ⁻ and HSe ⁻	10
4. Figure 2.3. (a) Preparation of NBu ₄ SeH. (b) Thermal ellipsoid diagram (at 50% probability) depicting the molecular structure of NBu ₄ SeH.	11
5. Figure 2.4. (a) Representation of the host guest equilibrium between 2.1^{tBu} and HSe ⁻ . (b) ¹ H NMR titration of 1.6 mM 2.1^{tBu} with NBu ₄ SeH in 10% DMSO- <i>d</i> ₆ in CD ₃ CN. (c) Representation of the host guest equilibrium between 2.2^{CF3} and HSe ⁻ . (d) ¹ H NMR titration of 2.0 mM 2.2^{CF3} with NBu ₄ SeH in CD ₃ CN.	13
6. Figure 2.5. Thermal ellipsoid diagram (at 50% probability) depicting the molecular structure of [2.1^{tBu} (SeH)] ⁻ . Hydrogen atoms not interacting with the bound HSe ⁻ are omitted for clarity.	18
7. Figure 3.1. Receptor scaffolds 3.1-3.3 all bind HS ⁻ reversibly and all contain C–H HB donors. Only receptor classes 3.1 and 3.2 have been shown to reversibly bind HSe ⁻ . The C–H HB donors that interact with the HCh ⁻ are shown in red for clarity.	21
8. Figure 3.2. The series of arylethynyl bisurea receptors used in this study.	24
9. Figure 3.3. ¹ H NMR spectra of six receptors 3.1^R in 10% DMSO- <i>d</i> ₆ /CD ₃ CN. The largest change in δ of possible HB donors occurs for the CH _a proton peak.	25
10. Figure 3.4. (a) Representation of the host–guest equilibrium between 3.1^{CF3} and HS ⁻ . (b) ¹ H NMR titration of 2.2 mM 3.1^{CF3} with NBu ₄ SH in 10% DMSO- <i>d</i> ₆ /CD ₃ CN.	27
11. Figure 3.5. LFER between ΔG _{binding} and σ _p values for 3.1^R with HS ⁻ , HSe ⁻ , Cl ⁻ , and Br ⁻ . Dashed lines represent the 95% confidence interval for each linear trend.	29

Figure	Page
12. Figure 3.6. Hammett plot between 3.1^R and HS ⁻ , HSe ⁻ , Cl ⁻ , and Br ⁻ . The slope of HS ⁻ is significantly different from HSe ⁻ , Cl ⁻ , and Br ⁻ illustrating the increased sensitivity of HS ⁻ to substituent effects.	32
13. Figure 3.7. (a) Free receptors 3.1^R can twist into the “W” conformation. ⁴⁴ (b) Representative ESP maps of 3.1^{CF3} , 3.1^H , and 3.1^{NMe2} , calculated at the PBE level of theory. The values describe the energy at the 0.02 Å isoelectric surface of the C–H HB donor <i>para</i> to the –R substituent.	36
14. Figure 3.8. Estimated aryl C–H···A ⁻ HB strengths for all six receptors, with all four anions. While HSe ⁻ , Cl ⁻ , and Br ⁻ show similar HB strengths, HS ⁻ shows a stronger binding with the C–H HB donor motif.	38
15. Figure 4.1. Arylethynyl bisurea receptors 4.1^H and 4.1^D used in our previous DEIE study of Cl ⁻ binding. Related receptors 4.2^H and 4.2^D are used in the current study to avoid reaction with HS ⁻	43
16. Figure 4.2. Representation of the host-guest equilibrium between 4.2^{H/D} and Cl ⁻ . Differences in the chemical shifts between the 4.2^H and 4.2^D isotopologues are observed in the ¹³ C NMR signals for the C ^{ab} , C ¹ , and C ² carbons. b) ¹³ C NMR signals for the C ^{ab} , C ¹ , and C ² carbons in 4.2^H and 4.2^D are tracked throughout a titration. c-e) Linearized plots from fitting the chemical shifts of the C ^{ab} , C ¹ , and C ² throughout a titration to Equation 4.1.	48
17. Figure 5.1. Bond lengths and bond angles often measured in HB systems and will be described throughout the text.	53
18. Figure 5.2. Absence and presence of C–H HB in <i>p</i> -toluic acid and <i>o</i> -toluic acid, respectively.	55
19. Figure 5.3. Crystal structures of arylethynyl bisurea receptors shown to bind (a) Cl ⁻ , (b) HS ⁻ , and (c) HSe ⁻ in the solid state. All three anions interact with the aryl C–H HB donor on the central ring.	58
20. Figure 5.4. The other two supramolecular hosts that have been shown to reversibly bind HS ⁻ . Both hosts feature C–H HB donors in their design (highlighted in red).	59
21. Figure 5.5. a) 3D histogram visualizing over 423,000 C–H···S contacts identified in the CSD. b) Cone angle of hydrogen bonding. c) Cone-corrected 3D histogram of all C–H···S contacts. The white dashed line represents estimate of the sum of the van der Waal radii of H and S.	62

Figure	Page
22. Figure 5.6. A relatively short and linear C–H···S contact in a disulfide cyclophane may help stabilize strained torsional angles.	64
23. Figure 5.7. 3D histogram of (a) N–H and b) O–H hydrogen bond donors with S.	65
24. Figure 5.8. Cone-corrected 3D histograms of C–H···A contacts found in the CSD with a) N, b) O, c) F, d) P, e) S, f) Cl, g) Se, h) Br, i) Te, and j) I. White dashed line represents estimate of the sum of the van der Waal radii of H and A.	67
25. Figure 5.9. a) <i>cis/trans</i> isomerization of synthetic peptoids. A C–H···A HB helps favor the <i>cis</i> conformation. b) Crystal structure shows a C–H···S HB in the solid state helps favor the <i>cis</i> conformation in the thioamide derivative.....	68
26. Figure 5.10. a) Crystal packing of the luminogen reveals C–H···O (atom denoted in red), C–H···N (blue) and C–H···S (yellow) intermolecular C–H HB.	69
27. Figure 5.11. Cone-corrected 3D histograms of S in different oxidation states: a) S ²⁻ , b) S ¹⁻ , and c) S ⁰	71
28. Figure 5.12. Cone-corrected 3D histograms of S bonded to a) one non-metal atom, b) two non-metal atoms, and c) three non-metal atoms.	73
29. Figure 5.13. a) <i>Out</i> isomer and b) <i>in</i> isomer of sulfur-strapped Zn-porphyrins.	74
30. Figure 5.14. Cone-corrected 3D histograms of C–H···S contacts with a) sp ³ alkyl C–H HB donors and b) sp ² aryl C–H HB donors.	75
31. Figure 5.15. Leucine and valine amino acid residues in contact with either Cl ⁻ or HS ⁻ in the first discovered bacterial ion channel for HS ⁻ . (PDB: 3TDX)	76
32. Figure 16. Tryptophan and threonine amino acid residues in contact with the biotin thioether in the streptavidin-biotin complex. (PDB: 6M9B)	76
33. Figure 5.17. Bi-weighted 3D histograms of C–H···A contacts found in the CSD with a) N, b) O, c) F, d) P, e) S, f) Cl, g) Se, h) Br, i) Te, and j) I.	79
34. Figure 5.18. C–H hydrogen bonding interactions in the primary coordination sphere of metal complexes as demonstrated by Szymczak and coworkers.	80

Figure	Page
35. Figure 5.19. Lengths and angles referred to in this section, where A is bound to a metal.	81
36. Figure 5.20. 3D histogram visualizing the cone corrected a) C–H···S–M, and b) C–H···Cl–M contacts in <i>d</i> -block metals where S or Cl are in the primary coordination sphere. The white line for each plot indicates the sum of the van der Waal radii between A and H.	83
37. Figure 5.21. Cone corrected histograms of C–H···S–M of groups a) 7, b) 8, c) 9, d) 10, e) 11, and f) 12 of the transition metals.	84
38. Figure 5.22. X-ray structures of (a) sulfide bound Hb1 isolated from <i>L. Pectinata</i> and (b) sulfide bound Hb isolated from human myoglobin. The labeled lengths correspond to C–S distances.	86
39. Figure 5.23. Cone corrected histograms of C–H···(SH)–M with <i>d</i> -block metals.	87
40. Figure 5.24. Graphical representation of C–H···S–Zn hydrogen bonding interactions observed in a ^{iPr} TpZnSH complex.	88
41. Figure 6.1. Supramolecular receptor for HS [−] used in this study.	92
42. Figure 6.2. a) UV-vis spectra of 6.2 (yellow trace) and 6.3 (pink trace) after reaction of 6.2 with HS [−] . b) UV-vis spectra of 6.2 and 5 equiv. 6.1 (orange trace) and 6.3 and 5 equiv. 6.1 (blue trace) after reaction of 6.2 with HS [−]	94
43. Figure 6.3. a) UV-vis spectra of the reaction of 10 μM TBASH with 10 μM 6.2 . b) UV-vis spectra of the reaction of 10 μM TBASH with 10 μM 6.2 in the presence of 5 equiv. 6.1 . b) Time course data of the absorbance at 570 nm in the presence (blue trace) and absence (red trace) of 5 equiv. 6.1 fit to a 2 nd order non-linear regression model (dashed black trace).	95
44. Figure 7.1. Anion receptors chosen for this study.	101
45. Figure 7.2. Experimentally determined log(D _{P,0}) values vs. log[TBPX] ₀ for a) TBPCl, b) TBPBr, c) TBPI, and d) TBPNO ₃	103
46. Figure 7.3. Equilibria present in host-mediated liquid-liquid extraction of TBPX salts.	105
47. Figure 7.4. Experimentally determined log(D _{P,TBPX}) values vs. log[7.1] for a) TBPCl, b) TBPBr, c) TBPI, and d) TBPNO ₃	106

48. Figure 7.5. a) Comparing the effect of 7.2 on distribution ratios of TBPX salts. b) Plots reveal the contribution of 7.2 towards the distribution ratio of TBPX.	109
--	-----

LIST OF TABLES

Table	Page
1. Table 2.1. Binding parameters for hosts 2.1^{tBu} and 2.2^{CF3} with the anions used in this study.	12
2. Table 2.2. Physical properties of the anions used in this study.	16
3. Table 2.3. Bond lengths and angles in [2.1^{tBu}(SeH)] ⁻	17
4. Table 3.1. Association constants and binding free energies for receptors 3.1^R at 1-3 mM with HS ⁻ , HSe ⁻ , Cl ⁻ , and Br ⁻ in 10% DMSO- <i>d</i> ₆ /CD ₃ CN at 25 °C.	28
5. Table 3.2. Fitting statistics for the LFER between ΔG _{binding} and σ _p for all four anions.	29
6. Table 3.3. Fitting statistics for Hammett plots for HS ⁻ , HSe ⁻ , Cl ⁻ , and Br ⁻	33
7. Table 3.4. Fitting statistics from the multivariable linear fit to the Swain-Lupton equation for the K _a values for HS ⁻ , HSe ⁻ , Cl ⁻ , and Br ⁻	35
8. Table 3.5. Fitting statistics for the LFER between ΔG _{binding} and ESP surfaces of the model compounds for HS ⁻ , HSe ⁻ , Cl ⁻ , and Br ⁻	36
9. Table 3.6. Estimated aryl C-H ^{···} A ⁻ HB strengths between 3.1^R and all four anions.	38
10. Table 4.1. Calculated DEIE for Cl ⁻ and Br ⁻ binding. Goodness of fit (R ²) of the titration data to Equation 4.1 through linear regression is included in parentheses.	48
11. Table 5.1. Parameters used to broadly categorize C-H HB as strong, moderate, and weak. Distance and angle ranges are inspired by analyses of hydrogen bonding in the solid state by Jeffrey and Steiner.	66
12. Table 6.1. Rate constant and initial starting material concentrations for the reaction of 10 μM TBASH with 10 μM 6.2 in the presence and absence of 5 equiv. 6.1 , calculated by the 2 nd order rate equation non-linear regression model.	95
13. Table 6.2. Rate constant and initial starting material concentrations for the reaction of 10 μM TBASH with 10 μM 6.2 in the presence of 1 equiv. 6.1 , calculated by the 2 nd order rate equation non-linear regression model.	97

Table	Page
14. Table 6.3. Initial rates of reaction of various concentrations of TBASH and 6.1 with 10 μM 6.2	98
15. Table 7.1. ΔG°_p (TBP^+) calculated from experimental $\log K_p$ for TBPCl, TBPBr, TBPI, and TBPNO ₃ partitioning from water into nitrobenzene at 25 $^\circ\text{C}$	104
16. Table 7.2. Experimental values determined through slope analysis for TBPCl, TBPBr, TBPI, and TBPNO ₃	106

LIST OF SCHEMES

Scheme	Page
1. Scheme 4.1. Synthetic route for the selective deuteration of anion receptor 4.2^D	45
2. Scheme 6.1. Reaction of HS ⁻ with 6.2 in the presence and absence of various equivalents of 6.1	92

CHAPTER I

INTRODUCTION

This chapter includes an excerpt from previously published and co-authored material from Eytel, L.M.; Fargher, H.A.; Haley, M.M.; Johnson, D.W. The road to aryl CH \cdots anion binding was paved with good intentions: fundamental studies, host design, and historical perspectives in CH hydrogen bonding. *Chem. Commun.* **2019**, 55, 5195–5206. This review was co-written by Dr. Lisa M. Eytel and Hazel A. Fargher, with editorial assistance from Professors Michael M. Haley and Darren W. Johnson.

Anionic species play diverse and complex roles in environmental, industrial, and biological systems, which necessitates chemical methods for detecting, sensing, sequestering, and selectively binding these negatively charged species to understand their fate, transport, and modes of action. As examples in the environment, anions are often found as natural and anthropogenic sources of pollution. Arsenate (AsO_4^{3-}) contamination in Bangladeshi wells has caused one of the largest mass-poisonings in history, affecting an estimated 85 million people.¹ Nitrate (NO_3^-) and dihydrogen phosphate (H_2PO_4^-) are essential for plant growth and are used in fertilizers to increase crop yield; however, over-application of these anions can be extremely detrimental to the environment, reaching surrounding bodies of water through agricultural run-off and promoting eutrophication.²⁻⁶ As an example in industrial processes, anions such as sulfate (SO_4^{2-}) also serve as major contaminants, and can thereby inhibit the effective vitrification of radioactive waste.⁷

In organisms, anions are essential for numerous biological processes. Chloride (Cl^-) is used to regulate membrane transport and control nervous system function, and the misregulation of Cl^- is linked with serious diseases such as cystic fibrosis.⁸ The hydrosulfide anion (HS^-) is currently being studied for its therapeutic potential as a signaling agent at low concentrations; at high concentrations, however, it is a deadly toxin and requires detailed monitoring in applications where exposure to the anion or its conjugate acid (hydrogen sulfide, H_2S) exists.⁹ Anions are even implicated in systems beyond our own planet. While perchlorate (ClO_4^-) serves as a rocket fuel additive and can lead to water contamination problems near terrestrial military bases (such as the Joint Base on Cape Cod, MA) and near flare manufacturing plants throughout California, perchlorate was also unexpectedly detected in soil on Mars.¹⁰⁻¹² This finding perhaps hints at past microbial life on the Red Planet,¹¹ and may suggest a future environmental cleanup challenge during terraforming by future humans seeking to populate other locations within the solar system.¹²

To understand, and potentially to monitor, the complicated roles that anions play in these many systems, the complex modes of action between an anionic “guest” and a molecular “host” have received increasing attention. Anions present several challenges as targets for molecular/ion recognition, including: (i) anions tend to be harder to bind by traditional electrostatic interactions because they are larger, more polarizable, and more diffuse than comparable cations. (ii) Anions exist in a diversity of molecular geometries, ranging from spherical (the halides) to planar (nitrate) to octahedral (SiF_6^{2-}), among other forms.¹³ (iii) Anions typically serve as weak to moderate bases, so their speciation can be pH dependent. As a result, proton transfer might occur rather than, *e.g.*, hydrogen bond

formation during their interactions with a host. (iv) Anions tend to be highly solvated and particularly mobile, especially in polar protic solvents. Despite these challenges, supramolecular host–guest systems have emerged over the past few decades as a way to continuously monitor anions through reversible, predominantly non-covalent interactions.^{13–15}

The first example of a supramolecular host for anion binding from our labs was published in 2008.¹⁶ The receptor features a pyridine hydrogen bond acceptor and sulfonamide N–H hydrogen bond donors (**1.1**, Figure 1.1a). Single crystal x-ray diffraction and ¹H NMR titrations in CDCl₃ revealed that the receptor bound H₂O, HCl, Cl[−], Br[−], and I[−] depending on the protonation state of the pyridine motif. Since our first introduction into anion binding, research within this collaboration has shifted towards a generalized arylolethynyl bisurea scaffold (**1.2**, Figure 1.1b). The rigid and conjugated scaffold imparts UV-vis absorption and fluorescent properties to the hosts, providing a useful handle to study anion binding through spectroscopic titrations, in addition to NMR titrations. Our labs have developed a modular approach for the synthesis of these hosts, providing a platform to design and study arylolethynyl bisurea receptors with various functional groups, binding pocket sizes, optoelectronic properties, and binding motifs. Over the 10+ years of research, we have designed receptors which are selective for H₂PO₄[−],¹⁷ NO₃[−],¹⁸ and Cl[−],¹⁹ elucidated host conformational change upon guest binding,^{17,20–22} and studied their optoelectronic properties.^{23,24} We have also used these hosts to study specific non-covalent interactions in host-guest binding. For example, we found that anion⋯π interactions can promote NO₃[−] selectivity¹⁸ and have studied the solvent effect on Cl[−] binding.²⁵ In addition, we highlighted a weak C–H⋯Cl[−] hydrogen

bond in receptor scaffold **1.2** ($X = CH$)²⁶ and subsequently used linear free energy relationships (LFER)²⁷ and deuterium equilibrium isotope effects (DEIE)²⁸ to further establish C–H hydrogen bond donors as important supramolecular motifs.

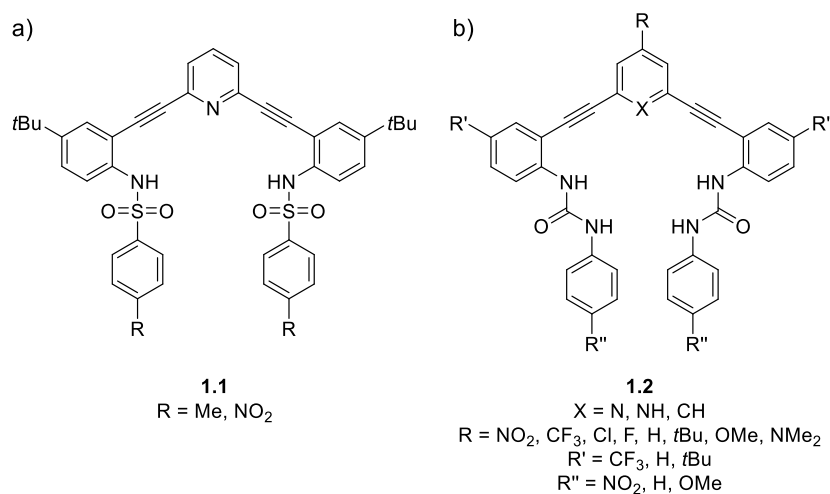


Figure 1.1. a) The first examples of supramolecular hosts for anion binding from our labs. b) The generalized arylethynyl bisurea scaffold that is well-studied as a supramolecular host for anion-binding in our labs.

From here, our research ventured into exploring supramolecular binding of understudied and reactive anions. In 2016, we published the first example of reversible supramolecular binding of HS^- .²⁹ HS^- has been classified as the third endogenously produced neurotransmitter and plays a role as a signaling molecule in major biological systems.^{9,30} As such, HS^- has been found to be essential for life, and recent interest in studying HS^- as a potential therapeutic for diseases has grown;⁹ however, HS^- is also nucleophilic, reducing, and basic ($pK_a = 7.0$) at physiological pH (7.4), and is sensitive to both water and oxygen. This reactivity has made the supramolecular chemistry of HS^- challenging to study. Since 2016, we are aware of only two other families of supramolecular receptors which have displayed reversible HS^- binding.^{31,32} Moving down

the periodic table, hydroselenide (HSe^-), another biologically essential yet highly reactive molecule,^{33,34} has been entirely overlooked by the anion binding community. Before 2019 there were no receptors published which had been shown to reversibly bind HSe^- .

Chapters II through V of this thesis investigate fundamental anion binding chemistry of the often-neglected hydrochalcogenide anions HS^- and HSe^- . We demonstrate how expanding the guest scope of our receptors to include these understudied anions has unearthed the importance of a specific weak non-covalent interaction in these supramolecular systems. Implementing the well-developed, modular approach to synthesizing the arylethynyl bisurea receptors allowed us to use systematic physical organic methods to untangle the non-covalent binding contributions amongst a mix of additive and competitive forces. Chapter II describes the first published examples of supramolecular receptors for HSe^- .³⁵ The participation of a depolarized aryl C–H hydrogen bond in anion binding with HSe^- and HS^- inspired a subsequent LFER outlined in Chapter III probing the effect C–H hydrogen bond donor polarity has on the strength of anion binding.³⁶ This study reveals an unexpected preference of the C–H hydrogen bond donor for HS^- over HSe^- , Cl^- , and Br^- . To investigate this finding further, Chapter IV follows work studying the DEIE of a C–H/D hydrogen bond donor on HS^- , Cl^- , and Br^- anion binding. This exploration culminates in an in-depth analysis of C–H \cdots S hydrogen bonds in the solid state, found in Chapter V.

Finally, with such a strong understanding of anion binding in these arylethynyl bisurea scaffolds, we can now study the utility of these molecules in more application-driven research. We have previously published a receptor with Cl^- selectivity and turn-on fluorescence upon binding in water,¹⁹ demonstrating the promise of these scaffolds as

fluorescent sensors in cells. Without water-solubilizing functional groups, however, these aryl ethynyl bisurea scaffolds display poor water solubility. This can be advantageous in applications such as liquid-liquid extraction, however. We previously developed a receptor with a high binding affinity and selectivity for HSO_4^- which was able to extract HSO_4^- from concentrated sulfuric acid.³⁷ In this thesis, we begin to explore new implementations for the hydrochalcogenide supramolecular receptors in organic solvents, as well as dive deeper into host-mediated liquid-liquid extraction. Inspired by supramolecular anion binding catalysis³⁸⁻⁴⁰ and the demonstrated success of supramolecular hosts to isolate and stabilize reactive and fleeting molecules,^{41,42} we use our anion receptors to modulate HS^- reactivity in Chapter VI. In doing so, we strive to gain new understanding into the design strategies used in nature to control this highly reactive molecule. In Chapter VII we expand upon earlier success in liquid-liquid extraction to initiate a collaboration at Oak Ridge National Laboratory to use our receptors to disrupt the Hoffmeister bias in liquid-liquid salt extraction.

Given the importance of anions in environmental (both terrestrial and extraterrestrial), industrial, and biological systems, this thesis highlights the utility of host-guest supramolecular chemistry to study both fundamental anion binding and application-driven research. This work also represents the combined effort of myself and many other undergraduate, graduate, post-doctoral, professorial, and research scientists. Chapters I through III include previously published co-authored material and Chapters IV through VII include unpublished co-authored material.

CHAPTER II

EXPANDING REVERSIBLE CHALCOGENIDE BINDING: SUPRAMOLECULAR RECEPTORS FOR THE HYDROSELENIDE (HSe⁻) ANION

This chapter includes previously published and co-authored material from Fargher, H.A.; Lau, N.; Zakharov, L.N.; Haley, M.M.; Johnson, D.W.; Pluth, M.D. Expanding Reversible Chalcogenide Binding: Supramolecular Receptors for the Hydroselenide (HSe⁻) Anion. *Chem. Sci.* **2019**, *10* (1), 67–72. This manuscript was co-written by Hazel A. Fargher and Nathanael Lau, with editorial assistance by Professors Michael M. Haley, Darren W. Johnson, and Michael D. Pluth. The project in this chapter was developed by Hazel A. Fargher, Nathanael Lau, and Professors Michael M. Haley, Darren W. Johnson, and Michael D. Pluth. The experimental work in this chapter was performed by Hazel A. Fargher and Nathanael Lau. The crystallographic data in this chapter was collected by Dr. Lev N. Zakharov.

2.1 Introduction

Synthetic supramolecular receptors have been used with great success for investigating the solution binding of biologically- and environmentally-relevant anions.^{13,43–46} By using reversible, mostly non-covalent interactions such as hydrogen bonding, electrostatic interactions, and anion- π interactions, a diverse palette of anions can be bound ranging from relatively inert anions such as halides and oxoanions^{47–51} to highly reactive anions.^{29,31,32,52–54} Although targeting the latter poses many challenges,

reversible binding in supramolecular hosts can be used to stabilize high-energy anions through non-covalent interactions in a manner reminiscent of certain active sites in proteins.⁵⁵ Despite this potential, examples of receptors targeting highly-reactive anions remain rare.^{29,31,32,52–54} In particular, the hydrochalcogenide anions hydroselenide (HSe^-) and hydrosulfide (HS^-) have been largely overlooked despite their considerable environmental and biological significance. These anions are weak bases that exist in equilibrium with their gaseous conjugate acids, hydrogen selenide (H_2Se , $pK_a = 3.74$) and hydrogen sulfide (H_2S , $pK_a = 7.00$).³⁴ The anionic species dominate at physiological pH, as H_2Se exists almost entirely as HSe^- and HS^- is favored over H_2S by a 3:1 ratio.^{9,33,56}

Although HSe^- and $\text{HS}^-/\text{H}_2\text{S}$ are highly toxic at elevated levels,^{9,57,58} both are essential to life at low concentrations and are produced endogenously.^{9,33,34} For example, H_2S has been classified as the third gasotransmitter alongside carbon monoxide (CO) and nitric oxide (NO) and plays regulatory roles in the cardiovascular, immune, and gastrointestinal systems, among others.^{9,30,59–61} Similarly, HSe^- is the common but highly-reactive intermediate generated in the metabolism of dietary selenium (Figure 2.1),^{33,34} and it is required for the synthesis of the essential 21st amino acid selenocysteine (Se-Cys).^{62,63} Se-Cys is then incorporated into selenoproteins, such as thioredoxin reductases and glutathione peroxidases^{33,34} that play important roles in redox biochemistry.^{64,65} However, the high reactivity of HSe^- toward both electrophiles and oxygen makes it difficult to observe directly in biological systems or to target through the design of selective synthetic receptors.^{33,66}

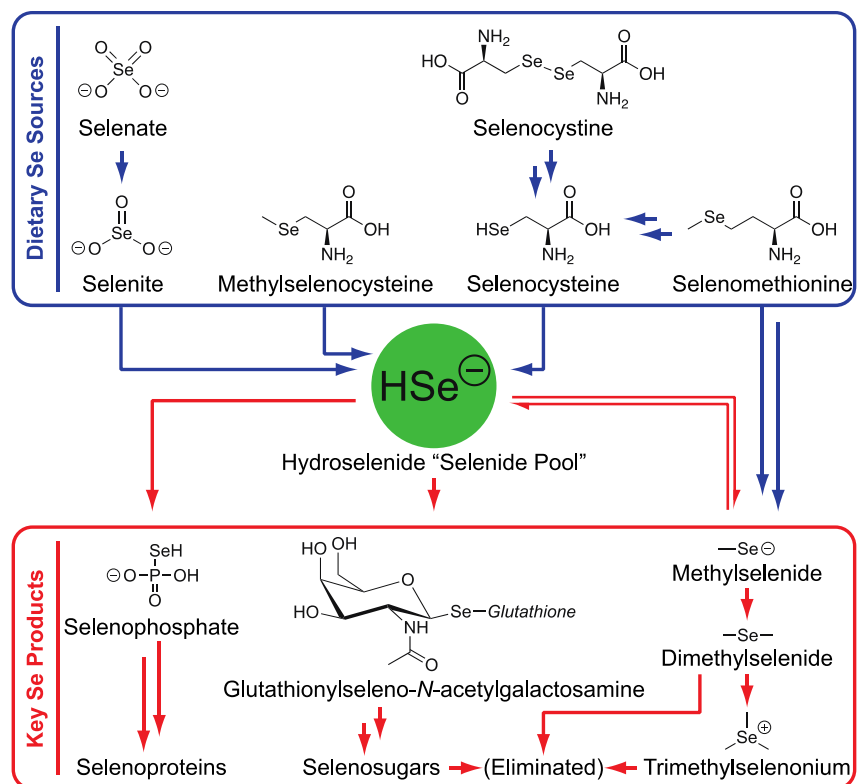


Figure 2.1. Summary of selenium metabolism in the human body.³³

Understanding the reversible binding requirements for hydrochalcogenides could provide valuable insights into possible receptor motifs in biological environments. However, we are not aware of any reports showing HSe^- as a viable target for molecular recognition by anion receptors. Similarly, few examples of reversible HS^- binding exist,^{29,31,32} the first of which were reported by our groups using two distinct families of modular receptor scaffolds (Figure 2.2). The initial report was based on a rigid arylethynyl bisurea receptor (**2.1^H**)²⁹ and the second on a flexible tripodal arylamide unit (**2.2^H**),³¹ both of which bound HS^- through $\text{N-H}\cdots\text{S}$ and aryl $\text{C-H}\cdots\text{S}$ hydrogen bonds. Building from these early insights into HS^- binding, we investigated whether these receptors could also bind and stabilize the substantially more reactive HSe^- anion. This was not a trivial descent down the periodic table; although sulfur and selenium share

similar chemical and physical properties, HSe^- is over three orders of magnitude more acidic and both a more potent nucleophile and reducing agent than HS^- .³⁴ In addition, selenium is larger and more diffuse than sulfur (Se^{2-} : 1.84 Å; S^{2-} : 1.70 Å),⁶⁷ making non-covalent and reversible binding more difficult.^{27,68}

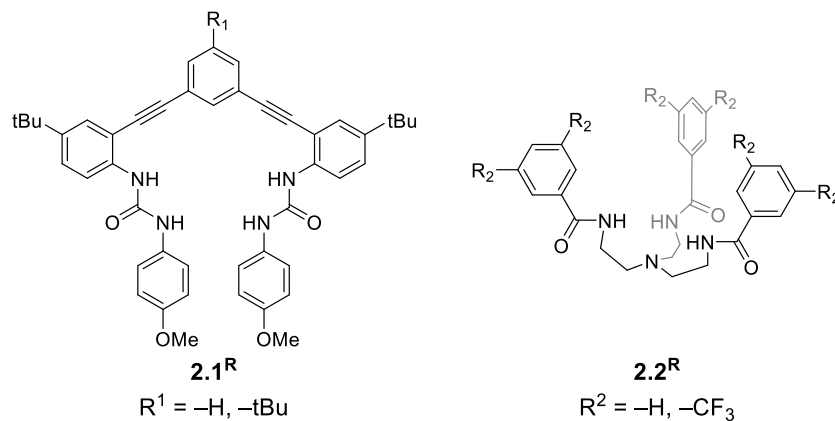


Figure 2.2. The two families of receptors used for binding HS^- and HSe^- .^{27,29,31}

Herein we report the first examples of using supramolecular receptors to reversibly bind the HSe^- anion, as clearly demonstrated by ^1H nuclear magnetic resonance (NMR) titration studies and X-ray crystallography. The binding affinities of our receptors to other related anions (HS^- , Cl^- , and Br^-) were also measured to determine the importance of factors such as anion size and basicity in binding. Our analysis revealed that our receptors favor smaller and more basic anions; thus, the greatest affinities observed were for HS^- . Ultimately, these studies provide a starting point for designing receptors capable of selective binding to HSe^- , which may provide future insights into the role of hydrochalcogenide anions in biology.

2.2 Results and Discussion

2.2.1 Synthesis of tetrabutylammonium hydroselenide (NBu₄SeH)

To investigate HSe⁻ binding to **2.1**^{tBu} and **2.2**^{CF₃}, which are both insoluble in water, we prepared NBu₄SeH by reducing elemental Se with NBu₄BH₄ in anhydrous CH₃CN (Figure 2.3a).⁶⁹ The crude NBu₄SeH oil was repeatedly washed with tetrahydrofuran (THF) to precipitate pure NBu₄SeH as a white powder. Single crystals of NBu₄SeH suitable for X-ray diffraction were obtained by layering a CH₃CN solution of NBu₄SeH with diethyl ether (Et₂O) (Figure 2.3b).

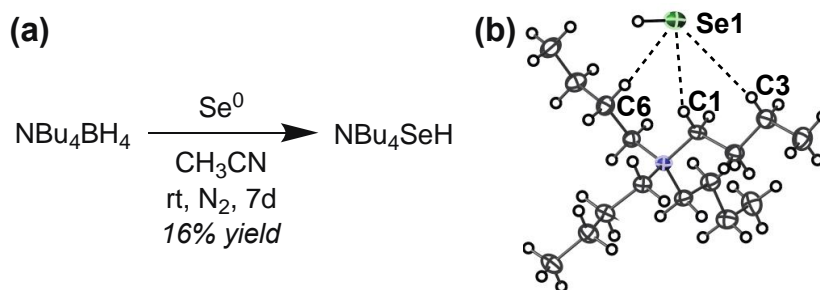


Figure 2.3. (a) Preparation of NBu₄SeH. (b) Thermal ellipsoid diagram (at 50% probability) depicting the molecular structure of NBu₄SeH.

Much like the related structure of NBu₄SH,⁷⁰ short contacts (3.954 – 4.248 Å) between the Se atom and C1, C2, and C6 of the NBu₄⁺ counterion are indicative of weak hydrogen bonding between the aliphatic C–H bonds of the counterion to the chalcogenide. The HSe⁻ proton was located in the solid-state structure and found to be pointed away from the NBu₄⁺ counterion. In addition, the ¹H NMR spectrum of NBu₄SeH showed the HSe⁻ resonance at –6.61 ppm in CD₃CN. The greater upfield shift of HSe⁻ compared to that of HS⁻ (–3.85 ppm)⁷⁰ is consistent with the greater electron density

around Se^{2-} relative to S^{2-} . We note that the salt is extremely sensitive to O_2 , and colorless solutions of NBu_4SeH turn dark green upon exposure to the atmosphere.

2.2.2 Binding experiments of **2.1^{tBu}** and **2.2^{CF3}** with HSe^-

Equipped with an organic soluble source of HSe^- , we next used ^1H NMR spectroscopy to investigate whether **2.1^{tBu}** and **2.2^{CF3}** could bind HSe^- (Figure 2.4). Solutions of each host (1.0–2.0 mM) were titrated with NBu_4SeH in either anhydrous 10% $\text{DMSO-}d_6/\text{CD}_3\text{CN}$ (for **2.1^{tBu}**) or anhydrous CD_3CN (for **2.2^{CF3}**), due to solubility differences between the hosts. We observed significant downfield shift in the urea N–H_{b/c} and aromatic C–H_a proton resonances in **2.1^{tBu}** and in the amide N–H_a and aromatic C–H_b proton resonances in **2.2^{CF3}**. Both of these results indicated that these protons are involved in binding HSe^- , and matched the recognition units that were previously observed to be involved in the binding of HS^- with **2.1^H** and **2.2^H**.^{29,31} Association constants (K_a) were determined by fitting the changes in the chemical shifts of these hydrogen bond donating moieties to a 1:1 host:guest model using Thordarson’s method (Table 2.1, *vide infra*).^{71,72}

Table 2.1. Binding parameters for hosts **2.1^{tBu}** and **2.2^{CF3}** with the anions used in this study.^a

Host	Solvent	HSe^-		Br^-		HS^-		Cl^-	
		K_a (M^{-1})	ΔG (kcal mol^{-1})	K_a (M^{-1})	ΔG (kcal mol^{-1})	K_a (M^{-1})	ΔG (kcal mol^{-1})	K_a (M^{-1})	ΔG (kcal mol^{-1})
2.1^{tBu}	10%	460 ±	-3.63 ±	110 ±	-2.79 ± 0.09	3600	-4.85 ±	1700	-4.41 ±
	DMSO- <i>d</i> ₆ /	50	0.06	20		±	0.09	± 200	0.06
	CD ₃ CN					500			
2.2^{CF3}	CD ₃ CN	290 ±	-3.35 ±	67 ±	-2.49 ± 0.06	840	-3.93 ±	430 ±	-3.59 ±
		50	0.10	7		± 80	0.06	50	0.07

^aThe minimum error is assumed to be 10% in cases where the standard deviation is less than 10%.

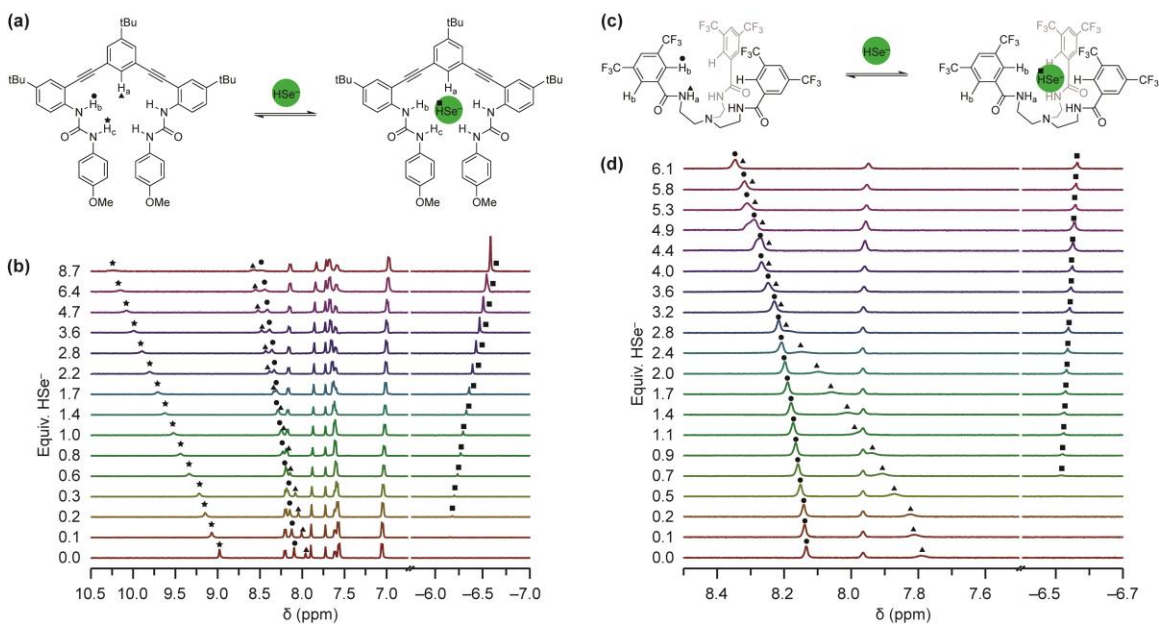


Figure 2.4. (a) Representation of the host guest equilibrium between **2.1^{tBu}** and HSe^- . (b) ^1H NMR titration of 1.6 mM **2.1^{tBu}** with NBu_4SeH in 10% $\text{DMSO-}d_6$ in CD_3CN . (c) Representation of the host guest equilibrium between **2.2^{CF3}** and HSe^- . (d) ^1H NMR titration of 2.0 mM **2.2^{CF3}** with NBu_4SeH in CD_3CN .

To ensure that the observed binding was reversible and not due to reaction with HSe^- as a nucleophile, we next looked for evidence of covalent modification of our receptors. In particular, **2.1^{tBu}** has several electrophilic sites, such as the urea carbonyl and alkyne moieties that could potentially undergo nucleophilic attack by HSe^- . Although no evidence of receptor modification was observed in titrations of **2.1^H** with HS^- ,²⁹ treatment of **2.1^{tBu}** with 20 equiv. HSe^- resulted in the appearance of new aromatic signals after approximately 30 min (Appendix A, Figure A.3).

To determine whether **2.1^{tBu}** was covalently modified by HSe^- over the course of the titration, 6 equiv. HSe^- were added to a 2 mM solution of **2.1^{tBu}** in 10% $\text{DMSO-}d_6/\text{CD}_3\text{CN}$ (Appendix A, Figure A.5). After 1 h there was little evidence of new aromatic signals; however, after 3 h new peaks appear in the spectra. Addition of 20 equiv. of zinc acetate ($\text{Zn}(\text{OAc})_2$) to the mixture removed HSe^- as ZnSe . The resulting ^1H NMR

spectrum showed that the receptor signals return to the same shifts as unmodified **2.1^{tBu}** along with the presence of smaller decomposition signals, demonstrating that the binding process of HSe⁻ is reversible within 1 h and over the timescale of the titration experiment.

To further investigate the minor decomposition products of **2.1^{tBu}** with HSe⁻, we used negative mode mass spectrometry (MS) to look for Se-containing species. We observed peaks consistent with fragments containing a molecule of HSe⁻ added across one alkyne bond (Appendix A, Figure A.4), which corroborates the observed desymmetrization of the aromatic peaks in the decomposition products in the ¹H NMR spectrum of **2.1^{tBu}**. Furthermore, the isotope patterns and mass accuracy of these peaks unambiguously show that these species incorporate HSe⁻. These results underscore the challenges in binding such a highly reactive species and confirm that careful receptor choice and design (e.g., bulky *t*-Bu group to protect **2.1^{tBu}** from nucleophilic aromatic substitution) is needed to accomplish this task.

The simpler tripodal receptor proved to be more resistant to attack by HSe⁻, since we have not observed any evidence of modification of **2.2^{CF3}** by HSe⁻, even though the electrophilicity of the amide carbonyl moieties should be enhanced due to the presence of the *meta* CF₃ groups. Coupled with the resistance of **2.1^{tBu}** to HSe⁻, this result demonstrates how the presence of relatively weak, non-covalent interactions can stabilize a normally reactive species. As with **2.1^{tBu}**, HSe⁻ binding was also shown to be reversible by conducting a similar Zn(OAc)₂ extrusion experiment (Appendix A, Figure A.5). After 2 equiv. HSe⁻ were added to **2.2^{CF3}**, the addition of 12 equiv. of Zn(OAc)₂ returned a ¹H NMR spectrum identical to that of pure **2.2^{CF3}**. The ability of these two distinct receptor

classes to reversibly bind HSe^- demonstrates the generality of binding of this previously uninvestigated anion, despite the highly reactive and reducing nature of HSe^- .

2.2.3 Binding experiments of **2.1^{tBu}** and **2.2^{CF3}** with other anions

To better understand the factors influencing HSe^- binding, we also measured the binding affinities of **2.1^{tBu}** and **2.2^{CF3}** towards the related anions HS^- , Cl^- , and Br^- (Table 2.1). Several notable trends emerged from these studies. For example, **2.1^{tBu}** maintains a higher binding affinity for HSe^- than **2.2^{CF3}**, even in a more competitive solvent system (10% $\text{DMSO-}d_6$ in CD_3CN vs. neat CD_3CN). This difference in binding affinity between the two receptors holds true for all of the other anions investigated and is consistent with our previous studies,^{29,31} and may reflect the increased number of N–H H-bond donors in **2.1^{tBu}** compared to **2.2^{CF3}**. Furthermore, this result underscores the importance of preorganization and directionality in hydrogen bonding in supramolecular systems, as the rigid ethynyl backbone of **2.1^{tBu}** offers more directed hydrogen bonds than the more flexible aliphatic backbone of **2.2^{CF3}**. Supporting this hypothesis, previous work on **2.1^{tBu}** and derivatives have shown that the central aromatic C–H hydrogen bond is unusually strong, contributing more than 1 kcal mol⁻¹ in anion binding energy.²⁷ In contrast, although receptor **2.2^{CF3}** should donate three hydrogen bonds between three *ortho* aromatic C–H hydrogen atoms to a guest molecule, ¹H NMR spectroscopy suggest that these interactions are relatively weak, as they are not strong enough to prevent free rotation of the aromatic rings since the *ortho* protons are not resolved.

Interestingly, both receptors demonstrated a clear preference for binding the hydrochalcogenide anions over the halide anions in the same row. By binding affinities,

2.1^{tBu} showed a two-fold preference for HS⁻ over Cl⁻ and a four-fold preference for HSe⁻ over Br⁻, despite the nearly identical ionic radii of anions within the same periodic row (Table 2.1). The protonation state of each anion is unlikely to explain the preferential binding towards hydrochalcogenide anions in **2.1^{tBu}** because this receptor contains no hydrogen bond accepting motifs in the binding pocket. The distinguishing factor may instead be basicity, as the chalcogenides are far better bases than the halides (Table 2.2) and should thus form stronger hydrogen bonds with the receptors. In contrast, the ionic size of the different anions appears to be a dominant factor in determining binding affinity in **2.1^{tBu}** and **2.2^{CF3}**. In both cases, the smaller row 3 anions (HS⁻ and Cl⁻) exhibit an order of magnitude stronger binding than those of the larger row 4 anions (HSe⁻ and Br⁻), despite the higher basicity of HSe⁻ over Cl⁻. Alternatively, because all the anions have the same charge, the row 3 anions have a higher surface charge density, which may result in greater electrostatic interactions between the anion and receptor, thus contributing to the stronger binding.

Table 2.2. Physical properties of the anions used in this study.

	HSe ⁻	Br ⁻	HS ⁻	Cl ⁻
Ionic Radius (Å)⁶⁷	1.70 ^a	1.84 ^b	1.67	1.82
pK_a (Conj. acid, H₂O)^{34,73}	7.0	3.7	-8.0	-9.0

^aIonic radius of S²⁻. ^bIonic radius of Se²⁻.

We further investigated the impact of anion size on receptor geometry in the solid-state. Single crystals of [NBu₄][**2.1^{tBu}**(SeH)] suitable for X-ray diffraction were obtained by layering an equimolar THF mixture of **2.1^{tBu}** and NBu₄SeH under Et₂O in a glovebox (Figure 2.5). We compared the metrical parameters of [**2.1^{tBu}**(SeH)]⁻ to those of

the previously reported $[\mathbf{2.1^H(SH)}]^{-29}$ and $[\mathbf{2.1^H(Cl)}]^{-26}$ to determine the effect of guest size on $\mathbf{2.1^R}$ receptors. The HSe^- guest is bound by $\mathbf{2.1^{tBu}}$ in the pocket created by one aromatic proton and four urea protons. The $\text{C}\cdots\text{Se}$ and $\text{N}\cdots\text{Se}$ distances suggest that the strongest hydrogen bonds are formed by the distal urea protons (N2 and N4, $(\text{N}\cdots\text{Se})_{\text{ave}} = 3.385 \text{ \AA}$), followed by the central aryl proton ($\text{C1}\cdots\text{Se} = 3.769 \text{ \AA}$) then the proximal urea protons (N1 and N3, $(\text{N}\cdots\text{Se})_{\text{ave}} = 3.892 \text{ \AA}$). These results suggested that the Se atom did not fit well inside the binding pocket of $\mathbf{2.1^{tBu}}$, since the more constrained proximal urea protons had weaker interactions to the anion than the more flexible distal urea protons. Additionally, none of the $\text{C}\cdots\text{H}\cdots\text{Se}$ or $\text{N}\cdots\text{H}\cdots\text{Se}$ angles formed were in the preferred linear geometry (Table 2.3). Although similar behavior was observed for $[\mathbf{2.1^H(SH)}]^{-29}$ and $[\mathbf{2.1^H(Cl)}]^{-26}$, the larger HSe^- guest distorted the binding pocket more than the smaller HS^- or Cl^- guests. When distances between the distal urea nitrogen atoms to the plane formed by the central aryl ring were investigated, $[\mathbf{2.1^{tBu}(SeH)}]^-$ (2.273 \AA) exhibited much longer average distance than $[\mathbf{2.1^H(SH)}]^-$ (2.109 \AA) or $[\mathbf{2.1^H(Cl)}]^-$ (2.029 \AA). In tandem, these results suggest that the larger HSe^- guest distorts the binding cavity more than related row 3 anions, perhaps explaining the poorer binding affinity for HSe^- in these systems.^{74,75}

Table 2.3. Bond lengths and angles in $[\mathbf{2.1^{tBu}(SeH)}]^-$.

	Atomic Distance (Å)	Bond Angle (°)
C1(H)⋯Se1	3.769	168.38
N1(H)⋯Se1	4.073	144.15
N2(H)⋯Se1	3.373	170.23
N3(H)⋯Se1	3.710	151.50
N4(H)⋯Se1	3.397	172.68

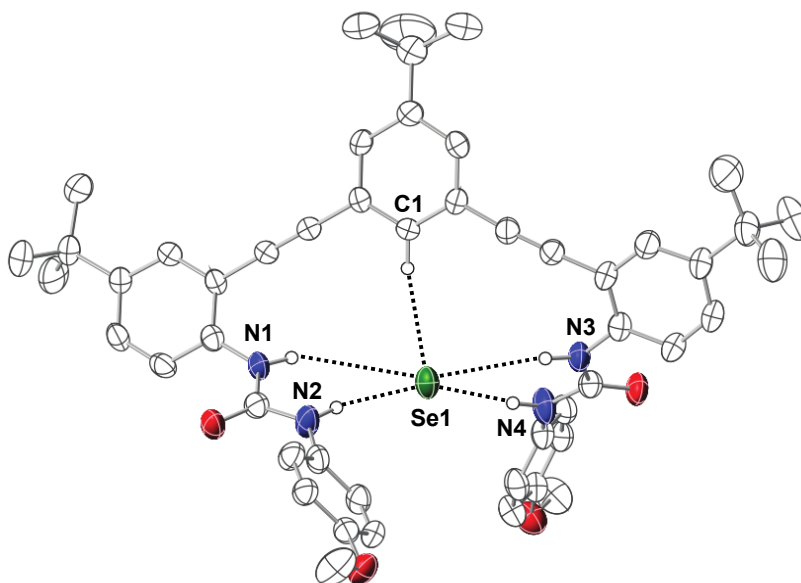


Figure 2.5. Thermal ellipsoid diagram (at 50% probability) depicting the molecular structure of $[2.1^{\text{tBu}}(\text{SeH})]^-$. Hydrogen atoms not interacting with the bound HSe^- are omitted for clarity.

2.3 Conclusions

In this study we have presented the first example of reversible HSe^- binding with two separate supramolecular receptors. Both receptors interact with HSe^- through N–H and aryl C–H hydrogen bonds and the ability of two structurally distinct receptors to bind HSe^- demonstrates the generality of this type of reversible supramolecular interaction. Additional studies with the related anions HS^- , Cl^- , and Br^- suggested basicity and anion size impact the binding affinities of the receptors in polar, aprotic organic solvents. Both receptors show the greatest binding affinity for the smallest and most basic anion, HS^- . The dramatic decrease in binding affinity for larger anions suggests that smaller anions fit better in these systems, giving our receptors a preference for HS^- over HSe^- . The size of the anion appears to impact binding more significantly than basicity, as the binding

affinity of the relatively basic anion HSe^- is surprisingly almost four times less than that of the substantially less basic but smaller anion Cl^- . The predictability of these trends suggests clear enthalpic driving forces behind binding preference, but the role of entropy cannot be discounted. The analysis of entropy versus enthalpy in our hosts will be followed up in a future report.

These results, coupled with the development of the first synthesis for NBu_4SeH , provide a solid platform for development of future supramolecular HSe^- receptors. Reversible receptors for HSe^- certainly require scaffolds resistant to nucleophilic attack and should be able to bind selenium through suitable hydrogen bond donors such as urea N–H, amide N–H, or aromatic C–H groups, likely among many others. Furthermore, receptors more selective for HSe^- may require binding cavities larger than either **2.1^{tBu}** or **2.2^{CF3}** possess. Such developments will ultimately provide better tools toward understanding the supramolecular chemistry of the biologically- and environmentally-relevant hydrochalcogenide anions.

CHAPTER III

TUNING SUPRAMOLECULAR SELECTIVITY FOR HYDROSULFIDE: LINEAR FREE ENERGY RELATIONSHIPS REVEAL PREFERENTIAL C–H HYDROGEN BOND INTERACTIONS

This chapter includes previously published and co-authored material from Fargher, H.A.; Lau, N.; Richardson, H.C.; Cheong, P.H.-Y.; Haley, M.M.; Pluth, M.D.; Johnson, D.W. Tuning Supramolecular Selectivity for Hydrosulfide: Linear Free Energy Relationships Reveal Preferential C–H Hydrogen Bond Interactions. *J. Am. Chem. Soc.* **2020**, *142* (18), 8243–8251. This manuscript was co-written by Hazel A. Fargher and Nathanael Lau, with editorial assistance by Professors Michael M. Haley, Michael D. Pluth, and Darren W. Johnson. The project in this chapter was developed by Hazel A. Fargher, Nathanael Lau, and Professors Michael M. Haley, Michael D. Pluth, and Darren W. Johnson. The experimental work in this chapter was performed by Hazel A. Fargher and Nathanael Lau. The computational experiments were performed by H. Camille Richardson, with assistance from Professor Paul H.-Y. Cheong.

3.1 Introduction

The hydrochalcogenide anions (HCh^- , Ch = Group 16 element) hydrosulfide (HS^-) and hydroselenide (HSe^-) are highly reactive species that play crucial roles in biological systems.^{9,33} At physiological pH, these anions are favored in solution over their diprotic counterparts hydrogen sulfide (H_2S) and hydrogen selenide (H_2Se), which are important as a biological gasotransmitter and in selenium metabolism, respectively.^{9,33,34,56} The high nucleophilicity and redox activity of these anions, however, has stymied many investigations.^{9,33} A better understanding of the molecular recognition

properties of these anions could aid our understanding of the non-covalent forces used to stabilize these reactive species in biology and enable the development of future probes for HCh^- binding and detection.

The well-known ability of supramolecular receptors to reversibly bind anionic guests through noncovalent interactions^{13,76,77} mimics strategies found in Nature to stabilize reactive species^{78–80} and offers an attractive approach for studying the supramolecular chemistry of HCh^- . Our groups recently reported the first examples of organic receptors that can reversibly bind HS^- and HSe^- by employing urea or amide N–H hydrogen bond (HB) donors and aromatic C–H HB donors (**3.1**, **3.2**, Figure 3.1).^{29,31,35} More recently, an additional report of reversible supramolecular HS^- binding was reported in a system that employs bambusuril C–H HB donors (**3.3**, Figure 3.1).³²

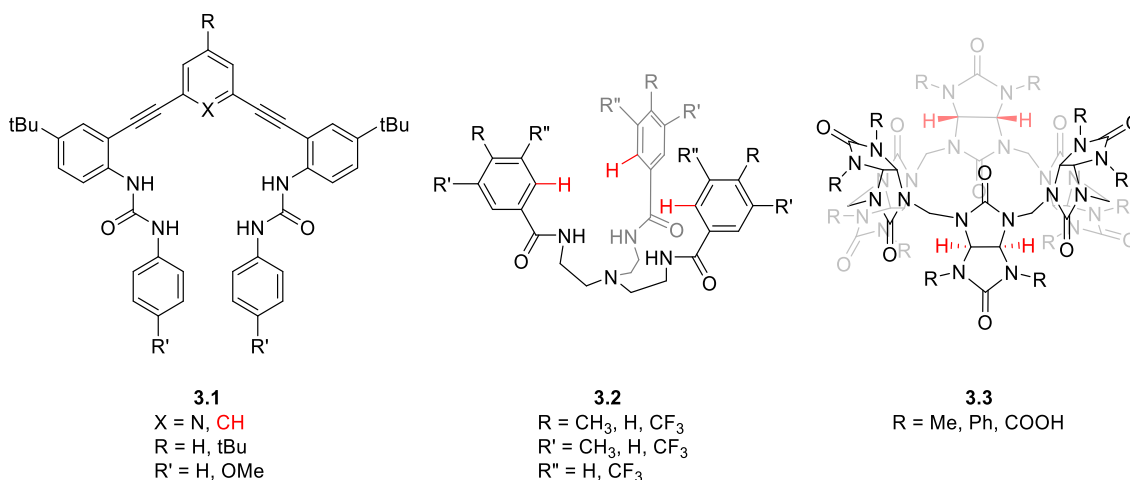


Figure 3.1. Receptor scaffolds **3.1-3.3** all bind HS^- reversibly and all contain C–H HB donors. Only receptor classes **3.1** and **3.2** have been shown to reversibly bind HSe^- . The C–H HB donors that interact with the HCh^- are shown in red for clarity.

One advantage of using synthetic supramolecular receptors is the ability to engineer the receptor scaffold to improve specificity for one guest over other competing

analytes. Supramolecular receptors with high selectivity could prove useful in applications such as sensing, extraction, controlled delivery, and cell-membrane transport.⁸¹⁻⁸³ Designing selective systems for HCh^- , however, is difficult given the similarity of size and shape to halides. This challenge in molecular recognition has not yet been solved and can be observed in all previously reported receptors **3.1-3.3** for HCh^- , all of which also bind Cl^- and Br^- with appreciable affinity to HCh^- of a similar size.^{29,32,35}

C-H HB donors serve as a unifying theme in receptors **3.1-3.3**, which hints that such moieties could be important for HCh^- binding. Broadening these types of interactions, methionine C-H \cdots S HBs have been reported to be critical in the substrate specificity and catalytic activity of methionine aminopeptidase.⁸⁴ These interactions are not limited to one protein, but rather have been observed in 20 other protein structures in the Protein Data Bank (PDB) prior to 2016.⁸⁴ These findings prompted us to investigate the importance of C-H HB donor motifs in driving selective recognition of HCh^- further. We have previously investigated the effect of polarization of an aryl C-H HB donor on various anions through modifying the *para*-substituent with electron-donating and -withdrawing groups of **3.1**.²⁷ Analysis of the linear free energy relationships (LFERs), including Hammett plots, revealed a significant relationship between substituent effects on polarization of the aryl C-H HB and anion binding energy, at a time when non-traditional C-H HB donors were perhaps still considered controversial by some.^{27,85} By conducting a similar LFER study with HCh^- , the effect of the C-H HB donor polarization on HCh^- binding could be compared directly to that on halides.

Moreover, these studies can begin to unravel the similarities and differences between selective recognition of halides and HCh^- . At first glance, these anions should behave drastically differently due to the differences in their polarizabilities, pK_{bs} ,^{73,86,87} solvation energies,^{88,89} and reactivities; yet they tend to behave surprisingly similarly in their molecular recognition behavior at first glance. Differences in the observed effects could indicate that C–H polarization influences the selectivity between the two classes of anions, which is supported by prior results with **3.1-3.3** and in biological systems. Additionally, the systematic investigation of a series of receptors with physical organic methods is a rigorous way to uncover other important details in anion binding mechanisms, binding selectivity, and other anion-dependent effects.^{90,91} Motivated by these needs, here we demonstrate that LFERs are a powerful tool that allow for not only anion-dependent solution binding energies ($\Delta G_{\text{binding}}$) to be measured, but also for observing anion-dependent substituent effects and estimating of the difference in aryl C–H \cdots Anion (A^-) HB strengths between HCh^- and halides. These insights can be used as a first step to understanding the supramolecular chemistry of these anions as well as provide design elements for developing selective receptors for these reactive, yet biologically relevant anions.

3.2 Results and Discussion

3.2.1 Synthesis and characterization

A series of six arylethynyl bisurea receptors (**3.1^R**, Figure 3.2), differing only by the substituent in the position *para* to the participating aryl C–H HB donor ($-\text{R}$, Figure 3.2), was prepared for LFER studies with HCh^- (HS^- and HSe^-) and halides (Cl^- and

Br⁻).²⁷ This host system, which can bind a guest molecule through HBs from one aryl C–H HB donor and four urea N–H HB donors, was chosen for its functional group tolerance of and compatibility with HCh⁻. Hosts in this series had been previously shown to resist irreversible nucleophilic attack from the HCh⁻ guests on the titration timescale by preferentially binding HS⁻ and HSe⁻ through primarily noncovalent HBs.^{29,31,35} The series of receptors featured one previously unreported host (**3.1**^{CF3}), which was prepared by similar synthetic methods and characterized by ¹H, ¹³C{¹H}, and ¹⁹F NMR spectroscopy (Appendix B, Figures B.4–B.6) as well as by mass spectrometry.

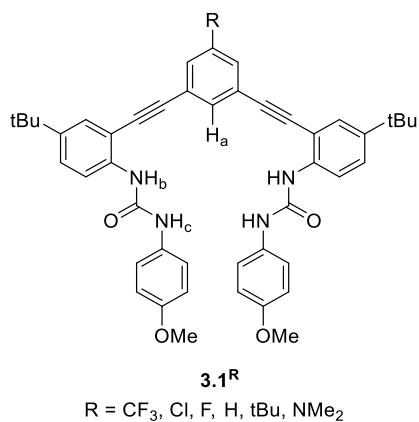


Figure 3.2. The series of arylethynyl bisurea receptors used in this study.

To ensure that modulating the electron-withdrawing or -donating character of the –R substituent only affected the polarity of the C–H_a HB donor and not the NH_{b/c} HB donors as well, we compared the ¹H NMR spectra of the six **3.1**^R free hosts (Figure 3.3). The ¹H NMR spectra of the most electron-donating (**3.1**^{NMe2}) and -withdrawing receptors (**3.1**^{CF3}) showed that the largest difference in chemical shift ($\Delta\delta$) occurred in the aryl CH_a proton ($\Delta\delta = 0.927$ ppm), followed by much smaller shifts in the proximal urea NH_b protons ($\Delta\delta = 0.058$ ppm) and distal urea NH_c protons ($\Delta\delta = 0.024$ ppm). We observed a

general trend of downfield shifting of CH_a resonance with increasing electron-withdrawing nature of the –R substituent, with the exception of **3.1**^{Cl} and **3.1**^F, perhaps revealing the importance of resonance effects in the electron-withdrawing ability of these two substituents.

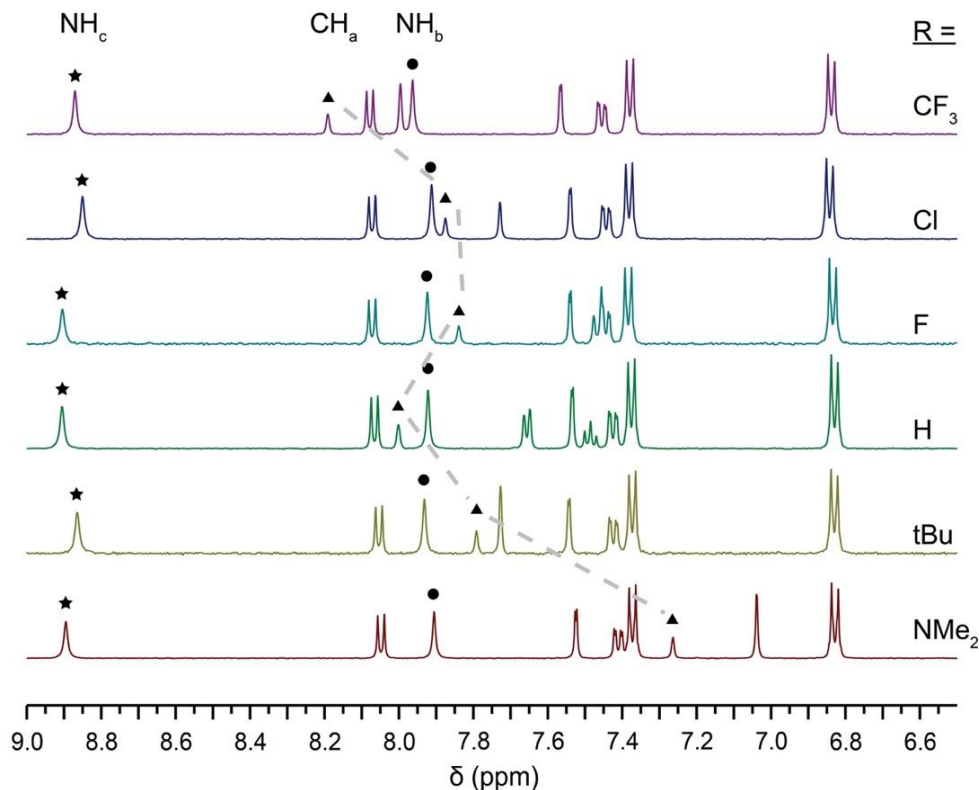


Figure 3.3. ¹H NMR spectra of six receptors **3.1**^R in 10% DMSO-*d*₆/CD₃CN. The largest change in δ of possible HB donors occurs for the CH_a proton peak.

Additionally, the LFER between the ¹H NMR chemical shift (δ) of H_{a-c} in 10% DMSO-*d*₆/CD₃CN and the Hammett parameter σ_p was used to quantitatively evaluate the influence of the electron-withdrawing and -donating nature of the –R substituent on δ of the free-host. Figure B.7 (Appendix B) and Table B.1 (Appendix B) show that the plot for the aryl C–H_a proton has a slope of 0.64 ± 0.11, with 90% of the change in δ stemming

from the electron-donating or -withdrawing nature of the substituent ($R^2 = 0.90$). Conversely, the fits for the urea $\text{NH}_{b/c}$ protons are poor ($0.13 \leq R^2 \leq 0.49$), and the slopes of the plots for these protons are close to 0, indicating that these protons are not significantly affected by the nature of the functional group. These data show that electronic communication between the urea protons and the $-\text{R}$ substituent diminishes with increasing distance, which is consistent with observations in other systems.^{91,92} Furthermore, the aryl $\text{C}-\text{H}$ bond is most affected by the *para*-substituent modifications, which is consistent with previous work from our group.²⁷

3.2.2 ^1H NMR spectroscopy titrations

Previous work from our lab tested the hypothesis that softer HCh^- could interact more favorably with aryl $\text{C}-\text{H}$ HB donors,²⁹ suggesting that substituent effects that polarize this motif may affect the binding affinity of HCh^- more than the presumptively harder halides. As a result, selectivity between these similar anions could potentially be achieved in this system by exploiting suitably polarized $\text{C}-\text{H}$ HB donor motifs. To test this hypothesis, we measured binding affinities (K_{as}) using ^1H NMR spectroscopy titration experiments between the six **3.1^R** hosts and HS^- , HSe^- , Cl^- , and Br^- guests as the tetrabutylammonium (NBu_4^+) salts^{35,70} in 10% $\text{DMSO}-d_6/\text{CD}_3\text{CN}$ at 25 °C, as shown for host **3.1^{CF3}** and HS^- (Figure 3.4). All experiments were performed under anaerobic and anhydrous conditions since the presence of oxygen or water resulted in brightly colored guest solutions, noisy NMR spectra, poor data fitting, and accelerated irreversible reactivity between hosts and HCh^- . Titrations were performed in triplicate (Method B.1 and B.2, Appendix B), and K_{as} and energy of binding in solution ($\Delta G_{\text{binding}}$) (Table 3.1)

were obtained by the Thordarson method.⁷¹ Note that some K_a values for **3.1^H** and **3.1^{tBu}** were previously reported by our groups^{29,35} and were reused in this study after replication under the exact conditions reported in this paper.

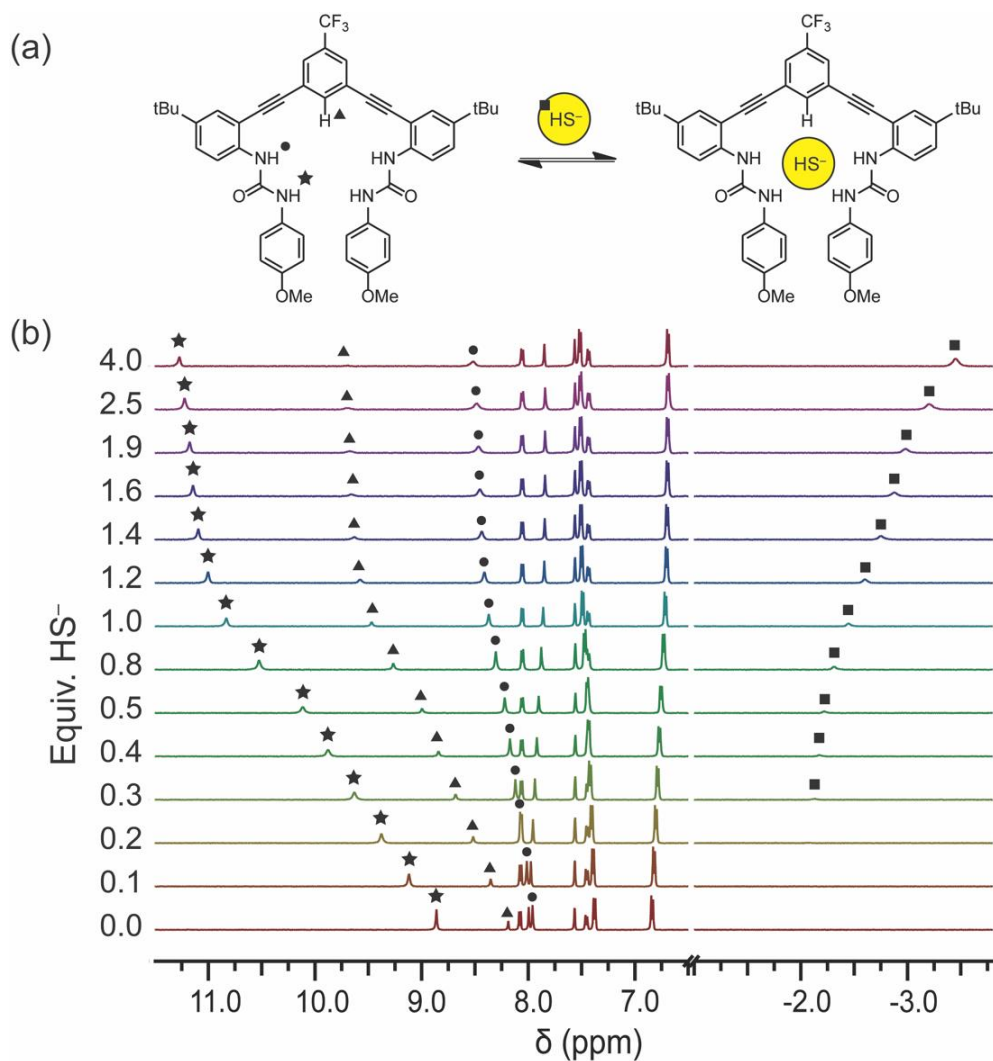


Figure 3.4. (a) Representation of the host–guest equilibrium between **3.1^{CF3}** and HS^- . (b) ^1H NMR titration of 2.2 mM **3.1^{CF3}** with NBu_4SH in 10% $\text{DMSO-}d_6/\text{CD}_3\text{CN}$.

Table 3.1. Association constants and binding free energies for receptors **3.1^R** at 1-3 mM with HS⁻, HSe⁻, Cl⁻, and Br⁻ in 10% DMSO-*d*₆/CD₃CN at 25 °C.^a

Host	HS ⁻		HSe ⁻		Cl ⁻		Br ⁻	
	<i>K</i> _a (M ⁻¹)	Δ <i>G</i> _{binding} (kcal mol ⁻¹)	<i>K</i> _a (M ⁻¹)	Δ <i>G</i> _{binding} (kcal mol ⁻¹)	<i>K</i> _a (M ⁻¹)	Δ <i>G</i> _{binding} (kcal mol ⁻¹)	<i>K</i> _a (M ⁻¹)	Δ <i>G</i> _{binding} (kcal mol ⁻¹)
3.1^{CF3}	15000 ± 1800	-5.69 ± 0.07	940 ± 80	-4.05 ± 0.05	2420 ± 120	-4.61 ± 0.03	173 ± 9	-3.05 ± 0.03
3.1^{Cl}	8480 ± 1170	-5.35 ± 0.08	810 ± 60	-3.96 ± 0.04	2300 ± 180	-4.58 ± 0.05	133 ± 7	-2.89 ± 0.03
3.1^F	8330 ± 940	-5.34 ± 0.07	610 ± 40	-3.79 ± 0.04	1890 ± 90	-4.47 ± 0.03	134 ± 7	-2.90 ± 0.03
3.1^{H^b}	5010 ± 810 ^b	-5.04 ± 0.10 ^b	530 ± 60	-3.71 ± 0.06	1780 ± 120 ^b	-4.43 ± 0.04 ^b	120 ± 7	-2.84 ± 0.03
3.1^{tBu^b}	3600 ± 500 ^b	-4.85 ± 0.08 ^b	460 ± 50 ^b	-3.63 ± 0.06 ^b	1700 ± 200 ^b	-4.40 ± 0.07 ^b	110 ± 20 ^b	-2.78 ± 0.11 ^b
3.1^{NMe2}	1660 ± 100	-4.39 ± 0.04	360 ± 40	-3.48 ± 0.06	1120 ± 150	-4.15 ± 0.08	85 ± 8	-2.63 ± 0.06

^aAll values were obtained by fitting ¹H NMR titration data to 1:1 binding isotherm model with the error as the standard deviation of three titrations.³⁰ Minimum error is assumed to be 5% of *K*_a value. ^bValues were previously reported by our groups in references 29 (**3.1^H**) and 35 (**3.1^{tBu}**).

3.2.3 LFERs reveal anion-dependent Δ*G*_{binding} trends

With *K*_as and Δ*G*_{binding} values determined for each host/guest combination, we endeavored to use LFERs to visualize binding energy trends within a host/guest series with one anion and across a range of anions. Plotting Δ*G*_{binding} of each host/guest complex against σ_p of the -R substituent (Figure 3.5) revealed a strong linear response of the HCh⁻ and halide anion binding energies to the electron-withdrawing or -donating nature of the -R substituent. Table 3.2 summarizes the parameters of the linear fit for each anion, determined through linear regression. For each anion, more than 90% of the change in Δ*G*_{binding} can be attributed to the electronics of the -R substituent (0.91 ≤ *R*² ≤ 0.97). The LFER for HSe⁻ has the lowest *R*² value, which we attribute to slight reactivity of HSe⁻ with the receptors that is not detectable by ¹H NMR spectroscopy over the titration timescale but has been observed previously over several hours.³⁵ Competing receptor

reactivity has been shown in other systems to adversely affect fits.⁹³ Importantly, the p -values for the contribution of the slopes and intercepts to all the regressions are statistically significant, meaning that both σ_p and $\Delta G_{\text{binding}}$ at the intercept are meaningful predictors of anion binding in our systems. The p -values for overall models also reveal that all the LFERs are statistically significant.

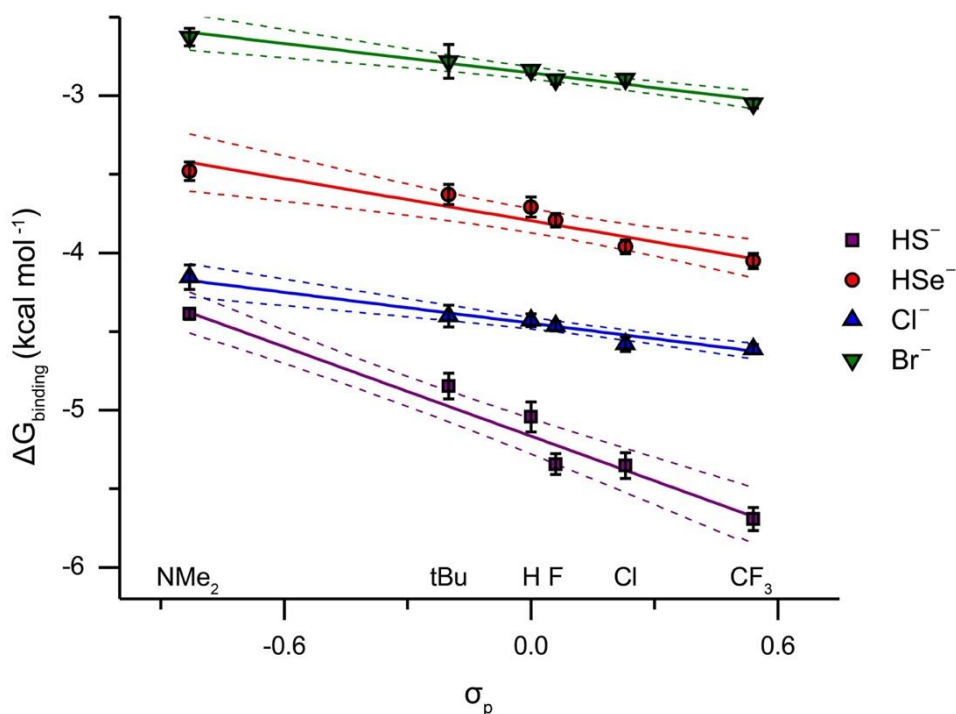


Figure 3.5. LFER between $\Delta G_{\text{binding}}$ and σ_p values for **3.1^R** with HS^- , HSe^- , Cl^- , and Br^- . Dashed lines represent the 95% confidence interval for each linear trend.

Table 3.2. Fitting statistics for the LFER between $\Delta G_{\text{binding}}$ and σ_p for all four anions.

Guest	Slope	Intercept	p -value		R^2	R^2_{adj}	
			Slope	Intercept			
HS⁻	-0.97 ± 0.10	-5.14 ± 0.04	< 0.01	< 0.01	< 0.01	0.96	0.95
HSe⁻	-0.43 ± 0.07	-3.78 ± 0.03	< 0.01	< 0.01	< 0.01	0.91	0.88
Cl⁻	-0.35 ± 0.03	-4.45 ± 0.01	< 0.01	< 0.01	< 0.01	0.97	0.96
Br⁻	-0.30 ± 0.03	-2.86 ± 0.01	< 0.01	< 0.01	< 0.01	0.96	0.96

Several trends can immediately be extracted from this LFER study. First, each LFER has a negative slope, indicating that more electron-withdrawing *para* substituents favor guest binding for all four anions as expected. This trend is likely due to the increasing polarization, and by extension acidity, of the C–H_a HB donor, as noted in previous LFERs of HB receptors with anionic guests.^{93,94} Additionally, we previously observed that **3.1**^{tBu} binds smaller, more basic anions with a higher affinity.³⁵ These trends were again observed in this study: for similarly sized anions (e.g., HS⁻ vs. Cl⁻ and HSe⁻ vs. Br⁻), the more basic anion is more strongly bound by each receptor, whereas between the anions in the same Group (e.g., HS⁻ vs. HSe⁻ and Cl⁻ vs. Br⁻), the smaller anion is more strongly bound. Stronger bases would clearly form stronger HBs with the host, and the more diffuse nature of the larger anions may weaken their HB affinity.

As a result of these trends, the LFERs reveal that all six receptors bind HS⁻ (a small, basic guest) the strongest, with a preference for this anion over the other anions investigated. Surprisingly, we also saw that when the polarization of the aryl C–H HB donor increases with more electron-withdrawing substituents, the preference of our receptors for HS⁻ over the other anions increases (Figure 3.5). The most electron-donating receptor **3.1**^{NMe2} shows little preference for HS⁻ over Cl⁻ ($\Delta\Delta G_{\text{binding}} = -0.24 \pm 0.09$ kcal mol⁻¹), whereas the most electron withdrawing receptor **3.1**^{CF3} has the largest difference in binding energy between the two anions ($\Delta\Delta G_{\text{binding}} = -1.30 \pm 0.08$ kcal mol⁻¹), which corresponds to an approximately nine-fold increase in selectivity (Table

3.2). This unexpected result is significant because polar C–H HB donors may provide a route to future, more selective supramolecular receptors for HS⁻.ⁱ

3.2.4 Hammett plots reveal anion-dependent substituent effects

To better understand and visualize differences in anion binding sensitivity, we used Hammett relationships ($\log(K_a^R/K_a^H)$ vs. σ_p) generated by fitting K_a data to Equation 3.1. Table 3.3 summarizes the parameters of each linear fit, determined through linear regression. These were fit to a modified Hammett equation that includes an origin offset value (ϵ). The reported p -values for each slope, ρ , indicate that σ_p is a significant predictor of anion sensitivity to the polarity of the C–H HB donor in our systems, and the p -values of the regression models show the Hammett plots for each anion are statistically significant. Non-significant p -values for the contribution of ϵ to the overall model indicates that factors beyond the electronics of the –R substituent described by σ_p do not have a meaningful effect on the change in binding energies for the individual anion guests. Indeed, forcing the Hammett plot through the origin of the graph does not result in appreciably different slopes (Appendix B, Table B.20).

$$\log \frac{K_a^R}{K_a^H} = \rho \sigma_p + \epsilon \quad (3.1)$$

The Hammett plots for HSe⁻, Cl⁻, and Br⁻ (Figure 3.6) show a smaller substituent effect than the benchmark deprotonation of benzoic acid in water at 25 °C,⁹⁵ with slopes ranging from 0.22 to 0.32. These slopes are similar to our previously reported receptors²⁷ and other HB donor and acceptor systems.⁹⁶ In our system these values represent a

ⁱ Exhaustive efforts to use computational experiments to explain the preference and increasing selectivity of our receptors for HS⁻ compared to the other anions unfortunately proved unfruitful. See Appendix C for more details.

description of how sensitive anion binding is to the polarization and strength of the aryl C–H HB donor. Using analysis of covariance (ANCOVA) to compare the linear regression models of HSe^- , Cl^- , and Br^- , we found that the slopes of the three Hammett plots are not statistically different (Appendix B, Table B.21). These anions may have very different binding energies in our host system (Table 3.1, Figure 3.5), but the substituent effect on binding is independent of the identity of the three anions. Stated another way, HSe^- , Cl^- , and Br^- have experimentally identical effects from C–H HB donor modulation in this receptor class.

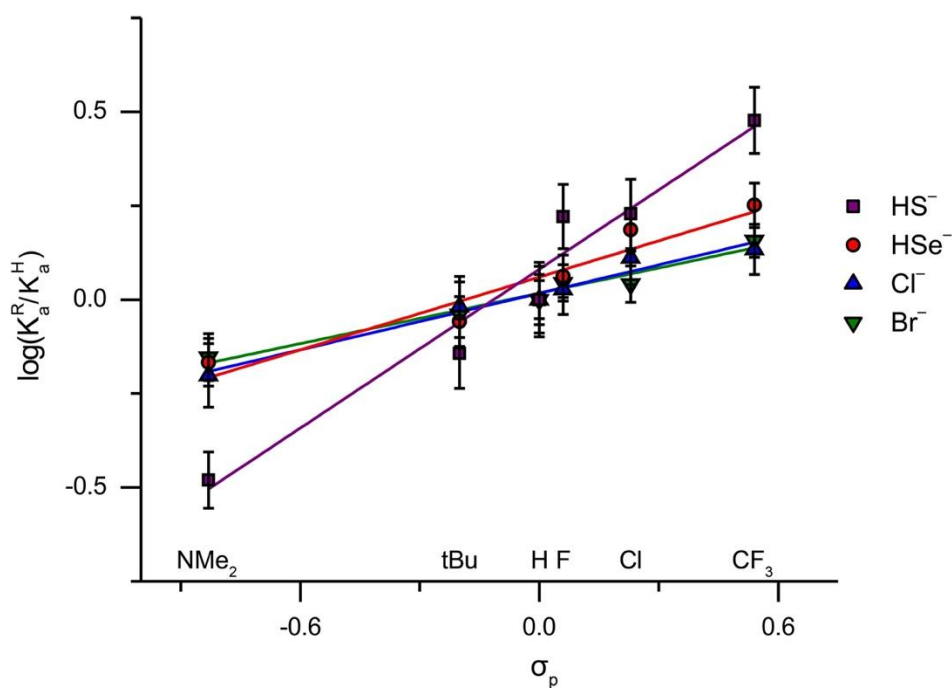


Figure 3.6. Hammett plot between $\mathbf{3.1^R}$ and HS^- , HSe^- , Cl^- , and Br^- . The slope of HS^- is significantly different from HSe^- , Cl^- , and Br^- illustrating the increased sensitivity of HS^- to substituent effects.

Intriguingly, the larger magnitude of the slope for the Hammett plot of HS⁻ binding ($\rho = 0.71 \pm 0.07$, Table 3.3) is statistically significantly larger than that of the other anions, confirmed by ANCOVA (Appendix B, Table B.21). These results show that HS⁻ is more sensitive to the polarization of the C–H HB donor than the other anions. To investigate these results further, we used Swain-Lupton parameters to investigate the relative inductive/field and resonance contributions to the observed substituent effect in each anion binding event, and electrostatic potential (ESP) surface maps to interrogate the strength of each C–H \cdots A⁻ HB.

Table 3.3. Fitting statistics for Hammett plots for HS⁻, HSe⁻, Cl⁻, and Br⁻.

Guest	ρ	ϵ	p-value			R ²	R ² _{adj.}
			ρ	ϵ	Model		
HS ⁻	0.71 ± 0.07	0.07 ± 0.03	< 0.01	0.08	< 0.01	0.96	0.95
HSe ⁻	0.32 ± 0.05	0.06 ± 0.02	< 0.01	0.06	< 0.01	0.90	0.88
Cl ⁻	0.25 ± 0.02	0.02 ± 0.01	< 0.01	0.16	< 0.01	0.97	0.96
Br ⁻	0.22 ± 0.02	0.02 ± 0.01	< 0.01	0.16	< 0.01	0.96	0.96

3.2.5 Field/inductive vs. resonance substituent effects on anion binding

We first hypothesized the increased sensitivity of HS⁻ to changing the –R substituent could be attributed to differences in the relative resonance contribution from the –R substituent to the aryl C–H HB in binding with each anion. To test this hypothesis we fit experimentally determined K_{as} to the Swain-Lupton equation (Equation 3.2), which splits the $\rho\sigma_p$ term in the Hammett equation (Equation 3.1) into contributions from field/inductive effects (denoted by ρ_{rF}) and contributions from resonance effects (denoted by ρ_{rR}).⁹⁷ Although our systems should not exhibit any important resonance contributors involving the aryl C–H HB donors (Appendix B, Figure B.37), resonance effects have been shown to play a significant role in anion binding within our scaffolds.²⁷ Table 3.4

summarizes the parameters of each linear fit, determined through multivariable linear regression. The linear regression of each anion has an excellent fit to Swain-Lupton parameters F and R ($0.96 \leq R^2 \leq 0.99$). The reported p -values for the contribution of ρ_f and ρ_r to the regressions for all anions indicate that inductive/field effects and resonance are both meaningful contributors to anion binding. In addition, the overall models for the Swain-Lupton plots are statistically significant. Non-significant p -values for the contribution of the intercept I to the regressions (Table 3.4) indicate that factors beyond field/inductive and resonance substituent effects, such as polarizability and steric interactions, do not make meaningful contributions to the change in binding energies. Again, forcing the plot through the origin of the graph does not significantly affect results (Appendix B, Table B.22).

$$\log \frac{K_a^R}{K_a^H} = \rho_f F + \rho_r R + I \quad (3.2)$$

To better compare the regression results in Table 3.4, we calculated the percent resonance contribution (%R) to anion binding with Equation 3.3.²⁷ Previous computational studies have shown no resonance contribution to anion binding in other C–H HB donor systems in the gas phase.^{90,98} This does not take into account the role of solvent, however, which may be crucial in allowing resonance effects to participate in anion binding; in fact, our system shows a high %R contribution to anion binding, ranging from 36 to 47%. We were also able to directly compare the %R contribution for the halides in 10% DMSO-*d*₆/CD₃CN (solvent dielectric constant $\epsilon \sim 42$)⁹⁹ with previously published %R for the halides in a similar receptor series in H₂O_{sat}/CHCl₃ ($\epsilon \sim 4.9$).^{27,99} We found that despite moving from a comparatively non-competitive solvent

system (H₂O_{sat.}/CHCl₃) to a competitive solvent system (10% DMSO-*d*₆/CD₃CN), all the %R contributions are identical within error.²⁷

$$\%R = \frac{\rho_r}{\rho_f + \rho_r} \times 100 \quad (3.3)$$

We also found that the %R contributions for all the anions in 10% DMSO-*d*₆/CD₃CN are identical within error, despite HS⁻ having much larger coefficients for ρ_f and ρ_r. Therefore, we cannot ascribe such a big difference in sensitivity seen for HS⁻ to a change in the relative contributions from resonances substituent effects. However, analysis of the linear fits of the anions with alternative Hammett parameters σ_m and σ_p⁺, which give more weight to field/inductive effects and resonance effects, respectively,⁹⁷ indicates that resonance contributions from the substituent may still play a larger role in binding the halides than HCh⁻ (Appendix B, Section B.8).

Table 3.4. Fitting statistics from the multivariable linear fit to the Swain-Lupton equation for the *K*_a values for HS⁻, HSe⁻, Cl⁻, and Br⁻.

Guest	ρ _f	ρ _r	<i>I</i>	<i>p</i> -value			R²	R²_{adj.}	%R	
				ρ _f	ρ _r	I				Model
HS⁻	1.00 ±	0.62 ±	-0.02 ±	< 0.01	< 0.01	0.50	< 0.01	0.99	0.99	38 ± 3
	0.08	0.04	0.03							
HSe⁻	0.48 ±	0.27 ±	0.00 ±	0.01	0.01	0.94	0.01	0.96	0.93	36 ± 8
	0.09	0.05	0.03							
Cl⁻	0.28 ±	0.25 ±	0.01 ±	0.02	< 0.01	0.71	0.01	0.97	0.94	47 ± 9
	0.06	0.03	0.02							
Br⁻	0.26 ±	0.20 ±	0.00 ±	0.01	< 0.01	0.96	0.01	0.97	0.95	43 ± 8
	0.05	0.03	0.02							

3.2.6 Estimation of aryl C–H⋯A⁻ strength through LFERs

Our next step was to analyze the LFER between Δ*G*_{binding} of each anion and the electrostatic potential (ESP) surface of the aryl hydrogen atom participating in anion binding (Figure 3.7), similar to previous work.²⁷ ESP maps at the 0.02 Å isoelectronic surface for the six receptors were computed at the PBE/6-31G(d) level of theory.^{100–102}

The ESP value of the C–H HB donor was used to ascertain the electronic effect that the –R substituent has on the C–H HB donor, and by extension the binding strength of the four anions. The statistically significant linear fit (Table 3.5) agrees with previous work that anion binding in our systems and others is often strongly governed by electrostatics.^{27,90,98,103} The fact that HS[−] and Cl[−] seem to have a better fit ($0.97 \leq R^2 \leq 0.98$) than HSe[−] and Br[−] ($0.93 \leq R^2 \leq 0.95$) could point to attractive binding forces other than electrostatics, such as induction and dispersion,¹⁰⁴ playing a more significant role in binding the larger anions in our systems. The ChelpG charges, which give atomic charges that map to the ESP,¹⁰⁵ for the key C–H HB donor did not reveal statistically significant linear fits. This showed that it is not the average charge of the C–H atoms that are meaningful to explain the binding; instead, the anisotropy of the ESP map is crucial to explain the chemistry of binding in these receptors.

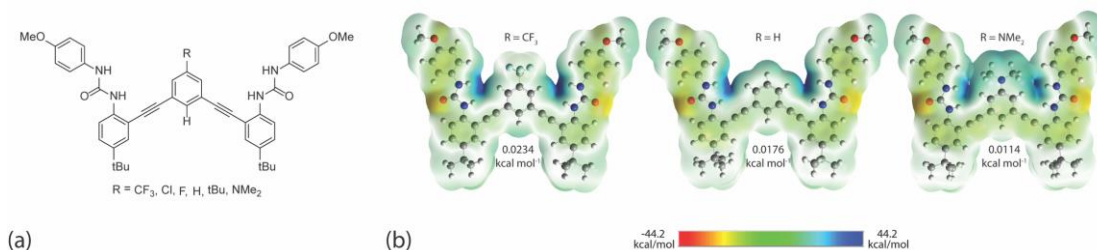


Figure 3.7. (a) Free receptors **3.1**^R can twist into the “W” conformation.⁴⁴ (b) Representative ESP maps of **3.1**^{CF₃}, **3.1**^H, and **3.1**^{NMe₂}, calculated at the PBE level of theory. The values describe the energy at the 0.02 Å isoelectric surface of the C–H HB donor *para* to the –R substituent.

Table 3.5. Fitting statistics for the LFER between $\Delta G_{\text{binding}}$ and ESP Surfaces of the model compounds for HS[−], HSe[−], Cl[−], and Br[−].

Guest	Slope	Intercept	<i>p</i> -value		R ²	R ² _{adj.}
			Slope	Intercept		
HS [−]	-105 ± 9	-3.17 ± 0.17	< 0.01	< 0.01	< 0.01	0.97
HSe [−]	-48 ± 5	-2.89 ± 0.10	< 0.01	< 0.01	< 0.01	0.95
Cl [−]	-37 ± 3	-3.75 ± 0.06	< 0.01	< 0.01	< 0.01	0.98
Br [−]	-31 ± 4	-2.27 ± 0.08	< 0.01	< 0.01	< 0.01	0.93

This LFER was used in conjunction with previously published Equation 3.4 to estimate the strength of the aryl C–H \cdots A $^-$ HB.²⁷ The equation assumes that at the intercept (when the ESP at the C–H HB is equal to 0), all of the remaining binding energy is due to attractive interactions other than the C–H HB. Subtracting out all other attractive interactions from the experimental $\Delta G_{\text{binding}}$ should provide an estimate for the C–H \cdots A $^-$ HB strength. Note that since the binding of anions in our hosts is a cooperative event between the N–H_{b/c} urea and aryl C–H_a HBs,²⁸ and other forces such as contribution from solvent are not accounted for, the following data are simply estimates.

$$\text{Aryl CH}\cdots\text{A}^- \text{ HB Strength} = \Delta G_{\text{binding}} - \text{intercept} \quad (3.4)$$

The estimated aryl C–H \cdots A $^-$ HB bond strengths for each of the six receptors with each of the four anions are shown in Table 3.6. Unlike the Swain-Lupton analysis, the plot of binding strengths vs. ESP shows a clear difference between HS $^-$ relative to the other three anions (Figure 3.8), reflecting the differences in Hammett plots of the anion guests. The strength of the aryl C–H \cdots A $^-$ HBs are very similar for each of the six receptors with HSe $^-$, Cl $^-$, and Br $^-$. Conversely, HS $^-$ shows considerably stronger C–H HB strengths for all the receptors in this system. From these data, it is clear that the aryl C–H donor has a preference for HS $^-$ binding over the other anions, emphasizing the importance of using such moieties in the design of HS $^-$ sensitive and selective probes and materials, and indicating that the nature of the C–H \cdots A $^-$ interaction is the cause of the difference in slopes in the Hammett plot.

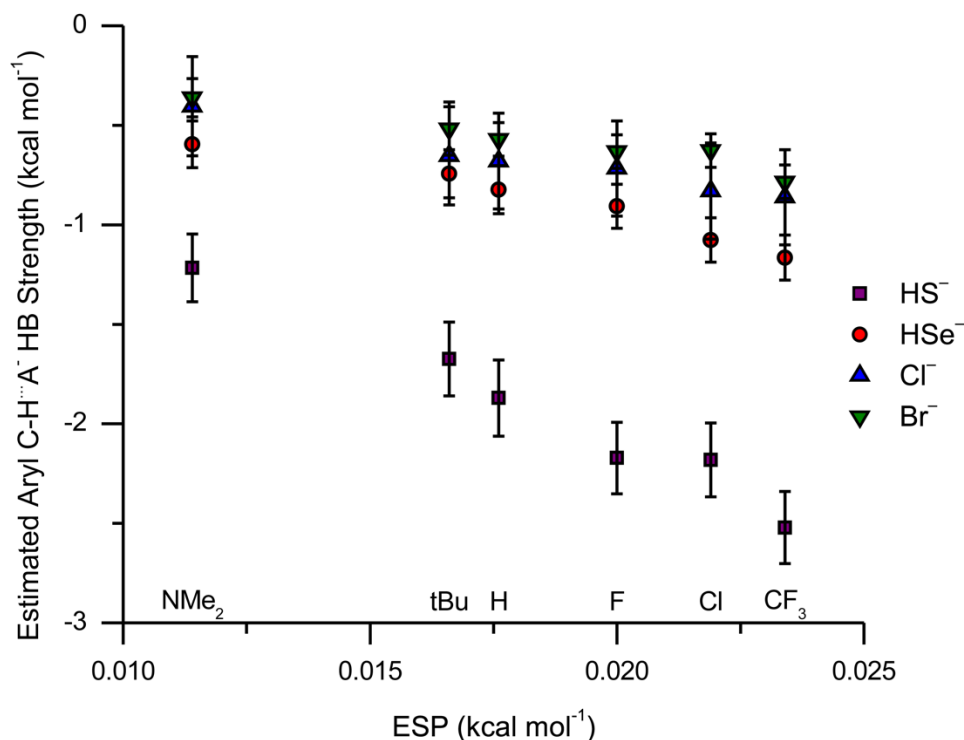


Figure 3.8. Estimated aryl C–H···A[−] HB strengths for all six receptors, with all four anions. While HSe[−], Cl[−], and Br[−] show similar HB strengths, HS[−] shows a stronger binding with the C–H HB donor motif.

Table 3.6. Estimated aryl C–H···A[−] HB strengths between **3.1^R** and all four anions.

Host	ESP (kcal mol ^{−1})	HS [−] Aryl C–H···A [−] HB Strength (kcal mol ^{−1})	HSe [−] Aryl C–H···A [−] HB Strength (kcal mol ^{−1})	Cl [−] Aryl C–H···A [−] HB Strength (kcal mol ^{−1})	Br [−] Aryl C–H···A [−] HB Strength (kcal mol ^{−1})
3.1^{CF3}	0.0234	−2.52 ± 0.18	−1.17 ± 0.11	−0.86 ± 0.24	−0.78 ± 0.08
3.1^{Cl}	0.0219	−2.18 ± 0.19	−1.08 ± 0.11	−0.83 ± 0.24	−0.63 ± 0.08
3.1^F	0.0200	−2.17 ± 0.18	−0.91 ± 0.11	−0.72 ± 0.24	−0.63 ± 0.08
3.1^H	0.0176	−1.87 ± 0.19	−0.82 ± 0.12	−0.68 ± 0.24	−0.57 ± 0.08
3.1^{tBu}	0.0166	−1.68 ± 0.19	0.74 ± 0.12	−0.65 ± 0.25	−0.52 ± 0.13
3.1^{NMe2}	0.0114	−1.22 ± 0.17	−0.60 ± 0.12	0.40 ± 0.25	−0.36 ± 0.10

3.3 Conclusions

Efforts by many others in the field,^{85,90,106–116} as well as our studies on equilibrium isotope effects²⁸ and LFERs on aryl C–H···A[−] HBs,²⁷ have helped establish C–H HBs as an important anion recognition motif in supramolecular chemistry. We endeavored to

apply this study to HCh^- , due to previous speculation that aryl $\text{C-H}\cdots\text{A}^-$ HBs could be important to binding these anions.^{26,29,35}

We therefore used our model aryl ethynyl bisurea anion-binding systems to report the first example of a LFER with HCh^- receptors in this manuscript. During this process, we also expanded the family of receptors shown to reversibly bind the reactive hydrochalcogenide anions. Importantly, we observed significant differences in HS^- binding in comparison to Cl^- , HSe^- , and Br^- anions. The LFERs of $\Delta G_{\text{binding}}$ vs. σ_p show that our receptors prefer to bind smaller, more basic anions. Additionally, selectivity for HS^- over the other anions increased with increasing C-H HB donor acidity. Furthermore, Hammett plots illustrated a significantly greater substituent effect on HS^- binding when compared to that of the other three anionic guests. Finally, the estimate of the aryl $\text{C-H}\cdots\text{A}^-$ HB bond strength again revealed unique behavior for HS^- binding, where significantly higher C-H HB strengths were observed.

Taken together, the insights from our investigation highlight the design principles needed for the next generation of selective hosts, materials, and probes for HCh^- anion binding. These studies demonstrate the importance of polarization of aryl C-H HB donors for HS^- , which may be utilized to bind this anion more tightly and selectively for a variety of applications in biomedical and environmental research. In addition, our studies on a fairly simple model systems may shed light on more complicated systems where $\text{C-H}\cdots\text{Ch}$ HBs and HCh^- recognition are gaining attention in molecular and structural biology. It has been well established that $\text{C-H}\cdots\text{O}$ HBs are important in organocatalysis^{117,118} and in defining the structure and function of biomolecules such as DNA, RNA, and proteins.^{119,120} Moving down the periodic table, C-H HBs and other

non-covalent binding interactions with chalcogens are less well studied. Methionine C–H \cdots S HBs have been found to be important in the catalytic activity and substrate specificity of methionine aminopeptidase.⁸⁴ Furthermore, a bacterial cell ion channel for HS⁻ was found to use only non-covalent molecular recognition in transport of the anion,¹²¹ and HS⁻ has been found in the turnover state of a nitrogenase enzyme, held in place by HB interactions.¹²² Perhaps our studies on fairly simple model systems lead to a hypothesis that CH HBs are over-represented in biological examples of sulfur compound recognition.

CHAPTER IV

DEUTERIUM EQUILIBRIUM ISOTOPE EFFECTS IN A SUPRAMOLECULAR RECEPTOR FOR THE HYDROCHALCOGENIDE AND HALIDE ANIONS

This chapter includes previously published and co-authored material from Fargher, H.A.; Nickels, R.A.; de Faria, T.P.; Haley, M.M.; Pluth, D.W.; Johnson, D.W. *RSC Adv.* **2021**, *11*, 26581–26585. This manuscript was written by Hazel A. Fargher with editorial support from Professors Michael M. Haley, Michael D. Pluth, and Darren W. Johnson. The project in this chapter was developed by Hazel A. Fargher and Professors Michael M. Haley, Michael D. Pluth, and Darren W. Johnson. Synthesis in this chapter was performed by Russell A. Nickels. Analytical work and data analysis was performed by Hazel A. Fargher. Mass spectra were obtained by Thaís P. de Faria.

4.1 Introduction

Molecular recognition and host-guest binding in both biological and synthetic systems are often driven by a mixture of competitive and additive primarily non-covalent interactions. Understanding the role of each of these forces in a host-guest system can reveal insights into the driving forces behind binding and help inform in the molecular design of future hosts.^{123–125} Equilibrium isotope effects (EIE), also referred to as binding isotope effects (BIE) in structural molecular biology,¹²⁶ measure the effect of isotopic substitution on supramolecular interactions through changes in the vibrational energy of the substituted bond. These studies can be used to elucidate the complex non-covalent forces involved in host conformational changes and host-guest binding.^{127–130}

Examples from structural molecular biology have demonstrated that EIEs can reveal mechanistic information in enzyme-ligand binding events.^{126,131} Isotopic substitution in synthetic supramolecular systems has been used both for labelling purposes and for studying individual non-covalent interactions. For example, Bergman, Raymond, and coworkers used deuterium equilibrium isotope effects (DEIE) to study benzylphosphonium cation guest binding in a self-assembled supramolecular complex in aqueous solution.¹³² From these DEIE studies, the authors found that attractive cation $\cdots\pi$ interactions in the interior of the host were important for promoting guest binding, and that C–H $\cdots\pi$ and $\pi\cdots\pi$ interactions were relatively small contributors. In another example, Shimizu and coworkers studied the DEIE on the strength of C–H $\cdots\pi$ interactions in their molecular balances.¹³³ Both computational and experimental results showed that the strength of C–H $\cdots\pi$ and C–D $\cdots\pi$ interactions were about equal, settling the debate on which interaction is stronger and easing concerns about using deuteration for spectroscopic and labelling applications.

Previously, we used a DEIE to study Cl[−] binding with the arylethynyl bisurea anion receptor **4.1**^{H/D} (Figure 4.1) in DMSO-*d*₆.²⁸ We found an experimental DEIE of 1.019 ± 0.010 , which matched the computationally-predicted DEIE of 1.020. Further computational analysis determined that the DEIE was due to a distorted N–H \cdots Cl[−] hydrogen bond geometry, which lead to changes in the C–H/D bond vibrational energy in the host-guest complex. In addition, Paneth and coworkers performed a computational study with **4.1**^H and other hydrogen bonding supramolecular Cl[−] receptors to determine the EIE of ^{35/37}Cl binding in these hosts.¹³⁴ Because isotope effects, both equilibrium and kinetic, originate solely from changes in the vibrational energy of the isotopically

labelled bond, the EIE arising from this study came from changes in the vibrational energies of the bonds in the supramolecular hosts when participating in hydrogen bonding with Cl^- isotopes. Indeed, a linear relationship was observed between the hydrogen bond donor (D) D–H bond lengths in the host-guest complex and the computed $^{35/37}\text{Cl}$ EIE.

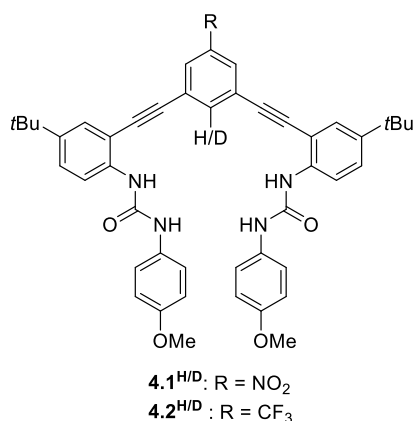


Figure 4.1. Arylolethynyl bisurea receptors 4.1^{H} and 4.1^{D} used in our previous DEIE study of Cl^- binding. Related receptors 4.2^{H} and 4.2^{D} are used in the current study to avoid reaction with HS^- .³⁶

Previous EIE studies with receptor $4.1^{\text{H/D}}$ have focused on Cl^- binding; however, to the best of our knowledge, no work has yet investigated the EIE of hydrosulfide (HS^-) binding in this or other systems. HS^- is a highly reactive anion that plays crucial roles in biology. At physiological pH, HS^- is favored in solution by a 3:1 ratio over its conjugate acid, hydrogen sulfide (H_2S). H_2S has been identified as the third physiological gasotransmitter alongside CO and NO and plays essential roles in physiological systems.⁹ Despite its high nucleophilicity and reducing potential, HS^- has been observed to be bound through non-covalent interactions in the protein crystal structure of a bacterial ion channel¹²¹ and in the turn-over state of vanadium-containing nitrogenase.¹²² The

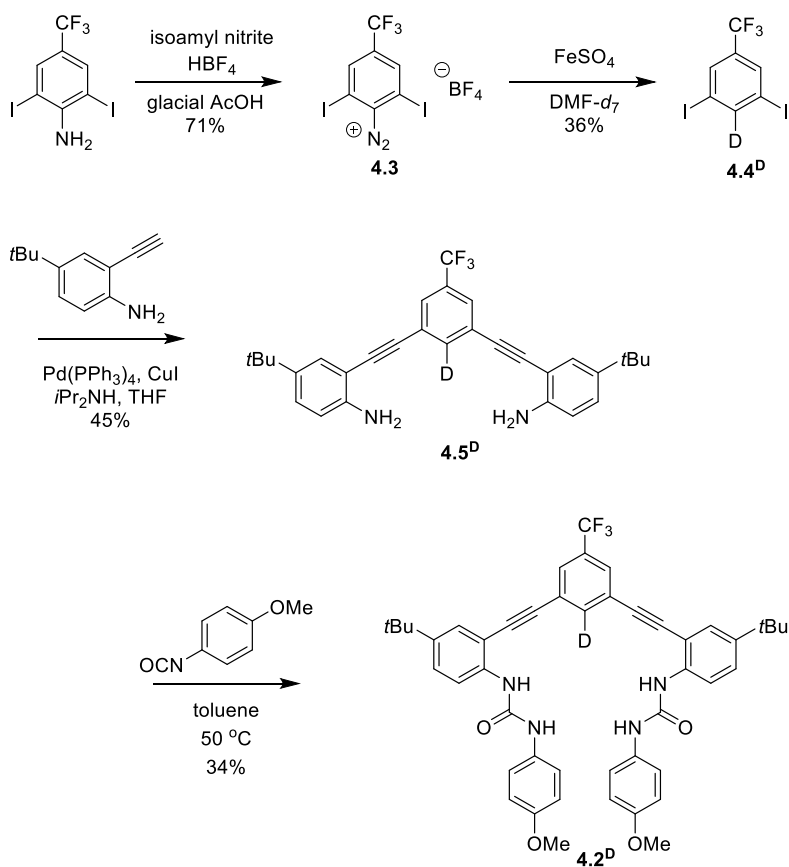
supramolecular chemistry of HS^- is under-studied in synthetic supramolecular receptors, likely due to the inherent high reactivity of HS^- . Indeed, we are aware of only three families of receptors that have been shown to reversibly bind HS^- .^{29,31,32,36}

Recently, we used a series of arylethynyl bisurea anion receptors to investigate and demonstrate a linear free energy relationship between the polarity of a non-traditional C–H hydrogen bond donor and the solution binding energy of HS^- , HSe^- , Cl^- , and Br^- .³⁶ A major and unexpected finding of this study was that HS^- demonstrated a significant increase in sensitivity towards the polarity of the C–H hydrogen donor over HSe^- , Cl^- , and Br^- . Although increasing the polarity of the C–H hydrogen bond donor did not lead to changes in selectivity between HSe^- , Cl^- , and Br^- , we observed a 9-fold increase in selectivity for HS^- over Cl^- , suggesting a fresh approach to selective HS^- recognition using non-covalent interactions. In this current study, we label the C–H hydrogen bond donor in an arylethynyl bisurea receptor with a deuterium atom (**4.2^{H/D}**, Figure 4.1) to further investigate this apparent preference of polar C–H hydrogen bond donors for HS^- over Cl^- and Br^- through DEIE.

4.2 Methods

Receptor **4.2^H** is a previously reported anion receptor for HS^- , Cl^- , and Br^- and was prepared by established methods.³⁶ Deuterium labelling of the isotopologue **4.2^D** was achieved by selective monodeuteration of intermediates through methods similar to those reported in the literature (Scheme 4.1).¹³⁵ The diazonium salt **4.3** was synthesized in a 71% yield from 2,6-diiodo-4-trifluoromethylaniline.¹³⁶ Dediazonation in $\text{DMF-}d_7$ is catalyzed by FeSO_4 and allows for selective synthesis of monodeuterated intermediate

4.4^D. The deuteration step proceeds through a radical pathway that uses DMF-*d*₇ as the deuterium source. This deuteration reaction provides efficient deuterium incorporation even with up to 50% by volume H₂O in the reaction solution due to the differential bond strengths in DMF and H₂O.¹³⁵ Sonogashira cross-coupling reaction of **4.4^D** and 4-*t*-butyl-2-ethynylaniline¹³⁷ afforded **4.5^D** in 45% yield. Subsequent addition with 4-methoxyphenyl isocyanate gave **4.2^D** in 34% yield. Compound **4.2^D** and intermediates were characterized through ¹H, ²H, ¹³C{¹H}, and ¹⁹F NMR spectroscopy and high-resolution mass spectrometry (see Appendix C).



Scheme 4.1. Synthetic route for the selective deuteration of anion receptor **4.2^D**.

Previous work on the DEIE of Cl⁻ binding with **4.1^{H/D}** in DMSO revealed an experimental isotope effect of 1.019 ± 0.010. Therefore, we expected similar small DEIEs for HS⁻, Cl⁻, and Br⁻ binding with **4.2^{H/D}**. Typical methods to determine binding constants (K_a) in supramolecular systems use non-linear regression fitting of titration data. Results from this method can be affected by small errors in the known initial host and guest concentration, quality of the titration isotherm, and subsequent data fitting, which when taken together often results in 2-15% errors in K_a . To increase the precision in K_a^H/K_a^D data for this study, we used the Perrin method of competitive titrations,¹³⁸ which has been shown previously to reduce errors in EIE values significantly with errors as small as 0.0004.¹³⁹ In this method, a linearized plot of the chemical shifts of **4.2^H** (δ_H) and **4.2^D** (δ_D) in fast exchange with an anionic guest is fit by linear regression to Equation 4.1. The slope of the linear regression is equal to the DEIE of the system. Because the linear regression only relies on chemical shift values and is independent of host and guest concentration, the precision of the method is limited to the precision of the NMR instrument and quality of data fitting.

$$(\delta_H^0 - \delta_H)(\delta_D - \delta_D^f) = DEIE(\delta_D^0 - \delta_D)(\delta_H - \delta_H^f) \quad (4.1)$$

In addition, ¹³C NMR spectroscopy is sensitive to isotopic labelling and can show changes in chemical shifts between isotopomers. We were able to differentiate between the ¹³C NMR signals for C^{ab}, C¹, and C² for free and bound **4.2^H** and **4.2^D** (Figure 4.2a) in 10% DMSO-*d*₆/CD₃CN, which were similar to those reported for **4.1^{H/D}** in DMSO.²⁸ Competitive ¹³C NMR spectroscopy titrations were performed in anaerobic and anhydrous 10% DMSO-*d*₆/CD₃CN at 25 °C with mixtures of **4.2^H** and **4.2^D** in combined concentrations between 5.71 and 13.46 mM. Aliquots of the tetrabutylammonium (TBA)

salts of HS^- , Cl^- , and Br^- were added until the system had reached saturation (Titration Method A, Appendix C). In an effort to decrease reactivity of HS^- with $\mathbf{4.2^{H/D}}$ and DMSO over long periods of time and decrease oxygen and water contaminations, some titrations with HS^- were performed by splitting the host solution of $\mathbf{4.2^{H/D}}$ between four J-young NMR tubes. For each point in the competitive titration, TBASH was added to a new solution of $\mathbf{4.2^{H/D}}$ inside an N_2 -glovebox shortly before obtaining a ^{13}C NMR spectra (Titration Method B, Appendix C). The C^{ab} , C^1 , and C^2 ^{13}C NMR signals were tracked for $\mathbf{4.2^H}$ and $\mathbf{4.2^D}$ in each titration for each anion. A representative competitive titration and linearized plots for Cl^- binding is shown in Figure 4.2.

4.3 Results and Discussion

The DEIE calculated from tracking the chemical shifts of the C^{ab} , C^1 , and C^2 ^{13}C NMR signals from Cl^- and Br^- binding are summarized in Table 4.1. The results shown are an average of three trials. Analysis of the data for competitive titrations of $\mathbf{4.2^{H/D}}$ with Cl^- reveals a normal DEIE of 1.014 ± 0.002 , calculated from monitoring the C^2 ^{13}C NMR signal. The C^{ab} and C^1 ^{13}C NMR signals have the largest percent error in the calculated DEIE and show no statistically significant DEIE (i.e., $\text{DEIE} = 1$) for Cl^- binding; however, because there is only one DEIE in the system, these positions must not be sensitive enough to the vibrational energy of the C–H/D bond in the free host and the host-guest complex to reveal the normal DEIE.

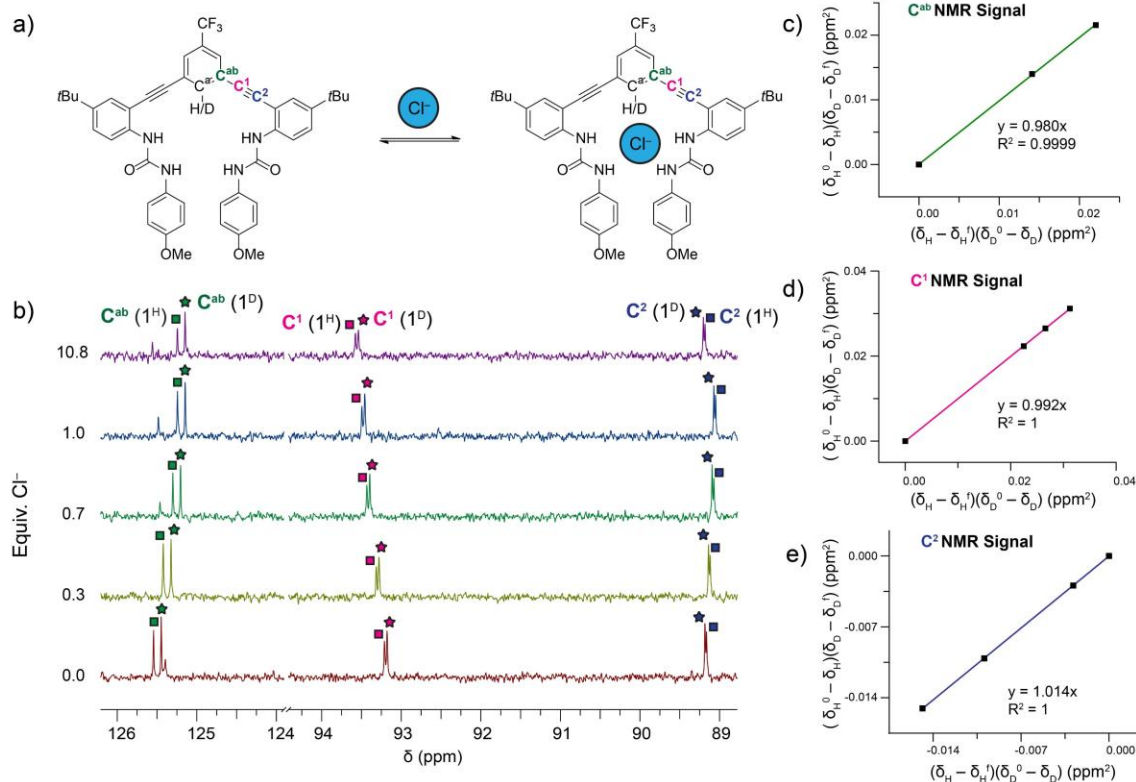


Figure 4.2. Representation of the host-guest equilibrium between $4.2^{H/D}$ and Cl^- . Differences in the chemical shifts between the 4.2^H and 4.2^D isotopologues are observed in the ^{13}C NMR signals for the C^{ab} , C^1 , and C^2 carbons. b) ^{13}C NMR signals for the C^{ab} , C^1 , and C^2 carbons in 4.2^H and 4.2^D are tracked throughout a titration. c-e) Linearized plots from fitting the chemical shifts of the C^{ab} , C^1 , and C^2 throughout a titration to Equation 4.1.

Table 4.1. Calculated DEIE for Cl^- and Br^- binding. Goodness of fit (R^2) of the titration data to Equation 4.1 through linear regression is included in parentheses.

^{13}C NMR Signal	DEIE (R^2)	
	Cl^-	Br^-
C^{ab}	0.983 ± 0.017 (0.997)	1.006 ± 0.010 (0.999)
C^1	1.006 ± 0.007 (0.999)	1.009 ± 0.018 (0.997)
C^2	1.014 ± 0.002 (1.00)	0.990 ± 0.046 (0.981)

Notably, our experimental DEIE value for Cl^- binding with $4.2^{H/D}$ in 10% DMSO- d_6/CD_3CN is smaller than the computed value of 1.020 for Cl^- binding with $4.1^{H/D}$ in DMSO- d_6 .²⁸ Our previously published computational study revealed that the DEIE of Cl^- binding resulted from distorted urea $N-H \cdots Cl^-$ hydrogen bonding geometry affecting the

vibrational frequency of the C–H/D bond in the host-guest complex. Replacing the NO₂ functional group in **4.1^{H/D}** ($\sigma_p = 0.78$) with a CF₃ functional group ($\sigma_p = 0.54$) in **4.2^{H/D}** decreases the polarization of the C–H/D bond and subsequently makes it a slightly poorer hydrogen bond donor. In addition, the DEIE of Cl[−] binding in this current study is in a less polar solvent system (10% DMSO/CH₃CN, $\epsilon \sim 42$) compared to the previous study (DMSO, $\epsilon = 47$). We hypothesize that the decreased polarization of the C–H/D bond and the lower solvent polarity either relieve the distorted N–H \cdots Cl[−] hydrogen bonding geometry or decreases its influence on the vibrational frequency of the C–H/D bond in the host-guest complex. To deconvolute and better understand the role of both C–H/D hydrogen bond donor polarity and solvent on the DEIE of Cl[−] binding in these receptors, a systematic study of these two variables would be required, similar to those previously reported.^{25,27,36}

Analysis of the data for competitive titrations of **4.2^{H/D}** with Br[−] revealed no DEIE at any of the tracked ¹³C NMR signals; however, each calculated DEIE has a relatively large percent error (0.99 – 4.64%, compared to 0.20% for the DEIE of Cl[−] binding), which could potentially obscure small DEIEs. We attribute these large percent errors to a limitation in the Perrin method that assumes that the hosts are fully bound by guest at saturation. This limitation can potentially decrease the precision of this method for weakly bound guests with low K_a , such as Br[−] which has a K_a of 173 ± 9 with **4.2^H** in 10% DMSO-*d*₆/CD₃CN at 25 °C.³⁶

Using the combined data from 11 experiments, we were unable to determine the DEIE for HS[−] binding. The C¹ ¹³C NMR signal appeared to be the most sensitive to the change in vibrational energy of the C–H/D bond in the free host and the host-guest

complex; however, in over half these trials, data from the C¹ ¹³C NMR signal showed a poor linear fit ($R^2 < 0.99$). In addition, we were unable to triplicate any DEIE from the data which showed a good linear fit ($R^2 > 0.99$). We hypothesize that the high nucleophilicity and air and water sensitivity of HS⁻ made it incompatible with the long experiment times needed for ¹³C NMR spectroscopy titrations. In addition, HS⁻ is the only protic guest investigated in these studies, and it is also possible that vibrational coupling between the S–H motif and the receptor may further complicate the measurement of these small EIEs. Such coupling between S–H and other motifs has been implicated previously in the IR inactivity of S–H stretching modes in many metal-sulfhydryl complexes.¹⁴⁰

4.4 Conclusion

Deuterium equilibrium isotope effects (DEIE) can be used to elucidate non-covalent driving forces behind anion binding in our arylolethynyl bisurea receptors. We endeavored to use DEIE studies to further investigate a preference of polarized C–H hydrogen bond donors for HS⁻ over Cl⁻ and Br⁻ which we reported previously.³⁶ In this current work, we highlight a convenient method to selectively and completely deuterate the aryl C–H hydrogen bond donor in our supramolecular anion receptors. We then found a DEIE of 1.014 ± 0.002 for Cl⁻ binding with **4.2**^{H/D}. This DEIE was smaller than the computed DEIE of Cl⁻ binding with **4.1**^{H/D} which features a more polarized C–H hydrogen bond donor and in a more polar solvent. Finally, we reveal challenges in using the Perrin method and ¹³C NMR spectroscopy titrations in determining small and precise EIE for weakly binding or highly reactive guests.

From this work, we have highlighted several areas that need further research. The first is to study how solvent and hydrogen bond donor polarity affect EIE of guest binding. A computational study from Paneth and coworkers suggest that both these variables can be used to influence $^{35/37}\text{Cl}$ EIE in supramolecular hosts.¹³⁴ We also were unable to determine a DEIE of HS^- binding in our receptors, likely due to its high reactivity. A new method to determine small, precise EIE of reactive species such as HS^- is needed in order to learn more about the supramolecular chemistry of this biologically relevant anion.

CHAPTER V

C–H···S HYDROGEN BONDING INTERACTIONS

This chapter includes unpublished and co-authored material. This manuscript was written by Hazel A. Fargher and Dr. Tobias J. Sherbow with editorial support from Professors Michael M. Haley, Darren W. Johnson, and Michael D. Pluth. The project in this chapter was developed by Hazel A. Fargher, Dr. Tobias J. Sherbow, and Professor Michael D. Pluth. Data collection and analysis was performed by Hazel A. Fargher and Dr. Tobias J. Sherbow.

5.1 Introduction

The past century has provided significant advances in understanding chemical bonding. Works such as “The Nature of the Chemical Bond” from Linus Pauling have detailed covalency through valence bond theory.¹⁴¹ More recently, “The Nature of the Mechanical Bond” expanded bonding ideas to include threaded supramolecular assemblies and molecular machines.¹⁴² We understand that non-covalent interactions play crucial roles in both small molecule and macromolecular structure, ranging from the impact of hydrogen bonding and π -stacking interactions in DNA to the London dispersion forces that stabilize sterically crowded inorganic and organometallic compounds.¹⁴³ While we continue to learn about these phenomena and their effects on contemporary chemical systems, we also understand that certain non-covalent interactions may have been overlooked and are just now being realized for their potential.^{144–146}

Hydrogen bonding (HB) interactions are among the strongest, most directional, and most dynamic of the many reversible, weak, primarily non-covalent interactions.

These are especially important interactions because without HB, terrestrial life would not exist. The HB is responsible for the increased density of frozen water, the folding of proteins, and the self-complementarity of nucleic acids. A HB must feature both an attractive interaction and evidence of bond formation between a hydrogen atom bonded to a donor (D), which is more electronegative than the hydrogen, and a HB acceptor (A).^{147–149} Parameters that are often measured in HB systems include the H···A (L1) and D···A (L2) distances, and the D–H···A (A1) and R–A···H (A2) bond angles. Generally, shorter L1 distances and A2 angles approaching 180° contribute to stronger HB interactions (Figure 5.1).

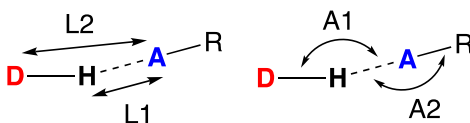


Figure 5.1. Bond lengths and bond angles often measured in HB systems and will be described throughout the text.

Hydrogen bonding interactions are derived from a mixture of attractive and repulsive forces that include electrostatics, polarization, charge transfer, dispersion, and exchange repulsion.¹⁴⁹ Electrostatic forces are typically the largest contributing force in a HB and are directional based on the electrostatic potential of the D–H and A atoms. Electrostatic interactions can be enhanced by increasing partial charges on the donor and acceptor atoms, and therefore can be easily modified through functionalization. The strength of electrostatic interactions diminishes the slowest of all the attractive forces with increasing H···A distances. Polarization relates to the ability of the HB acceptor to reorganize electron density to better participate in hydrogen bonding. Charge transfer

forces are caused by the overlap of a filled lone pair orbital on the HB Acceptor with the empty D–H antibonding orbital. These forces require high linearity and diminish greatly with deviation from optimal HB geometry and with increasing distance. Finally, dispersion and exchange repulsion forces are often referred together as van der Waals forces, which when combined can be approximated by the Lennard-Jones potential.¹⁵⁰ These forces are isotropic and generally weak, which often makes them primary contributors to non-linear hydrogen bonds.

5.1.1 C–H hydrogen bond donors

Studies surrounding the large field of hydrogen bonding are generally focused on traditional, strong hydrogen bonds, which are typically found between a highly electronegative HB donor, such as oxygen or nitrogen, and an electronegative HB acceptor. These strong interactions tend to be short and highly linear, with the D–H⋯A bond angle between 170 and 180°. The strength of these HB is generally measured by the distance between the hydrogen and acceptor atom in the solid state; however, spectroscopic techniques, such as ¹H NMR and vibrational spectroscopy, can also be used to characterize hydrogen bonds. With this emphasis on strong hydrogen bonds, weaker HB—which rely on a mixture of electrostatic, polarization, and Van der Waals forces—have historically been overlooked. For example, despite the moderate electronegativity of carbon, C–H motifs have emerged as a newly recognized class of HB donors.^{85,107,114,116,151} Early pK_a measurements of substituted benzoic acids showed an increased acidity of *ortho*-toluic acid in comparison to the *para* structural isomer, which was postulated to be due to a C–H⋯O intramolecular interaction between the methyl

group and the carboxylate to stabilize the conjugate base (Figure 5.2).¹⁵² With many additional examples, including extensive theoretical calculations, of C–H···O HB interactions demonstrated since this initial observation, it is now widely accepted that C–H···O interactions can be classified as a hydrogen bond.¹⁵³ This classification has been expanded to include C–H···O, C–H···N, C–H···Cl, and C–H···Br HB interactions and has been well established in molecular biology,¹⁵⁴ organocatalysis,^{155,156} and molecular recognition.^{157,158} In fact, recent studies indicate C–H HB acidities follow predictable linear free energy relationships (LFER) and show modest isotope effects.^{27,28}

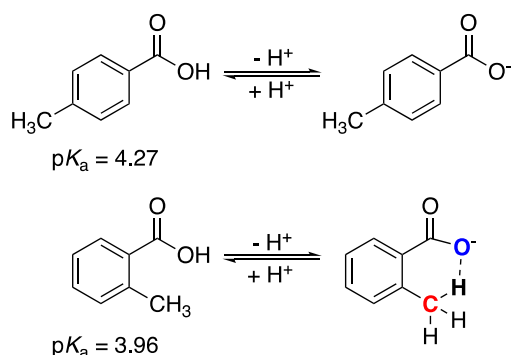


Figure 5.2. Absence and presence of C–H HB in *p*-toluic acid and *o*-toluic acid, respectively.

5.1.2 C–H···S hydrogen bonding

Simply moving one row down the periodic table, however, we find that C–H···S HB interactions are underappreciated. Studies of S-based HB acceptors generally focus on N–H, O–H, and other more traditional HB donors, with little investigation of C–H···S HB.^{159–162} We find this omission surprising, as both work from our labs and others has shown that C–H HB donors exhibit a specific preference for sulfur-based HB acceptors.^{36,106,108} In our work in supramolecular anion recognition, we were inspired to

investigate C–H HB donors for binding hydrosulfide (HS^-) after successful application of these receptors for Cl^- binding.²⁶ In 2016 we published an archetypal example of supramolecular receptors for HS^- . Using ^1H NMR spectroscopy titrations and single crystal X-ray diffraction structural analysis of the host-guest complex, we showed that an aryl C–H functional group in the binding pocket participated in hydrogen bonding with HS^- and Cl^- (Figures 5.3a-5.3b).²⁹ In 2019 we found that even when the aryl C–H bond was depolarized by an electron donating *t*-Bu functional group (Figure 5.3c), it still participated in hydrogen bonding with HS^- , HSe^- , Cl^- , and Br^- .³⁵ This finding inspired a subsequent LFER investigation, in which we studied how modulating the polarity of the aryl C–H HB donor affected the anion-binding strength of HS^- , HSe^- , Cl^- , and Br^- .³⁶ We found that our hosts displayed a preference for HS^- over the other three anions, which increased with increasing polarization of the C–H HB donor. In fact, HS^- was significantly more sensitive towards changing C–H HB donor polarity than the other three anions, which suggests a distinct sensitivity to C–H hydrogen bonding to the sulfur-containing guest. The only other two supramolecular hosts for HS^- ,^{31,32} both published in 2018, also use C–H HB donors (Figure 5.4) in the anion binding pocket, which further supports the idea that polarized C–H HB donors may be particularly important in HS^- recognition.

Recent work from our laboratory has also studied how reactive sulfur species (RSS) interact with metal-sulfur containing bonds which lead to the further isolation of compounds containing short C–H \cdots S stabilizing contacts. The reactivity of a molybdenum tetrasulfido complex, $[\text{NBu}_4][\text{TpMoS}(\text{S}_4)]$ (Tp = hydrotris(3,5-dimethylpyrazol-1-yl)borate), was studied with HS^- and we found that HS^- is oxidized to

form polysulfides and a *tris*(sulfido) Mo complex [NBu₄][TpMoS₃] byproduct.¹⁶³ Upon further inspection of the molecular structure of the [NBu₄][TpMoS₃] byproduct, we found that the Mo=S bond lengths vary by up to 0.019 Å and that the longest Mo=S moieties displayed C–H⋯S contacts as short as 2.681 Å to the [NBu₄]⁺ counterion. Further evidence of a HB interaction was confirmed by comparing the ¹H NMR spectroscopic resonances of the [NBu₄]⁺ in the starting [NBu₄][TpMoS(S₄)] complex, in which short C–H⋯S contacts were not observed, to the ¹H NMR resonances of the [NBu₄]⁺ in the [NBu₄][TpMoS₃] byproduct, where shifts of up to 0.65 ppm were observed for [NBu₄]⁺ resonances. As described later in this manuscript, there are numerous examples of C–H⋯S–M contacts with sulfur-metal bound species, and many of these may help to stabilize reactive species and promote reactivity in catalysis and enzymatic systems.

Additional evidence for C–H⋯S HB interactions is supported by a recent study by Wategaonkar and coworkers using both gas-phase vibrational spectroscopy and *ab initio* quantum chemical calculations.¹⁶⁴ Despite the weak nature of both the HB donor and acceptor, C–H⋯S interactions exhibited all the characteristics of a conventional hydrogen bond, and even displayed binding strengths comparable to more traditional HB in their system. Although S is a less electronegative element than other traditional HB acceptors, S is large and polarizable, allowing it to better participate in dispersion interactions. Indeed, using natural energy decomposition analysis calculations, they found that dispersion was the dominant hydrogen bonding force in all the C–H⋯S interactions in their system.¹⁶⁴ Importantly, because dispersion is an isotropic component of hydrogen bonding, it is possible that C–H⋯S HB in the solid state that deviate from linearity are commonly overlooked.

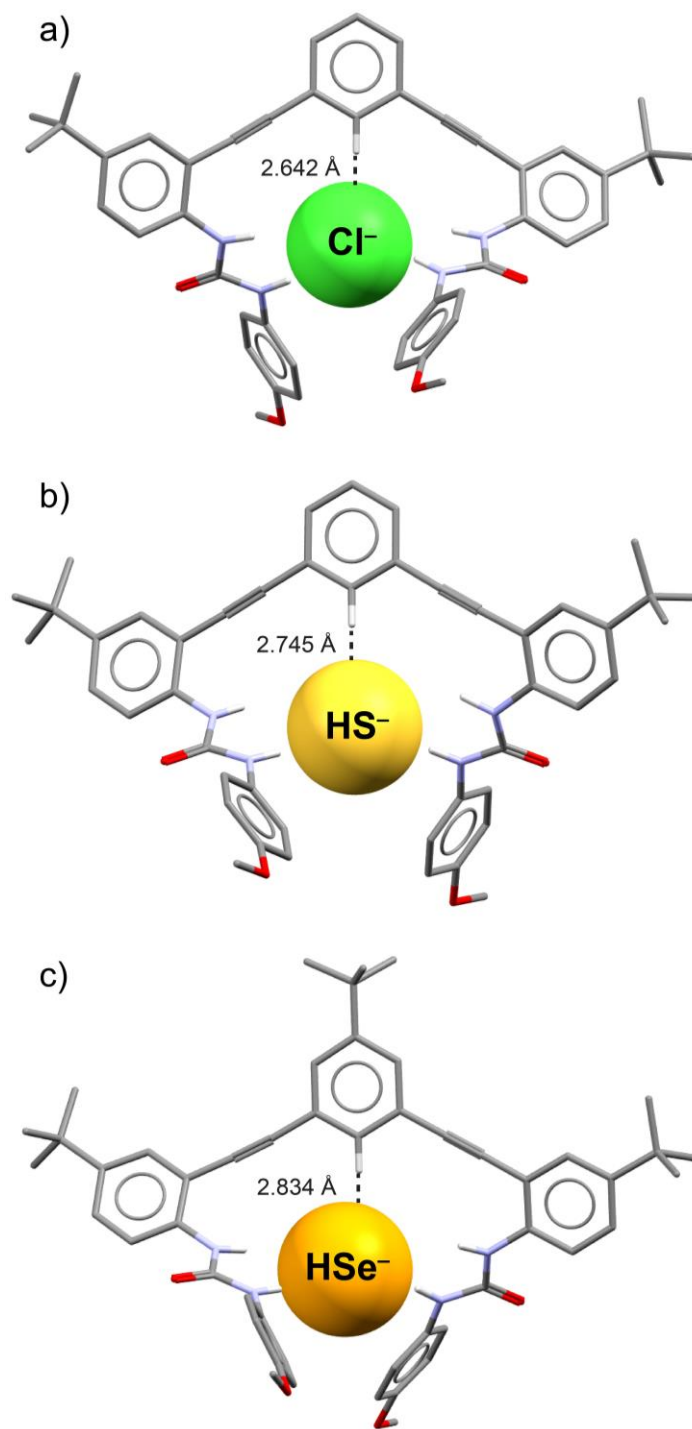


Figure 5.3. Crystal structures of arylethynyl bisurea receptors shown to bind (a) Cl^- , (b) HS^- , and (c) HSe^- in the solid state. All three anions interact with the aryl C–H HB donor on the central ring.

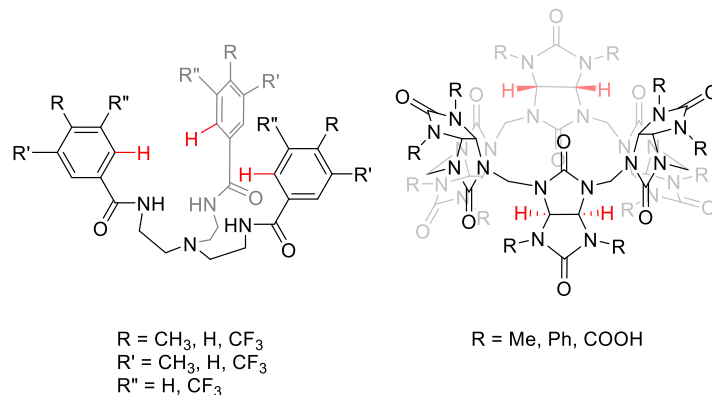


Figure 5.4. The other two supramolecular hosts that have been shown to reversibly bind HS^- . Both hosts feature C–H HB donors in their design (highlighted in red).

More broadly, other researchers have specifically commented on the consequential roles of C–H \cdots S interactions in enzymatic binding pockets. For example, work by Addlagatta and coworkers studying the substrate specificity and catalytic cycle of type 1 methionine aminopeptidase, an enzyme responsible for cleaving methionine from around 70% of proteins in living cells, identified a key C–H HB donor that had been evolutionarily preserved in the enzyme.⁸⁴ The authors showed that a hydrogen bond between a S HB acceptor in cysteine and a C–H HB donor in methionine was responsible for the substrate specificity and efficiency in the catalytic cycle. As part of this work, a search of the Protein Databank (PDB) found 20 other instances of C–H \cdots S contacts with a maximum distance of 4 Å between methionine and methionine analog C–H HB donors in ligands and S cysteine and methionine HB acceptors. Only a few of the 20 instances were from methionine aminopeptidase enzymes, which suggests a broader generality of this interaction among other types of enzymes.

In general, attractive non-covalent interactions with S may be more important than has been previously appreciated. For example, in a review by Meanwell and coworkers¹⁴⁶ that focused on the role of the S σ -hole in S \cdots O, S \cdots N, and S \cdots π interactions

in medicinal and organic chemistry, the authors point out that “because the role of noncovalent interactions involving sulfur in compound conformation and ligand-protein interactions may be underappreciated, this phenomenon may have been overlooked in many drug design campaigns”. Similarly, other research on more electron-rich sulfur species has revealed that $S \cdots \pi$ and $S-H \cdots \pi$ interactions may be particularly important stabilizing forces in both biological and synthetic systems.¹⁶⁵

5.1.3 Scope of review

Inspired by these prior examples pointing to an increased potential importance of non-covalent interactions, our work here advances our understanding of $C-H \cdots S$ interactions by analyzing existing data on $C-H \cdots S$ interactions across multiple disciplines. Using the CSD, we interrogate these short $C-H \cdots S$ contacts and we have grouped these interactions into different categories: 1) the S atom coordination number, 2) the types of $C-H$ HB donors, and 3) its varying oxidation state. We then also compare $C-H \cdots S$ interactions when S is bound to an organic molecule or a metal. We present the analysis of these results using 3D histograms and compare these interactions to other established HB acceptors to further cement that $C-H \cdots S$ interactions should not be neglected. Lastly, we provide examples from our own work as well as others that contain previously overlooked $C-H \cdots S$ interactions that may have influenced reactivity and the stabilization of unusual conformations in the solid state. In this process, we demonstrate that these underappreciated interactions are found in molecular biology, catalysis, and supramolecular systems, and may even be a privileged interaction providing stronger and more selective HB in the overall molecular architecture. More broadly, this work shows

that non-traditional hydrogen bonding, such as C–H \cdots S HB interactions, should not be overlooked and instead should be considered in the further development of research where non-covalent interactions are used to direct reactivity and/or enhance stability.

5.2 Results and Discussion

5.2.1 Organic molecules with sulfur hydrogen bond acceptors.

C–H \cdots S HB have higher dispersion character than more traditional HB motifs, therefore these C–H \cdots S contacts likely have different angle and distance preferences. To better understand these angle and distance HB metrics, we used available solid-state structural information from the CSD to find all C–H \cdots S contacts with organic based S HB acceptors. Contacts used in this study were restrained to only include instances where the C–H \cdots S (Figure 5.1, A1) and H \cdots S---R (Figure 5.1, A2) angles fell between 90–180° and H \cdots S (Figure 5.1, L1) and C \cdots S (Figure 5.1, L1) bond lengths fell between 0–4.0 Å and 0–5.0 Å, respectively. These L1 and A1 parameters provide search parameters that encompass a wide array of contacts including weaker interactions, in which A1 is closer to 90° and L1 distances are longer, as well as stronger interactions, in which A1 is more linear and L1 distances are shorter. The L2 and A2 parameters are also incorporated to filter out longer contacts and angles that would not be considered hydrogen bonding interactions.

To visualize the >423,000 C–H \cdots S contacts from this dataset we plotted a 3D histogram of H \cdots S distance (Å) versus C–H \cdots S bond angle (°) (Figure 5.5a). The plot reveals that the majority of C–H \cdots S contacts are not linear. The most common H \cdots S contact is found between 3.125–3.250 Å and 121.5–126.0°, which encompasses 6,615

contacts. Any hydrogen bonding occurring at this contact angle and distance would likely be classified as a weak interaction due to the primary attractive forces being entirely electrostatic and dispersion type interactions. These contacts can be significant, however, because numerous weak inter- and intramolecular forces are additive and can greatly affect the physical and chemical properties of an overall system.^{166,ii}

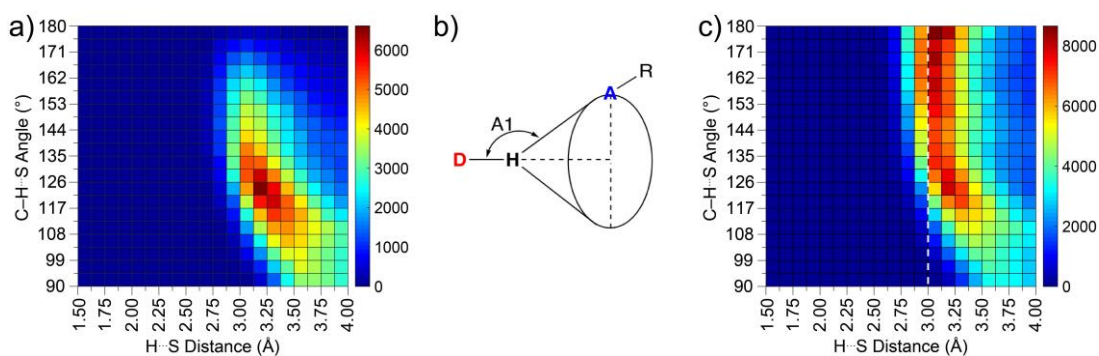


Figure 5.5. a) 3D histogram visualizing over 423,000 C–H···S contacts identified in the CSD. b) Cone angle of hydrogen bonding. c) Cone-corrected 3D histogram of all C–H···S contacts. The white dashed line represents estimate of the sum of the van der Waal radii of H and S.

Although a 3D histogram can provide useful information about the most common interaction geometry in the solid state, the low angle contacts are statistically favored due to the HB “cone-angle” (Figure 5.5b), which biases interpretations of the 3D histogram. This phenomenon has previously been shown to skew 2D histograms of contact angles of traditional O–H HB systems away from linearity.⁷⁴ This statistical bias toward low-angles can be removed by applying a simple cone-angle correction that weights each bin of the

ⁱⁱ For example, the presence of multiple low-angle C–H···S HB were shown to significantly affect the overall structure and host-guest ability in perthio-bambusuril macrocycles. Unlike bambus[6]urils, which bind anions through C–H···anion HB inside a macrocycle cavity, Reany and coworkers showed that perthio-bambus[6]urils did not exhibit any significant anion binding ability due to several low-angle C–H···S interactions that led to a compact structure and weakened the anion binding ability of the macrocycle. See reference 166 for more details.

histogram by $1/\sin(\theta)$, where θ is the C–H \cdots S contact angle. The resultant cone-corrected data reveals the relative importance and preferred geometry of high-angle contacts in the solid state (Figure 5.5c).¹⁶⁷

The cone-corrected 3D histogram displays a clear geometric preference of C–H \cdots S contacts. Many of the contacts fall below the sum of the van der Waal radii of H and S ($r_w^H + r_w^S$, shown as a white dashed line in Figure 5.5c). At these shortest distances ($< 3.00 \text{ \AA}$), high-angle contacts are favored, revealing an attractive interaction promoting linear contacts. Even at distances greater than the sum of the van der Waals radii, the C–H \cdots S contacts show strong geometric preferences. For example, there is a preference for linear contacts between $3.00\text{--}3.125 \text{ \AA}$, and as the distance increases ($3.125\text{--}3.625 \text{ \AA}$) the low-angle contacts become equally or more important than high-angle (linear) contacts. Finally, at longer distances ($3.625\text{--}4.00 \text{ \AA}$) the angle dependence decreases, and it is less likely that strong, directional hydrogen bonding occurs at these distances; instead, we see more random, geometrically- and statistically-driven contacts, more reminiscent of interactions dominated by dispersion interactions.^{168,169}

As an example of such C–H \cdots S interactions impacting structural outcomes, we have re-assessed work from our own group and have identified previously overlooked C–H \cdots S contacts that likely contribute to the observed solid-state packing. In 2016 we isolated a crystal of a novel tetrameric disulfide cyclophane (Figure 5.6), which surprisingly was found to fold in on itself and form several strained C–S–S–C torsional angles rather than bind a smaller solvent or guest molecule.¹⁷⁰ Reanalysis of this structure revealed a very short, linear intramolecular C–H \cdots S contact (2.810 \AA , 170.4° , highlighted in Figure 5.6), which may contribute to the stabilization of the more compact structure.

Further analysis also identified three additional intramolecular C–H \cdots S contacts with longer H \cdots S distances of 3.682–3.935 Å. These distances, however, fall within the region of the weighted histogram that shows little contact angle preference, and so are likely not forming a HB. Finally, we identified 27 intermolecular contacts with C–H \cdots S angles ranging between 100.8 and 174.9° and H \cdots S distances ranging between 2.811 and 3.890 Å, some of which may have directed and stabilized the overall compact packing of the macrocycle in the solid state.

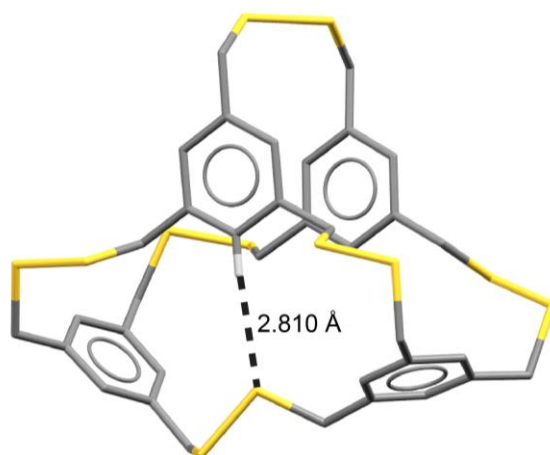


Figure 5.6. A relatively short and linear C–H \cdots S contact in a disulfide cyclophane may help stabilize strained torsional angles.

5.2.1.1 S HB acceptors with traditional HB donors

Comparing the cone-corrected 3D histograms of S contacts with traditional N–H (Figure 5.7a) and O–H (Figure 5.7b) donors displayed different interaction profiles. C–H HB donors show flexible geometric preference for either high-angle or low-angle contacts and support a wide range of H \cdots S distances, whereas weighted contacts with N–H and O–H HB donors are only found in a narrow geometric window. These traditional N–H and O–H HB donors prefer to only make short and linear contacts with

few examples in the CSD showing deviations from this idealized geometry. These data suggest that the hydrogen bonding interaction between sulfur and traditional N–H and O–H HB donors is generally stronger than with C–H hydrogen bond donors and likely have more charge-transfer character at these short distances and linear contact angles. However, C–H \cdots S interactions, which have more dispersion character, can out-perform N–H and O–H HB donors at long distances and more bent contact angles.

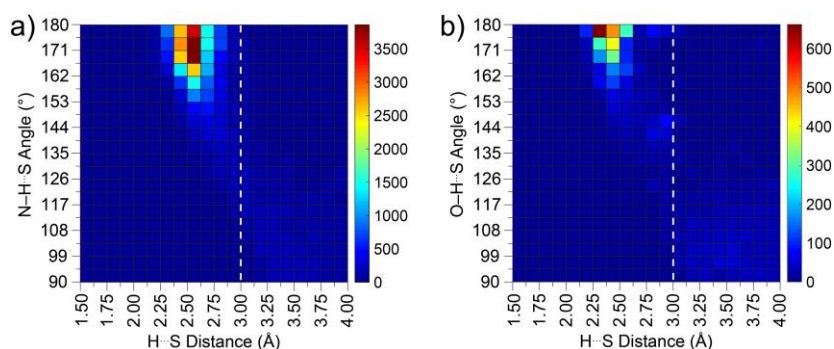


Figure 5.7. 3D histogram of (a) N–H and b) O–H hydrogen bond donors with S.

5.2.1.2 Comparing hydrogen bond acceptors

We also analyzed the C–H \cdots S contacts with other HB acceptors from neighboring elements on the periodic table (N, O, F, P, Cl, Se, Br, Te, I) (Figure 5.8). Oxygen had the greatest number of inter- and intramolecular contacts (>7,898,000), followed by F (>3,540,000), Cl (>1,338,000), and N (>1,082,000), perhaps suggesting that the acceptance of C–H HB with O, Cl, and N may be in part due to their ubiquity in the solid state. Comparison of the resultant histograms shows that the flexible contact angle geometry of the C–H HB donor is conserved. In addition, almost all C–H \cdots A contacts occur at distances greater than 2.2 Å, which is significant because contacts greater than this distance have generally been defined as weak HB with mostly electrostatic and dispersion

character by Jeffrey¹⁷¹ and later Steiner.⁷⁴ Although these data do not allow for determination of the absolute strength of these interactions, we used distances and contact angles inspired by Jeffrey and Steiner to broadly categorize ‘strong’, ‘moderate’, and ‘weak’ C–H···A interactions (Table 5.1). C–H···A contacts that fall in the region of the cone corrected 3D histogram that shows little preference for either high- or low-angle contacts are likely not being driven by significant attractive interactions.

Table 5.1. Parameters used to broadly categorize C-H HB as strong, moderate, and weak. Distance and angle ranges are inspired by analyses of hydrogen bonding in the solid state by Jeffrey and Steiner.^{74,171}

	Strong	Moderate	Weak
H···A Distance	$\leq r_w^H + r_w^A$	$> r_w^H + r_w^A$	$> r_w^H + r_w^A$
C–H···A Angle (°)	> 130	> 130	> 90

The second-row elements N, O, and F are among the smallest, least polarizable, and most electronegative atoms (Figure 5.8a-c). In their weighted 3D histograms, these elements make the highest proportion of strong HB contacts. This driving force toward short contacts, however, makes these elements poor C–H HB acceptors at longer distances. An example of this point is highlighted in work studying *cis/trans* isomerization in amide and thioamide containing peptoids.¹⁷² The authors found that a C–H···S interaction in the thioamide derivative caused a greater preference for the *cis* conformer than was observed in the amide derivative. A crystal structure of the thioamide showed that the key intramolecular C–H···S HB had a bond length of 2.9 Å (Figure 5.9), which could be considered a strong C–H···S HB but is much longer than most C–H···O interactions. Despite generally being a weaker HB acceptor than O, the S-containing thioamide formed a strong HB over the greater distance whereas the O-containing amide

could not. This observation is further reflected by work from the Shimizu group, which shows that S- π interactions are more favorable than O- π interactions at long distances.¹⁶⁵

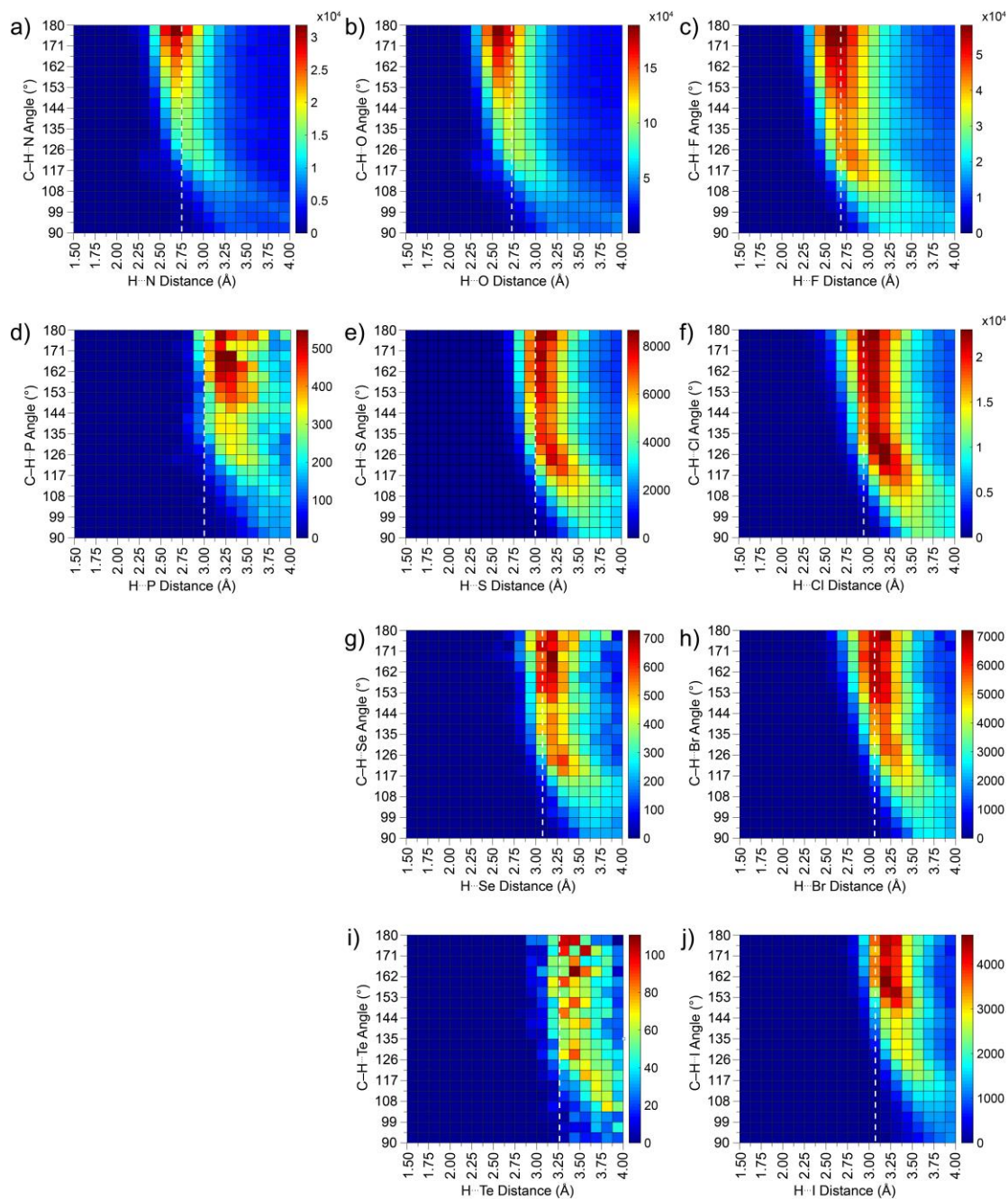


Figure 5.8. Cone-corrected 3D histograms of C-H...A contacts found in the CSD with a) N, b) O, c) F, d) P, e) S, f) Cl, g) Se, h) Br, i) Te, and j) I. White dashed line represents estimate of the sum of the van der Waal radii of H and A.

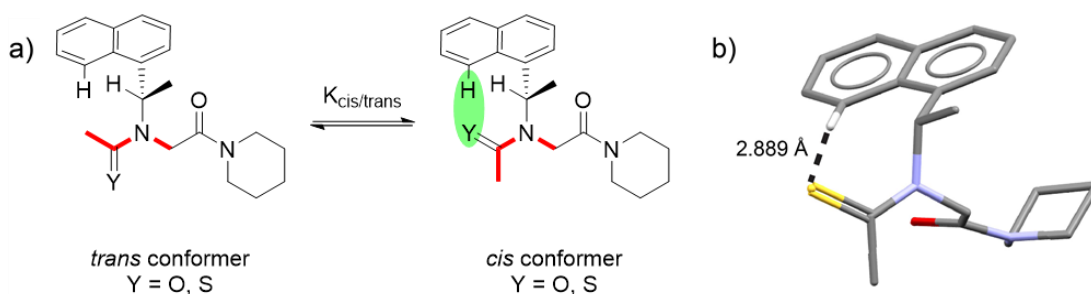


Figure 5.9. a) *cis/trans* isomerization of synthetic peptoids. A C–H···A HB helps favor the *cis* conformation. b) Crystal structure shows a C–H···S HB in the solid state helps favor the *cis* conformation in the thioamide derivative.

The propensity for S acceptors to make longer contacts with C–H donors than N, O, and F may contribute to prior underappreciation of C–H···S interactions. For example, Goel and coworkers found that inter- and intramolecular C–H···N and C–H···O HB were crucial in the aggregation induced emission (AIE) mechanism for a novel class of luminogens (Figure 5.10). Studying the published crystal structure, we also find highly linear C–H···S contacts (177.6°) that may assist in rigidifying the aggregates. The C–H···S contacts were found at a much longer C–H···A distance (3.191 \AA) than the other types of C–H contacts ($2.52\text{--}2.58 \text{ \AA}$).¹⁷³ Other work by Tang and coworkers supports this possibility, showing that strong, linear C–H···S HB contribute to AIE in their systems.¹⁷⁴

Although the second-row elements favor short contacts, the rest of the HB acceptors in the third, fourth, and fifth-rows tend toward making moderate-to-weak contacts. In this regime, as the electronegativity of the HB acceptor decreases, more linear C–H···A contacts are favored. This trend is best seen in third row elements P, S, and Cl. Chlorine, the most electronegative atom in this series, has the highest number of weighted low-angle contacts and P, the least electronegative atom in this series, has the least number of weighted low-angle contacts. This across-row trend also holds true for the small, electronegative second-row elements. From the third-row down, we also see

that this trend holds down a periodic column, which is best visualized by comparing Cl, Br, and I. Cl, the most electronegative atom in this series, again has the greatest number of weighted low-angle contacts, whereas I, the least electronegative in this series, has the least. To explain this trend, we have to consider each attractive force in a HB. The attractive interaction from charge transfer decreases the fastest over distance (diminishing approximately following e^{-r}), and therefore cannot explain the trends in the weak-to-moderate contacts that extend past the sum of the van der Waal radii of H and A. Electronegativity does not increase the preference for linearity, so electrostatic interactions also likely do not explain the trends. Furthermore, dispersion interactions are isotropic and so would not favor any contact angle. Polarizability, which is the ability of the HB acceptor to redistribute its electron density, must be the most important acceptor character driving linear contact angles. This observation would explain why the second-row elements, which are small, and not very polarizable, behave differently from the rest of the acceptors.

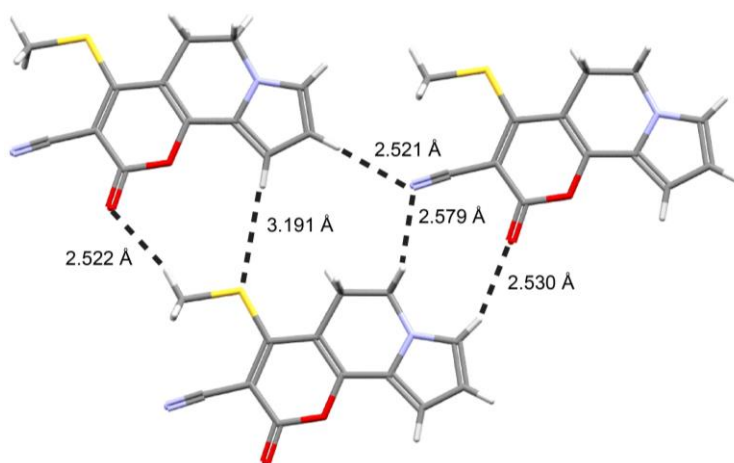


Figure 5.10. a) Crystal packing of the luminogen reveals C–H···O (atom denoted in red), C–H···N (blue) and C–H···S (yellow) intermolecular C–H HB.

The chalcogen atoms S and Se have generally been considered poor HB acceptors due to their low electronegativity. Both these elements, however, are polarizable and therefore are more likely to be C–H HB acceptors. C–H \cdots S/Se contacts behave similarly, with a strong preference for linear contacts and a weaker preference for low-angle contacts. Even Te appears to show a preference for linear contacts, although there are far fewer of these instances (3,677 inter- and intra-molecular contacts), perhaps reflecting the synthetic challenges working with this highly reactive element. Nevertheless, there are two published examples of C–H \cdots Te interactions.^{175,176} The most recent example, published in 2020, studied the C–H \cdots A interactions of a series of *bis*(silanechalcogenones). Using evidence from crystal structures and computations, the authors found that S made the strongest C–H HB bonds compared to Se and Te; however, the size of Te allowed it to make both inter- and intramolecular HB. Given that the weighted 3D histogram of C–H \cdots Te contacts reveals a preference for linear geometries, perhaps there are already examples of these contacts that have been missed.

Finally, we note the striking similarity between the behavior of C–H \cdots S contacts and C–H \cdots Cl contacts. Cl is a well-established C–H HB acceptor. The S and Cl contacts occur at similar distances, but S is a more polarizable element, and so should act as a better C–H HB acceptor. Indeed, we see more of a linear preference in S contacts. If C–H \cdots Cl HB have been identified as salient non-covalent interactions, C–H \cdots S HB should be equally established.

5.2.1.3 S-character affects preferred hydrogen bonding angles

5.2.1.3.1 S oxidation state

For a main group element, sulfur is unique because it is readily found in many stable oxidation states, ranging from -2 to $+6$.¹⁷⁷ 3D cone-corrected histograms of C–H \cdots S interactions of sulfur in the S^{2-} , S^{1-} , and S^0 oxidation states clearly show that oxidation state influences the preferred geometry of this interaction (Figure 5.11).

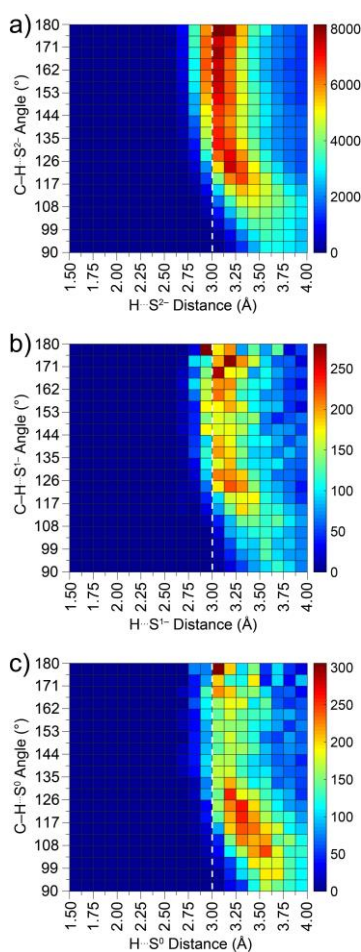


Figure 5.11. Cone-corrected 3D histograms of S in different oxidation states: a) S^{2-} , b) S^{1-} , and c) S^0 .

Roughly 93% of the C–H \cdots S contacts identified in our CSD analysis were found in the oxidation state -2 . S^{2-} is the best oxidation state for hydrogen bonding because it is in the most electron-rich state and is most polarizable than other oxidation states. In addition, S^{2-} is more prevalent than S^{1-} and S^0 in crystal structures containing S and C–H functional groups, regardless of whether a contact is occurring. Only about 6% of C–H \cdots S contacts were in the S^0 and S^{1-} oxidation state, combined. These contacts are longer than those to S^{2-} and almost none of the weighted contacts can be considered strong. Although these are weaker interactions, S^{1-} and S^0 HB acceptors still play important roles in crystal packing. For example, Hisaki and coworkers found C–H \cdots S contacts between a trisdehydrotribenzo[12]annulene derivative and DMSO, a commonly used organic solvent containing S^0 , to be essential in the supramolecular assembly of the system.¹⁷⁸ The overall ordered architecture formed from C–H \cdots S^0 HB allowed the structure to have anisotropic charge mobility, making it a candidate for organic semiconductor materials.

5.2.1.3.2 S coordination number

The number of atoms that S is bonded to, defined here as the coordination number, can affect the electrostatic and steric environment as well as the polarizability of the HB acceptor, which should in turn change the nature of the C–H \cdots S interactions. Indeed, the weighted 3D histograms of C–H \cdots S contacts when S is bonded to one (SR), two (SR₂), and three (SR₃) other non-metal atoms reveal major differences in the important contact geometries (Figure 5.12). When the S HB acceptor is bonded to one other atom, the contacts are shorter and more linear, perhaps due to less steric crowding around the S HB acceptor. Regions of both high-angle and low-angle contacts are

important when S is bonded to two other atoms, and most contacts are moderate to weak. The 3D histogram of C–H···S contacts when S is bonded to three other atoms closely resembles that of S⁰ (Figure 5.11c) as the contacts in these two categories largely overlap.

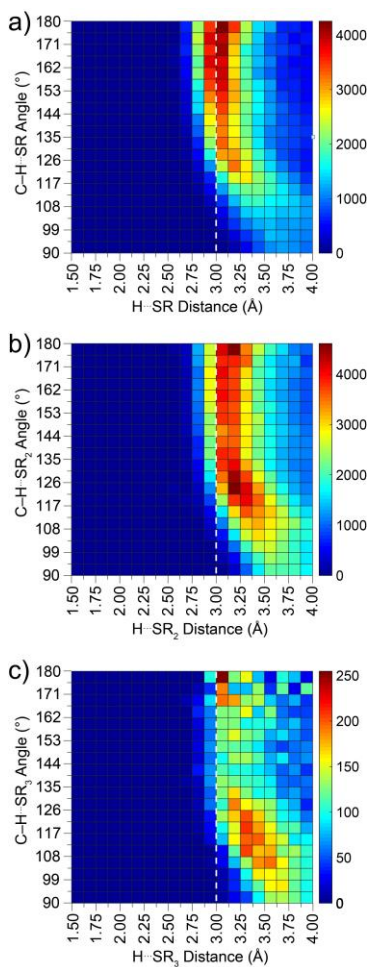


Figure 5.12. Cone-corrected 3D histograms of S bonded to a) one non-metal atom, b) two non-metal atoms, and c) three non-metal atoms.

Although we cannot definitively identify why bent interactions are favored in SR₂ and SR₃ contacts, we can see evidence of their importance in published examples. For example, in 2017 Anderson and coworkers reported an unexpected attractive interaction between a pyridine ligand and the alkyl straps in sulfur-strapped Zn-porphyrins.¹⁷⁹ 2D

NMR spectroscopy, UV-vis spectroscopy, and crystal structure analysis revealed the formation of both an expected *out* isomer (Figure 5.13a) and also an unexpected, more sterically hindered *in* isomer (Figure 5.13b). The formation of the *in* isomer is attributed to C–H \cdots π interactions between the alkyl C–H groups on the strap and the pyridine ring. The authors also comment that “there may also be an attractive interaction between the sulfur atom and the α C–H of the pyridine”. Investigating the published crystal structure, we clearly see that while the C–H \cdots S contacts are bent, one falls squarely in the region of important low-angle C–H \cdots S contacts with an H \cdots S distance of 3.140 Å and a C–H \cdots S contact angle of 123.5°.

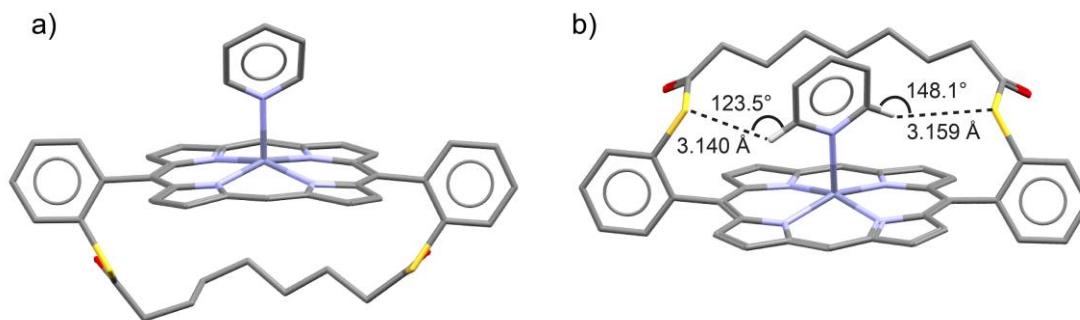


Figure 5.13. a) *Out* isomer and b) *in* isomer of sulfur-strapped Zn-porphyrins.

5.2.1.4 Alkyl vs. aryl based C–H donors

In general, the C–H atoms of carbons with more *s*-character are more acidic and are typically viewed as better HB donors. When comparing cone corrected 3D histograms of alkyl and aryl C–H HB donors, however, we observed that linear contacts are more important with alkyl C–H HB donors whereas low angle contacts are more important with aryl C–H HB donors (Figure 5.14). Even though this outcome seems counter-intuitive, it may reflect that aryl C–H HB donors are better at accommodating bifurcated

hydrogen bonds than alkyl C–H donors. For example, we found that about 37% of C–H⋯S contacts with aryl C–H HB donors are bifurcated between two adjacent aryl C–H HB donors. A 3D histogram of just these bifurcated C–H⋯S⋯H–C contacts (Appendix D, Figure D.3) shows a strong preference for the same low-angle contacts that are observed for all aryl C–H⋯S contacts.

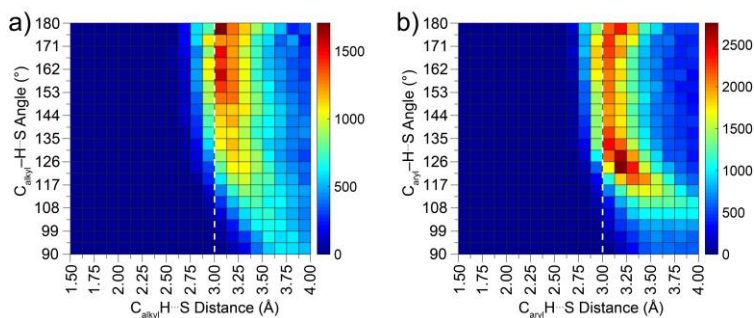


Figure 5.14. Cone-corrected 3D histograms of C–H⋯S contacts with a) sp^3 alkyl C–H HB donors and b) sp^2 aryl C–H HB donors.

Alkyl and aryl C–H HB donors are not relegated to synthetic systems, and there is also evidence for both sp^3 and sp^2 C–H HB donors interacting with sulfur in biological systems. For example, we revisited the crystal structure of the first discovered bacterial ion channel for HS^- and found C⋯S contact distances between valine and leucine amino acids and HS^- that were about the same distance or shorter than the majority of weighted C–H⋯S contacts (Figure 5.15, Figure D.2e).¹²¹ In addition, we found evidence of both sp^3 and sp^2 C–H HB donors from threonine and tryptophan residues in streptavidin in contact with the thioether (Figure 5.16). The streptavidin-biotin complex is one of the strongest non-covalent binding events known in nature, in part due to the high geometric complementarity of the host-guest complex and a high degree of hydrogen bonding.

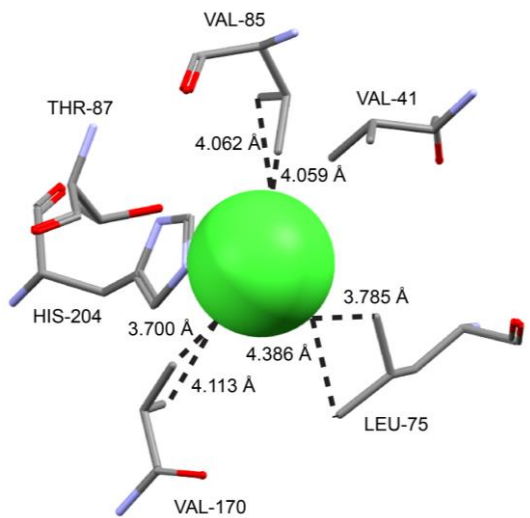


Figure 5.15. Leucine and valine amino acid residues in contact with either Cl^- or HS^- in the first discovered bacterial ion channel for HS^- . (PDB: 3TDX)

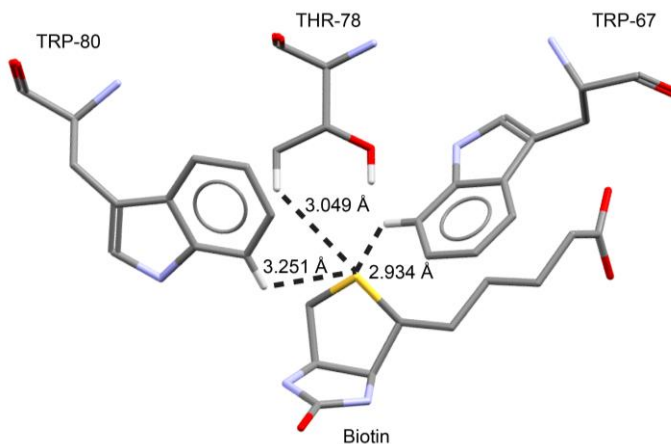


Figure 16. Tryptophan and threonine amino acid residues in contact with the biotin thioether in the streptavidin-biotin complex. (PDB: 6M9B)

5.2.1.5 Hydrogen bond acceptor directionality

Geometric preference of hydrogen bonding in the solid state also extend to the HB acceptor. Strong HB often have clear $\text{R}\cdots\text{A}\cdots\text{H}$ acceptor directionality (A2, Figure 5.1), whereas weak HB lose this directionality. For example, the acceptor directionality in a strong HB may be driven by the required geometry of charge transfer or electrostatic

potential. On the other hand, a weak HB with high dispersion character would lose much of its directionality.

The acceptor directionality in both linear and bent C–H···S contacts can be visualized by using a 3D histogram of C–H···S contact angle vs. R---S···H contact angle in which both axes of contact angles are weighted by the cone angle correction (Figure 5.17e). These bi-weighted 3D histograms do not show the most common donor and acceptor contact angles, but rather show what combinations of C–H···A and R---A···H angles are particularly important geometries. For example, at C–H···S angles between 90° and 94.5° there is no preferred R---S···H directionality, meaning that each bin should have about the same low importance. These contacts are either statistically-driven or Van der Waals contacts. On the other hand, C–H···S angles between 175.5 and 180° either prefer a linear R---S···H acceptor angle or a bent acceptor angle between about 108–126°. As the C–H···S bond angle deviates farther from linearity, specific acceptor directionalities start to lose importance, perhaps reflecting the increasing dispersion contribution to hydrogen bonding at bent contact angles.

Most HB acceptors with C–H HB donors favor a highly linear acceptor directionality and only occur at linear C–H···A contact angles (Figure 5.17). As the C–H···A angle deviates from linearity, preference for any acceptor directionality gradually disappears. Sulfur is the exception to this trend. Sulfur HB acceptors show an ‘island’ of important R---S···H angles at low-angle C–H···S contacts. Although the donor directionality in this island is weak, S is the only HB acceptor that shows any acceptor directionality for this bent, weak HB. This unique geometry is completely removed with SR₁ acceptors (Figure D.4), and is exaggerated with SR₂ acceptors (Figure D.5b).

Notably, this geometry is not seen with OR₂ acceptors (Figure D.5a) but is present with SeR₂ acceptors (Figure D.5c). Because there is some (albeit weak) attractive interaction or environment that is promoting this unique contact geometry, S may be a stronger C–H HB acceptor at bent angles compared to other acceptors.

5.2.2 Sulfur hydrogen bonding interactions in metal sulfur ligated complexes

Similar to the established hydrogen bonding interactions between sulfur as a HB acceptor with N–H and O–H HB donors in organic molecules, sulfur atoms coordinated to metal centers also participate in hydrogen bonding. S HB donor ligands are widely known in many subfields of inorganic chemistry ranging from the active site of bioinorganic cofactors, such as nitrogenase, to catalytic systems. Model systems have highlighted how certain R–H···S HB motifs can be consequential in catalytic turnover and reactivity. An example from Riordan and coworkers in 2003 focused on investigating sulfur alkylation rates by functionalized zinc thiophenolates in the presence of *ortho* and *para* N–H amide HB donors.¹⁸⁰ In this work, the second-order rate constants for the alkylation of functionalized zinc thiophenolates with BnBr in the presence of *ortho* and *para* N–H amide HB donors were $1.3 \times 10^4 \text{ M}^{-1}\text{s}^{-1}$ and $44 \times 10^4 \text{ M}^{-1}\text{s}^{-1}$, respectively. The different rates were attributed to stabilizing *ortho*-N–H HB donors significantly diminishing the nucleophilicity of the bound thiophenolates. This interaction was confirmed by ¹H NMR and IR spectroscopy and observed by the short N–H···S distance in the solid state with a H···S bond length of 2.49(2) Å. The authors speculate that similar R–H···S HB interactions may play a role in other zinc thiolates of metalloproteins.

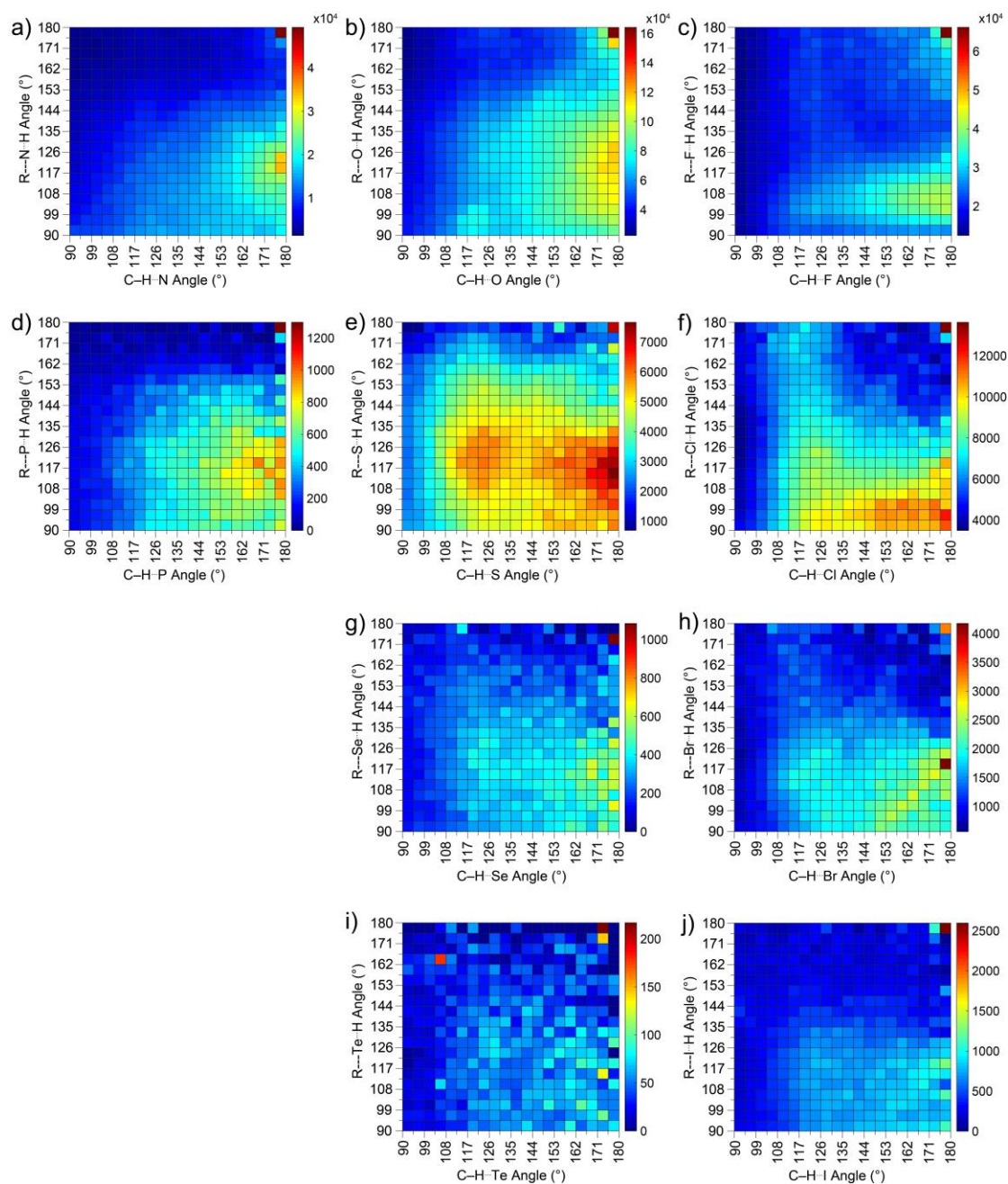


Figure 5.17. Bi-weighted 3D histograms of C–H···A contacts found in the CSD with a) N, b) O, c) F, d) P, e) S, f) Cl, g) Se, h) Br, i) Te, and j) I.

Efforts to establish C–H HB interactions with atoms in the primary coordination sphere of metal complexes has been studied and an elegant example was recently shown using a modified phenanthroline (phen) ligand. Functionalization of the phen ligand with

–CF₂H, a known C–H HB donor with similar donating strength to amines and thiols,¹⁸¹ at the 2-position allowed for close contacts between the CF₂H group and the primary coordination sphere of the metal. Szymczak and coworkers synthesized complexes of Pd (PdX₂(phen) where X = F[–], Cl[–], Br[–], and OR[–]) and showed a C–H···X HB interaction between the CF₂H group and the X-type ligand in the primary coordination sphere of the Pd complex (Figure 5.18).¹⁸² These results were shown by solid state structural analysis and confirmed by spectroscopic data and computational studies. Hydrogen bonding interactions with H···O distances were found to be as short as 2.002 Å. Furthermore, an interesting result from this work showed that while the CF₂H group is a great HB donor, the CH(CH₃)₂ group is also capable of providing stabilizing HB interactions. Both PdCl₂(phen) complexes where an *ortho*-CF₂H and *ortho*-CH(CH₃)₂ of the phen ligand were synthesized and comparative bond lengths of the C–H···Cl interaction were observed with distances of 2.339 and 2.496 Å for *ortho*-CF₂H and *ortho*-CH(CH₃)₂ complexes, respectively. While this example does not include S-based HB acceptors, it demonstrates that C–H HB donors can dramatically affect the stability and reactivity of ligand donor atoms in the primary coordination sphere.

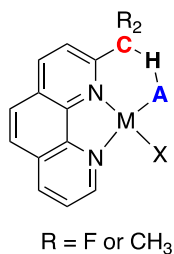


Figure 5.18. C–H hydrogen bonding interactions in the primary coordination sphere of metal complexes as demonstrated by Szymczak and coworkers.

To expand the analysis of C–H···S HB interactions in organic molecules (vide supra), we searched for hydrogen bonding interactions involving C–H···S–M motifs where S is bound to a metal. This analysis knits together work by others that highlight the importance of hydrogen bonding through influencing model chemistry of metalloenzymatic reaction pathways through N–H···S HB and the ability of C–H HB donors to form C–H···X–M HB interactions in the primary coordination spheres of metal complexes. Similar to the metal sulfur interactions observed in organic compounds, we focused on CSD search parameters for C–H···S–M contacts to included C–H···S (A1) and H···S–M (A2) angles of 90–180° and H···S (L1) and C···S (L2) bond lengths of 0–4.0 Å and 0–5.0 Å, respectively. Our initial searches were aimed at determining whether short C–H···S–M contacts are common in *d*-block metals. The results of the initial search provided 45,733 molecules with these parameters and a total of 487,171 intra- and intermolecular C–H···S–M contacts (Figure 5.19).

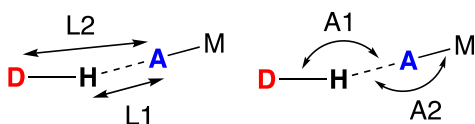


Figure 5.19. Lengths and angles referred to in this section, where A is bound to a metal.

The cone corrected 3D histogram for the C–H···S–M contacts for *d*-block metals reveals that the majority of the weighted contacts include bond lengths between 3.00–3.25 Å at angles > 144°, with notable ‘islands’ of favorable contact geometry at lower angles of 12–135° and at longer distances of 3.00–3.375 Å. We also compared C–H···Cl–M HB contacts based on the similarity of Cl and S as well as prior work demonstrating the importance of C–H···Cl–M interactions. Chlorine and S are nearly

identical in size with van der Waals radii of 2.05 and 2.06 Å, respectively,¹⁸³ and so a comparison of these H···Cl contacts would validate the observed H···S seen in Figures 5.20 as HB interactions. The cone corrected C–H···Cl–M contacts plotted in Figure 5.20b shows data from 77,677 molecules with 920,886 inter- and intramolecular contacts. The major difference between the plots of Cl HB contacts and S HB contacts is that Cl HB contacts show a greater consolidation of contacts above 100 ° and at distances between 2.750–3.000 Å. These data suggest that C–H···Cl–M contacts may be stronger and more directional than C–H···S–M contacts, and may be attributed to higher steric bulk of thiolates in comparison to bound Cl in coordination complexes, or to slight differences in the dipole moment between Cl and S because Cl is more electronegative than S. It is worth noting that such discrepancies between Cl HB contacts and S HB contacts is not observed when A is not bonded to a metal. Differences between Cl and S may also be attributed to their valency. Chloride is a monovalent ligand, while sulfide-based ligands are divalent and the ability for a shorter and more directional HB interaction for chloride could be due to steric interactions. The similarities in shape and localization of areas with high frequency in Figure 5.20 do suggest that Cl and S behave similarly as HB acceptors despite a weaker interaction with S. Lastly, the cone corrected 3D histogram of C–H···S contacts where the S atom is bonded to a metal (Figure 5.20a) and non-metal (Figure 5.5c and 5.8e) look strikingly similar. The majority of the contacts include bond lengths between 3.00–3.25 Å at angles > 135 °, which further validates that both organic molecules and metal complexes engage in C–H···S HB.

We next aimed to identify if certain groups in the *d*-block contained more C–H···S–M contacts than others. In comparison to nitrogen and oxygen, S is relatively

large and polarizable, and so we expect that complexes with the more polarizable late transition metals will have greater affinity for thiolate and S-bound ligands, resulting in more HB contacts. A survey of groups 3-12 from the periodic table confirms that early transition metals have far fewer C–H···S–M contacts in comparison to groups 7-12. Cone corrected 3D histograms are shown for groups 7-12 (Figure 5.21). The group with the shortest C–H···S–M contacts was group 10, which included 11,986 molecules with 96,423 inter- and intramolecular contacts. As we move from left to right in the periodic table across the *d*-block elements, a trend emerges where the most concentrated or highest frequency of weighted C–H···S–M contacts occurs with less directionality. For group 1 metals, only 170 molecules matched the search criteria. Although there were regions of increased C–H···S–M contacts near 3.125 Å and angles above 155° the small data set does not allow for further analysis.ⁱⁱⁱ

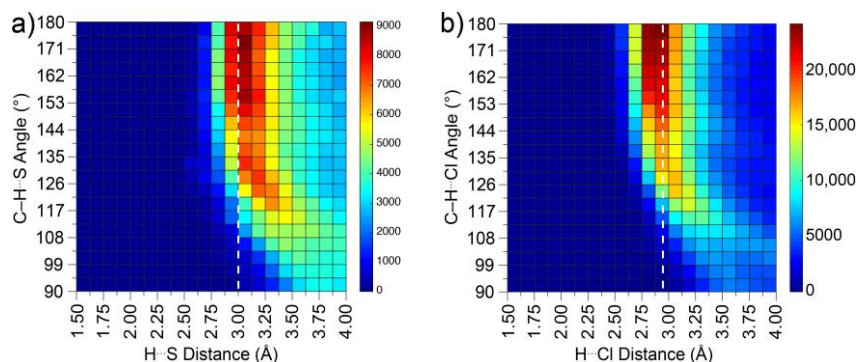


Figure 5.20. 3D histogram visualizing the cone corrected a) C–H···S–M, and b) C–H···Cl–M contacts in *d*-block metals where S or Cl are in the primary coordination sphere. The white line for each plot indicates the sum of the van der Waal radii between A and H.

ⁱⁱⁱ We observed similar trends for groups 3-5. Group 6 metals (Cr, Mo and W), did show localized trends C–H···S–M at higher angles and shorter distances. With 4,589 molecules found from the search criteria in the CSD, we observe many contacts at distances shorter than 3.125 Å and angles above 135 degrees. Group 13 metals (Al, Ga, and In) included 1,089 molecules matching the search criteria; however, the data depicted in the cone corrected histogram demonstrated a more delocalized pattern of contacts ranging in H···S between 2.00 and 3.50 Å.

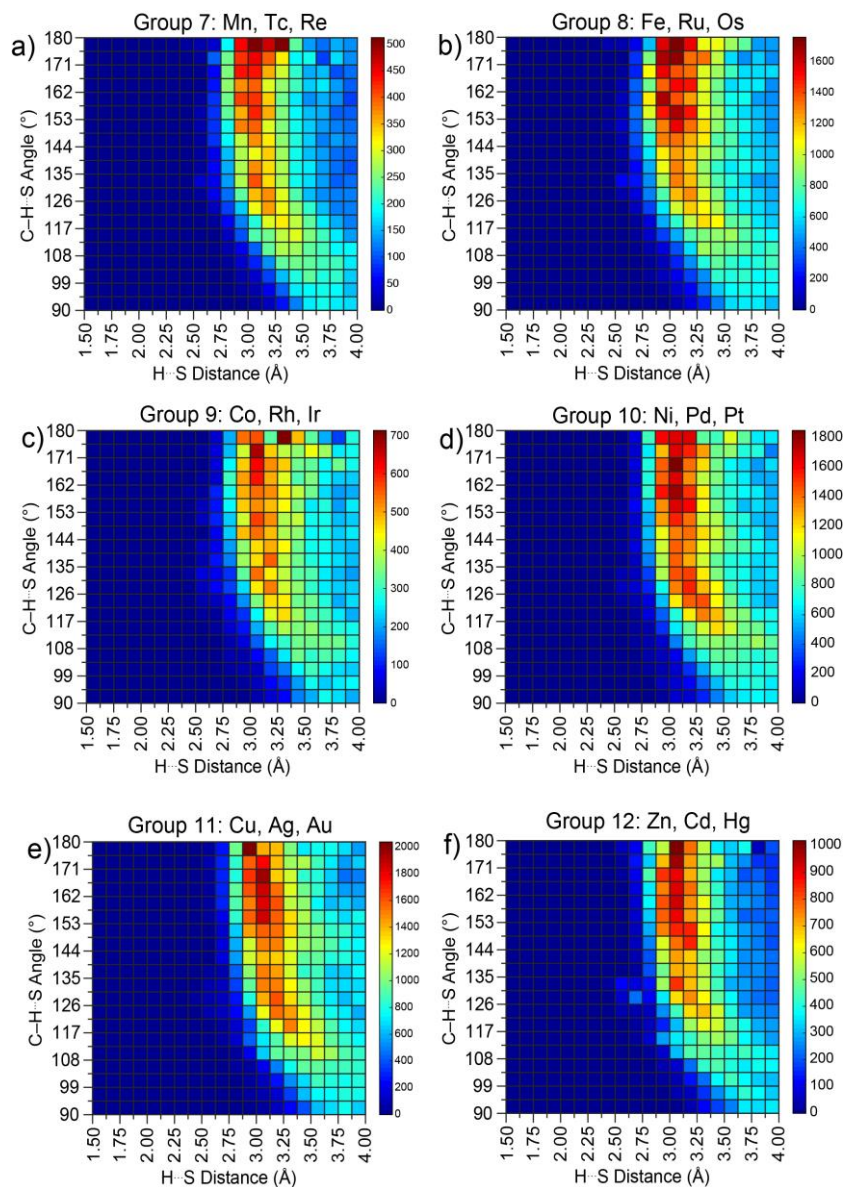


Figure 5.21. Cone corrected histograms of C-H \cdots S-M of groups a) 7, b) 8, c) 9, d) 10, e) 11, and f) 12 of the transition metals.

5.2.2.1 Structures exhibiting short C-H \cdots S-M contacts

With the designation of H₂S as the third gasotransmitter, extensive research has focused on understanding its role as a signaling molecule, transport throughout biological systems, and reactivity with metalloproteins.^{9,184–187} The bivalve mollusk *Lucina Pectinata* is a species of clam that has been found in sulfur rich environments and further

found to bind hydrosulfide with high affinities. We revisited the HS⁻-bound hemoglobin I (HbI) structure determined in 1994 by Bolognesi and coworkers.¹⁸⁸ The active site revealed what is now referred to as the “Phe cage”, which is a hydrophobic pocket around the HbI, and a glycine residue that is a hydrogen bond acceptor to HS⁻ to further stabilize the reactive HS⁻ anion. In tandem, the Phe cage, which is believed to prevent water molecules from displacing the bound HS⁻, and the glycine residue, which aids in HS⁻ coordination, are thought to be the major contributing factors for the high binding affinities of HS⁻ to the Fe center. Reanalysis of the structural data of sulfide-bound HbI from *L. Pectinata* showed that there is a short C··S contact of 3.9 Å between the Phe-43 residue and the S atom bound to Fe. Although the H atom on the metal sulfide was not located, the short C··S distance suggests that the H··S distance could be as short as 2.8 Å, which would be considered one of the stronger C–H··S–M contacts according to the data collected by Bolognesi shown in Figure 5.22 (PDB: 1MOH).

Later work by Banerjee and coworkers discovered that human Hb can support catalytic H₂S oxidation to form thiosulfate and polysulfides prompting further investigation of how sulfide binds human Hb.¹⁸⁵ In subsequent work focused on structural and mechanistic insights into this process, the crystal structure of sulfide bound human Hb was reported (Figure 5.22b, PDB: 5UCU).¹⁸⁹ There are key differences in the active site between the sulfide bound Hb structures from *L. Pectinata* and humans. In human Hb, the hydrogen bond acceptor to the bound sulfide is His rather than Gly in *L. Pectinata*. In addition, the Phe residue in the human Hb has a longer C··S contact at 4.3 Å, which would suggest a weaker C–H··S–M interaction. Single site mutagenesis of Hb1 from *L. Pectinata* has been studied to understand how H₂S oxidation is affected by the

hydrophobic pocket of *L. Pectinata*.¹⁹⁰ When the Phe residues are modified with more polar, hydrogen bond accepting residues, which are more similar to those of human Hb, the rate of H₂S oxidation is increased. Based on the short, potentially strong C–H··S contact in the primary coordination sphere of sulfide bound to Hb1 from *L. Pectinata*, we postulate that these short stabilizing contacts may contribute to the slowed rate of sulfide oxidation. It is possible that the C–H··S–Fe hydrogen bond causes the bound sulfide to be less readily oxidized by Fe due to an attractive force between the partial negative charge on S and the partial positive charge of the hydrogen atom involved in hydrogen bonding, thus limiting its reducing power and slowing down the oxidation process.

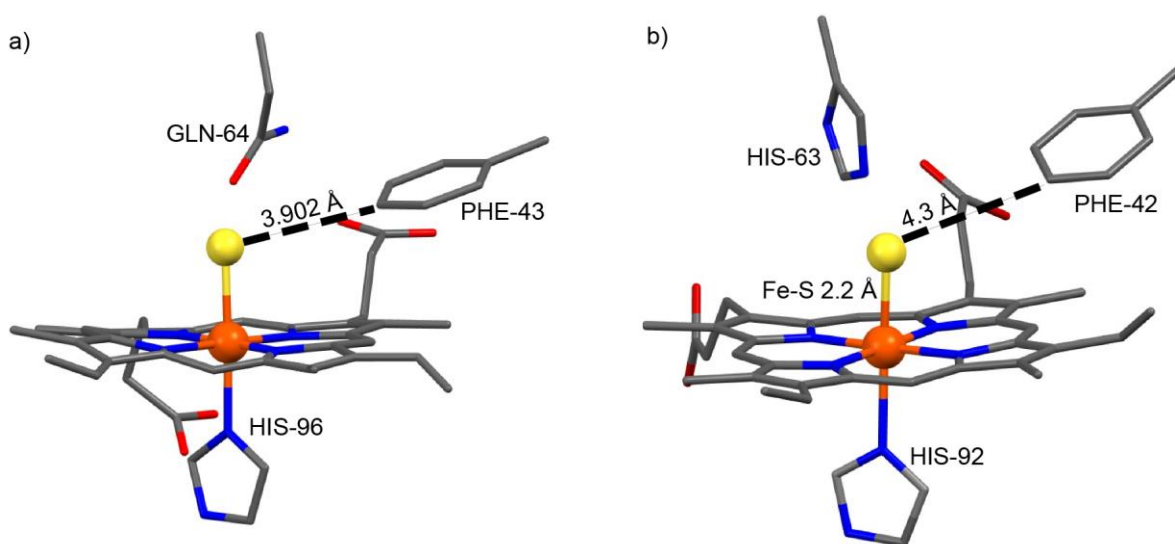


Figure 5.22. X-ray structures of (a) sulfide bound Hb1 isolated from *L. Pectinata* and (b) sulfide bound Hb isolated from human myoglobin. The labeled lengths correspond to C–S distances.

Stabilizing interactions within other metal hydrosulfide complexes by C–H··S–M interactions were also found when using the same search criteria for C–H··S–M contacts of the *d*-block. Searching the CSD for short contacts for structures in which the sulfur HB

acceptor was a M–SH moiety revealed 202 molecules with 1,476 contacts (Figure 5.23). The cone corrected 3D histogram shows the majority of contacts have an angle greater than 150 ° at distances < 3.125 Å. Such interactions, which include the example from *L. Pectinata*, would be considered moderate in strength.

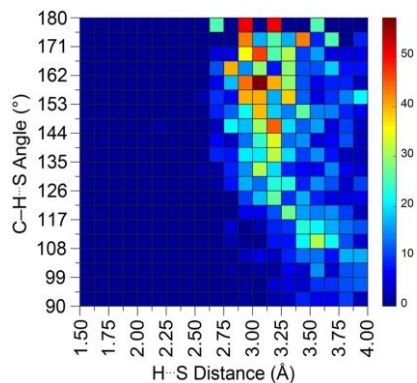


Figure 5.23. Cone corrected histograms of C–H \cdots (SH)–M with *d*-block metals.

Zn–S complexes are widely studied in biological sulfur chemistry due to the known affinity for the formation of Zn–S bonds, such as in Zn finger proteins. Zn–SH have been demonstrated to form through ligand metathesis reactions of Zn–OH with H₂S, leading others to study the reactivity of these compounds as models in biological reactivity. For example, Galardon and Artaud have studied *tris*(pyrazol)boratezinc hydrosulfide (TpZnSH) species, in which the TpZnOH precursors are structurally similar to the carbonic anhydrase active site, to further understand their roles in persulfidation reactivity *via* Zn–SH intermediates.¹⁹¹ In this work, an isopropyl functionalized Tp ligand (ⁱPrTp) is used to isolate a ⁱPrTpZnSH complex. Further inspection of this structure shows multiple short C–H \cdots S–Zn hydrogen bonding interactions (Figure 5.24). All three isopropyl groups of the ⁱPrTp ligand show the tertiary C–H bond pointing towards the

bound Zn–S. The H \cdots S bond lengths and C–H \cdots S bond angles are 3.066, 3.110, 3.289 Å and 150.5, 153.6, 135.5 °, respectively. The Zn–S bond distance is 2.230 Å and slightly shorter in comparison to some other Zn–SH species where C–H \cdots S hydrogen bonds are weaker.¹⁹²

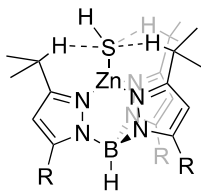


Figure 5.24. Graphical representation of C–H \cdots S–Zn hydrogen bonding interactions observed in a ⁱPrTpZnSH complex.

5.3 Conclusions

This work provides evidence for hydrogen bonding interactions between C–H bonds as hydrogen bond donors and sulfur atoms as hydrogen bond acceptors. Although specific C–H \cdots S have been observed previously in selected systems, the analyses provided here highlight that these close contacts are significantly more common than currently appreciated. This generality is supported by the tens of thousands of solid-state structures with C–H \cdots S interactions that provide the framework to study the details of such contacts and associated trends. Following the standard definition of a hydrogen bond, we establish that C–H \cdots S close contacts are indeed hydrogen bonding interactions, with the most defining factor being the distance between a hydrogen atom and the acceptor. The prevalence of such contacts in organic molecules and metal complexes with S in the primary coordination sphere provides the ability to compare these

interactions through the use of 3D histograms. These analyses provide clear trends for preferential distances and angles for C–H···S close contacts.

These analyses reveal that that C–H···S hydrogen bonds out-perform more traditional N–H···S and O–H···S hydrogen bonds at long distances and bent contact angles. This marked difference in contact angle geometry and distance may help explain why C–H···S contacts have been traditionally overlooked. Prior work by Addlagatta and coworkers⁸⁴ identified 20 C–H···S contacts with C···S distances up to 4 Å in enzyme-ligand binding sites reported in the PDB. Now, informed by the over 423,000 C–H···S contacts found in molecular structures of small molecules, we see that this 4 Å cut-off may be too short (Figure D.2e). We suspect lengthening the allowed range of C···S contact distances would reveal even more overlooked C–H···S hydrogen bonds present in enzyme-ligand binding sites in the PDB. In addition to our own analyses that establishes C–H···S close contacts as hydrogen bonds, we highlighted selected prior examples in which C–H···S contacts are present, but that were not identified in the earlier analyses. One such example from the hydrosulfide Hb complexes in *L. Pectinata* and human myoglobin may explain the disparate reactivity observed between the two Hb species.

As a whole, this work demonstrates that C–H···S close contacts can be classified as hydrogen bonding interactions and should no longer be overlooked. The 3D histograms presented provide a convenient tool for identifying relatively strong, moderate, and weak C–H···S hydrogen bonds present in the solid state. Moving forward, C–H···S interactions should be included in the design, analysis, and function of compounds in diverse areas of chemistry ranging from supramolecular chemistry to structural biology to materials characterization.

CHAPTER VI

CONTROLLING THE REACTIVITY OF HYDROSULFIDE WITH A SUPRAMOLECULAR HOST

This chapter includes unpublished co-authored material from Fargher, H.A.; Longnight, F.; de Faria, T. P.; Nickels, R.A.; Haley, M.M.; Johnson, D.W.; Pluth, M.D. This manuscript was written by Hazel A. Fargher with editorial assistance by Professors Michael M. Haley, Darren W. Johnson, and Michael D. Pluth. The project in this chapter was developed by Hazel A. Fargher, Michael M. Haley, Darren W. Johnson, and Michael D. Pluth. The experimental work and data analysis were performed by Faith Longnight. Mass spectra were obtained by Thaís P. de Faria. Supramolecular receptors were synthesized by Russell A. Nickels.

6.1 Introduction

Supramolecular host-guest chemistry studies the non-covalent, intermolecular binding interactions between two or more molecules, and often serves as a simplified synthetic imitation of protein-ligand binding in biology. Much like protein-ligand interactions, the supramolecular host binding pocket can control the microenvironment of a bound guest and as a result catalyze reactions,^{38-40,193-196} change the product distribution of a reaction,¹⁹⁷⁻¹⁹⁹ and shift equilibria.²⁰⁰⁻²⁰² Host-guest chemistry can even stabilize highly reactive and fleeting molecules.²⁰³⁻²⁰⁵ Notably, in 1991 Cram and coworkers found that dimerization of the highly reactive, antiaromatic molecule cyclobutadiene was prevented when incarcerated inside a hemicarcerand supramolecular host.⁴¹ This host-guest stabilization allowed the authors to study the spectroscopic

properties of this otherwise unstable molecule for the first time. Another representative example highlighting the effectiveness of host-guest stabilization includes research by Nitschke and coworkers who showed that white phosphorus (P_4), a highly pyrophoric compound when exposed to air, is unreactive towards water and oxygen when encapsulated in a tetrahedral container molecule.⁴²

Recently, we have reported an arylethynyl bisurea supramolecular receptor for hydrosulfide (HS^-) with high binding affinities ($K_a \sim 15,000 M^{-1}$) in organic solvents (**6.1**, Figure 6.1).³⁶ HS^- is an important biomolecule; at physiological pH, HS^- is favored over its conjugate acid hydrogen sulfide (H_2S , $pK_a = 7.00$), which has been classified as the third endogenously produced gasotransmitter and plays a role as a signaling molecule in major biological systems.^{9,30} The supramolecular chemistry of HS^- , however, remains understudied. HS^- is a nucleophilic and reducing anion and as such supramolecular hosts must be carefully designed to prevent undergoing reaction with this guest. As a result, we are aware of only three families of supramolecular receptors that have shown reversible, non-covalent binding with HS^- .^{29,31,32,35,36} Nonetheless, evidence of the importance of supramolecular interactions with HS^- has emerged in nature. For example, HS^- has been found bound by hydrogen bonding interactions in the turn-over state of vanadium-containing nitrogenase.¹²² In addition, a recently discovered bacterial ion channel uses non-covalent interactions for the molecular recognition and cell membrane transport of HS^- .¹²¹

In this work, we study how supramolecular anion binding modulates the reactivity of HS^- in organic solvents. The rate of reaction of HS^- with a nitrobenzoxadiazole (7-nitro-1,2,3-benzoxadiazole, NBD) thioether (**6.2**, Scheme 6.1) is monitored in the

presence and absence of supramolecular receptor **6.1**. NBD thioether derivatives have been established as a colorimetric probe for HS^- in aqueous solution and are known to undergo nucleophilic aromatic substitution ($\text{S}_{\text{N}}\text{Ar}$) with the analyte.²⁰⁶ Reaction product **6.3** is UV-active and can be used to monitor the reaction progress *via* UV-vis spectroscopy. By comparing rate constants (k) and rate of reactions (v), we aim to understand the extent of HS^- stabilization through supramolecular binding with **6.1**, and perhaps mimic design strategies of nature in controlling this reactive biomolecule.

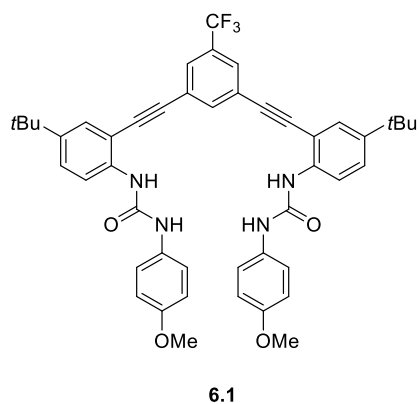
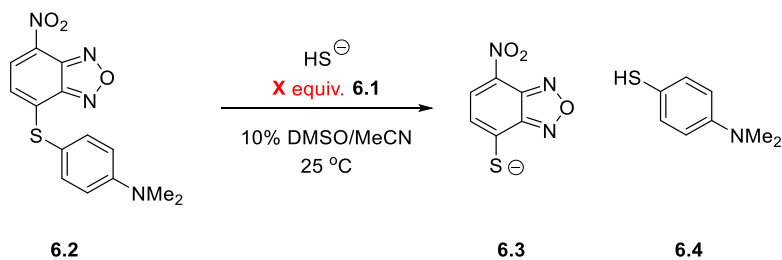


Figure 6.1. Supramolecular receptor for HS^- used in this study.



Scheme 6.1 Reaction of HS^- with **6.2** in the presence and absence of various equivalents of **6.1**.

6.2 Methods

Host **6.1** is a previously reported anion receptor for HS^- and was prepared by established methods.³⁶ **6.2** was chosen for this study as the rate of reaction with HS^- was slow enough to be measured *via* UV-vis spectroscopy but proceeded to completion before HS^- reactivity with **6.1** could occur.^{35,36} Furthermore, both NBD-thioether **6.2** and reaction products **6.3** and **6.4** are unlikely to compete with HS^- binding with **6.1**. NBD-thioether **6.2** was synthesized through methods similar to those reported in literature²⁰⁶ and was characterized through ^1H and ^{13}C NMR spectroscopy and high-resolution mass spectrometry (Appendix E).

The reaction of HS^- with NBD thioether derivative **6.2** in anhydrous and anaerobic 10%-DMSO/MeCN at 25 °C was monitored *via* UV-vis spectrophotometry in the presence and absence of supramolecular receptor **6.1** (see Appendix E for experimental details). NBD-thioether **6.2** absorbs around 420 nm in 10% DMSO/MeCN, consistent with other NBD-thioether derivatives in aqueous 50 mM PIPES buffer (Figure 6.2a).²⁰⁶ After reaction with HS^- , the UV-vis trace of reaction product **6.3** can be observed with a local λ_{max} at around 570 nm. This local λ_{max} is more red-shifted than **6.3** in aqueous 50 mM PIPES buffer which is consistent with fewer hydrogen bond donors in the organic solvent compared to water (Figure 6.2a).²⁰⁶ Derivatives of receptor **6.1** have previously been shown to absorb in the UV-vis region;^{26,27,29} however, the UV-vis trace of **6.2** and **6.3** in the presence of 5 equiv. **6.1** revealed similar local λ_{max} for **6.1** + **6.2** (420 nm) and **6.1** + **6.3** (570 nm) (Figure 6.2b).

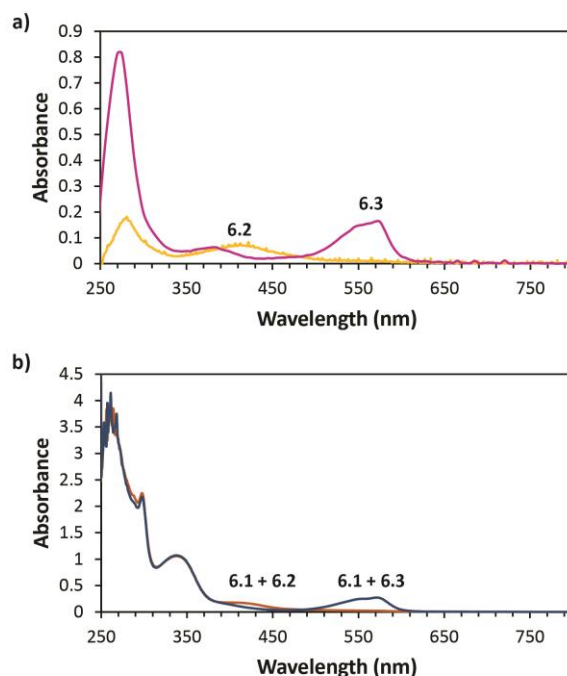


Figure 6.2. a) UV-vis spectra of **6.2** (yellow trace) and **6.3** (pink trace) after reaction of **6.2** with HS⁻. b) UV-vis spectra of **6.2** and 5 equiv. **6.1** (orange trace) and **6.3** and 5 equiv. **6.1** (blue trace) after reaction of **6.2** with HS⁻.

6.3 Results and Discussion

To best understand the effect of **6.1** on the rate of the reaction in Scheme 6.1, we compared the reaction kinetics of 1 equiv. TBASH with 1 equiv. NBD-thioether **6.2** in the presence and absence of 5 equiv. **6.1**. The reaction progress in both cases were monitored by collection of UV-vis absorption data of the reaction product **6.3** at 570 nm in 0.9 s intervals (Figure 6.3a-b). Initial data points before ~5 s were not observed due to the speed of the reaction; however, we were able to determine a rate constants (k) for the reaction with and without **6.1** present by fitting UV-vis absorption data to the 2nd order rate equation through non-linear regression (Figure 6.3c). Kinetic experiments were performed in duplicate or triplicate. Table 6.1 summarizes the results from a representative trial and average rate constants (k_{ave}) from multiple trials. Comparing k_{ave}

for the two reactions, we see that even at the 99.7% confidence interval the reaction proceeds significantly slower in the presence of 5 equiv. **6.1**.

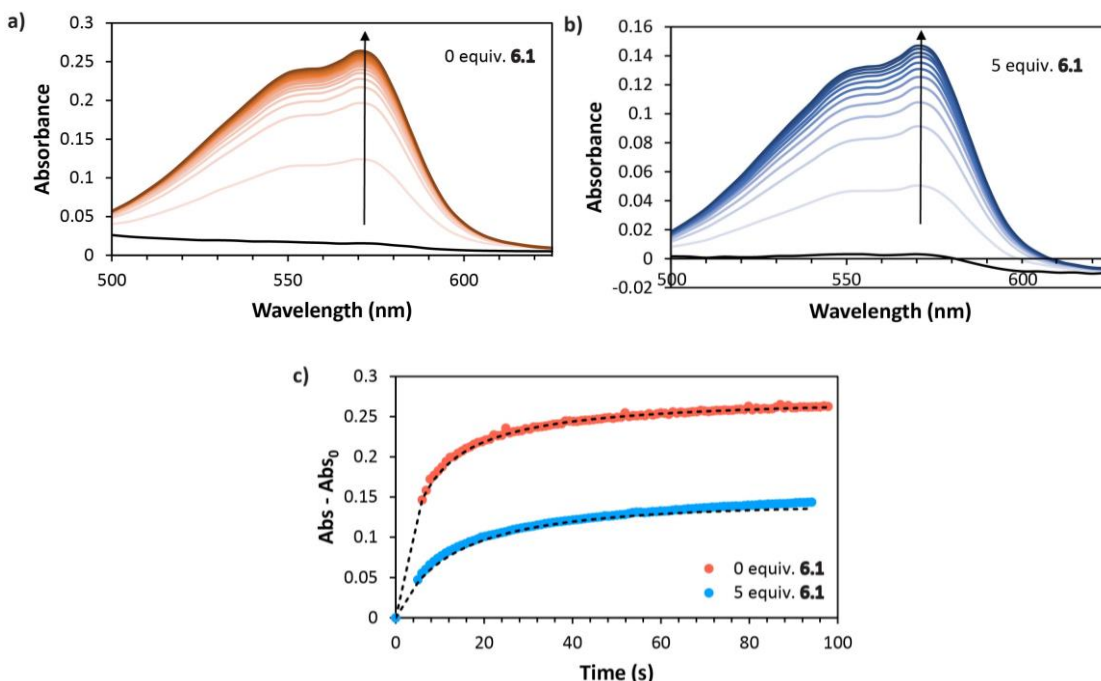


Figure 6.3. a) UV-vis spectra of the reaction of 10 μM TBASH with 10 μM **6.2**. b) UV-vis spectra of the reaction of 10 μM TBASH with 10 μM **6.2** in the presence of 5 equiv. **6.1**. c) Time course data of the absorbance at 570 nm in the presence (blue trace) and absence (red trace) of 5 equiv. **6.1** fit to a 2nd order non-linear regression model (dashed black trace).

Table 6.1. Rate constant and initial starting material concentrations for the reaction of 10 μM TBASH with 10 μM **6.2** in the presence and absence of 5 equiv. **6.1**, calculated by the 2nd order rate equation non-linear regression model.

Equiv. 6.1	Representative results from one trial				k_{ave} ($\text{M}^{-2}\cdot\text{s}^{-1}$)
	k ($\text{M}^{-2}\cdot\text{s}^{-1}$)	[TBASH] ₀ (Abs)	[6.2] ₀ (Abs)	R^2	
0	0.681 ± 0.009	0.270 ± 0.002	0.283 ± 0.002	0.995	0.670 ± 0.008
5	0.44 ± 0.02	0.140 ± 0.002	0.196 ± 0.004	0.994	0.44 ± 0.03

In addition, the initial concentrations for TBASH and **6.2**, calculated by the non-linear regression model, can provide more information about the equilibria and kinetics happening in solution. To the best of our efforts, we keep the TBASH and **6.2** initial

equivalent ($[\text{TBASH}]_0$ and $[\mathbf{6.2}]_0$, respectively), unless otherwise noted. In the absence of **6.1**, the non-linear regression model consistently returns 1.06 ± 0.01 for the ratio of $[\mathbf{6.2}]_0/[\text{TBASH}]_0$, confirming a 1:1 starting concentration equivalency. However, in the presence of 5 equiv. **6.1**, despite aiming for a 1:1 equivalency, the non-linear regression model returns a $[\mathbf{6.2}]_0/[\text{TBASH}]_0$ ratio of 1.406 ± 0.002 , suggesting that 0.4 equiv. of the injected TBASH is not contributing to the rate of reaction in the 2nd order rate equation. This may suggest that the rate of dissociation (k_{off}) of the host-guest complex of $[\mathbf{6.1}\cdot\text{HS}^-]$ is slower than the rate of the reaction. More work to determine k_{on} and k_{off} is required to further explore this idea. Furthermore, $k_{\text{on}}/k_{\text{off}}$ may not be equal to the association equilibrium constant ($K_a \sim 15,000 \text{ M}^{-1}$) if the reaction with NBD-thioether **6.2** proceeds faster than equilibrium can be reached in solution.

Finally, we also studied the kinetics of the reaction in Scheme 6.1 in the presence of 1 equiv. **6.1**. Time course data of the absorbance of reaction product **6.3** was fit to the 2nd order rate equation through non-linear regression. Although each of the three trials are well-fit by the model, k is inconsistent across the three trials (Table 6.2), and at times greater than the rate constant in the absence of a receptor (Table 6.1). We hypothesize that small changes in the absorbance at 570 nm due to host-guest complexation with **6.1** may contribute to more variability at a 1:1 host:guest equivalency. In addition, developing a model which better reflects the k_{on} and k_{off} rate constants is likely more important at a 1:1 host:guest equivalency, and could contribute to more consistent results.

Table 6.2. Rate constant and initial starting material concentrations for the reaction of 10 μM TBASH with 10 μM **6.2** in the presence of 1 equiv. **6.1**, calculated by the 2nd order rate equation non-linear regression model.

Trial	k ($\text{M}^{-2}\cdot\text{s}^{-1}$)	[TBASH] ₀ (Abs)	[6.2] ₀ (Abs)	R ²
1	0.63 ± 0.01	0.241 ± 0.002	0.278 ± 0.003	0.996
2	0.519 ± 0.008	0.380 ± 0.003	0.39 ± 0.01	0.997
3	0.75 ± 0.02	0.278 ± 0.002	0.299 ± 0.003	0.995

6.4 Conclusion and Future Outlook

Inspired by supramolecular hosts which have been shown to stabilize reactive species, we show that receptor **6.1**, which has a strong affinity for HS^- , reduces the reactivity of the anion in organic solvent and slows down the rate of reaction of HS^- towards $\text{S}_{\text{N}}\text{Ar}$ with NBD thioether **6.2**. Although this study serves as a proof of concept, future generations of supramolecular hosts may be used to control the equilibria and product distribution of systems with HS^- as a starting material.

Future work includes further characterizing the kinetics of the reaction with and without the receptor present. Kinetic experiments must be performed to determine k_{on} and k_{off} of the host-guest complex. In addition, work is already underway comparing the effect of **6.1** on the initial rate (v_0) of reaction. Table 6.3 summarizes those results so far. By changing the concentration of **6.1** and keeping TBASH concentration constant we will be able to determine at what point the reaction is saturated by receptor. By changing the concentration of TBASH throughout these studies we will be able to better discern important differences in v_0 stemming from host:guest equivalency.

Finally, this system allows us to compare the effect of different supramolecular receptors on the rate of reaction. In particular, supramolecular host **4.2^D** (a deuterium-labelled isotopologue of **6.1**) was used in Chapter IV to study the deuterium equilibrium isotope effect (DEIE) of a C–H/D hydrogen bond donor on anion binding. Because of the

reactivity of HS^- , we were unable to determine the DEIE of HS^- binding with **4.2^D**; however, the use of a fast, high-precision instrument that could monitor all reactants in solution, such as a reactIR, could provide insight into the rate constants and association constants in Scheme 6.1, and ultimately allow us to determine the DEIE of anion binding through kinetic experiments.

Table 6.3. Initial rates of reaction^a of various concentrations of TBASH and **6.1** with 10 μM **6.2**.

TBASH conc. (μM)	v_0 ($\Delta\text{Abs}/\Delta\text{s}$)				
	0 μM 6.1	10 μM 6.1	20 μM 6.1	50 μM 6.1	100 μM 6.1
0	0	0	0	0	0
2.5	—	—	—	—	—
5	0.008 ± 0.004	—	—	—	—
10	0.020 ± 0.001	0.028 ± 0.005	—	0.0087 ± 0.0004	—
20	—	—	—	—	—

^aRates determined over 6.8 ± 0.1 s.

CHAPTER VII

ARYLETHYNYL UREA ANION RECEPTORS FOR DISRUPTION OF THE HOFMEISTER BIAS IN TETRABUTYLPHOSPHONIUM SALT LIQUID- LIQUID EXTRACTION

This chapter includes unpublished co-authored material from Fargher, H.A.; Haley, M.M.; Johnson, D.W.; Moyer B.A. This manuscript was written by Hazel A. Fargher with editorial assistance by Professors Michael M. Haley and Darren W. Johnson and Dr. Bruce A. Moyer. The project in this chapter was developed by Hazel A. Fargher and Dr. Bruce A. Moyer. The experimental work and data analysis were performed by Hazel A. Fargher with support from Dr. Bruce A. Moyer.

7.1 Introduction

Separation of inorganic salts for purification is a major challenge in industry, mining,^{207,208} environmental remediation,^{209,210} sensing,²¹¹ and waste treatment.^{212,213} Host-mediated liquid-liquid extraction, in which a host is employed in extraction of salt guests from one immiscible liquid to another (typically water and an organic solvent, respectively), has emerged as a powerful technology in the separation of salts.^{214,215} Hosts can be designed to impart selectivity and high binding affinities for extracted salts.²¹⁶

Research into host-mediated liquid-liquid extraction has explored the influence of receptors on cation,^{217–219} anion,⁷⁷ and ion-pair^{220,221} extraction. A significant body of this work has focused on the development and study of cation receptors in liquid-liquid extraction; lagging behind is the study of anion receptors in extraction.²¹⁴ This constitutes a major gap in research in the field of salt extraction and separation. Co-extraction of the

counter anion will strongly influence the extractability and even selectivity of the targeted cation.^{222,223}

Without the presence of a receptor for the counter anion, extraction of a salt from water into an organic phase is strongly related to the hydrophilicity or lipophilicity of the anion. Therefore, salt extraction is highly dependent on the position of the counter anion in the Hofmeister series (an empirical ranking of ions based on their hydrophilicity or lipophilicity) making the selective liquid-liquid extraction of a salt with a hydrophilic counter anion challenging with only a cation receptor.²²² Selective anion receptors with strong binding affinities could disrupt this Hofmeister bias in anion extraction, much in the same way cation receptors have been shown to impart selectivity for specific cations.

In this work, we use previously published arylolethynyl urea anion receptors **7.1** and **7.2** (Figure 7.1a and b, respectively) to study their impact in disrupting the Hofmeister bias in liquid-liquid salt extraction. **7.1** was chosen due to its high affinity for Cl^- ($K_a \sim 7,900$) and NO_3^- ($K_a \sim 5,520$) and simple 1:1 host:guest binding in chloroform.²⁷ **7.2** was chosen for its selectivity for NO_3^- over Cl^- , Br^- , and I^- in 10% $\text{DMSO-}d_6/\text{CDCl}_3$.¹⁸ In addition, the tripodal architecture of **7.2** may be useful for extracting larger oxoanions such as ReO_4^- and TcO_4^- in future work.

7.2 Methods

Anion receptors **7.1** and **7.2** were used in liquid-liquid extraction of tetrabutylphosphonium (TBP^+) salts from water into nitrobenzene. **7.1** and **7.2** have previously been reported and were synthesized according to established methods.^{18,27} TBP^+ salts were chosen for extraction experiments because P concentration in aqueous

solution can be determined by ICP-MS with limits of detection (LOD) in the ppt range and background equivalent concentrations (BEC) in the ppb range. TBP salts were synthesized by reaction of TBPOH with various acids and characterized by ^{31}P NMR (Appendix F). Nitrobenzene was chosen as the extractant solvent to minimize ion-pairing in the organic phase and was purified according to previous methods.²²⁴

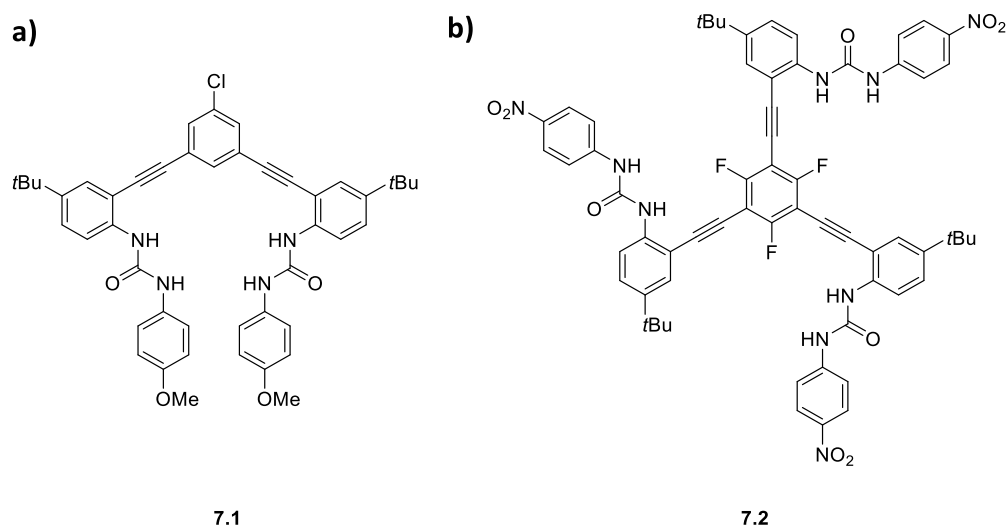


Figure 7.1. Anion receptors chosen for this study.

7.2.1 Liquid-liquid extraction experiments

Aqueous phases of 18 M Ω deionized water contained variable concentrations of TBP salts (TBPX, where X⁻ = Cl⁻, Br⁻, I⁻, and NO₃⁻). The organic phases of nitrobenzene contained variable concentrations of **7.1**, **7.2**, or no receptor. Equal volumes (0.3 mL each) of the organic and aqueous phases were equilibrated by repeated inversion at 8 RPM by a rotator for 2 h. Temperature was held around 25 °C by heating a bead bath beneath the rotator and covering the bead bath, rotator, and headspace with a double layer of aluminum foil. After rotation, samples were centrifuged at 3000 RCF for 20 min at 25

°C in a refrigerated centrifuge. After centrifugation, 0.2 mL of the aqueous phase was removed and prepared for analysis by ICP-MS (Appendix F). All extractions were performed in duplicate or triplicate.

7.3 Results and Discussion

7.3.1 Calculating energy of partitioning for TBP⁺

Gibbs free energy of extraction of dissociated TBPX ions ($\Delta G^{\circ}_{ex\pm}$) in host-mediated liquid-liquid extraction is the sum of Gibbs free energy of partitioning (ΔG°_p) of both TBP⁺ and X⁻ and Gibbs free energy of formation (ΔG°_f) of the host-guest complex (Equation 7.1). Therefore, understanding salt partitioning from water into nitrobenzene is a key first step before studying the effect of an anion receptor on salt extraction. ΔG°_p values for anion partitioning from water into nitrobenzene have been well-documented;²²⁵ however, $\Delta G^{\circ}_p(\text{TBP}^+)$ is so-far unknown. $\Delta G^{\circ}_p(\text{TBPX})$ can be represented as the partition equilibrium constant (K_p) according to Equation 7.2. In the following equations y represents the Debye-Hückel activity coefficients of the species in solution and a bar denotes that the species is in the organic phase.

$$\Delta G^{\circ}_{ex\pm} = \Delta G^{\circ}_p(\text{TBP}^+) + \Delta G^{\circ}_p(\text{X}^-) + \Delta G^{\circ}_f(\text{R}_m\text{X}^-) \quad (7.1)$$

$$\frac{\Delta G^{\circ}_p(\text{TBP}^+) + \Delta G^{\circ}_p(\text{X}^-)}{2.303RT} = \log \left(K_p(\text{TBPX}) \right) = \log \left(\frac{\bar{y}_{\text{TBP}^+} [\overline{\text{TBP}^+}] \bar{y}_{\text{X}^-} [\overline{\text{X}^-}]}{y_{\text{TBP}^+} [\text{TBP}^+] y_{\text{X}^-} [\text{X}^-]} \right) \quad (7.2)$$

The distribution ratio (D_P) is a measure of TBP⁺ concentration in the organic and aqueous phase after extraction and is represented by Equation 7.3. D_P can be substituted into Equation 7.2, thereby relating $\Delta G^{\circ}_p(\text{TBP}^+)$ to D_P .

$$D_P = \frac{[\overline{\text{TBP}^+}]}{[\text{TBP}^+]} = \frac{[\overline{\text{X}^-}]}{[\text{X}^-]} \quad (7.3)$$

Liquid-liquid extractions of various concentrations of TBPX salts were performed with nitrobenzene in the absence of a host. ICP-MS analysis of P concentration in the aqueous phase before and after extraction was used to calculate the distribution ratio in the absence of any receptor ($D_{P,0}$). Experimental $\log(D_{P,0})$ were plotted against initial salt concentration ($[TBPX]_0$) for Cl^- , Br^- , I^- , and NO_3^- . (Figure 7.2a–7.2d, respectively) to reveal that $\log(D_{P,0})$ is independent of salt concentration, consistent with Equation 7.2.

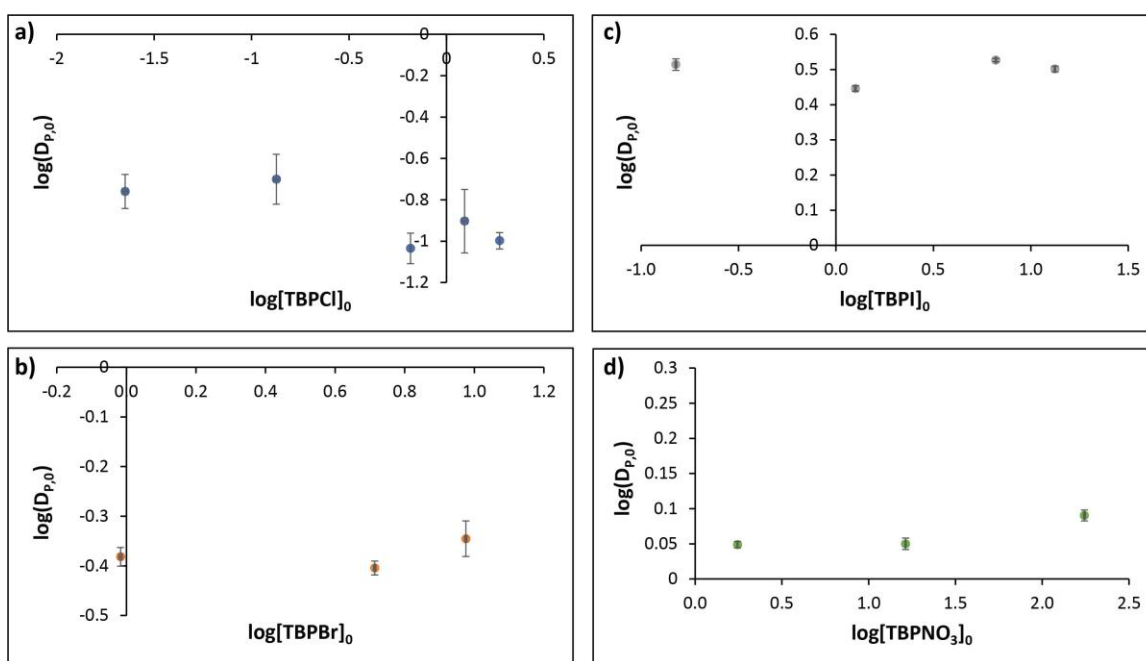


Figure 7.2. Experimentally determined $\log(D_{P,0})$ values vs. $\log[TBPX]_0$ for a) TBPCl, b) TBPBr, c) TBPI, and d) TBPNO₃.

Values for $\log(K_p)$ for TBPCl, TBPBr, TBPI, and TBPNO₃ were calculated from $D_{P,0}$ according to Equation 7.2. An average K_p for each salt was used to independently calculate $\Delta G^\circ_p(TBP^+)$ (Table 7.1). An average of these values reveals a favorable Gibbs free energy of $-24 \pm 1 \text{ kJ mol}^{-1}$ for TBP^+ partitioning from water into nitrobenzene at 25 °C. A large negative partitioning energy means that TBP^+ is a highly lipophilic cation,

making TBP salts an excellent candidate for studying extraction with hydrophilic anions. In addition, TBP^+ is more lipophilic than the tetrabutylammonium (TBA^+) cation which has a ΔG_p° of -9 kJ mol^{-1} , perhaps due to the greater dispersion character of P compared to N. With a value for $\Delta G_p^\circ(\text{TBP}^+)$ we can now study the effect of an anion receptor on the extraction of TBP salts.

Table 7.1. ΔG_p° (TBP^+) calculated from experimental $\log K_p$ for TBPCl, TBPBr, TBPI, and TBPNO₃ partitioning from water into nitrobenzene at 25 °C.

Salt	Average $\log K_p$	$\Delta G_p^\circ (\text{X}^-)$ (kJ mol^{-1}) ²²⁵	$\Delta G_p^\circ (\text{TBP}^+)$ (kJ mol^{-1})
TBPCl	-1.8 ± 0.3	35	-25 ± 1
TBPBr	-0.79 ± 0.04	29	-25 ± 1
TBPI	0.98 ± 0.06	18	-24 ± 1
TBPNO ₃	0.06 ± 0.01	24	-24 ± 1
Average $\Delta G_p^\circ (\text{TBP}^+)$ (kJ mol^{-1})			-24 ± 1

7.3.2 Host-mediated extraction by 7.1

Host-mediated liquid-liquid extraction can be represented as a series of equilibria (Figure 7.3). Under conditions in which ions are dissociated in both phases, the extraction constant of dissociated ions (K_{ex^\pm} , Equation 7.4) is the product of $K_p(\text{TBPX})$ and the formation constant (K_f , Equation 7.5) of anion binding with host R. When initial anion receptor concentration ($[\text{R}]_0$) is much greater than the concentration of TBPX in the organic phase after equilibrium is reached ($[\text{TBPX}]_{\text{org}}$, $\sim 10x$) we can make two key assumptions: 1) $[\text{R}]_0$ is approximately equal to free receptor concentration ($[\text{R}]$); and 2) almost all X^- in the nitrobenzene phase are bound by R, i.e. $D_{\text{P,TBPX}} = [\text{R}_n\text{X}^-]_{\text{org}}/[\text{X}^-]_{\text{aq}}$. With these two key assumptions we can substitute $D_{\text{P,TBPX}}$ into Equation 7.4 and rearrange to give Equation 7.6. Equation 7.6 can be analyzed through linear slope analysis in which $[\text{R}]_0$ is the independent variable and $\log D_{\text{P,TBPX}}$ is the dependent variable.

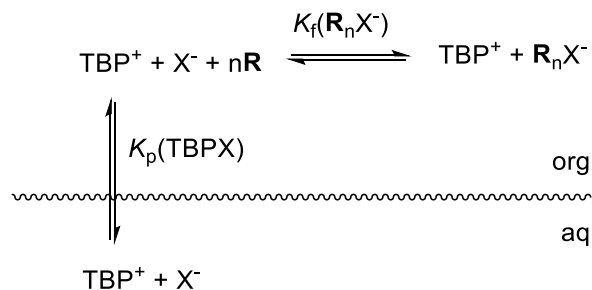


Figure 7.3. Equilibria present in host-mediated liquid-liquid extraction of TBPX salts.

$$K_{ex\pm}(\text{TBPX}) = \frac{\bar{y}_{\text{TBP}^+}[\text{TBP}^+] \bar{y}_{\text{R}_n\text{X}^-}[\text{R}_n\text{X}^-]}{y_{\text{TBP}^+}[\text{TBP}^+] y_{\text{X}^-}[\text{X}^-] (\bar{y}_{\text{R}})^n [\bar{\text{R}}]^n} = K_p \cdot K_f \quad (7.4)$$

$$K_f = \frac{\bar{y}_{\text{R}_n\text{X}^-}[\text{R}_n\text{X}^-]}{y_{\text{X}^-}[\text{X}^-] (\bar{y}_{\text{R}})^n [\bar{\text{R}}]^n} \quad (7.5)$$

$$2 \log D_P = n \log[\bar{\text{R}}] + \log K_{ex\pm} + \log \left(\frac{y_{\text{TBP}^+} \cdot y_{\text{X}^-}}{\bar{y}_{\text{TBP}^+} \cdot \bar{y}_{\text{R}_n\text{X}^-}} \right) \quad (7.6)$$

Liquid-liquid extractions of a fixed concentration of TBPX salts (0.02 – 0.03 mM) were performed with nitrobenzene as the water-immiscible high-dielectric-constant organic diluent in the presence of various concentrations of host **7.1** (1, 0.5, 0.1, 0.07, and 0.05 mM) (See Appendix F). ICP-MS analysis of P concentration in the aqueous phase before and after extraction was used to calculate $D_{P,\text{TBPX}}$. Experimental $\log(D_{P,\text{TBPX}})$ were plotted against free receptor concentration (**[7.1]**) for Cl^- , Br^- , I^- , and NO_3^- (Figures 7.4a–7.4d, respectively) to reveal that $\log(D_{P,\text{TBPX}})$ is linearly related to **[7.1]**, consistent with Equation 7.6. Note, for each data point **[7.1]** was estimated by assuming that the concentration of the host-guest complex is far greater than the concentration of free guest in organic solution and subtracting $n \times [\text{X}^-]_{\text{org}}$ (where n is the binding stoichiometry) from initial receptor concentration, **[7.1]**₀. This assumption becomes weaker at lower **[7.1]**₀.

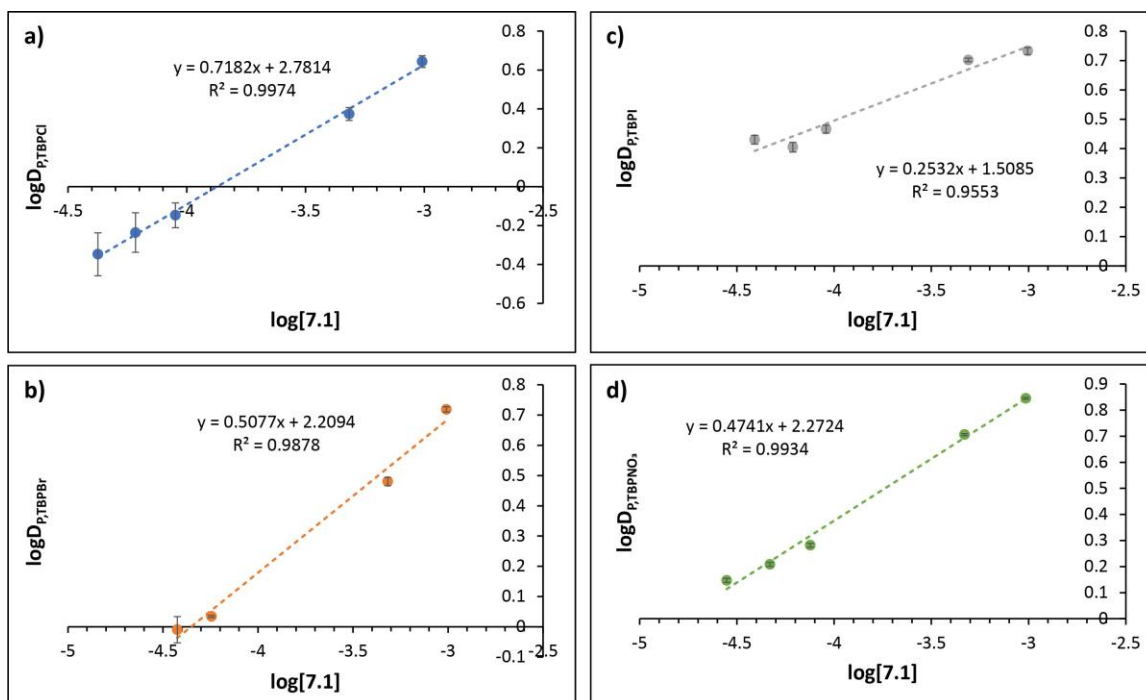


Figure 7.4. Experimentally determined $\log(D_{P,TBPX})$ values vs. $\log[7.1]$ for a) TBPCl, b) TBPBr, c) TBPI, and d) TBPNO₃.

Equations 7.1 and 7.6 and our calculated $\Delta G^\circ_p(\text{TBP}^+)$ were used to determine $K_{\text{ex}\pm}$, $\Delta G^\circ_{\text{ex}\pm}$, host:guest binding stoichiometry, $K_f(\text{R}_n\text{X}^-)$, and $\Delta G^\circ_f(\text{R}_n\text{X}^-)$ (Table 7.2). In cases where a 1:1 host:guest binding stoichiometry is determined (i.e., slope = 0.5, and $n = 1$), $K_f(\text{RX}^-)$ is equal to the association constant (K_a) of 1:1 host-guest formation. Otherwise, $K_f(\text{R}_n\text{X}^-)$ is the product of association constants in the step-wise formation of R_nX^- .

Table 7.2. Experimental values determined through slope analysis for TBPCl, TBPBr, TBPI, and TBPNO₃.

	n	$K_f(\text{R}_n\text{X}^-)$ M⁻¹	$\Delta G^\circ_f(\text{R}_n\text{X}^-)$ (kJ mol⁻¹)	$K_{\text{ex}\pm}$ (M⁻¹)	$\Delta G^\circ_{\text{ex}\pm}$ (kJ mol⁻¹)	R^2_{model}
TBPCl	1.44 ± 0.04	—	—	—	—	0.997
TBPBr	1.02 ± 0.08	900 ± 300	-17.1 ± 0.9	160 ± 60	-12.6 ± 0.9	0.988
TBPI	—	—	—	—	—	—
TBPNO ₃	0.95 ± 0.04	160 ± 30	-13.0 ± 0.5	180 ± 40	-12.6 ± 0.5	0.993

Comparing the binding stoichiometry (n , Table 7.2) of **7.1** with each anion, we see that binding stoichiometry is anion dependent, even among these simpler anions. We were only able to calculate a 1:1 host:guest binding stoichiometry for Br^- and NO_3^- . We found the slope of the linear analysis with Cl^- to be 1.44, suggesting complex binding stoichiometry and may even be indicative of multiple species in solution. Because of this complex binding stoichiometry, we were unable to determine any more extraction parameters with Cl^- . Finally, we were unable to determine a binding stoichiometry with I^- due to low extraction efficiency. We found that at the lowest receptor concentrations (0.05, 0.07, and 0.1 mM), $\log(D_{\text{P,TBPBr}})$ is within error of background extraction by nitrobenzene alone. Therefore, these three points cannot be used in slope analysis. These findings were somewhat unexpected as previous work had determined 1:1 binding stoichiometry with all of these anions with 1 – 5 mM **7.1** and closely related derivatives in CDCl_3 ,^{26,27} 10% $\text{DMSO-}d_6/\text{CD}_3\text{CN}$,^{36,29,35} CH_3CN ,²⁹ and $\text{CD}_2\text{Cl}_2:\text{DMSO-}d_6$ mixtures²⁵ through ^1H NMR and UV-vis spectroscopy titrations. However, previous work also notes an anion-dependence in linear free energy relationships of derivatives of host **7.1** with the halides, nitrate, and hydrochalcogenide anions,^{27,36} perhaps suggesting that host binding stoichiometry and conformation with these anions is more diverse than previously appreciated.

We were only able to determine $K_{\text{f}}(\text{R}_n\text{X}^-)$ values for TBPBr and TBPNO₃, due to their host:guest binding stoichiometry of 1:1. We calculated a $K_{\text{f}}(\text{R}\cdot\text{Br}^-)$ of $900 \pm 300 \text{ M}^{-1}$ and a $K_{\text{f}}(\text{R}\cdot\text{NO}_3^-)$ of $180 \pm 40 \text{ M}^{-1}$ which are similar to K_{a} of Cl^- binding with a derivative of **7.1** in $\text{DMSO-}d_6$,²⁵ an organic solvent with a similar dielectric constant to nitrobenzene (46.7 and 34.8, respectively).

Finally, we calculated $\Delta G^{\circ}_{\text{ex}\pm}$ for TBPBr and TBPNO₃ (Table 7.2) and see some evidence of disruption of the Hofmeister series. Although Br⁻ and NO₃⁻ have different ΔG_p° (29 and 24 kJ mol⁻¹, respectively)²²⁵ they have the same $\Delta G^{\circ}_{\text{ex}\pm}$. This result can only be due to the presence of a receptor, highlighting the utility of future generations of anion receptors in selective extraction of anions, despite their position on the Hofmeister series.

7.3.3 Host-mediated extraction by **7.2**

We also investigated host-mediated liquid-liquid extraction of TBPX salts (0.03–0.06 mM) with variable concentration **7.2** (0.4, 0.1, 0.07, 0.04, 0.004 mM). Due to limitations with host solubility in nitrobenzene (~0.4 mM), and ICP-MS limit of detection and precision for P concentrations in aqueous solution, we were unable to get sufficient data for linear slope analysis; however, analysis of log(D_P) values can still give us valuable information about the influence of **7.2** on salt extraction.

Plotting log(D_{P,TBPX}) vs. log([R]₀/[TBPX]₀) we can more easily compare the effect of **7.2** on distribution ratios of TBPCl, TBPBr, TBPI, and TBPNO₃ (Figure 7.5a). Despite partitioning energies which range from the unfavorable (TBPCl and TBPBr) to the favorable (TBPI), the presence of excess **7.2** (log([R]₀/[TBPX]₀) > 0) result in similar log(D_{P,TBPX}) values across the range of salts. Furthermore, plotting log(D_{P,TBPX}) – log(D_{P,0}) vs. logK_P([R]₀/[TBPX]₀), where D_{P,0} represents the distribution ratio of TBPX salts in the absence of any receptor, shows the increase in the log(D_P) due to anion binding with **7.2** (Figure 7.5b). Figure 7.5b shows that TBPCl enjoys the greatest increase in D_P due to the presence of **7.2**, at all ratios of [R]₀/[TBPX]₀. This is indicative of

stronger binding of Cl^- with **7.2** compared to the other anions, consistent with its greater charge density. D_P values for TBPBr and TBPNO₃ are similarly affected. Binding may be seen to follow the Hofmeister order in Fig. 7.5b. This result is somewhat surprising; we chose to study **7.2** for its selectivity for NO₃⁻ in anion binding in 10% DMSO-*d*₆/CDCl₃. However, selectivity in 10% DMSO-*d*₆/CDCl₃ was found to be due to favorable anion- π interactions between NO₃⁻ and **7.2**. Perhaps this decrease in selectivity for NO₃⁻ in nitrobenzene is indicative of competing anion- π interactions from the solvent. Finally, we see that D_P values for I⁻ are least affected by the presence of **7.2**, suggesting weaker anion binding. While we see that binding follows the Hofmeister order, the order of extraction overall does not follow this order (Fig. 7.5a). Nitrate is most strongly extracted overall.

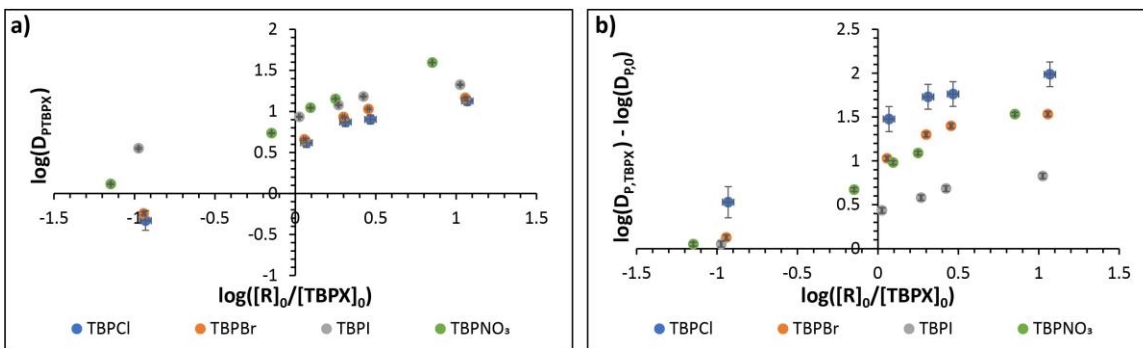


Figure 7.5. a) Comparing the effect of **7.2** on distribution ratios of TBPX salts. b) Plots reveal the contribution of **7.2** towards the distribution ratio of TBPX.

7.4 Conclusion

Host-mediated liquid-liquid extraction has proven a useful method in the separation and purification of salts in industrial, environmental, and waste management settings. In particular, work on cation receptors has now allowed for the selective

extraction of targeted salts, for example the use of cation receptors in the removal of Cs^+ from radioactive waste. Lagging far behind, however, is the use of anion receptors for the selective removal of the counter anion. Development of such receptors could be hugely beneficial in liquid-liquid extraction applications, from helping to improve extraction efficiencies, to targeting anions of interest, and even influencing cation selectivity.

In this work, we study the effect of two previously published arylolethynyl urea receptors on TBPX salt extraction from water into nitrobenzene. Both receptors have previously been shown to bind the halides and NO_3^- in organic solvents, allowing us to study anion receptor effect on a series of TBPX salts with anions from across the Hofmeister series. A tetrabutylphosphonium (TBP^+) counter cation was chosen so that salt distribution ratios could be determined through ICP-MS analysis of phosphorus concentration in aqueous solution.

Herein, we report the Gibbs free energy of partitioning of TBP^+ into nitrobenzene at 25 °C, previously unreported. This value will be useful for other researchers using TBP^+ to study anion extraction. In addition, we show that receptors **7.1** and **7.2** significantly disrupt the anion Hofmeister bias in extraction, and at the highest concentration of receptors (0.4 – 1 mM) studied, we see similar distribution ratios for all TBPX salts, regardless of the hydrophilicity or lipophilicity of the anion. Finally, we explain the equilibria in host-mediated liquid-liquid extraction and show how slope-analysis can be used to determine host-guest binding stoichiometry and the formation equilibrium constant of anion binding. Research and progress in this field should lead to the development of selective extraction of anions through host-mediated liquid-liquid extraction, regardless of the anion's place on the Hofmeister series.

CHAPTER VIII

CONCLUSIONS AND FUTURE OUTLOOK

The research in this thesis highlights the utility of supramolecular host-guest chemistry in both fundamental and application-driven work. Steady advancements in the field of organic synthetic chemistry have given the supramolecular chemist the freedom to design, build, and study the binding properties of almost any supramolecular host. Size, geometry, and non-covalent interactions are all factors that can be tailored in a binding pocket and studied to ask questions about the strength and specificity of host-guest interactions. The careful design of a series of supramolecular hosts allows for physical organic methods to isolate the role of specific non-covalent interactions amongst a mixture of additive and competitive forces. In addition, targeting new and understudied guests can provide insights into their unique supramolecular chemistry, both in biological and abiological settings.

Asking these fundamental questions is an essential first step before useful and relevant applications can be developed. At the time this thesis was written, a search on Google Scholar for “chloride supramolecular ‘anion binding’” returns 4,830 results. This plethora of research has led to innovative applications for Cl^- host-guest chemistry. These include mapping Cl^- concentrations in subcellular organelles,²²⁶ Cl^- transport across cell membranes as a potential therapeutic for disease states such as cystic fibrosis,^{82,83,227} detection of Cl^- in sweat as a non-invasive method to monitor disease,²²⁸ organocatalysis,^{229,230} and even NaCl extraction from water.¹⁰⁷ In Chapters II–IV of this thesis, we use Cl^- binding as a benchmark to understand hydrochalcogenide binding and

in Chapter V, C–H \cdots S contact geometry is compared with C–H \cdots Cl contact geometry to establish the former as an important non-covalent interaction in supramolecular chemistry. Finally, in Chapter VII, we explore how supramolecular receptors can be used to improve Cl $^-$ extraction from water. In contrast, a search on Google Scholar for “hydrosulfide OR hydroselenide OR hydrochalcogenide supramolecular ‘anion binding’” returns 234 results, and we are only aware of three families of supramolecular receptors which have been shown to reversibly bind the hydrochalcogenide anions.^{29,31,32,35,36} As the research on these anions expands, so too should their supramolecular applications.

The work in this thesis has revealed design elements in supramolecular hosts that are both compatible and show a preference for the hydrochalcogenide anions. This is somewhat unusual; although reports have shown the importance of non-covalent interactions in binding with the hydrochalcogenide anions in biology,^{121,122} the high reactivity of these anions can make their supramolecular chemistry challenging to study. We have shown that unreactive and poorly acidic hydrogen bond donors such as urea and amide N–H functional groups are compatible with the nucleophilic, reducing, and basic nature of the hydrochalcogenide anions. In Chapter II we warn of slow addition of the hydrochalcogenide anions to hosts with an alkyne functional group and in Chapter VI demonstrate nucleophilic aromatic substitution of HS $^-$ with sufficiently electron-deficient aromatic rings. Chapters II through IV highlight challenges in studying the host-guest chemistry of HS $^-$ in organic solvent that is contaminated with small amounts of oxygen and water, and over long experiment times. Finally, in Chapter III, we found a preference of a polarized C–H hydrogen bond donor for HS $^-$ over other anions studied, which suggests that future generations of HS $^-$ selective supramolecular hosts should employ this

motif. C–H \cdots S hydrogen bonds may already be a key factor in a published chemical field-effect transistor for HS $^-$ detection in aqueous solution²³¹ and has inspired the use of our supramolecular receptors in an ion-selective electrode.²³²

Despite these advances in our understanding of hydrochalcogenide anion binding, we are still lagging far behind the extensive work on Cl $^-$ binding. The S–H and Se–H bonds in the hydrochalcogenide anions set them apart from other spherical mono-atomic anions such as the halides. In addition, the hydridic nature of these hydrogens differ from other protic anions. We do not believe that these hydrogens interact with traditional hydrogen bond acceptors. On the contrary, in Chapters II and III we show that the hydrochalcogenide hydrogens have chemical shifts in the hydride region of ^1H NMR spectra and shift upfield upon binding with a supramolecular host. A greater understanding of the behavior and character of these hydrogens during host-guest binding can inform design rules for the geometry and types of non-covalent interactions used in future host binding pockets.

Other binding motifs such as anion $\cdots\pi$ interactions and σ -hole interactions such as halogen, chalcogen, and pnictogen bonding, need to be explored further for compatibility and binding strength. Solvent studies to understand the effect of solvation, polarity, and solvent hydrogen bonding on the supramolecular chemistry of HS $^-$ and HSe $^-$ are needed to eventually translate understanding of synthetic supramolecular host-guest chemistry to protein-ligand interactions in biological settings. Finally, further EIE studies are needed to elucidate how binding affects the vibrational energy of the bonds present in both host and guest.

In conclusion, we have demonstrated that aryl ethynyl urea anion receptors provide a versatile and modifiable scaffold for supramolecular host-guest binding with a variety of guests, from the well-behaved halide anions, to large protic oxoanions, and the highly reactive and understudied hydrochalcogenide anions. In using these receptors to understand the fundamental supramolecular host-guest chemistry of the hydrochalcogenide anions, we have explored compatible and preferable hydrochalcogenide binding motifs which inform the design of supramolecular hosts in future applications. The insights gained from expanding the scope of supramolecular anion binding to the hydrochalcogenide anions should inspire future work on other understudied biologically relevant anions and small molecules such as nitrosopersulfide (SSNO^-) and nitroxyl (HNO), respectively.

APPENDIX A

SUPPLEMENTARY CONTENT FOR CHAPTER II

Experimental Details

Materials and Methods.

All manipulations were performed under an inert atmosphere using an Innovative Atmospheres N₂-filled glove box unless otherwise noted. All reagents were purchased from commercial sources and used as received, unless otherwise noted. Solvents were degassed by sparging with Ar followed by passage through a Pure Process Technologies solvent purification system to remove water and stored over 4Å molecular sieves in an inert atmosphere glove box. CD₃CN and DMSO-d₆ were distilled from calcium hydride then deoxygenated by three freeze-pump-thaw cycles and stored in an inert atmosphere glove box. Tetrabutylammonium hydrosulfide (NBu₄(SH))⁷⁰ and host **2.1**^{IBu} were all synthesized according to previous reports.^{27,70} Note: Hydrogen sulfide, hydrogen selenide, and related salts are highly toxic and should be handled carefully to avoid exposure. MS was collected on a Xevo Waters ESI LC/MS instrument. The following naming conventions were used to describe NMR couplings: (s) singlet, (d) doublet, (t) triplet, (q) quartet, (dd) doublet of doublets, (m) multiplet, (b) broad.

Guest and Receptor Synthesis.

Tetrabutylammonium hydroselenide (NBu₄SeH). This preparation was adapted from previous reports.⁶⁹ NBu₄BH₄ (0.743 g, 2.90 mmol) was dissolved in dry CH₃CN (10 mL) and treated with Se⁰ (0.242 g, 3.10 mmol) in a dry box. After stirring for 7 d, the solvent was removed *in vacuo* and the resulting yellow oil was washed with THF. The resulting white powder was filtered using a fine porosity glass-fritted funnel and redissolved in CH₃CN and layered under Et₂O to afford colorless crystals (0.152 g, 0.500 mmol, 16% yield). ¹H NMR (600 MHz, CD₃CN) δ: 3.09 (m, 8H), 1.60 (p, *J* = 7.9 Hz, 8H), 1.35 (h, *J* = 7.3 Hz, 8H), 0.97 (t, *J* = 7.4 Hz, 12H), -6.61 (SeH, s, 1H). ¹³C{¹H} NMR (150 MHz, CD₃CN) δ: 59.3, 24.32, 20.34, 13.79.

N,N',N''-(Nitrilotris(ethane-2,1-diyl))tris(3,5-bis(trifluoromethyl)benzamide) (2.2^{CF3}).

This preparation was adapted from previous reports.^{31,233} Tris(2-aminoethyl)amine (0.0770 g, 0.530 mmol) and NaOH (0.230 g, 5.75 mmol) were dissolved in H₂O (20 mL), and a solution of 3,5-bis(trifluoromethyl)benzoyl chloride (0.437 g, 1.58 mmol) in ethyl acetate (EtOAc, 20 mL) was added dropwise and the reaction mixture was stirred overnight under N₂ at room temperature. The organic layer was washed three times with H₂O (30 mL) then dried with Na₂SO₄. After filtration, the solvent was removed under vacuum to afford a white powder (0.246 g, 54% yield). ¹H NMR (600 MHz, DMSO-*d*₆) δ: 8.86 (NH, t, *J* = 5.5 Hz, 3H), 8.29 (s, 6H), 8.14 (s, 3H), 3.34 (q, *J* = 5.9 Hz, 6H), 2.75 (t, *J* = 6.2 Hz, 6H). ¹³C{¹H} NMR (150 MHz, DMSO-*d*₆) δ: 163.36, 136.37, 130.14 (q, *J* = 33.3 Hz), 127.78, 124.49, 122.98 (q, *J* = 272.8 Hz), 53.44, 38.10.

NMR Studies.

General Methods. NMR spectra were acquired on a Bruker Avance-III-HD 600 spectrometer with a Prodigy multinuclear broadband cryoProbe at 25.0 °C or on a Varian 500 MHz spectrometer. Chemical shifts are reported in parts per million (δ) and are referenced to residual solvent resonances (CD_3CN ^1H 1.94 ppm, $^{13}\text{C}\{^1\text{H}\}$ 118.26 ppm and $\text{DMSO-}d_6$ ^1H 2.50 ppm, $^{13}\text{C}\{^1\text{H}\}$ 39.52 ppm).

General Procedure for NMR Titrations. Method A. A solution of host in 10% $\text{DMSO-}d_6/\text{CD}_3\text{CN}$ or CD_3CN (1.8-2.2 mM, 3 mL) was prepared and 500 μL was added to a septum-sealed NMR tube. The remaining host solution (2.5 mL) was used to prepare a host/guest (10-25 mM) stock solution. Aliquots of the host/guest solution were added to the NMR tube using Hamilton gas-tight syringes, and ^1H NMR spectra were recorded at 25 °C after each addition of guest. The $\Delta\delta$ of the various NH and aromatic CH protons were used to follow the progress of the titration, and association constants were determined using the Thordarson method.^{71,72}

Method B. A solution of receptor **2.1^{tBu}** in 10% $\text{DMSO-}d_6/\text{CD}_3\text{CN}$ (0.8-1.2 mM) was prepared and 500 μL was added to a septum-sealed NMR tube. A stock solution of guest (NBu_4SeH) was prepared in 10% $\text{DMSO-}d_6/\text{CD}_3\text{CN}$ (18.6-27.0 mM). Aliquots of the guest solution were added to the NMR tube using Hamilton gas-tight syringes, and ^1H NMR spectra were recorded at 25 °C after each addition of guest. The $\Delta\delta$ of the NH and

the central aromatic CH proton was used to follow the progress of the titration, and association constants were determined using the Thordarson method.^{71,72}

Decomposition Studies with 2.1^{tBu} and HSe⁻. Stock solutions in 10% DMSO-*d*₆/CD₃CN of **2.1^{tBu}** (2 mM,) and NBu₄(SeH) (25 mM) were prepared. A septum sealed NMR tube was charged with 500 μL of the **2.1^{tBu}** solution. 20 equiv. NBu₄SeH was added to the receptor solution using a Hamilton gas-tight syringe, and the δ of the NH and various aromatic CH protons were monitored by ¹H NMR at 25 °C to determine the effect of HSe⁻ binding on **2.1^{tBu}** (Figure A.3). These samples were then collected and the solvent removed under vacuum for MS analysis.

HSe⁻ Binding Reversibility Studies with 2.1^{tBu} and Zn(OAc)₂. Stock solutions in 10% DMSO-*d*₆/CD₃CN of receptor **2.1^{tBu}** (2 mM,) and NBu₄SeH (11 mM) were prepared, as was a stock solution of Zn(OAc)₂ (78 mM) in DMSO-*d*₆. A septum sealed NMR tube was charged with 500 μL of **2.1^{tBu}**. After 6 equiv. NBu₄SeH was added using a Hamilton gas-tight syringe, the δ of the NH and various aromatic CH protons were monitored by ¹H NMR at 25 °C over the course of 3 h. (Figure A.5) 20 equiv. Zn(OAc)₂ was added using a Hamilton gas-tight syringe to determine the effect of Zn(OAc)₂ on HSe⁻ binding.

HSe⁻ Binding Reversibility Studies with 2.2^{CF3} and Zn(OAc)₂. Stock solutions in 10% DMSO-*d*₆/CD₃CN of **2.2^{CF3}** (2 mM,), NBu₄SeH (20 mM), and Zn(OAc)₂ (40 mM) were prepared. A septum sealed NMR tube was charged with 350 μL of the **2.2^{CF3}** solution,

then 2 equiv. NBu₄SeH and 12 equiv. Zn(OAc)₂ were sequentially added using Hamilton gas-tight syringes. The δ of the NH and various aromatic CH protons were monitored by ¹H NMR at 25 °C to determine the effect of Zn(OAc)₂ on HSe⁻ binding.

X-ray Crystallography

General Methods. Diffraction intensities for NBu₄SeH, **2.2**^{CF₃}, and NBu₄[**2.1**^{tBu}(SeH)] were collected at 173 K on a Bruker Apex2 CCD diffractometer using CuK α radiation, $\lambda = 1.54178$ Å. Space groups were determined based on systematic absences (NBu₄SeH, NBu₄[**2.1**^{tBu}(SeH)]) and intensity statistics (**2.2**^{CF}). Absorption corrections were applied by SADABS.²³⁴ Structures were solved by direct methods and Fourier techniques and refined on F^2 using full matrix least-squares procedures. All non-H atoms were refined with anisotropic thermal parameters. H atoms in all structures were refined in calculated positions in a rigid group model, except the H atom bonded to the Se atom in NBu₄SeH. Position of this H atom was found on the residual density map and refined with isotropic thermal parameters. Solvent molecules (hexane in **2.2**^{CF₃} and diethyl ether in NBu₄[**2.1**^{tBu}(SeH)]) fill out a large empty space between the main molecules in the packing. They are highly disordered and were treated by SQUEEZE.²³⁵ The corrections of the X-ray data by SQUEEZE are 132 and 212 electron/cell; the expected values are 100 and 168 electron/cell, respectively, for **2.2**^{CF₃} and NBu₄[**2.1**^{tBu}(SeH)]. Due to a lot of disordered -CF₃ groups in the structure of **2.2**^{CF₃}, diffraction at high angles from crystals of this compound is very weak and reflection statistics at high angles are poor. Even using a strong *Incoatec* I μ S Cu source it was possible to collect data only up to $2\theta_{\max} =$

99.98°. However, diffraction data collected for **2.2**^{CF₃} provide appropriate numbers of measured reflections per refined parameters: 8261 per 1118. Thermal parameters for the F atoms in the disordered –CF₃ groups are significantly elongated displaying their significant disorder. Diffraction data for NBu₄[**2.1**^{tBu}(SeH)] has been collected up to $2\theta_{\max} = 133.46^\circ$ but reflection at high angles are also very weak due to disordered terminal groups in a counter-ion NBu₄ and solvent Et₂O molecule. The disordered fragments have been refined with restrictions on its geometry and using RIGU option in SHELXL. All calculations were performed by the Bruker SHELXL-2014 package.²³⁶

In contrast to the structure of NBu₄SH,⁷⁰ determined in high symmetry *R-3c* with the H atom at the S atom disordered over several positions, the structure of NBu₄SeH was determined in monoclinic system with one position for the H atom on the Se atom. The difference in size of the S and Se atoms appear to provide the difference in crystal packing and as a result crystal symmetry in case of the Se atom is reduced from hexagonal to monoclinic.

Table A.1. Crystallographic data for NBu₄SeH, **2.2**^{CF₃}, and NBu₄[**2.1**^{tBu}(SeH)].

	NBu ₄ SeH	2.2 ^{CF₃}	NBu ₄ [2.1 ^{tBu} (SeH)]
formula	C ₁₆ H ₃₇ NSe	C ₃₆ H ₃₁ F ₁₈ N ₄ O ₃	C ₇₄ H ₁₁₁ N ₅ O ₆ Se
fw	322.42	909.65	1245.63
T (K)	173(2)	173(2)	173(2) K
crystal system	Monoclinic	Triclinic	Monoclinic
space group	<i>C2/c</i>	<i>P-1</i>	<i>P2₁/n</i>
a (Å)	14.1628(5)	13.8015(7)	9.5547(4)
b (Å)	14.0547(5)	18.0488(9)	30.3155(13)
c (Å)	19.8443(7)	18.1383(9)	26.1228(10)
α (°)	90	103.008(3)	90
β (°)	110.832(2)	102.996(3)	90.476(2)
γ (°)	90	105.924(3)	90
Z	8	4	4
V (Å³)	3691.9(2)	4030.4(4)	7566.4(5)
δ_{calc} (mg/m³)	1.160	1.499	1.093
indep. reflections	3260	8261	13148
R1	0.0442	0.0656	0.0921
R1(I>2σ(I))	0.0722	0.0899	0.1124
wR2	0.1118	0.1674	0.2381
GOF	1.025	1.047	1.050
max/min res. e⁻ den. (eÅ⁻³)	+0.377/-0.337	+0.672/-0.343	+1.061/-0.814
CCDC#	1846890	1846891	1846892

$$wR2 = [\Sigma[w(F_o^2 - F_c^2)^2] / \Sigma[w(F_o^2)^2]]^{1/2}$$

$$R1 = \Sigma||F_o| - |F_c|| / \Sigma|F_o|$$

GOF = S = $[\Sigma[w(F_o^2 - F_c^2)^2] / (n-p)]^{1/2}$ where n is the number of reflections and p is the total number of parameters refined.

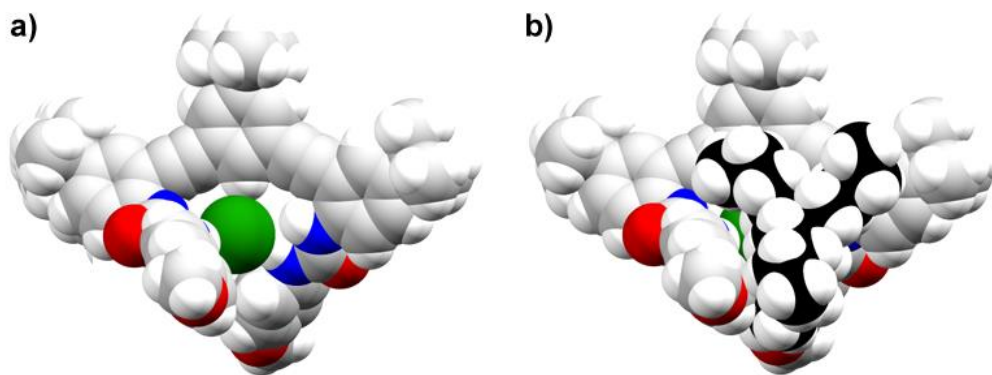


Figure A.1. Space-filling model of (a) [2.1^{tBu}(SeH)]⁻ and (b) NBu₄⁺ [2.1^{tBu}(SeH)], (C atoms of NBu₄⁺ in black) demonstrating that the aliphatic C–H bonds of NBu₄⁺ counterion interacts with the bound HSe⁻ anion.

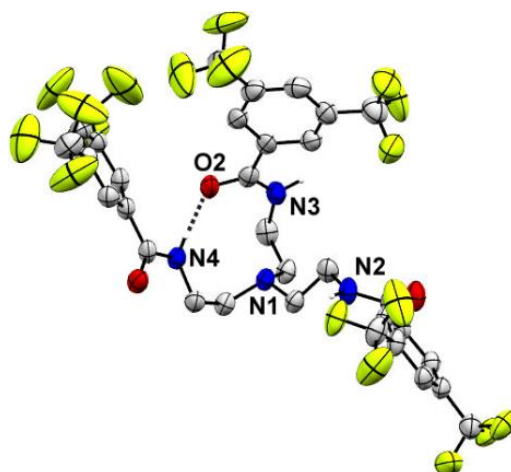


Figure A.2. Thermal ellipsoid diagram (at 50% probability) depicting the molecular structure of 2.2^{CF3}. Only N–H hydrogen atoms are shown for clarity.

NMR Studies

Decomposition Studies with 2.1^{tBu} and HSe⁻. Stock solutions in 10% DMSO-*d*₆/CD₃CN of 2.1^{tBu} (2 mM,) and NBu₄(SeH) (25 mM) were prepared. A septum sealed NMR tube was charged with 500 μL of the 2.1^{tBu} solution. 20 equiv. NBu₄SeH was added to the receptor solution using a Hamilton gas-tight syringe, and the δ of the NH and various aromatic CH protons were monitored by ¹H NMR at 25 °C to determine the effect of HSe⁻ binding on 2.1^{tBu} (Figure A.3).

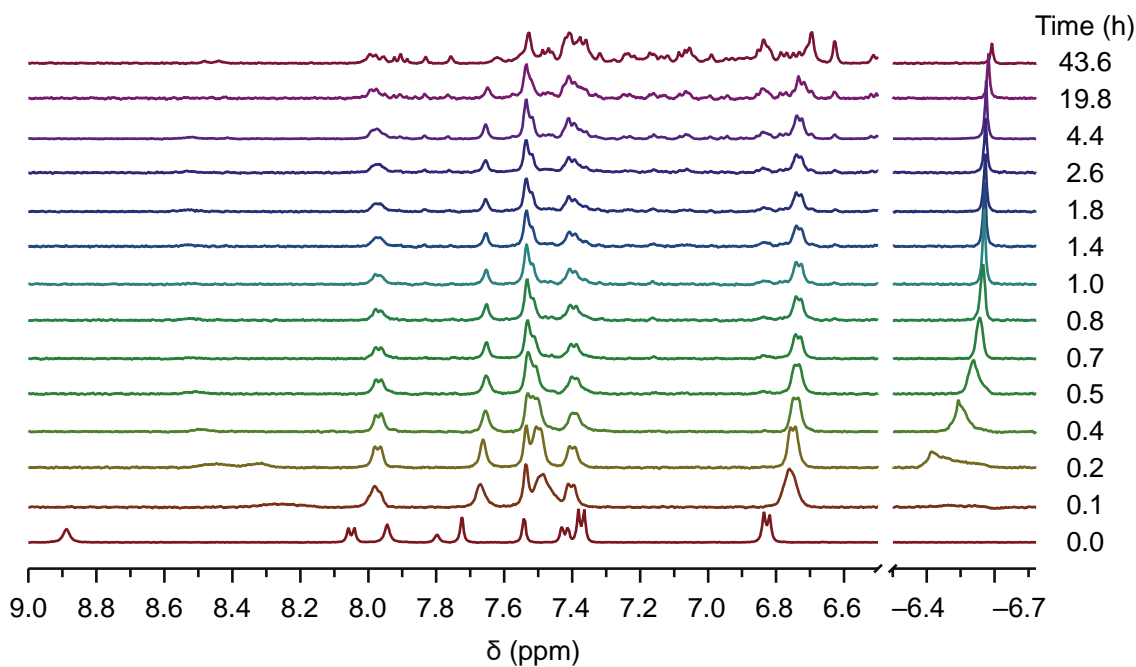


Figure A.3. Stacked ¹H spectrum of receptor 2.1^{tBu} and subsequent decomposition over 43 h upon addition of 20 equiv. NBu₄SeH.

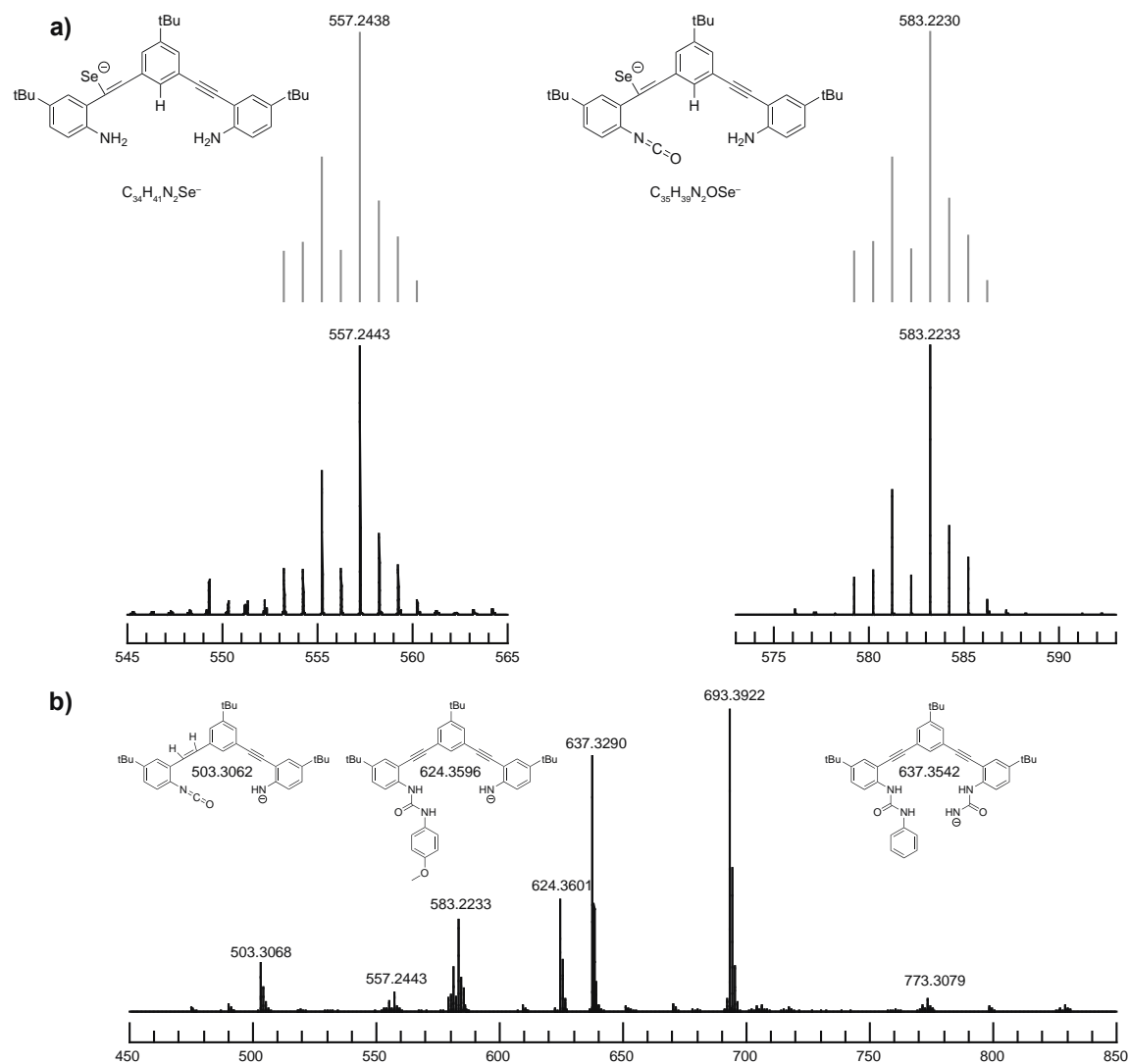


Figure A.4. (a) Zoomed MS (negative mode, ESI) of further reacted products, with the proposed identity of these fragments, from the reaction of receptor **2.1^{tBu}** with 20 equiv. NBu_4SeH . Simulated spectra are in grey above the experimental spectra. (b) Full MS (negative mode, ESI) with the proposed identity of certain peaks specified.

HSe⁻ Binding Reversibility Studies with 2.1^{tBu} and Zn(OAc)₂. Stock solutions in 10% DMSO-*d*₆/CD₃CN of receptor **2.1^{tBu}** (2 mM,) and NBu₄SeH (11 mM) were prepared, as was a stock solution of Zn(OAc)₂ (78 mM) in DMSO-*d*₆. A septum sealed NMR tube was charged with 500 μL of **2.1^{tBu}**. After 6 equiv. NBu₄SeH was added using a Hamilton gas-tight syringe, the δ of the NH and various aromatic CH protons were monitored by ¹H NMR at 25 °C over the course of 3 h. (Figure A.5) 20 equiv. Zn(OAc)₂ was added using a Hamilton gas-tight syringe to determine the effect of Zn(OAc)₂ on HSe⁻ binding.

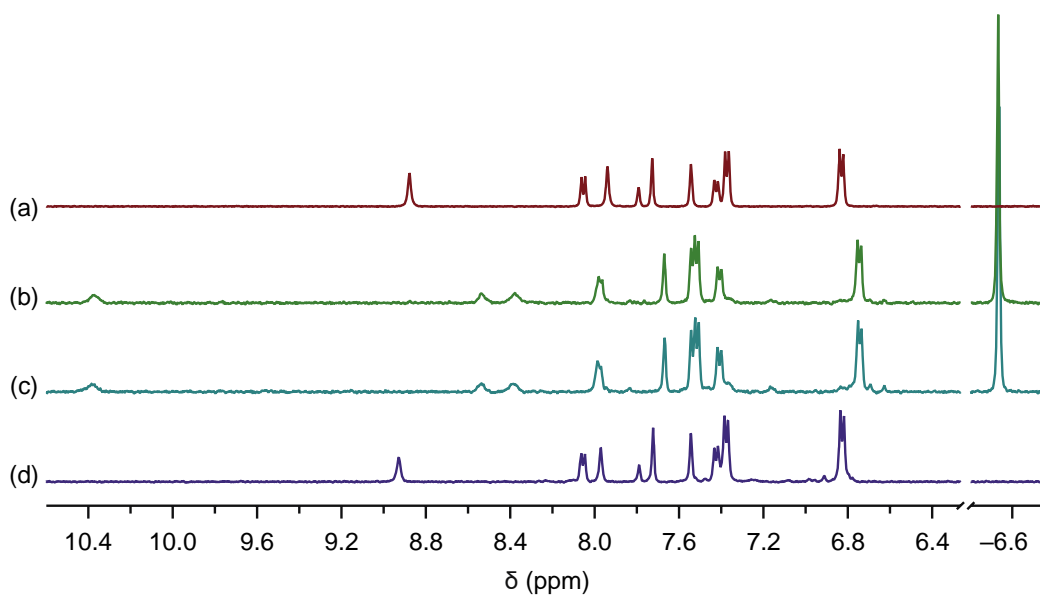


Figure A.5. (a) ¹H spectrum of unbound **2.1^{tBu}**. (b) ¹H spectrum of **2.1^{tBu}** bound with HSe⁻ after 1 h and (c) after 3 h. (d) Addition of Zn(OAc) shows a return to the original, unbound spectrum of **2.1^{tBu}**, demonstrating reversibility.

HSe⁻ Binding Reversibility Studies with 2.2^{CF3} and Zn(OAc)₂. Stock solutions in 10% DMSO-*d*₆/CD₃CN of **2.2^{CF3}** (2 mM), NBu₄SeH (20 mM), and Zn(OAc)₂ (40 mM) were prepared. A septum sealed NMR tube was charged with 350 μL of the **2.2^{CF3}** solution, then 2 equiv. NBu₄SeH and 12 equiv. Zn(OAc)₂ were sequentially added using Hamilton gas-tight syringes. The δ of the NH and various aromatic CH protons were monitored by ¹H NMR at 25 °C to determine the effect of Zn(OAc)₂ on HSe⁻ binding.

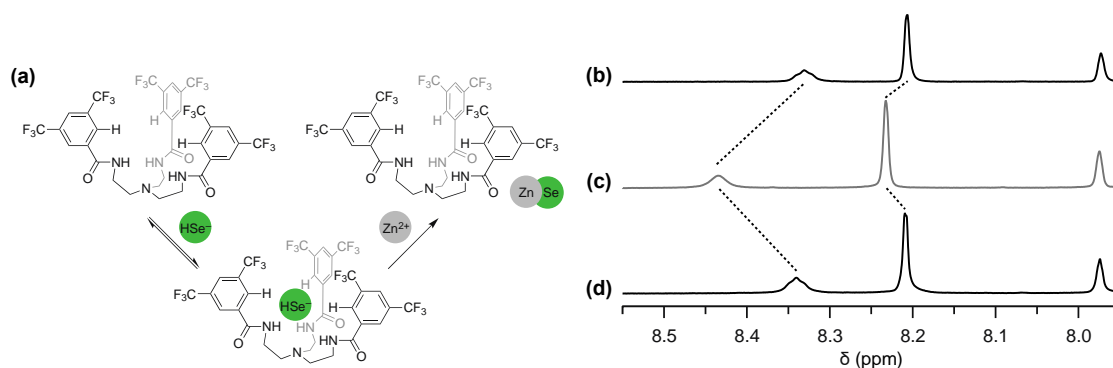


Figure A.3. (a) Molecular depiction of Zn extrusion to show reversibility of receptor **2.2^{CF3}**. (b) ¹H spectrum of unbound **2.2^{CF3}**. (c) ¹H NMR spectrum of **2.2^{CF3}** bound with HSe⁻. (d) Addition of Zn(OAc)₂ shows a return to the original, unbound spectrum of **2.2^{CF3}**, demonstrating reversibility.

^1H NMR Data

Table A.2. Representative titration of receptor **2.1^{tBu}** with HSe^- in 10% $\text{DMSO-}d_6/\text{CD}_3\text{CN}$.

Entry	V_{Guest} (μL)	$[\text{Host}]$ (M)	$[\text{HSe}^-]$ (M)	Equiv.	δNH_f (ppm)	δNH_g (ppm)	δCH_a (ppm)
0	0	2.0E-03	0.0E+00	0.00	8.873	7.937	7.790
1	5	2.0E-03	2.7E-04	0.13	8.991	7.969	7.854
2	10	2.0E-03	5.3E-04	0.27	9.098	8.000	7.906
3	15	2.0E-03	7.9E-04	0.40	9.187	8.028	7.950
4	25	1.9E-03	1.3E-03	0.67	9.343	8.071	8.035
5	35	1.9E-03	1.8E-03	0.94	9.475	8.101	8.101
6	55	1.8E-03	2.7E-03	1.47	9.670	8.165	8.201
7	95	1.7E-03	4.3E-03	2.55	9.913	8.229	8.327
8	145	1.6E-03	6.1E-03	3.89	10.078	8.274	8.405
9	205	1.4E-03	7.8E-03	5.50	10.176	8.312	8.456
10	265	1.3E-03	9.3E-03	7.10	10.254	8.336	8.489
11	325	1.2E-03	1.1E-02	8.71	10.307	8.354	8.507
12	385	1.1E-03	1.2E-02	10.32	10.331	8.361	8.516
13	485	1.0E-03	1.3E-02	13.00	10.367	8.380	8.525

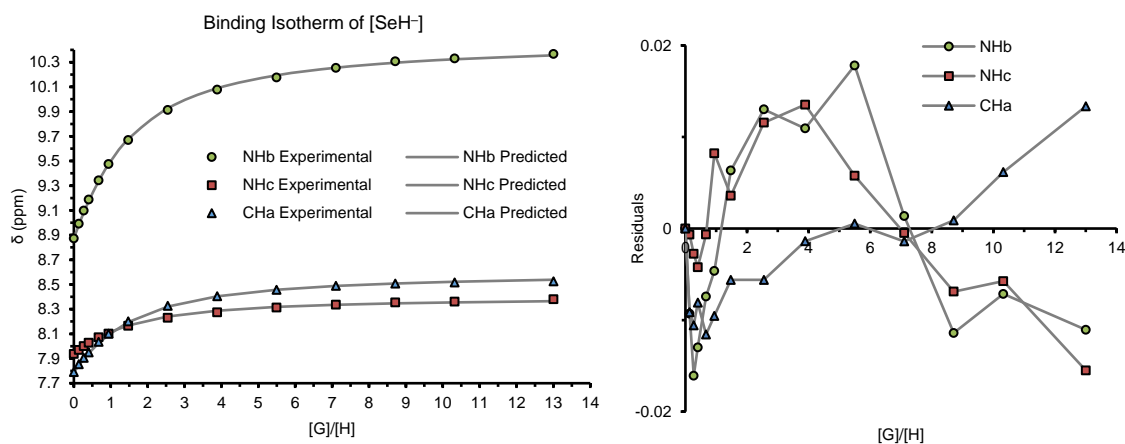


Figure A.7. Representative binding isotherm for HSe^- titration of receptor **2.1^{tBu}** in 10% $\text{DMSO-}d_6/\text{CD}_3\text{CN}$ determined by ^1H NMR spectroscopy.

Table A.3. Representative titration of receptor **2.1^{tBu}** with HS⁻ in 10% DMSO-*d*₆/CD₃CN.

Entry	V _{Guest} (μL)	[Host] (M)	[HS ⁻] (M)	Equiv.	δ NH _f (ppm)	δ NH _g (ppm)	δ CH _a (ppm)
0	0	1.0E-03	0.0E+00	0.00	8.868	7.934	7.790
1	5	1.0E-03	1.8E-04	0.18	9.205	8.003	7.969
2	10	1.0E-03	3.6E-04	0.36	9.507	8.060	8.153
3	15	1.0E-03	5.3E-04	0.53	9.770	8.116	8.313
4	20	1.0E-03	7.0E-04	0.70	9.999	8.161	8.448
5	30	1.0E-03	1.0E-03	1.04	10.363	8.233	8.644
6	40	1.0E-03	1.4E-03	1.36	10.580	8.282	8.758
7	50	1.0E-03	1.7E-03	1.67	10.723	8.314	8.835
8	65	1.0E-03	2.1E-03	2.11	10.857	8.340	8.908
9	80	1.0E-03	2.5E-03	2.53	10.944	8.361	8.953
10	95	1.0E-03	2.9E-03	2.93	10.993	8.373	8.963
11	115	1.0E-03	3.4E-03	3.43	11.036	8.385	8.970
12	140	1.0E-03	4.0E-03	4.01	11.080	8.410	9.002
13	170	1.0E-03	4.7E-03	4.65	11.110	8.407	9.005
14	210	1.0E-03	5.4E-03	5.42	11.130	8.419	9.005
15	260	1.0E-03	6.3E-03	6.27	11.155	8.413	9.013
16	360	1.0E-03	7.7E-03	7.67	11.174	8.434	9.022
17	510	1.0E-03	9.3E-03	9.25	11.206	8.445	9.032
18	710	1.0E-03	1.1E-02	10.75	11.223	8.467	9.028

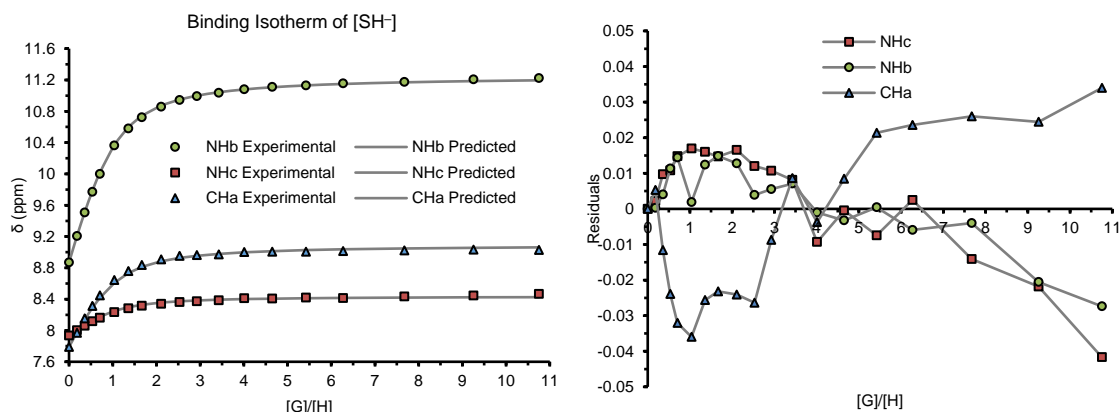


Figure A.4. Representative binding isotherm for HS⁻ titration of receptor **2.1^{tBu}** in 10% DMSO-*d*₆/CD₃CN determined by ¹H NMR spectroscopy.

Table A.2. Representative titration of receptor **2.1^{tBu}** with Br⁻ in 10% DMSO-*d*₆/CD₃CN.

Entry	V _{Guest} (μL)	[Host] (M)	[Br ⁻] (M)	Equiv.	δ NH _f (ppm)	δ NH _g (ppm)	δ CH _a (ppm)
0	0	1.0E-03	0.0E+00	0.00	8.878	7.936	7.797
1	5	1.0E-03	2.5E-04	0.25	8.906	7.941	7.820
2	10	1.0E-03	4.9E-04	0.49	8.923	7.945	7.836
3	15	1.0E-03	7.2E-04	0.72	8.946	7.947	7.854
4	20	1.0E-03	9.5E-04	0.95	8.967	7.952	7.875
5	30	1.0E-03	1.4E-03	1.40	9.003	7.956	7.906
6	40	1.0E-03	1.8E-03	1.83	9.035	7.962	7.939
7	50	1.0E-03	2.3E-03	2.25	9.069	7.965	7.965
8	65	1.0E-03	2.9E-03	2.85	9.108	7.971	8.002
9	80	1.0E-03	3.4E-03	3.41	9.143	7.976	8.033
10	95	1.0E-03	4.0E-03	3.95	9.177	7.982	8.066
11	115	1.0E-03	4.6E-03	4.63	9.214	7.987	8.105
12	135	1.0E-03	5.3E-03	5.26	9.247	7.991	8.132
13	160	1.0E-03	6.0E-03	6.00	9.281	7.995	8.164
14	190	1.0E-03	6.8E-03	6.82	9.318	8.001	8.196
15	225	1.0E-03	7.7E-03	7.68	9.352	8.006	8.225
16	265	1.0E-03	8.6E-03	8.58	9.385	8.011	8.256
17	315	1.0E-03	9.6E-03	9.57	9.420	8.016	8.289
18	375	1.0E-03	1.1E-02	10.61	9.455	8.022	8.316
19	455	1.0E-03	1.2E-02	11.79	9.488	8.022	8.345
20	555	1.0E-03	1.3E-02	13.02	9.516	8.030	8.367
21	695	1.0E-03	1.4E-02	14.40	9.530	8.036	8.383
22	885	1.0E-03	1.6E-02	15.82	9.560	8.036	8.410

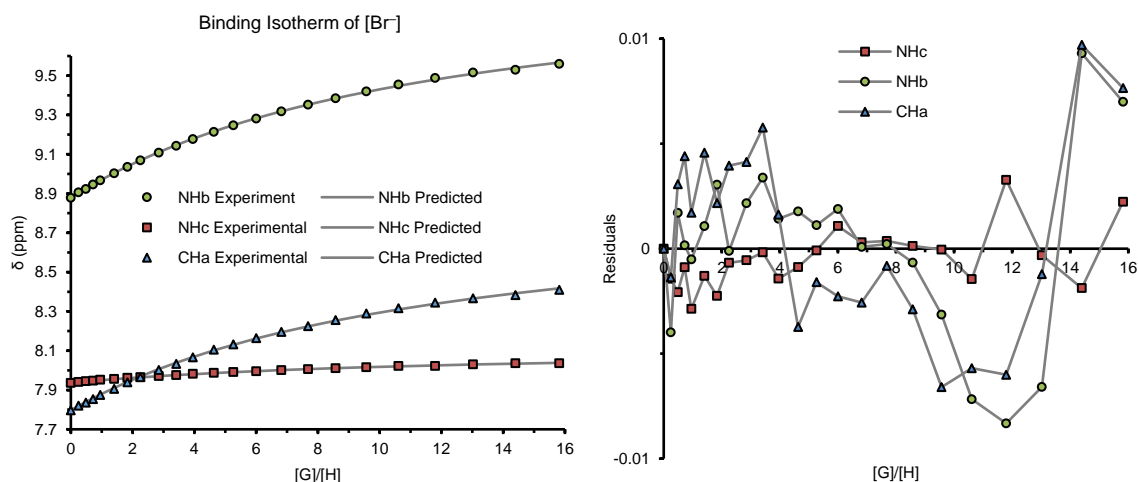


Figure A.5. Representative binding isotherm for Br⁻ titration of receptor **21^{tBu}** in 10% DMSO-*d*₆/CD₃CN determined by ¹H NMR spectroscopy.

Table A.5. Representative titration of receptor **2.1^{tBu}** with Cl⁻ in 10% DMSO-*d*₆/CD₃CN.

Entry	V _{Guest} (μL)	[Host] (M)	[Cl ⁻] (M)	Equiv.	δ NH _f (ppm)	δ NH _g (ppm)	δ CH _a (ppm)
0	0	8.8E-04	0.0E+00	0.00	8.866	7.934	7.788
1	5	8.8E-04	2.0E-04	0.23	9.083	7.956	7.969
2	10	8.8E-04	4.0E-04	0.45	9.256	7.973	8.117
3	15	8.8E-04	5.9E-04	0.67	9.397	7.989	8.238
4	20	8.8E-04	7.7E-04	0.88	9.514	8.001	8.336
5	30	8.8E-04	1.1E-03	1.30	9.696	8.018	8.484
6	40	8.8E-04	1.5E-03	1.70	9.820	8.031	8.593
7	50	8.8E-04	1.8E-03	2.09	9.910	8.039	8.667
8	65	8.8E-04	2.3E-03	2.64	10.006	8.050	8.746
9	80	8.8E-04	2.8E-03	3.17	10.069	8.061	8.800
10	100	8.8E-04	3.4E-03	3.83	10.130	8.062	8.847
11	125	8.8E-04	4.0E-03	4.59	10.181	8.073	8.891
12	155	8.8E-04	4.8E-03	5.43	10.219	8.080	8.920
13	195	8.8E-04	5.7E-03	6.44	10.259	8.082	8.946
14	245	8.8E-04	6.6E-03	7.55	10.293	8.090	8.969
15	345	8.8E-04	8.2E-03	9.38	10.328	8.100	8.988
16	495	8.8E-04	1.0E-02	11.42	10.361	8.108	9.006
17	695	8.8E-04	1.2E-02	13.36	10.374	8.114	9.013

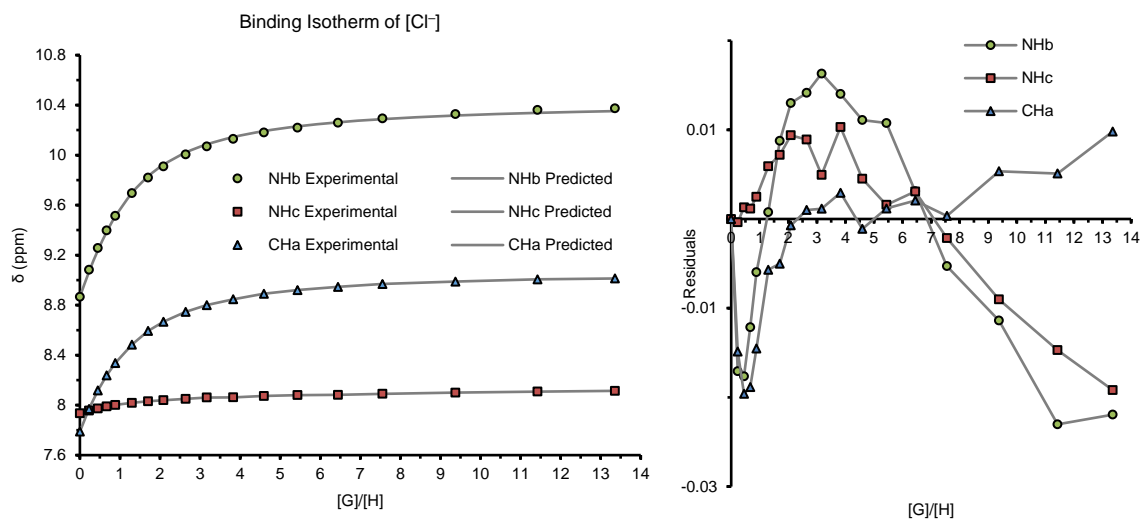


Figure A.6. Representative binding isotherm for Cl⁻ titration of receptor **2.1^{tBu}** in 10% DMSO-*d*₆/CD₃CN determined by ¹H NMR spectroscopy.

Table A.3. Representative titration of receptor **2.2^{CF3}** with HSe⁻ in CD₃CN.

Entry	V _{Guest} (μL)	[Host] (M)	[HSe ⁻] (M)	Equiv.	δ NH (ppm)	δ CH (ppm)
0	0	1.1E-03	0.00E+00	0.00	7.79	8.13
1	5	1.1E-03	8.99E-05	0.08	7.81	8.14
2	10	1.1E-03	1.78E-04	0.16	7.82	8.14
3	20	1.1E-03	3.49E-04	0.32	7.85	8.15
4	30	1.1E-03	5.14E-04	0.47	7.87	8.15
5	45	1.1E-03	7.49E-04	0.68	7.91	8.16
6	60	1.1E-03	9.72E-04	0.89	7.94	8.17
7	80	1.1E-03	1.25E-03	1.14	7.97	8.17
8	100	1.1E-03	1.51E-03	1.38	8.01	8.18
9	130	1.1E-03	1.87E-03	1.71	8.06	8.19
10	160	1.1E-03	2.20E-03	2.01	8.1	8.2
11	200	1.1E-03	2.59E-03	2.37	8.15	8.21
12	250	1.1E-03	3.03E-03	2.76	8.19	8.22
13	310	1.1E-03	3.47E-03	3.17	8.23	8.23
14	380	1.1E-03	3.92E-03	3.57	8.25	8.25
15	460	1.1E-03	4.35E-03	3.97	8.27	8.27
16	560	1.1E-03	4.79E-03	4.37	8.28	8.28
17	710	1.1E-03	5.33E-03	4.86	8.3	8.29
18	910	1.1E-03	5.86E-03	5.34	8.31	8.31
19	1160	1.1E-03	6.34E-03	5.78	8.32	8.32

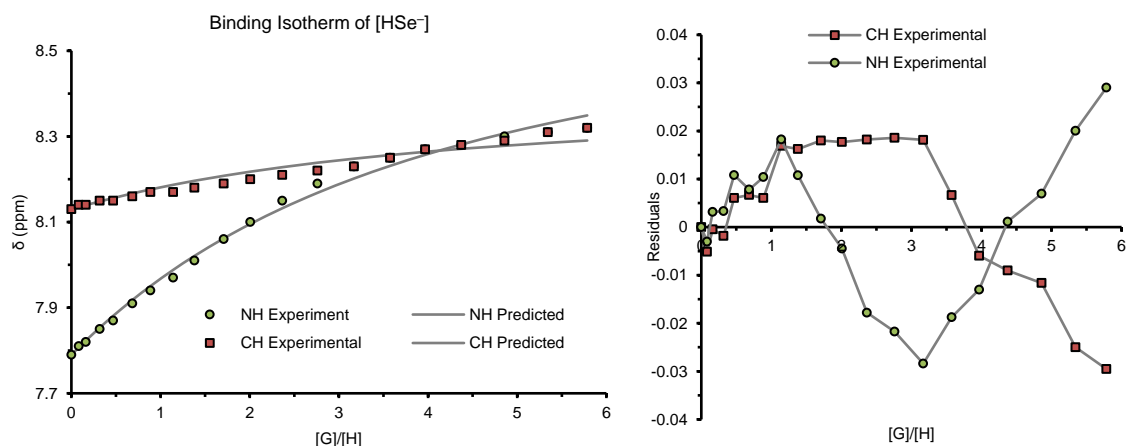


Figure A.7. Representative binding isotherm for HSe⁻ titration of receptor **2.2^{CF3}** in CD₃CN determined by ¹H NMR spectroscopy.

Table A.4. Representative titration of receptor **2.2^{CF3}** with HS⁻ in CD₃CN.

Entry	V _{Guest} (μL)	[Host] (M)	[HS ⁻] (M)	Equiv.	δ NH (ppm)	δ CH (ppm)
0	0	1.2E-03	0.0E+00	0.00	7.79	8.14
1	10	1.2E-03	2.3E-04	0.19	7.99	8.18
2	20	1.2E-03	4.5E-04	0.37	8.12	8.21
3	30	1.2E-03	6.6E-04	0.54	8.28	8.24
4	45	1.2E-03	9.6E-04	0.79	8.47	8.29
5	60	1.2E-03	1.2E-03	1.03	8.65	8.32
6	80	1.2E-03	1.6E-03	1.32	8.83	8.37
7	100	1.2E-03	1.9E-03	1.60	8.99	8.4
8	125	1.2E-03	2.3E-03	1.92	9.14	8.43
9	150	1.2E-03	2.7E-03	2.21	9.24	8.46
10	180	1.2E-03	3.1E-03	2.54	9.35	8.48
11	210	1.2E-03	3.4E-03	2.83	9.43	8.5
12	250	1.2E-03	3.9E-03	3.19	9.50	8.51
13	300	1.2E-03	4.4E-03	3.59	9.58	8.53
14	360	1.2E-03	4.9E-03	4.01	9.63	8.54
15	440	1.2E-03	5.4E-03	4.49	9.68	8.56
16	540	1.2E-03	6.0E-03	4.98	9.72	8.57
17	640	1.2E-03	6.5E-03	5.38	9.75	8.57
18	790	1.2E-03	7.1E-03	5.87	9.80	8.58
19	990	1.2E-03	7.7E-03	6.37	9.79	8.58
20	1240	1.2E-03	8.3E-03	6.83	9.82	8.14

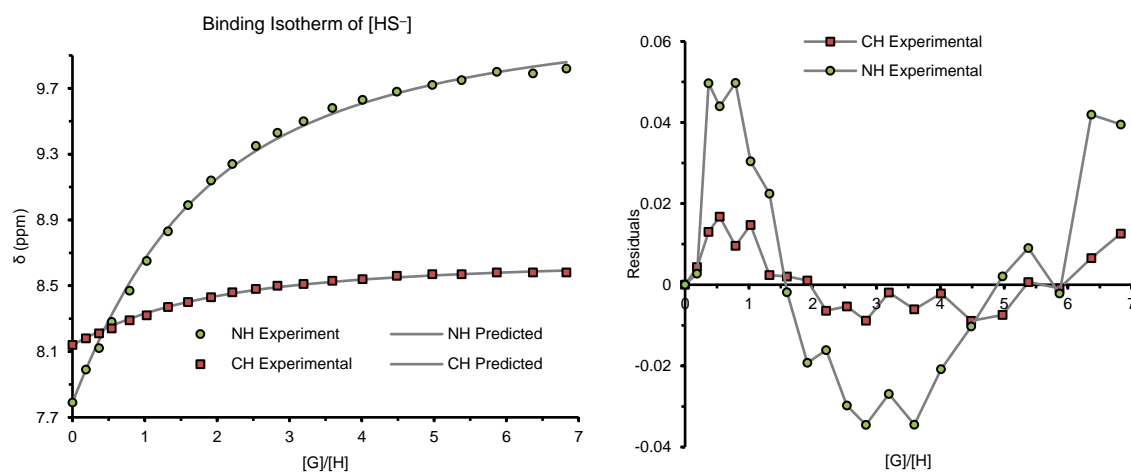


Figure A.8. Representative binding isotherm for HS⁻ titration of receptor **2.2^{CF3}** in CD₃CN determined by ¹H NMR spectroscopy.

Table A.8. Representative titration of receptor **2.2**^{CF3} with Br⁻ in CD₃CN.

Entry	V _{Guest} (μL)	[Host] (M)	[HS ⁻] (M)	Equiv.	δ NH (ppm)	δ CH (ppm)
0	0	1.2E-03	0.0E+00	0	7.79	8.14
1	5	1.2E-03	2.6E-04	0.21	7.81	8.14
2	10	1.2E-03	5.1E-04	0.42	7.83	8.15
3	20	1.2E-03	1.0E-03	0.83	7.86	8.15
4	30	1.2E-03	1.5E-03	1.22	7.89	8.16
5	45	1.2E-03	2.2E-03	1.78	7.93	8.17
6	60	1.2E-03	2.8E-03	2.30	7.97	8.18
7	80	1.2E-03	3.6E-03	2.97	8.01	8.19
8	100	1.2E-03	4.3E-03	3.58	8.05	8.2
9	130	1.2E-03	5.4E-03	4.44	8.1	8.21
10	160	1.2E-03	6.3E-03	5.21	8.13	8.22
11	200	1.2E-03	7.4E-03	6.14	8.17	8.23
12	240	1.2E-03	8.5E-03	6.97	8.21	8.24
13	290	1.2E-03	9.7E-03	7.89	8.25	8.25
14	350	1.2E-03	1.1E-02	8.85	8.28	8.26
15	430	1.2E-03	1.2E-02	9.94	8.32	8.27
16	530	1.2E-03	1.3E-02	11.07	8.35	8.27
17	680	1.2E-03	1.5E-02	12.39	8.38	8.28
18	880	1.2E-03	1.7E-02	13.71	8.42	8.29
19	1130	1.2E-03	1.8E-02	14.91	8.43	8.29
20	1380	1.2E-03	1.9E-02	15.79	8.45	8.3

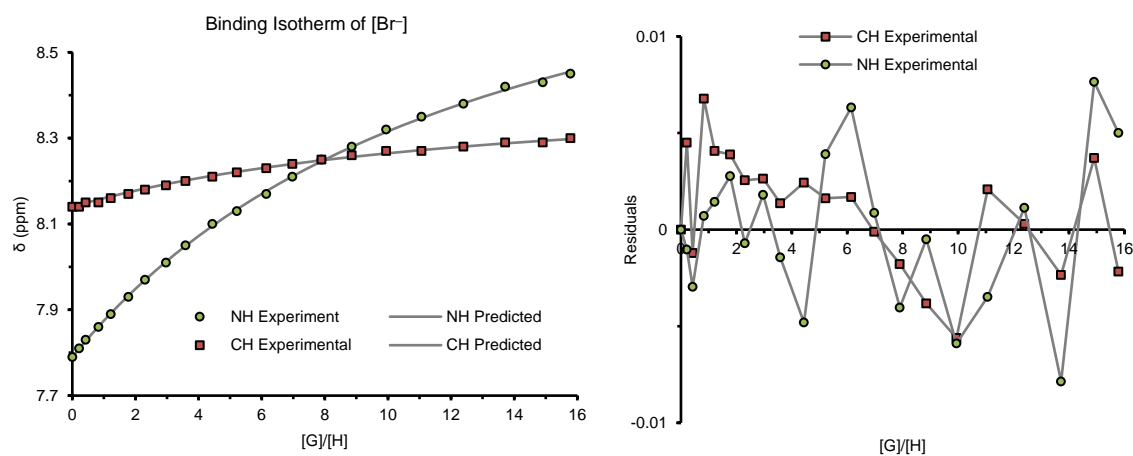


Figure A.9. Representative binding isotherm for Br⁻ titration of receptor **2.2**^{CF3} in CD₃CN determined by ¹H NMR spectroscopy.

Table A.5. Representative titration of receptor **2.2^{CF3}** with Cl⁻ in CD₃CN.

Entry	V _{Guest} (μL)	[Host] (M)	[HS ⁻] (M)	Equiv.	δ NH (ppm)	δ CH (ppm)
0	0	1.33E-03	0.00E+00	0.00	7.79	8.14
1	10	1.33E-03	4.23E-04	0.32	8	8.19
2	20	1.33E-03	8.30E-04	0.63	8.17	8.22
3	30	1.33E-03	1.22E-03	0.92	8.32	8.26
4	45	1.33E-03	1.78E-03	1.34	8.49	8.3
5	60	1.33E-03	2.31E-03	1.74	8.63	8.33
6	80	1.33E-03	2.98E-03	2.24	8.77	8.36
7	100	1.33E-03	3.60E-03	2.71	8.87	8.39
8	125	1.33E-03	4.32E-03	3.25	8.97	8.41
9	150	1.33E-03	4.98E-03	3.75	9.04	8.43
10	180	1.33E-03	5.71E-03	4.31	9.11	8.44
11	210	1.33E-03	6.39E-03	4.81	9.16	8.46
12	250	1.33E-03	7.20E-03	5.42	9.22	8.47
13	300	1.33E-03	8.10E-03	6.10	9.26	8.48
14	360	1.33E-03	9.04E-03	6.81	9.31	8.49
15	440	1.33E-03	1.01E-02	7.61	9.35	8.5
16	540	1.33E-03	1.12E-02	8.45	9.38	8.51
17	690	1.33E-03	1.25E-02	9.43	9.42	8.52
18	890	1.33E-03	1.38E-02	10.42	9.41	8.52
19	1140	1.33E-03	1.50E-02	11.31	9.45	8.52
20	1390	1.33E-03	1.59E-02	11.96	9.46	8.53

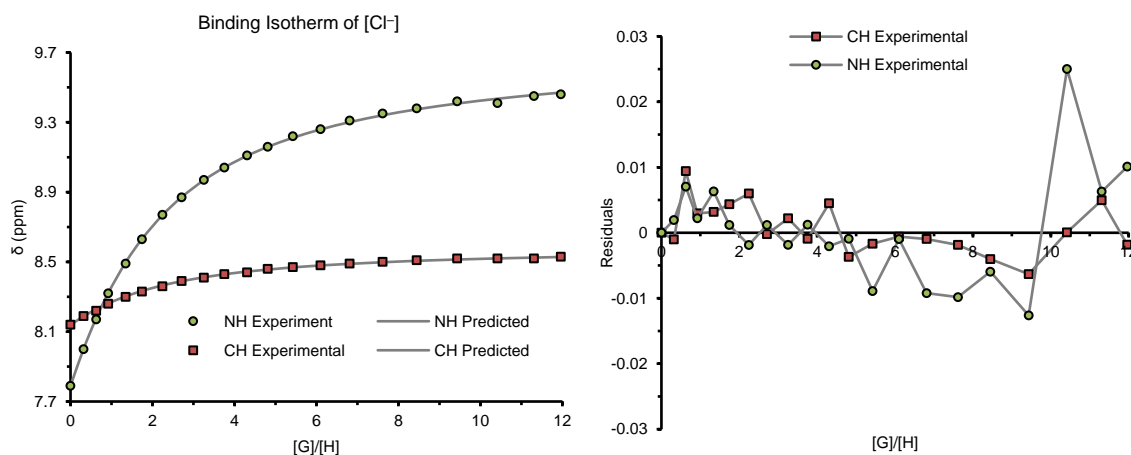


Figure A.10. Representative binding isotherm for Cl⁻ titration of receptor **2.2^{CF3}** in CD₃CN determined by ¹H NMR spectroscopy.

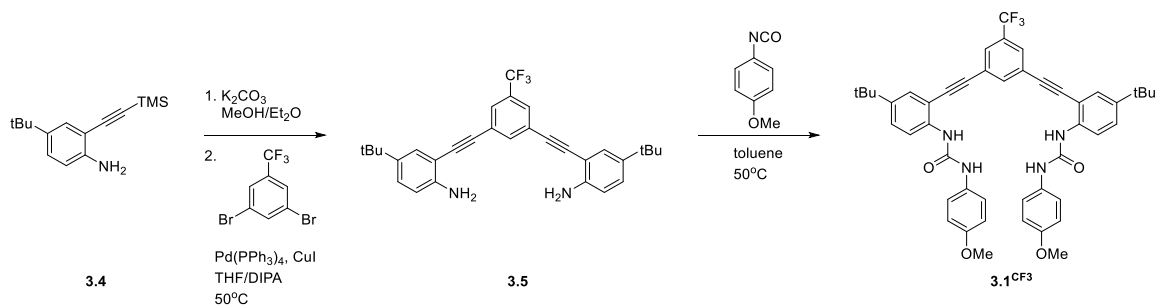
APPENDIX B

SUPPLEMENTARY CONTENT FOR CHAPTER III

Experimental Details

General Methods. All manipulations were performed under an inert atmosphere using an Innovative Atmospheres N₂-filled glove box unless otherwise noted. NMR spectra were acquired at room temperature on a Bruker Avance III HD 600 equipped with a Prodigy multinuclear cryoprobe (¹H: 600 MHz, ¹³C: 151 MHz, ¹⁹F: 565 MHz). ¹H and ¹³C chemical shifts (δ) are reported in ppm relative to residual CHCl₃ (¹H: 7.26 ppm, ¹³C: 77.16 ppm) or DMSO (¹H: 2.50 ppm, ¹³C: 39.52 ppm) shifts. ¹⁹F NMR shifts are referenced to CFC₃ (δ 0 ppm) as an external standard. Mass spectra data were acquired on a Waters SYNAPT HDMS ToF in positive ion mode with a Shimadzu Prominence LC front end. CD₃CN and DMSO-*d*₆ were distilled from calcium hydride then deoxygenated by purging with N₂ and stored over 4Å molecular sieves in an inert atmosphere glove box. Tetrabutylammonium chloride (NBu₄Cl) and tetrabutylammonium bromide (NBu₄Br) were recrystallized by layering an anhydrous THF solution under anhydrous Et₂O. Tetrabutylammonium hydrosulfide (NBu₄SH),⁷⁰ tetrabutylammonium hydroselenide (NBu₄SeH),³⁵ 1,3-dibromo-5-(trifluoromethyl)benzene,^{237,238} 4-*tert*-butyl-2-((trimethylsilyl)ethynyl)-aniline (**3.4**),^{137,239} and hosts **3.1**^{NMe₂}, **3.1**^{tBu}, **3.1**^H, **3.1**^F, and **3.1**^{Cl₂} were all synthesized according to previous reports. All other reagents were purchased from commercial sources and used as received. *Note:* Hydrogen sulfide, hydrogen selenide, and related salts are highly toxic and should be handled carefully to avoid exposure.

Receptor Synthesis and Characterization.



Scheme B.1. Synthetic scheme for **3.1**^{CF3} starting from previously published intermediate **3.4**.^{137,239}

Dianiline 3.5. This preparation was adapted from previous reports.²⁷ A suspension of 4-*tert*-butyl-2-((trimethylsilyl)ethynyl)aniline^{137,239} (**3.4**, 2.40 g, 9.77 mmol), K₂CO₃ (6.04 g, 43.70 mmol), MeOH (20 mL), and Et₂O (10 mL) was stirred at 25 °C for 3 h. The suspension was diluted with water and extracted with CH₂Cl₂ (3x) and washed with brine (2x). The organic layer was dried (Na₂SO₄) and concentrated *in vacuo* to afford a dark brown oil. The oil was dissolved in THF (10 mL) and DIPA (10 mL) and purged with N₂ for 1 h. The solution was cannulated into an N₂-purged solution of 1,3-dibromo-5-(trifluoromethyl)benzene^{240,241} (0.81 g, 2.7 mmol), Pd(PPh₃)₄ (0.15 g, 0.13 mmol), CuI (0.02 g, 0.1 mmol), THF (20 mL), and *i*-PrNH₂ (20 mL). The solution was stirred for 12 h at 50 °C, cooled, and concentrated *in vacuo*. The resulting oil was dissolved in CH₂Cl₂ and filtered through a 3 cm silica plug, which was washed with additional CH₂Cl₂. The filtrate was concentrated *in vacuo* and the resulting brown oil was purified by column chromatography (5:1 hexanes/EtOAc) to afford **3.5** (0.48 g, 0.98 mmol, 37%) as a beige solid. ¹H NMR (600 MHz, CDCl₃) δ 7.84 (s, 1H), 7.71 (s, 2H), 7.39 (d, *J* = 2.1 Hz, 2H), 7.23 (dd, *J* = 8.5, 2.1 Hz, 2H), 6.70 (d, *J* = 8.5 Hz, 2H), 4.18 (s, 4H), 1.30 (s, 18H). ¹³C

NMR (151 MHz, CDCl₃) δ 145.84, 141.19, 137.01, 131.55 (q, $J = 32.8$ Hz), 129.05, 128.03, 127.37 (q, $J = 3.6$ Hz), 124.99, 123.52 (q, $J = 272.7$ Hz), 114.64, 106.61, 92.12, 89.07, 34.09, 31.52. ¹⁹F NMR (565 MHz, CDCl₃) δ -63.09. HRMS (ESI-TOF-MS⁺) m/z calcd for C₃₁H₃₂N₂F₃ [M+H]⁺ 489.2518, found 489.2523.

Receptor 3.1^{CF3}. This preparation was adapted from previous reports.²⁷ All glassware was dried in a 150 °C oven overnight. A round bottom flask was charged with dry toluene (100 mL) and dianiline **3.5** (0.41 g, 0.84 mmol). 4-Methoxyphenyl isocyanate (0.40 mL, 3.1 mmol) was added dropwise and the solution was stirred for 12 h at 50 °C. The reaction became cloudy upon completion, and the precipitate was collected, then recrystallized in toluene to afford **3.1^{CF3}** (0.15 g, 0.20 mmol, 24%) as a fine white powder. ¹H NMR (600 MHz, DMSO-*d*₆) δ 9.31 (s, 2H), 8.32 (s, 1H), 8.17 (s, 2H), 8.11 (s, 2H), 8.04 (d, $J = 8.8$ Hz, 2H), 7.56 (d, $J = 2.4$ Hz, 2H), 7.46 (dd, $J = 8.8, 2.4$ Hz, 2H), 7.38 (d, $J = 8.9$ Hz, 4H), 6.85 (d, $J = 8.9$ Hz, 4H), 3.70 (s, 6H), 1.30 (s, 18H). ¹³C NMR (151 MHz, DMSO-*d*₆) δ 154.65, 152.40, 144.47, 138.33, 137.79, 132.41, 130.36 (q, $J = 31.7$ Hz), 128.96, 127.82 (q, $J = 3.9$ Hz), 127.46, 124.29, 123.41 (q, $J = 273.3$ Hz), 120.24, 119.74, 114.06, 110.26, 92.27, 88.58, 55.15, 33.98, 31.0. ¹⁹F NMR (565 MHz, DMSO-*d*₆) δ -61.47. HRMS (ESI-TOF-MS⁺) m/z calcd for C₄₇H₄₆N₄O₄F₃ [M+H]⁺ 787.3471, found 787.3457.

NMR Spectra.

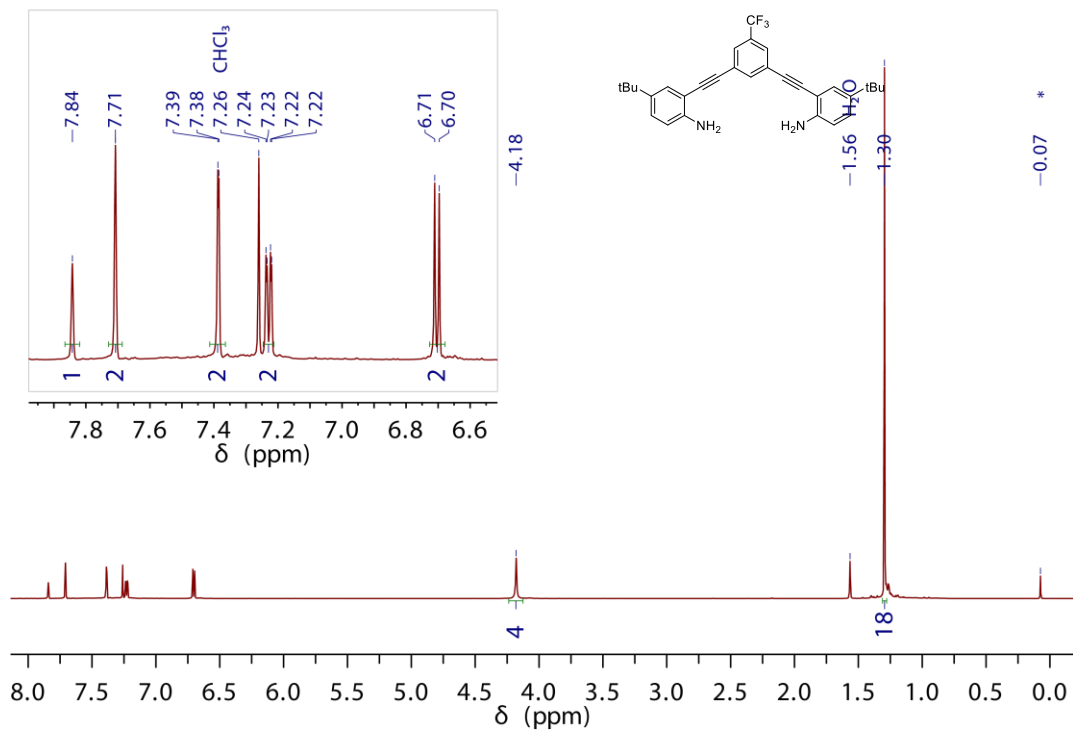


Figure B.1. ¹H NMR spectrum of dianiline **3.5**. * = silicon grease

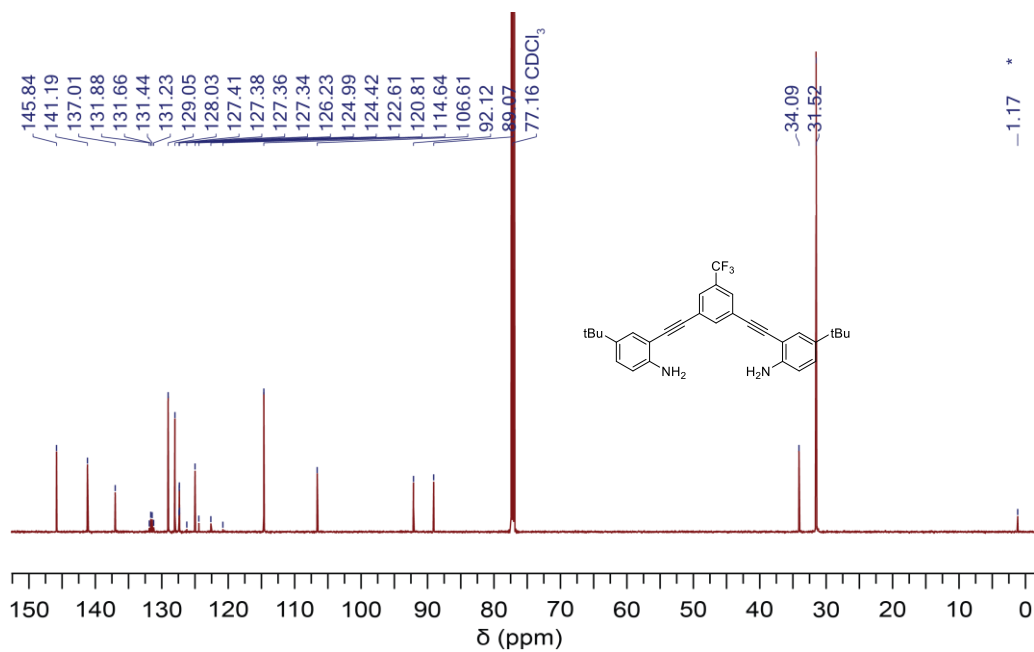


Figure B.2. ¹³C{¹H} NMR spectrum of dianiline **3.5**. * = silicon grease

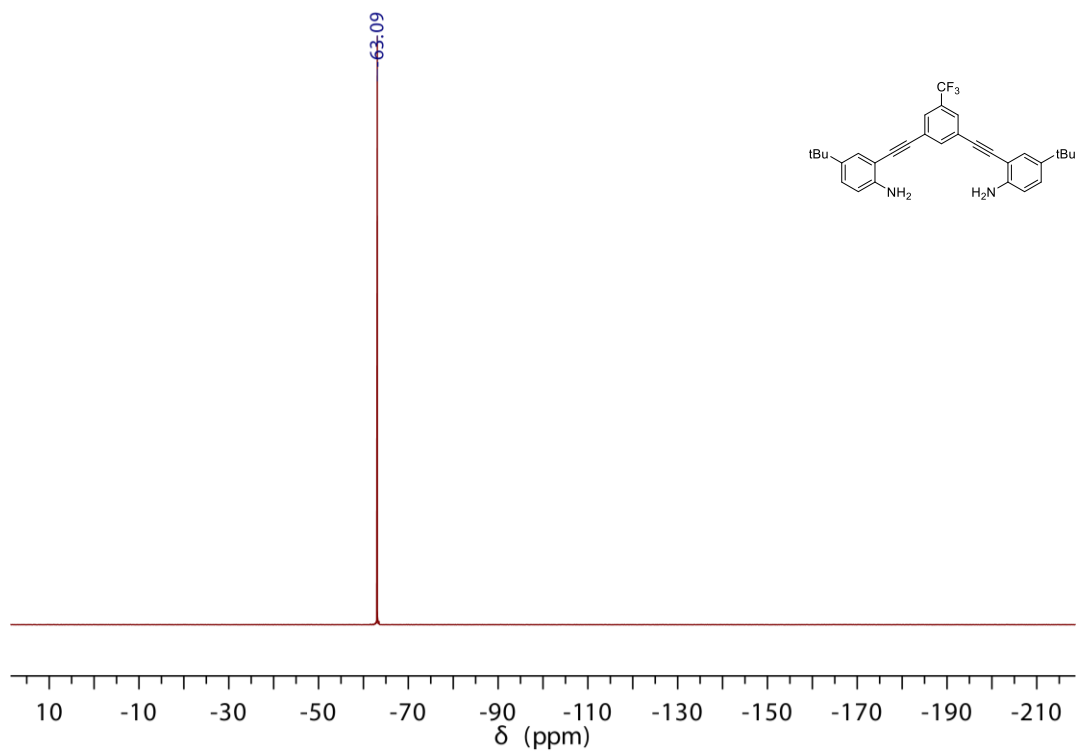


Figure B.3. ^{19}F NMR spectrum of dianiline **3.5**.

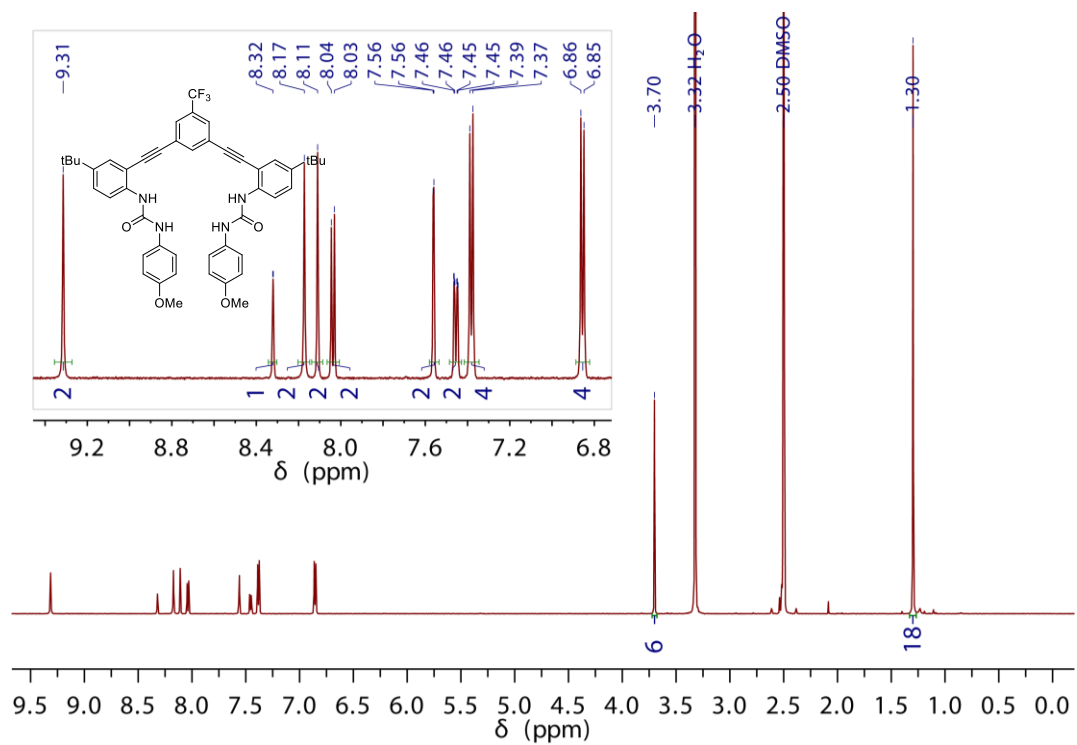


Figure B.4. ^1H NMR spectrum of receptor **3.1** $^{\text{CF}_3}$.

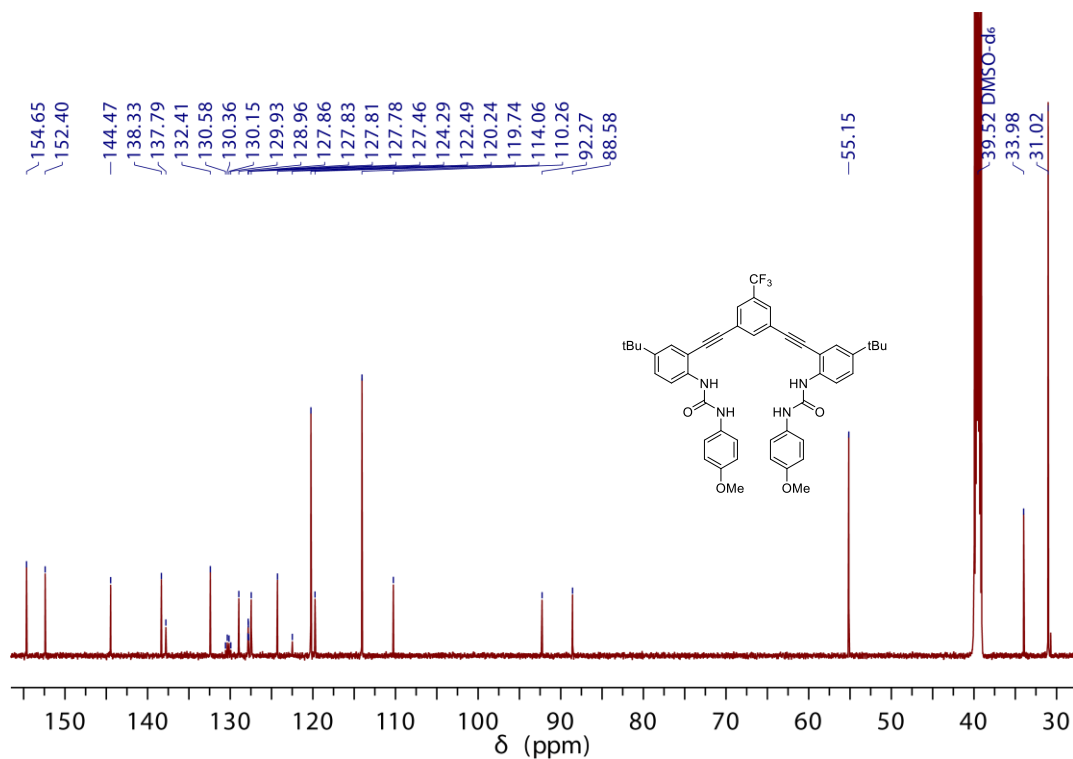


Figure B.5. $^{13}\text{C}\{^1\text{H}\}$ NMR spectrum of receptor **3.1**^{CF₃}.

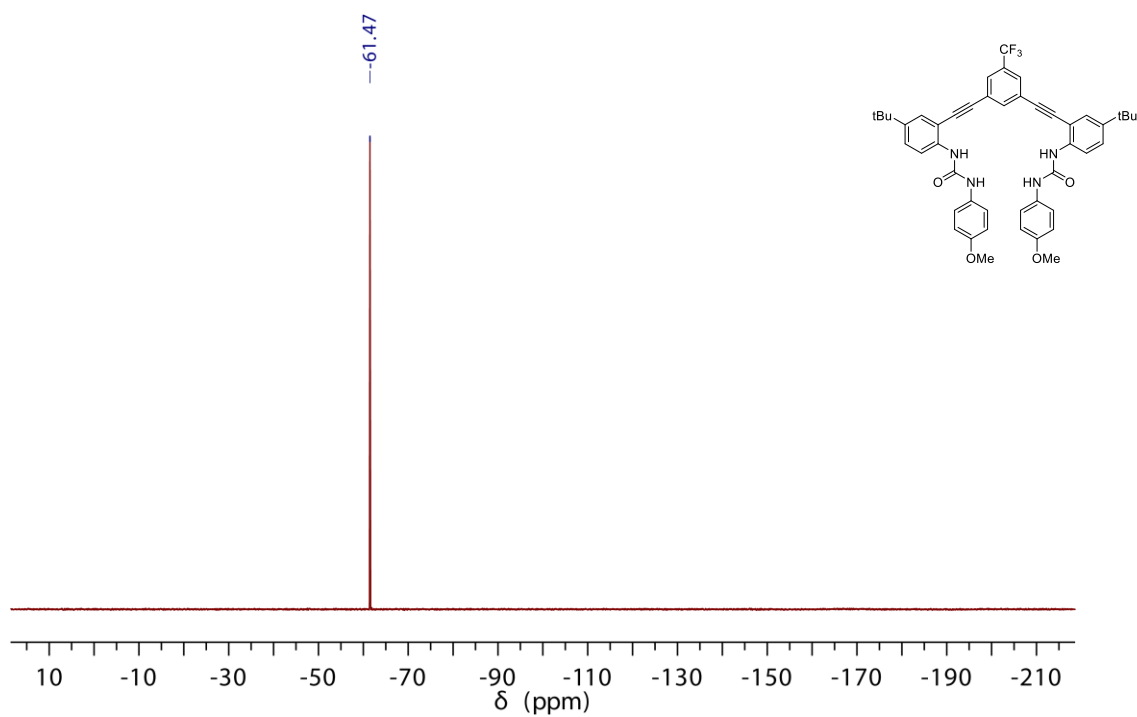


Figure B.6. ^{19}F NMR spectrum of receptor **3.1**^{CF₃}.

Linear free energy relationship (LFER) analysis of substituent effect on ^1H NMR chemical shift (δ) of free host hydrogen bond (HB) donors at 0.8-2.2 mM in 10% DMSO- d_6 / CD $_3$ CN at 25 °C.

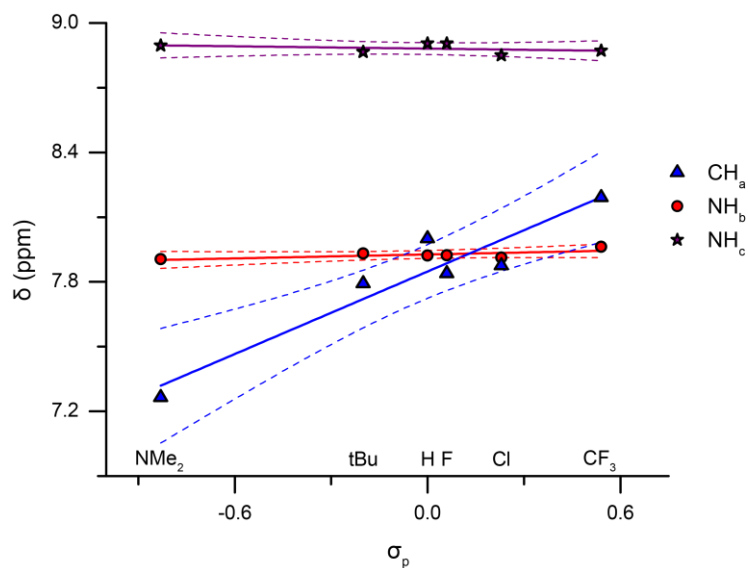


Figure B.7. LFER between δ of HB donors in free host **3.1^R** and σ_p . Dashed lines represent the 95% confidence interval for each linear trend.

Table B.1. Fitting statistics for the LFER between δ of HB donors in free host **3.1^R** and σ_p .

HB Donor	Slope	Intercept	p-value			R ²	R ² _{adj.}
			Slope	Intercept	Model		
CH _a	0.64 ± 0.11	7.85 ± 0.04	< 0.01	< 0.01	< 0.01	0.90	0.88
NH _b	0.03 ± 0.02	7.93 ± 0.01	0.12	< 0.01	0.12	0.49	0.36
NH _c	-0.02 ± 0.02	8.88 ± 0.01	0.48	< 0.01	0.48	0.13	-0.09

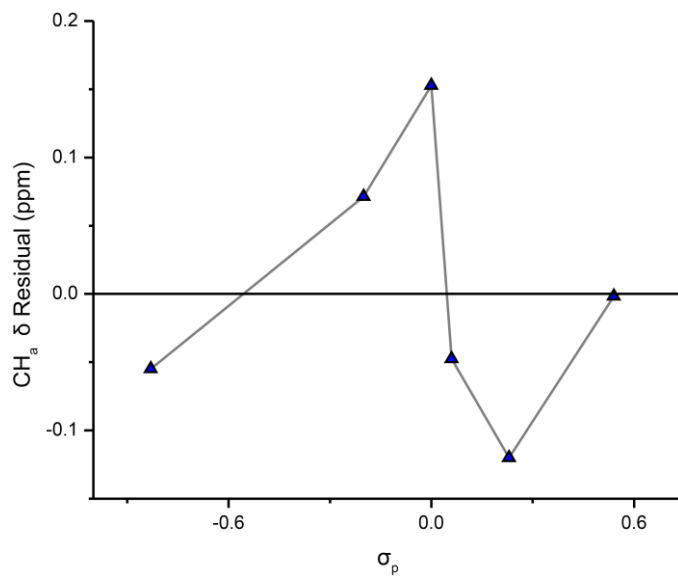


Figure B.8. Linear regression residuals of δ of CH_a in free host **3.1^R** and σ_p .

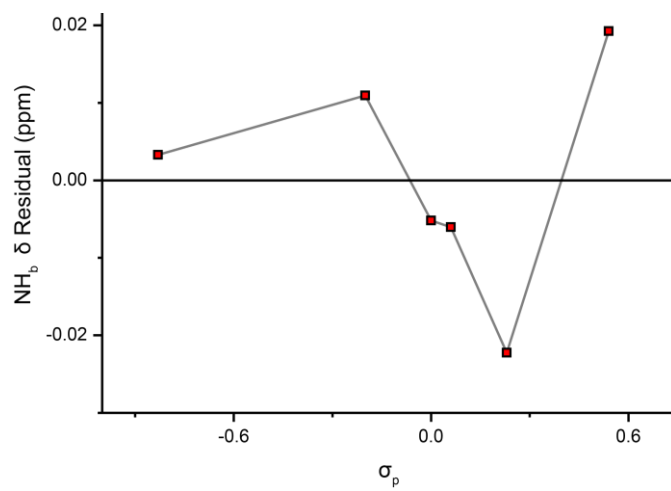


Figure B.9. Linear regression residuals of δ of NH_b in free host **3.1^R** and σ_p .

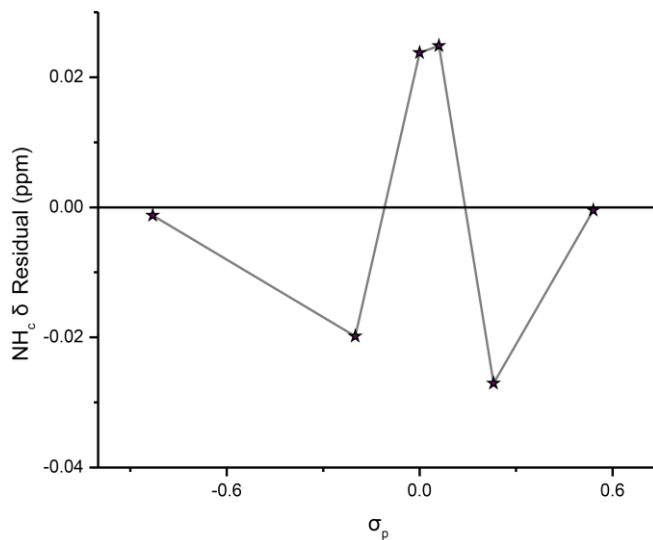


Figure B.10. Linear regression residuals of δ of NH_c in free host **3.1^R** and σ_p .

¹H NMR Titrations.

General Methods. ¹H NMR spectra were acquired at room temperature on a Varian Inova 500 MHz spectrometer (¹H: 500.11 MHz). ¹H chemical shifts (δ) are expressed in ppm relative to residual CH_3CN (¹H: 1.94 ppm) shifts.

General Procedure for NMR Titrations. Method A. A solution of host in 10% $\text{DMSO-}d_6/\text{CD}_3\text{CN}$ (0.8-2.1 mM) was prepared and 500 μL was added to a septum-sealed NMR tube. The remaining host solution (2.5 mL) was used to prepare a host/guest (NBu_4Cl or NBu_4Br) (18.5-27.9 mM) stock solution. Aliquots of the host/guest solution were added to the NMR tube using Hamilton gas-tight syringes, and ¹H NMR spectra were recorded at 25 °C after each addition of guest. The $\Delta\delta$ of the various NH and aromatic CH protons

were used to follow the progress of the titration, and association constants were determined using the Thordarson method.⁷¹

Method B. A solution of receptor host in 10% DMSO-*d*₆/CD₃CN (1.8-2.2 mM) was prepared and 500 μL was added to a septum-sealed NMR tube. A stock solution of guest (NBu₄SH or NBu₄SeH) was prepared in 10% DMSO-*d*₆/CD₃CN (14.6-24.3 mM).

Aliquots of the guest solution were added to the NMR tube using Hamilton gas-tight syringes, and ¹H NMR spectra were recorded at 25 °C after each addition of guest. The Δδ of the NH and the central aromatic CH proton was used to follow the progress of the titration, and association constants were determined using the Thordarson method.⁷¹

¹H NMR Titration Representative Data

Table B.2. Representative titration of receptor 1^{CF3} with HS^- in 10% DMSO-*d*₆/CD₃CN at 25 °C.

Entry	V _{Guest} (μL)	[Host] (M)	[HS ⁻] (M)	Equiv.	δ NH _c (ppm)	δ NH _b (ppm)	δ CH _a (ppm)
0	0	2.2E-03	0.0E+00	0.00	8.861	7.959	8.187
1	5	2.2E-03	2.4E-04	0.11	9.12	8.013	8.351
2	5	2.2E-03	4.8E-04	0.22	9.376	8.067	8.516
3	5	2.2E-03	7.1E-04	0.33	9.628	8.119	8.68
4	5	2.1E-03	9.4E-04	0.44	9.872	8.17	8.844
5	5	2.1E-03	1.2E-03	0.55	10.118	8.22	8.996
6	10	2.1E-03	1.6E-03	0.77	10.521	8.305	9.265
7	10	2.0E-03	2.0E-03	0.98	10.827	8.366	9.471
8	10	2.0E-03	2.4E-03	1.20	11	8.408	9.574
9	10	2.0E-03	2.8E-03	1.42	11.093	8.438	9.618
10	10	1.9E-03	3.2E-03	1.64	11.143	8.449	9.654
11	10	1.9E-03	3.5E-03	1.86	11.174	8.469	9.667
12	30	1.8E-03	4.5E-03	2.51	11.222	8.485	9.681
13	70	1.6E-03	6.6E-03	4.05	11.268	8.522	9.681

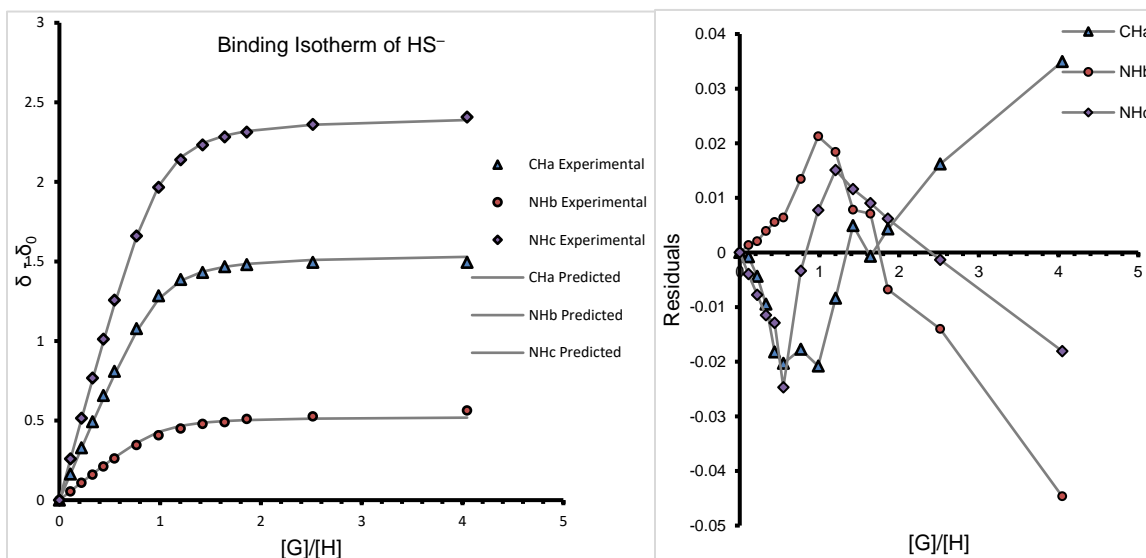


Figure B.11. Representative binding isotherm and residuals for HS^- titration of receptor 3.1^{CF3} in 10% DMSO-*d*₆/CD₃CN at 25 °C determined by ¹H NMR spectroscopy.

Table B.3. Representative titration of receptor **3.1**^{CF3} with HSe⁻ in 10% DMSO-*d*₆/CD₃CN at 25 °C.

Entry	V _{Guest} (μL)	[Host] (M)	[HSe ⁻] (M)	Equiv.	δ NH _c (ppm)	δ NH _b (ppm)	δ CH _a (ppm)
0	0	2.0E-03	0.0E+00	0.00	8.883	7.965	8.203
1	5	2.0E-03	0.2E-03	0.12	9.039	8.007	8.299
2	5	1.9E-03	0.5E-03	0.25	9.166	8.042	8.38
3	5	1.9E-03	0.7E-03	0.37	9.281	8.07	8.455
4	10	1.9E-03	1.2E-03	0.62	9.476	8.124	8.585
5	10	1.8E-03	1.6E-03	0.87	9.637	8.167	8.687
6	10	1.8E-03	2.0E-03	1.12	9.757	8.203	8.77
7	15	1.8E-03	2.6E-03	1.50	9.898	8.236	8.854
8	15	1.7E-03	3.2E-03	1.87	10.001	8.271	8.935
9	15	1.7E-03	3.7E-03	2.24	10.081	8.298	8.983
10	20	1.6E-03	4.4E-03	2.74	10.15	8.32	9.032
11	20	1.5E-03	5.0E-03	3.24	10.223	8.336	9.063
12	25	1.4E-03	5.7E-03	3.86	10.283	8.353	9.105
13	30	1.4E-03	6.5E-03	4.61	10.325	8.373	9.133
14	40	1.3E-03	7.4E-03	5.61	10.367	8.379	9.141
15	60	1.2E-03	8.7E-03	7.11	10.429	8.425	9.172

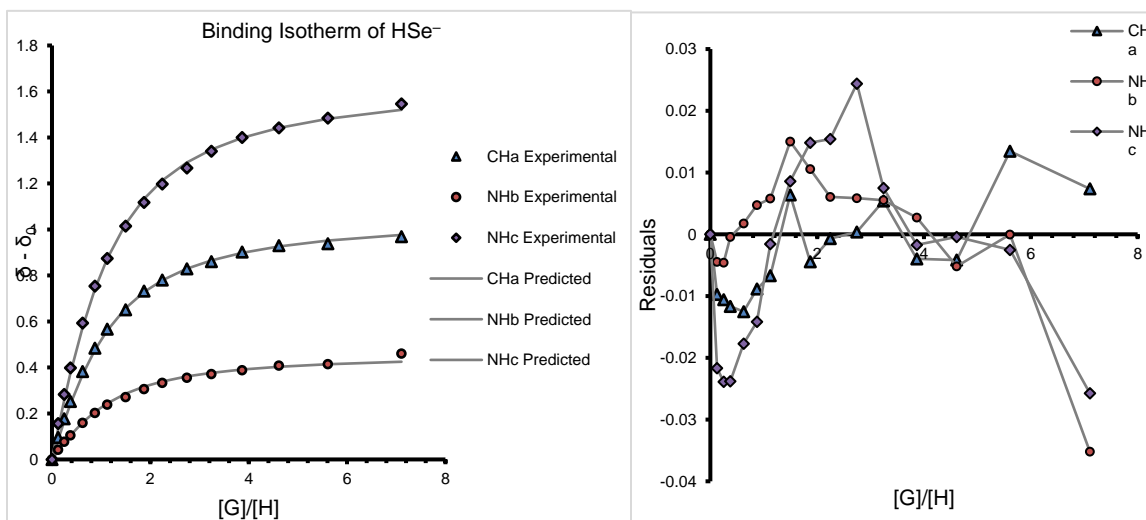


Figure B.12. Representative binding isotherm and residuals for HSe⁻ titration of receptor **3.1**^{CF3} in 10% DMSO-*d*₆/CD₃CN at 25 °C determined by ¹H NMR spectroscopy.

Table B.4. Representative titration of receptor **3.1**^{CF3} with Cl⁻ in 10% DMSO-*d*₆/CD₃CN at 25 °C.

Entry	V _{Guest} (μL)	[Host] (M)	[Cl ⁻] (M)	Equiv.	δ NH _c (ppm)	δ NH _b (ppm)	δ CH _a (ppm)
0	0	2.0E-03	0.0E+00	0.00	8.882	7.964	8.203
1	5	2.0E-03	2.0E-04	0.10	9.011	7.982	8.324
2	5	2.0E-03	4.0E-04	0.20	9.133	7.992	8.44
3	5	2.0E-03	6.0E-04	0.30	9.249	8.005	8.555
4	5	2.0E-03	7.9E-04	0.40	9.356	8.017	8.653
5	10	2.0E-03	1.2E-03	0.58	9.54	8.038	8.829
6	10	2.0E-03	1.5E-03	0.76	9.692	8.054	8.974
7	10	2.0E-03	1.9E-03	0.93	9.819	8.068	9.097
8	10	2.0E-03	2.2E-03	1.10	9.916	8.082	9.187
9	10	2.0E-03	2.5E-03	1.25	9.993	8.084	9.262
10	15	2.0E-03	2.9E-03	1.48	10.078	8.097	9.339
11	15	2.0E-03	3.4E-03	1.69	10.134	8.105	9.393
12	15	2.0E-03	3.8E-03	1.90	10.176	8.107	9.434
13	20	2.0E-03	4.3E-03	2.15	10.215	8.115	9.466
14	20	2.0E-03	4.7E-03	2.39	10.245	8.121	9.49
15	30	2.0E-03	5.4E-03	2.71	10.276	8.125	9.515
16	50	2.0E-03	6.4E-03	3.19	10.308	8.133	9.544
17	100	2.0E-03	7.9E-03	3.97	10.344	8.143	9.567
18	200	2.0E-03	1.0E-02	5.06	10.377	8.155	9.578

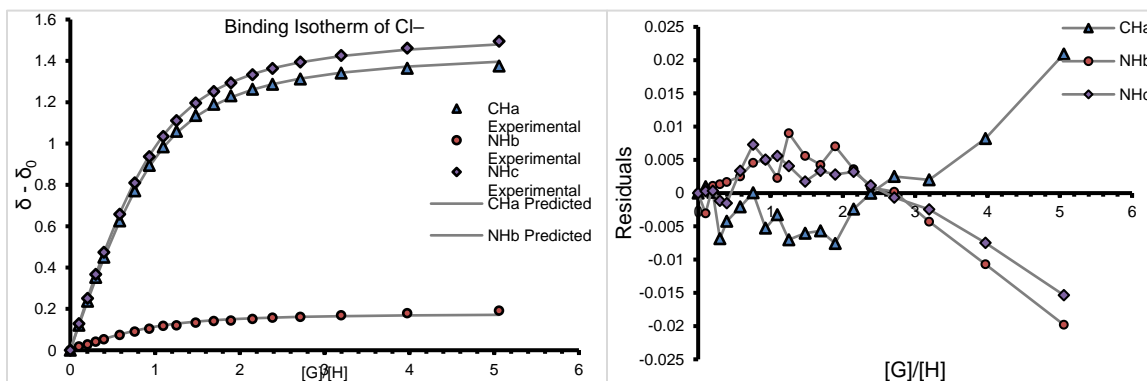


Figure B.13. Representative binding isotherm and residuals for Cl⁻ titration of receptor **3.1**^{CF3} in 10% DMSO-*d*₆/CD₃CN at 25 °C determined by ¹H NMR spectroscopy.

Table B.5. Representative titration of receptor **3.1**^{CF3} with Br⁻ in 10% DMSO-*d*₆/CD₃CN at 25 °C.

Entry	V _{Guest} (μL)	[Host] (M)	[Br ⁻] (M)	Equiv.	δ NH _c (ppm)	δ NH _b (ppm)	δ CH _a (ppm)
0	0	2.0E-03	0.0E+00	0.00	8.869	7.961	8.192
1	5	2.0E-03	2.8E-04	0.14	8.921	7.969	8.247
2	10	2.0E-03	8.1E-04	0.42	9.009	7.985	8.34
3	15	2.0E-03	1.6E-03	0.81	9.119	7.996	8.457
4	20	2.0E-03	2.5E-03	1.30	9.243	8.011	8.586
5	20	2.0E-03	3.4E-03	1.75	9.34	8.025	8.689
6	25	2.0E-03	4.5E-03	2.28	9.438	8.035	8.787
7	30	2.0E-03	5.6E-03	2.85	9.526	8.047	8.877
8	35	2.0E-03	6.8E-03	3.46	9.603	8.06	8.953
9	40	2.0E-03	8.0E-03	4.08	9.669	8.064	9.017
10	45	2.0E-03	9.2E-03	4.69	9.725	8.072	9.07
11	50	2.0E-03	1.0E-02	5.29	9.772	8.079	9.114
12	60	2.0E-03	1.2E-02	5.92	9.817	8.086	9.155
13	70	2.0E-03	1.3E-02	6.55	9.856	8.093	9.191
14	80	2.0E-03	1.4E-02	7.17	9.889	8.097	9.217
15	100	2.0E-03	1.5E-02	7.81	9.913	8.102	9.239
16	130	2.0E-03	1.7E-02	8.49	9.938	8.108	9.257
17	140	2.0E-03	1.8E-02	9.08	9.956	8.11	9.273

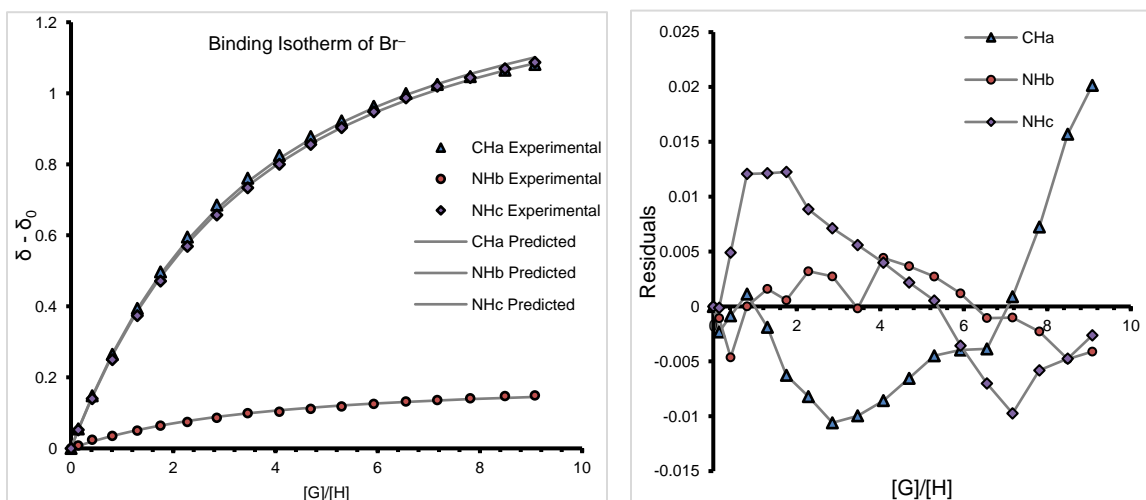


Figure B.14. Representative binding isotherm and residuals for Br⁻ titration of receptor **3.1**^{CF3} in 10% DMSO-*d*₆/CD₃CN at 25 °C determined by ¹H NMR spectroscopy.

Table B.6. Representative titration of receptor **3.1^{Cl}** with HS⁻ in 10% DMSO-*d*₆/CD₃CN at 25 °C.

Entry	V _{Guest} (μL)	[Host] (M)	[HS ⁻] (M)	Equiv.	δ NH _c (ppm)	δ NH _b (ppm)	δ CH _a (ppm)
0	0	2.0E-03	0.0E+00	0.00	8.874	7.923	7.879
1	5	2.0E-03	2.0E-04	0.10	9.086	7.972	8.011
2	5	2.0E-03	3.9E-04	0.20	9.302	8.018	8.139
3	5	2.0E-03	5.8E-04	0.29	9.514	8.063	8.269
4	5	2.0E-03	7.7E-04	0.39	9.712	8.112	8.392
5	5	1.9E-03	9.5E-04	0.49	9.903	8.158	8.51
6	10	1.9E-03	1.3E-03	0.69	10.25	8.243	8.72
7	10	1.9E-03	1.6E-03	0.88	10.534	8.301	8.901
8	10	1.8E-03	2.0E-03	1.08	10.737	8.353	9.023
9	10	1.8E-03	2.3E-03	1.27	10.878	8.393	9.103
10	15	1.8E-03	2.8E-03	1.57	11.008	8.423	9.172
11	15	1.7E-03	3.2E-03	1.86	11.048	8.457	9.209
12	15	1.7E-03	3.6E-03	2.16	11.078	8.489	9.203
13	20	1.6E-03	4.1E-03	2.55	11.114	8.531	9.209
14	40	1.5E-03	5.1E-03	3.33	11.154	8.539	9.232
15	80	1.4E-03	6.7E-03	4.90	11.188	8.573	9.219

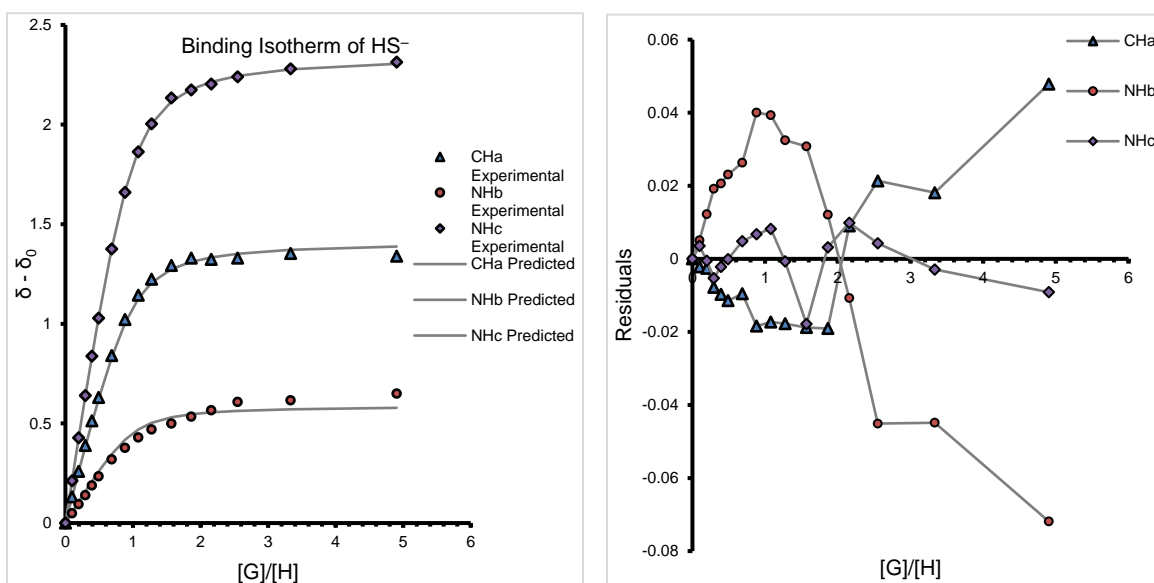


Figure B.15. Representative binding isotherm and residuals for HS⁻ titration of receptor **3.1^{Cl}** in 10% DMSO-*d*₆/CD₃CN at 25 °C determined by ¹H NMR spectroscopy.

Table B.7. Representative titration of receptor **3.1^{Cl}** with HSe⁻ in 10% DMSO-*d*₆/CD₃CN at 25 °C.

Entry	V _{Guest} (μL)	[Host] (M)	[HSe ⁻] (M)	Equiv.	δ NH _c (ppm)	δ NH _b (ppm)	δ CH _a (ppm)
0	0	1.8E-03	0.0E+00	0.00	8.869	7.92	7.88
1	5	1.8E-03	1.7E-04	0.10	8.957	7.943	7.934
2	5	1.8E-03	3.3E-04	0.19	9.054	7.973	7.991
3	5	1.7E-03	5.0E-04	0.29	9.125	7.993	8.033
4	5	1.7E-03	6.6E-04	0.38	9.196	8.012	8.068
5	5	1.7E-03	8.1E-04	0.48	9.257	8.036	8.112
6	10	1.7E-03	1.1E-03	0.67	9.372	8.064	8.175
7	10	1.6E-03	1.4E-03	0.86	9.456	8.092	8.227
8	10	1.6E-03	1.7E-03	1.05	9.543	8.118	8.279
9	10	1.6E-03	2.0E-03	1.24	9.615	8.14	8.32
10	15	1.5E-03	2.4E-03	1.52	9.705	8.169	8.377
11	15	1.5E-03	2.7E-03	1.81	9.789	8.194	8.418
12	15	1.5E-03	3.1E-03	2.09	9.853	8.214	8.461
13	20	1.4E-03	3.5E-03	2.47	9.925	8.239	8.503
14	20	1.4E-03	3.9E-03	2.86	9.978	8.258	8.534
15	25	1.3E-03	4.4E-03	3.33	10.036	8.281	8.568
16	35	1.3E-03	5.0E-03	4.00	10.11	8.3	8.603
17	60	1.2E-03	6.0E-03	5.14	10.182	8.336	8.642
18	100	1.0E-03	7.3E-03	7.04	10.244	8.362	8.676

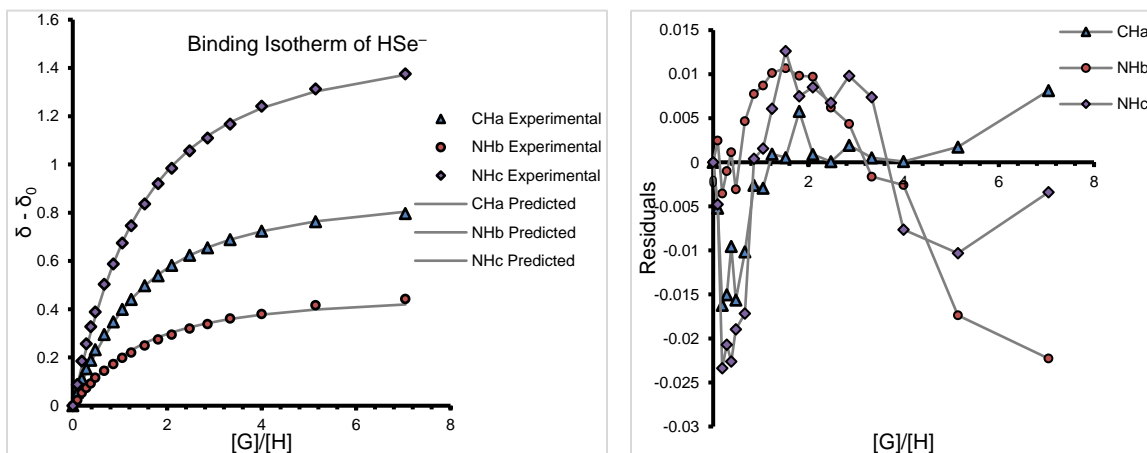


Figure B.16. Representative binding isotherm and residuals for HSe⁻ titration of receptor **3.1^{Cl}** in 10% DMSO-*d*₆/CD₃CN at 25 °C determined by ¹H NMR spectroscopy.

Table B.8. Representative titration of receptor **3.1**^{Cl} with Cl⁻ in 10% DMSO-*d*₆/CD₃CN at 25 °C.

Entry	V _{Guest} (μL)	[Host] (M)	[Cl ⁻] (M)	Equiv.	δ NH _c (ppm)	δ NH _b (ppm)	δ CH _a (ppm)
0	0	8.2E-04	0.0E+00	0.00	8.859	7.912	7.89
1	5	8.2E-04	2.3E-04	0.28	9.166	7.952	8.174
2	5	8.2E-04	4.6E-04	0.56	9.37	7.977	8.363
3	5	8.2E-04	6.8E-04	0.83	9.551	8.001	8.531
4	10	8.2E-04	1.1E-03	1.35	9.794	8.032	8.756
5	10	8.2E-04	1.5E-03	1.86	9.935	8.05	8.885
6	10	8.2E-04	1.9E-03	2.35	10.026	8.063	8.967
7	15	8.2E-04	2.5E-03	3.04	10.112	8.075	9.044
8	15	8.2E-04	3.1E-03	3.71	10.167	8.086	9.089
9	15	8.2E-04	3.6E-03	4.33	10.204	8.09	9.121
10	20	8.2E-04	4.2E-03	5.12	10.24	8.098	9.15
11	25	8.2E-04	5.0E-03	6.04	10.269	8.105	9.172
12	30	8.2E-04	5.8E-03	7.05	10.294	8.112	9.187
13	40	8.2E-04	6.8E-03	8.26	10.316	8.119	9.201
14	50	8.2E-04	7.9E-03	9.60	10.339	8.128	9.21
15	70	8.2E-04	9.2E-03	11.19	10.357	8.136	9.216
16	100	8.2E-04	1.1E-02	13.06	10.377	8.148	9.218
17	150	8.2E-04	1.3E-02	15.20	10.39	8.155	9.217
18	200	8.2E-04	1.4E-02	17.27	8.859	7.912	7.89

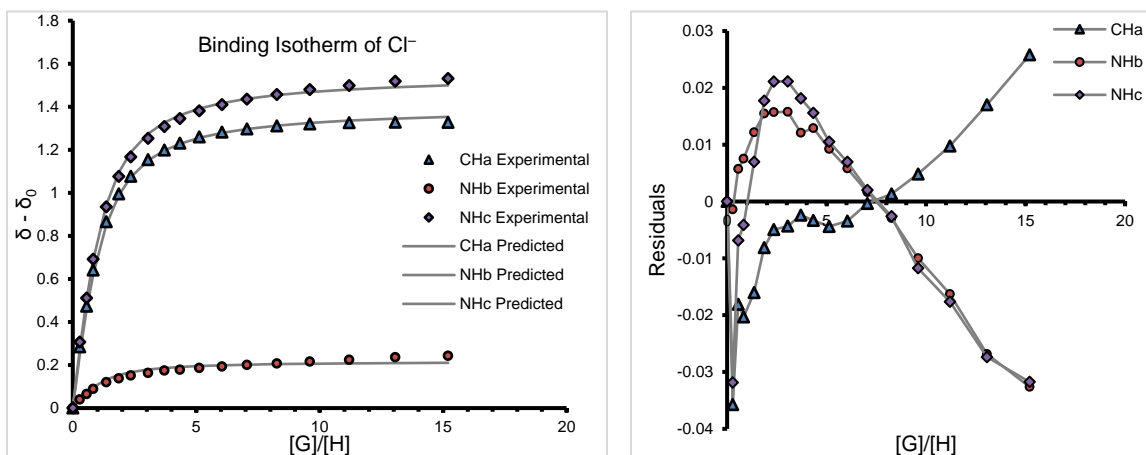


Figure B.17. Representative binding isotherm and residuals for Cl⁻ titration of receptor **3.1**^{Cl} in 10% DMSO-*d*₆/CD₃CN at 25 °C determined by ¹H NMR spectroscopy.

Table B.9. Representative titration of receptor **3.1^{Cl}** with Br⁻ in 10% DMSO-*d*₆/CD₃CN at 25 °C.

Entry	V _{Guest} (μL)	[Host] (M)	[Br ⁻] (M)	Equiv.	δ NH _c (ppm)	δ NH _b (ppm)	δ CH _a (ppm)
0	0	1.4E-03	0.0E+00	0.00	8.852	7.912	7.882
1	10	1.4E-03	5.9E-04	0.42	8.936	7.926	7.966
2	10	1.4E-03	1.2E-03	0.82	8.995	7.937	8.025
3	10	1.4E-03	1.7E-03	1.21	9.044	7.946	8.073
4	10	1.4E-03	2.2E-03	1.58	9.093	7.954	8.122
5	15	1.4E-03	3.0E-03	2.11	9.16	7.963	8.193
6	15	1.4E-03	3.7E-03	2.62	9.212	7.974	8.244
7	20	1.4E-03	4.6E-03	3.25	9.273	7.983	8.306
8	20	1.4E-03	5.4E-03	3.85	9.326	7.993	8.359
9	25	1.4E-03	6.4E-03	4.53	9.383	8.003	8.415
10	25	1.4E-03	7.3E-03	5.17	9.428	8.01	8.459
11	30	1.4E-03	8.3E-03	5.87	9.471	8.018	8.501
12	30	1.4E-03	9.2E-03	6.52	9.51	8.025	8.54
13	40	1.4E-03	1.0E-02	7.30	9.545	8.03	8.571
14	50	1.4E-03	1.2E-02	8.16	9.581	8.037	8.605
15	60	1.4E-03	1.3E-02	9.07	9.616	8.045	8.637
16	80	1.4E-03	1.4E-02	10.10	9.636	8.053	8.657
17	100	1.4E-03	1.6E-02	11.17	9.674	8.052	8.692

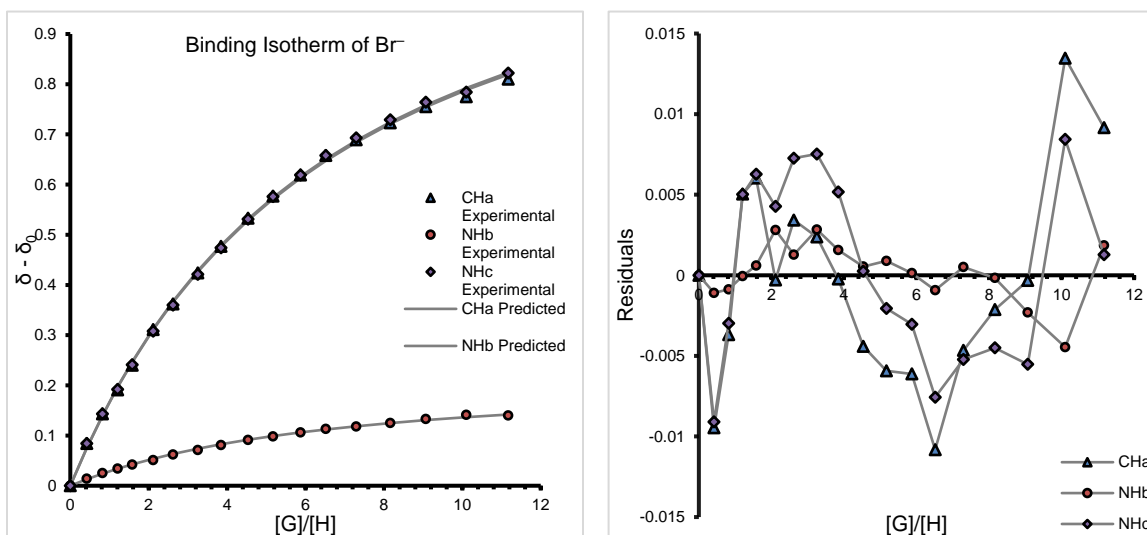


Figure B.18. Representative binding isotherm and residuals for Br⁻ titration of receptor **3.1^{Cl}** in 10% DMSO-*d*₆/CD₃CN at 25 °C determined by ¹H NMR spectroscopy.

Table B.10. Representative titration of receptor **3.1^F** with HS⁻ in 10% DMSO-*d*₆/CD₃CN at 25 °C.

Entry	V _{Guest} (μL)	[Host] (M)	[HS ⁻] (M)	Equiv.	δ NH _c (ppm)	δ NH _b (ppm)	δ CH _a (ppm)
0	0	2.0E-03	0.0E+00	0.00	8.861	7.919	7.797
1	5	2.0E-03	1.9E-04	0.10	9.074	7.969	7.923
2	5	2.0E-03	3.8E-04	0.19	9.291	8.051	8.019
3	5	1.9E-03	5.6E-04	0.29	9.511	8.063	8.182
4	5	1.9E-03	7.4E-04	0.38	9.721	8.121	8.309
5	5	1.9E-03	9.2E-04	0.48	9.928	8.167	8.43
6	10	1.9E-03	1.3E-03	0.67	10.294	8.249	8.646
7	10	1.8E-03	1.6E-03	0.86	10.582	8.316	8.821
8	10	1.8E-03	1.9E-03	1.05	10.785	8.366	8.939
9	10	1.8E-03	2.2E-03	1.25	10.92	8.398	9.012
10	10	1.7E-03	2.5E-03	1.44	10.997	8.429	9.054
11	15	1.7E-03	2.9E-03	1.72	11.072	8.446	9.092
12	20	1.6E-03	3.5E-03	2.11	11.128	8.467	9.119
13	50	1.5E-03	4.7E-03	3.06	11.188	8.499	9.114
14	100	1.3E-03	6.6E-03	4.98	11.243	8.515	9.145

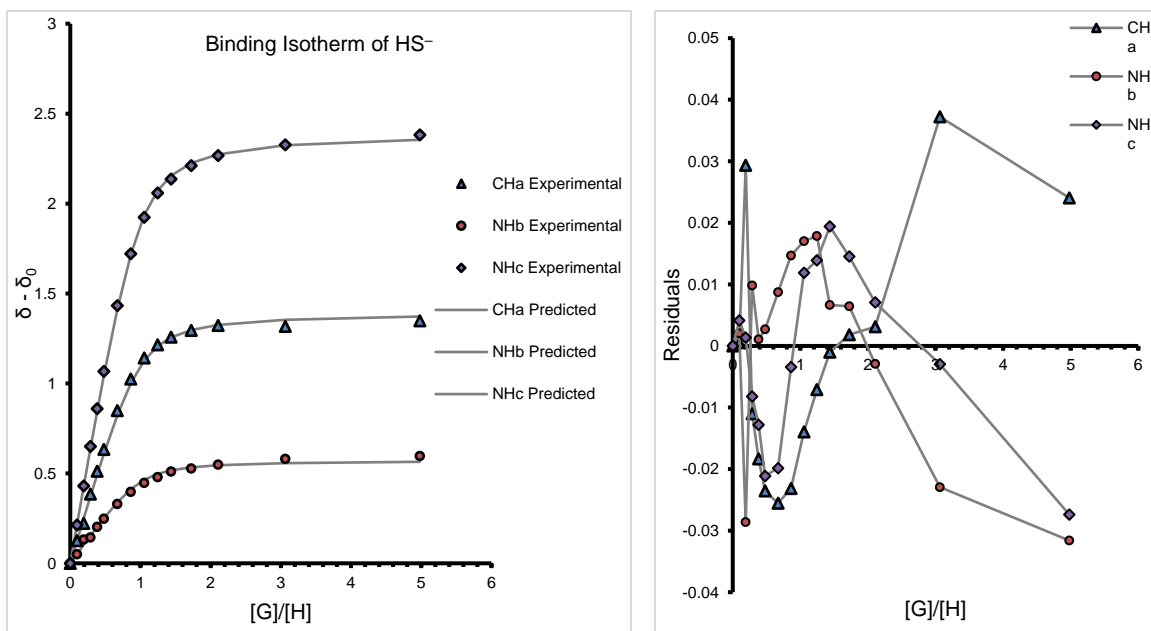


Figure B.19. Representative binding isotherm and residuals for HS⁻ titration of receptor **3.1^F** in 10% DMSO-*d*₆/CD₃CN at 25 °C determined by ¹H NMR spectroscopy.

Table B.11. Representative titration of receptor **3.1^F** with HSe⁻ in 10% DMSO-*d*₆/CD₃CN at 25 °C.

Entry	V _{Guest} (μL)	[Host] (M)	[HSe ⁻] (M)	Equiv.	δ NH _c (ppm)	δ NH _b (ppm)	δ CH _a (ppm)
0	0	2.0E-03	0.0E+00	0.00	8.862	7.926	7.785
1	5	2.0E-03	1.4E-04	0.07	8.923	7.94	7.822
2	5	2.0E-03	2.9E-04	0.14	8.992	7.959	7.856
3	5	2.0E-03	4.2E-04	0.21	9.047	7.977	7.892
4	5	2.0E-03	5.6E-04	0.29	9.102	7.995	7.92
5	10	1.9E-03	8.3E-04	0.43	9.198	8.022	7.979
6	10	1.9E-03	1.1E-03	0.57	9.285	8.049	8.025
7	10	1.9E-03	1.3E-03	0.72	9.37	8.074	8.074
8	15	1.8E-03	1.7E-03	0.93	9.464	8.103	8.125
9	15	1.8E-03	2.0E-03	1.15	9.55	8.13	8.182
10	20	1.7E-03	2.4E-03	1.43	9.651	8.16	8.238
11	25	1.6E-03	2.9E-03	1.79	9.748	8.191	8.293
12	30	1.6E-03	3.4E-03	2.22	9.842	8.217	8.352
13	35	1.5E-03	4.0E-03	2.72	9.922	8.246	8.398
14	40	1.4E-03	4.6E-03	3.29	9.992	8.274	8.438
15	50	1.3E-03	5.2E-03	4.01	10.085	8.333	8.464
16	70	2.0E-03	0.0E+00	0.00	8.862	7.926	7.785

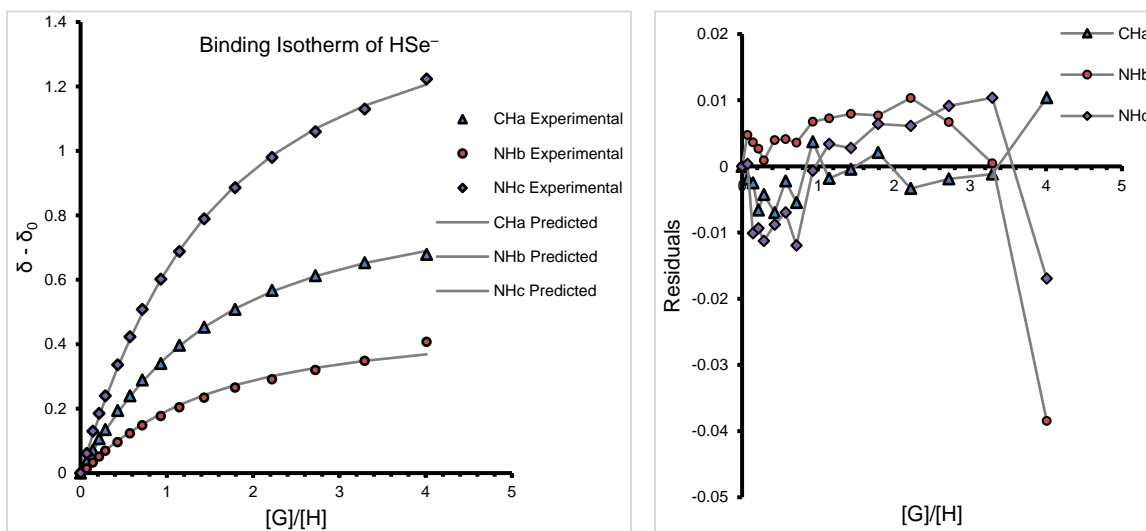


Figure B.20. Representative binding isotherm and residuals for HSe⁻ titration of receptor **3.1^F** in 10% DMSO-*d*₆/CD₃CN at 25 °C determined by ¹H NMR spectroscopy.

Table B.12. Representative titration of receptor **3.1^F** with Cl⁻ in 10% DMSO-*d*₆/CD₃CN at 25 °C.

Entry	V _{Guest} (μL)	[Host] (M)	[Cl ⁻] (M)	Equiv.	δ NH _c (ppm)	δ NH _b (ppm)	δ CH _a (ppm)
0	0	1.1E-03	0.0E+00	0.00	8.849	7.916	7.79
1	5	1.1E-03	1.9E-04	0.17	9.018	7.940	7.904
2	5	1.1E-03	3.7E-04	0.34	9.177	7.96	8.07
3	5	1.1E-03	5.4E-04	0.50	9.31	7.979	8.194
4	10	1.1E-03	8.9E-04	0.82	9.538	8.009	8.398
5	10	1.1E-03	1.2E-03	1.12	9.715	8.033	8.559
6	15	1.1E-03	1.7E-03	1.56	9.875	8.064	8.695
7	20	1.1E-03	2.3E-03	2.11	10.013	8.083	8.817
8	25	1.1E-03	3.0E-03	2.74	10.116	8.091	8.903
9	30	1.1E-03	3.7E-03	3.43	10.185	8.101	8.959
10	40	1.1E-03	4.6E-03	4.26	10.239	8.115	9
11	50	1.1E-03	5.6E-03	5.16	10.279	8.123	9.029
12	70	1.1E-03	6.8E-03	6.23	10.312	8.133	9.045
13	100	1.1E-03	8.1E-03	7.47	10.344	8.141	9.057
14	150	1.1E-03	9.7E-03	8.88	10.374	8.157	9.064
15	200	1.1E-03	1.1E-02	10.22	10.381	8.165	9.064

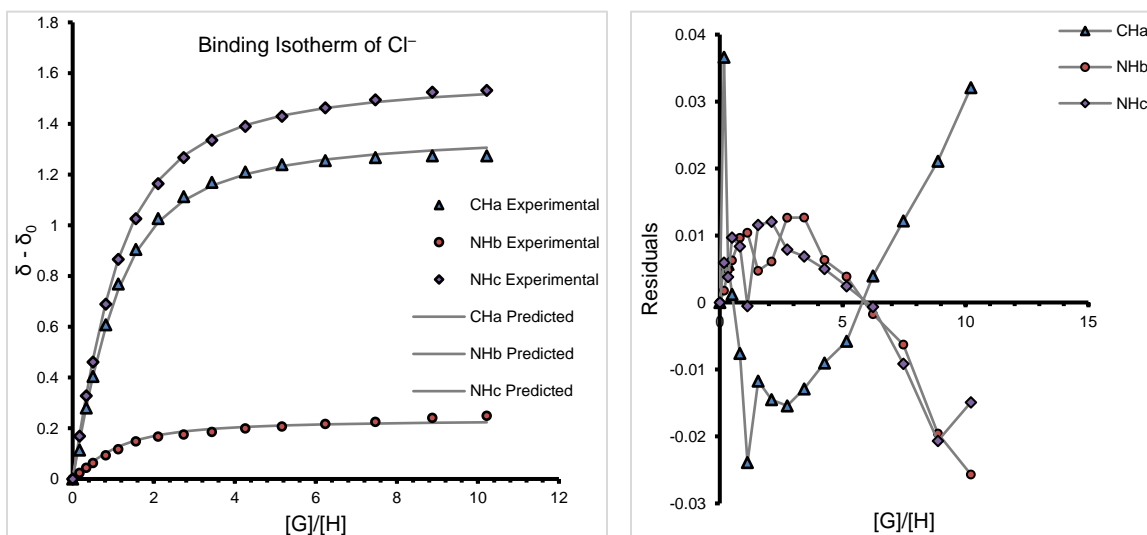


Figure B.21. Representative binding isotherm and residuals for Cl⁻ titration of receptor **3.1^F** in 10% DMSO-*d*₆/CD₃CN at 25 °C determined by ¹H NMR spectroscopy.

Table B.13. Representative titration of receptor **3.1^F** with Br⁻ in 10% DMSO-*d*₆/CD₃CN at 25 °C.

Entry	V _{Guest} (μL)	[Host] (M)	[Br ⁻] (M)	Equiv.	δ NH _c (ppm)	δ NH _b (ppm)	δ CH _a (ppm)
0	0	2.0E-03	0.0E+00	0.00	8.841	7.913	7.79
1	10	2.0E-03	8.2E-04	0.41	8.96	7.935	7.898
2	10	2.0E-03	1.6E-03	0.81	9.045	7.949	7.98
3	10	2.0E-03	2.4E-03	1.19	9.114	7.962	8.051
4	10	2.0E-03	3.1E-03	1.55	9.172	7.973	8.101
5	15	2.0E-03	4.1E-03	2.08	9.25	7.986	8.175
6	15	2.0E-03	5.1E-03	2.58	9.316	7.997	8.238
7	20	2.0E-03	6.4E-03	3.20	9.381	8.009	8.298
8	20	2.0E-03	7.5E-03	3.78	9.438	8.019	8.35
9	25	2.0E-03	8.9E-03	4.46	9.497	8.029	8.404
10	25	2.0E-03	1.0E-02	5.09	9.547	8.037	8.448
11	30	2.0E-03	1.2E-02	5.78	9.595	8.047	8.488
12	30	2.0E-03	1.3E-02	6.41	9.635	8.052	8.523
13	40	2.0E-03	1.4E-02	7.18	9.663	8.06	8.546
14	50	2.0E-03	1.6E-02	8.03	9.71	8.068	8.582
15	60	2.0E-03	1.8E-02	8.93	9.732	8.074	8.597
16	80	2.0E-03	2.0E-02	9.94	9.774	8.084	8.631
17	100	2.0E-03	2.2E-02	10.99	9.797	8.09	8.647
18	150	2.0E-03	2.4E-02	12.24	9.822	8.097	8.671

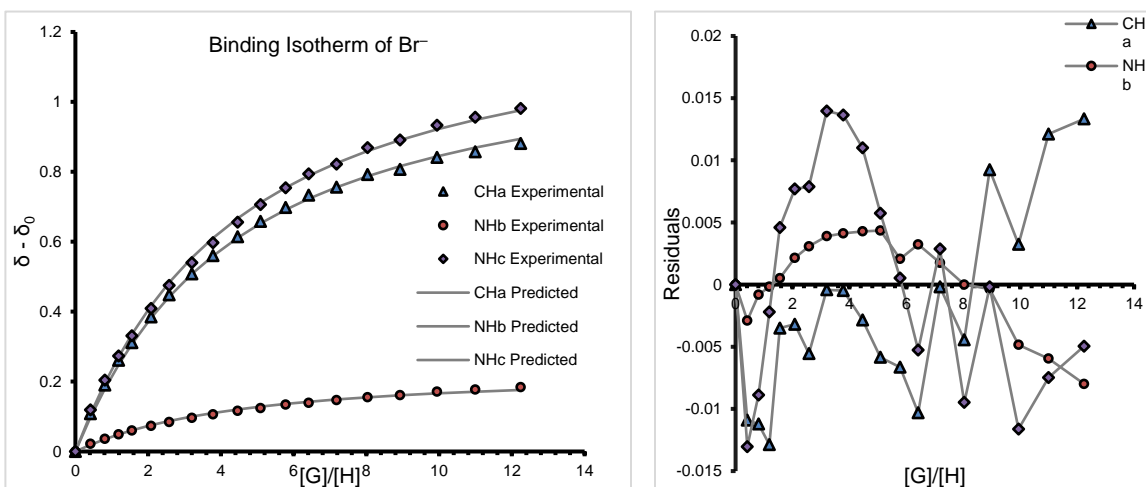


Figure B.22. Representative binding isotherm and residuals for Br⁻ titration of receptor **3.1^F** in 10% DMSO-*d*₆/CD₃CN at 25 °C determined by ¹H NMR spectroscopy.

Table B.14. Representative titration of receptor **3.1^H** with HSe⁻ in 10% DMSO-*d*₆/CD₃CN at 25 °C.

Entry	V _{Guest} (μL)	[Host] (M)	[HSe ⁻] (M)	Equiv.	δ NH _c (ppm)	δ NH _b (ppm)	δ CH _a (ppm)
0	0	2.0E-03	0.0E+00	0.00	8.907	7.922	8.002
1	5	2.0E-03	1.4E-04	0.07	8.974	7.939	8.041
2	5	2.0E-03	2.9E-04	0.15	9.039	7.958	8.079
3	5	1.9E-03	4.2E-04	0.22	9.092	7.976	8.104
4	5	1.9E-03	5.6E-04	0.29	9.144	7.991	8.129
5	10	1.9E-03	8.3E-04	0.44	9.226	8.018	8.179
6	10	1.8E-03	1.1E-03	0.58	9.304	8.039	8.222
7	10	1.8E-03	1.3E-03	0.73	9.373	8.065	8.26
8	15	1.8E-03	1.7E-03	0.95	9.472	8.092	8.312
9	15	1.7E-03	2.0E-03	1.17	9.553	8.118	8.354
10	20	1.7E-03	2.4E-03	1.46	9.638	8.143	8.411
11	25	1.6E-03	2.9E-03	1.83	9.733	8.175	8.457
12	30	1.5E-03	3.4E-03	2.27	9.83	8.199	8.508
13	35	1.4E-03	4.0E-03	2.78	9.902	8.223	8.547
14	40	1.4E-03	4.6E-03	3.36	9.977	8.265	8.58
15	45	2.0E-03	0.0E+00	0.00	8.907	7.922	8.002

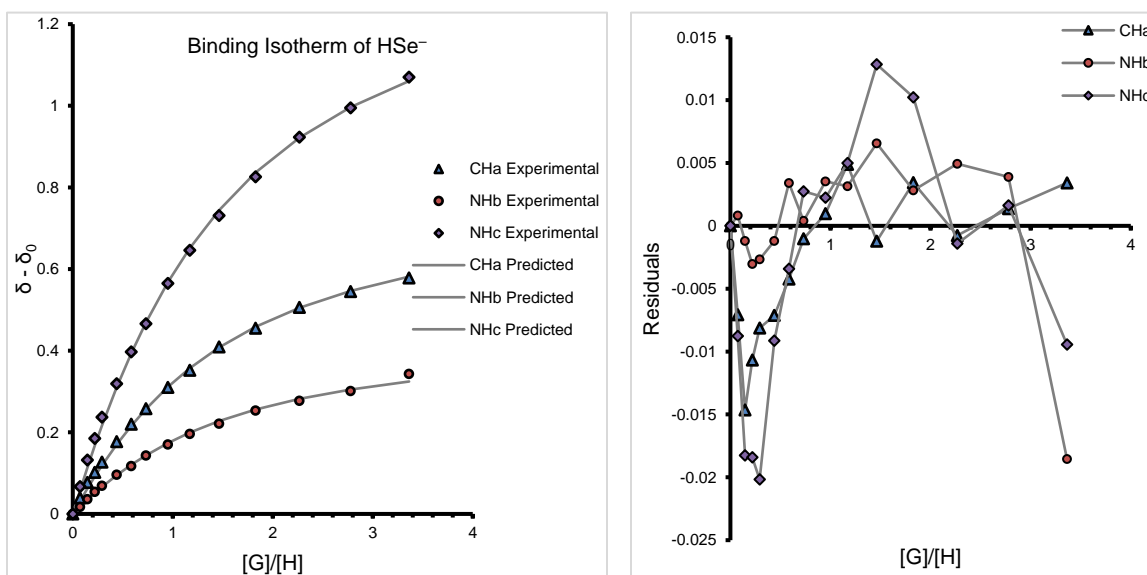


Figure B.23. Representative binding isotherm and residuals for HSe⁻ titration of receptor **3.1^H** in 10% DMSO-*d*₆/CD₃CN at 25 °C determined by ¹H NMR spectroscopy.

Table B.15. Representative titration of receptor **3.1^H** with Br⁻ in 10% DMSO-*d*₆/CD₃CN at 25 °C.

Entry	V _{Guest} (μL)	[Host] (M)	[Br ⁻] (M)	Equiv.	δ NH _c (ppm)	δ NH _b (ppm)	δ CH _a (ppm)
0	0	1.0E-03	0.0E+00	0.00	8.843	7.905	7.974
1	10	1.0E-03	6.5E-04	0.62	8.942	7.918	8.071
2	10	1.0E-03	1.3E-03	1.22	9.021	7.932	8.144
3	10	1.0E-03	1.9E-03	1.80	9.086	7.941	8.208
4	10	1.0E-03	2.5E-03	2.35	9.15	7.95	8.27
5	15	1.0E-03	3.3E-03	3.14	9.222	7.961	8.339
6	15	1.0E-03	4.1E-03	3.89	9.286	7.97	8.4
7	20	1.0E-03	5.0E-03	4.84	9.361	7.982	8.469
8	20	1.0E-03	6.0E-03	5.72	9.419	7.989	8.526
9	25	1.0E-03	7.0E-03	6.74	9.48	7.997	8.583
10	25	1.0E-03	8.0E-03	7.69	9.532	8.005	8.63
11	30	1.0E-03	9.1E-03	8.73	9.581	8.012	8.678
12	30	1.0E-03	1.0E-02	9.69	9.62	8.017	8.712
13	40	1.0E-03	1.1E-02	10.85	9.662	8.024	8.748
14	50	1.0E-03	1.3E-02	12.14	9.701	8.031	8.786
15	60	1.0E-03	1.4E-02	13.49	9.73	8.031	8.807
16	80	1.0E-03	1.6E-02	15.02	9.775	8.039	8.851
17	100	1.0E-03	1.7E-02	16.61	9.805	8.046	8.874

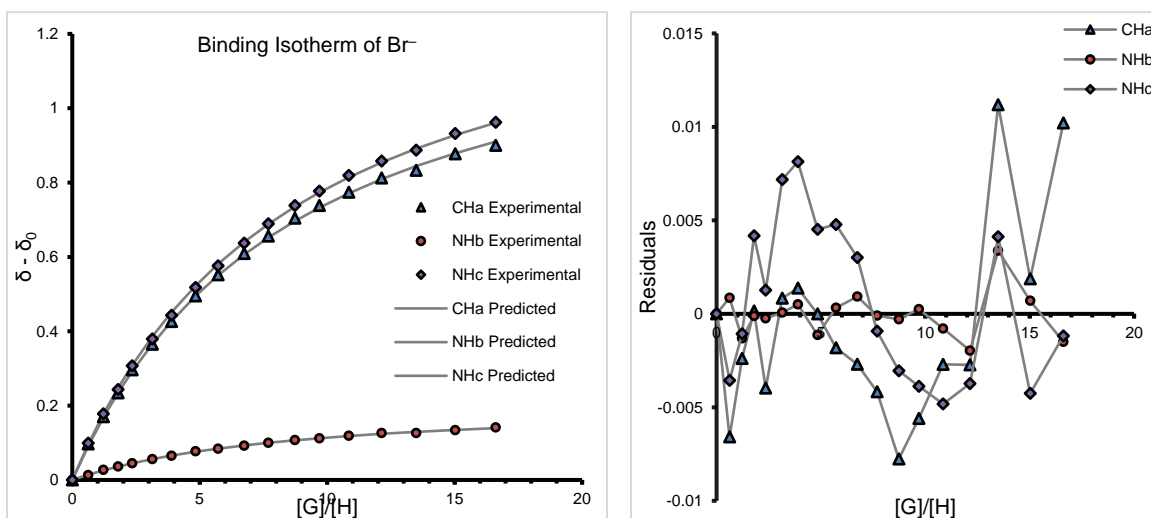


Figure B.24. Representative binding isotherm and residuals for Br⁻ titration of receptor **3.1^H** in 10% DMSO-*d*₆/CD₃CN at 25 °C determined by ¹H NMR spectroscopy.

Table B.16. Representative titration of receptor **3.1**^{NMe₂} with HS⁻ in 10% DMSO-*d*₆/CD₃CN at 25 °C.

Entry	V _{Guest} (μL)	[Host] (M)	[HS ⁻] (M)	Equiv.	δ NH _c (ppm)	δ NH _b (ppm)	δ CH _a (ppm)
0	0	2.1E-03	0.0E+00	0.00	8.885	7.903	7.265
1	10	2.1E-03	2.1E-04	0.10	9.047	7.943	7.345
2	20	2.0E-03	4.0E-04	0.20	9.221	7.981	7.431
3	30	2.0E-03	6.0E-04	0.30	9.38	8.017	7.52
4	40	1.9E-03	7.8E-04	0.40	9.55	8.051	7.601
5	55	1.9E-03	1.0E-03	0.55	9.762	8.1	7.72
6	70	1.8E-03	1.3E-03	0.70	9.979	8.148	7.828
7	90	1.8E-03	1.6E-03	0.90	10.216	8.199	7.955
8	110	1.7E-03	1.9E-03	1.10	10.412	8.244	8.061
9	135	1.7E-03	2.2E-03	1.35	10.601	8.287	8.157
10	160	1.6E-03	2.6E-03	1.60	10.746	8.321	8.23
11	190	1.5E-03	2.9E-03	1.90	10.857	8.354	8.288
12	220	1.5E-03	3.2E-03	2.21	10.92	8.37	8.339
13	260	1.4E-03	3.6E-03	2.61	10.982	8.391	8.391
14	310	1.3E-03	4.0E-03	3.11	11.041	8.411	8.411
15	370	1.2E-03	4.5E-03	3.71	11.08	8.437	8.437
16	450	1.1E-03	5.0E-03	4.51	11.094	8.451	8.451
17	550	1.0E-03	5.5E-03	5.51	11.126	8.459	8.459

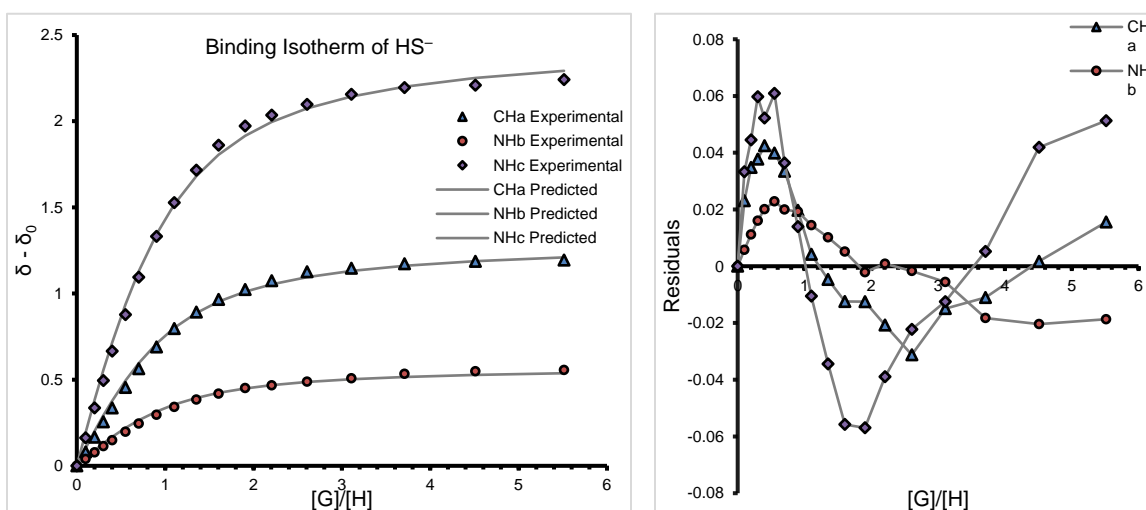


Figure B.25. Representative binding isotherm and residuals for HS⁻ titration of receptor **3.1**^{NMe₂} in 10% DMSO-*d*₆/CD₃CN at 25 °C determined by ¹H NMR spectroscopy.

Table B.17. Representative titration of receptor **3.1^{NMe2}** with HSe⁻ in 10% DMSO-*d*₆/CD₃CN at 25 °C.

Entry	V _{Guest} (μL)	[Host] (M)	[HSe ⁻] (M)	Equiv.	δ NH _c (ppm)	δ NH _b (ppm)	δ CH _a (ppm)
0	0	2.0E-03	0.0E+00	0.00	8.902	7.909	7.266
1	5	2.0E-03	1.7E-04	0.09	8.991	7.935	7.307
2	5	2.0E-03	3.4E-04	0.17	9.052	7.953	7.337
3	5	1.9E-03	5.1E-04	0.26	9.109	7.97	7.363
4	5	1.9E-03	6.7E-04	0.35	9.159	7.985	7.38
5	10	1.9E-03	9.8E-04	0.52	9.242	8.02	7.417
6	10	1.9E-03	1.3E-03	0.69	9.327	8.033	7.465
7	10	1.8E-03	1.6E-03	0.86	9.397	8.062	7.498
8	10	1.8E-03	1.9E-03	1.04	9.472	8.086	7.52
9	15	1.7E-03	2.3E-03	1.30	9.556	8.113	7.566
10	15	1.7E-03	2.6E-03	1.56	9.634	8.138	7.601
11	20	1.6E-03	3.1E-03	1.90	9.71	8.168	7.638
12	25	1.6E-03	3.7E-03	2.34	9.803	8.192	7.675
13	30	1.5E-03	4.3E-03	2.85	9.872	8.222	7.71
14	40	1.4E-03	5.1E-03	3.55	9.957	8.25	7.746
15	50	1.3E-03	5.9E-03	4.41	10.025	8.275	7.778
15	70	1.2E-03	6.8E-03	5.62	10.107	8.308	7.808

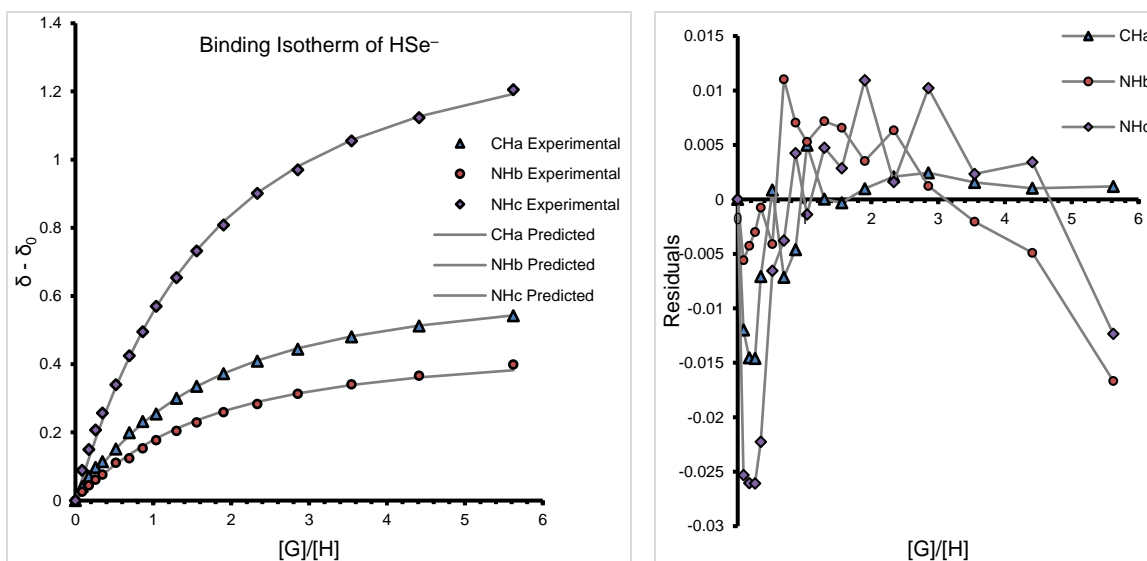


Figure B.26. Representative binding isotherm and residuals for HSe⁻ titration of receptor **3.1^{NMe2}** in 10% DMSO-*d*₆/CD₃CN at 25 °C determined by ¹H NMR spectroscopy.

Table B.18. Representative titration of receptor **3.1**^{NMe₂} with Cl⁻ in 10% DMSO-*d*₆/CD₃CN at 25 °C.

Entry	V _{Guest} (μL)	[Host] (M)	[Cl ⁻] (M)	Equiv.	δ NH _c (ppm)	δ NH _b (ppm)	δ CH _a (ppm)
0	0	2.1E-03	0.0E+00	0.00	8.875	7.901	7.257
1	5	2.1E-03	2.2E-04	0.11	8.988	7.915	7.345
2	5	2.1E-03	4.4E-04	0.21	9.092	7.928	7.428
3	5	2.1E-03	6.5E-04	0.31	9.19	7.941	7.507
4	10	2.1E-03	1.1E-03	0.51	9.364	7.963	7.648
5	10	2.1E-03	1.5E-03	0.70	9.503	7.981	7.759
6	10	2.1E-03	1.8E-03	0.88	9.621	7.996	7.853
7	15	2.1E-03	2.4E-03	1.14	9.764	8.014	7.966
8	15	2.1E-03	2.9E-03	1.39	9.868	8.028	8.05
9	20	2.1E-03	3.6E-03	1.70	9.966	8.041	8.126
10	20	2.1E-03	4.2E-03	1.99	10.04	8.053	8.181
11	25	2.1E-03	4.9E-03	2.32	10.103	8.061	8.228
12	30	2.1E-03	5.7E-03	2.70	10.157	8.071	8.266
13	40	2.1E-03	6.6E-03	3.14	10.205	8.08	8.298
14	60	2.1E-03	7.8E-03	3.73	10.254	8.091	8.327
15	100	2.1E-03	9.5E-03	4.52	10.302	8.104	8.349
16	180	2.1E-03	1.2E-02	5.56	10.346	8.12	8.366
17	300	2.1E-03	1.4E-02	6.69	10.342	8.118	8.367

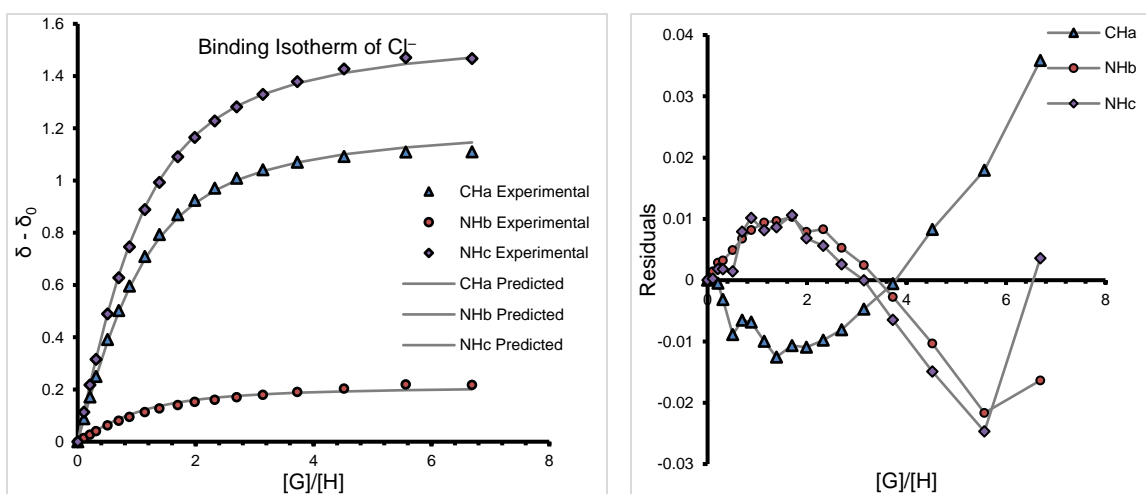


Figure B.27. Representative binding isotherm and residuals for Cl⁻ titration of receptor **3.1**^{NMe₂} in 10% DMSO-*d*₆/CD₃CN at 25 °C determined by ¹H NMR spectroscopy.

Table B.19. Representative titration of receptor **3.1^{NMe2}** with Br⁻ in 10% DMSO-*d*₆/CD₃CN at 25 °C.

Entry	V _{Guest} (μL)	[Host] (M)	[Br ⁻] (M)	Equiv.	δ NH _c (ppm)	δ NH _b (ppm)	δ CH _a (ppm)
0	0	2.0E-03	0.0E+00	0.00	8.895	7.906	7.264
1	5	2.0E-03	2.6E-04	0.13	8.92	7.910	7.283
2	10	2.0E-03	7.6E-04	0.39	8.961	7.919	7.315
3	15	2.0E-03	1.5E-03	0.75	9.021	7.93	7.362
4	20	2.0E-03	2.4E-03	1.20	9.089	7.942	7.396
5	25	2.0E-03	3.4E-03	1.73	9.164	7.956	7.478
6	30	2.0E-03	4.5E-03	2.30	9.233	7.967	7.535
7	40	2.0E-03	5.9E-03	2.98	9.31	7.98	7.595
8	50	2.0E-03	7.3E-03	3.71	9.387	7.993	7.657
9	60	2.0E-03	8.8E-03	4.47	9.453	8.006	7.708
10	80	2.0E-03	1.0E-02	5.31	9.512	8.016	7.754
11	100	2.0E-03	1.2E-02	6.16	9.567	8.025	7.794
12	130	2.0E-03	1.4E-02	7.02	9.612	8.034	7.829
13	170	2.0E-03	1.6E-02	7.88	9.653	8.043	7.857
14	120	2.0E-03	1.6E-02	8.35	9.671	8.047	7.871

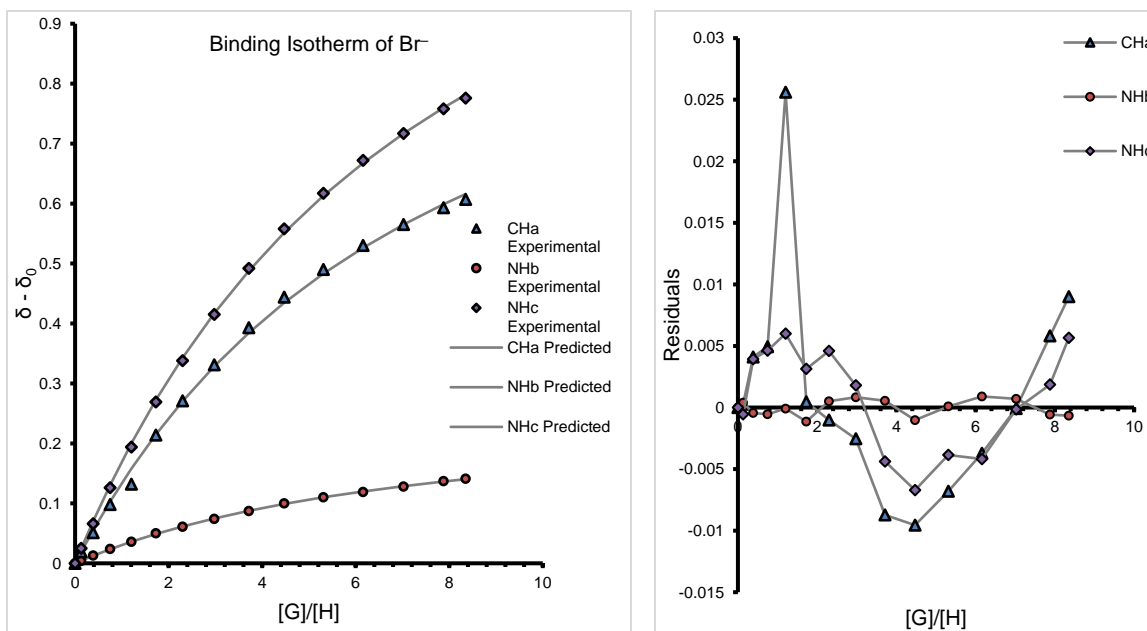


Figure B.28. Representative binding isotherm and residuals for Br⁻ titration of receptor **3.1^{NMe2}** in 10% DMSO-*d*₆/CD₃CN at 25 °C determined by ¹H NMR spectroscopy.

Linear Regression Fitting and Statistics of $\Delta G_{\text{binding}}$ and σ_p .

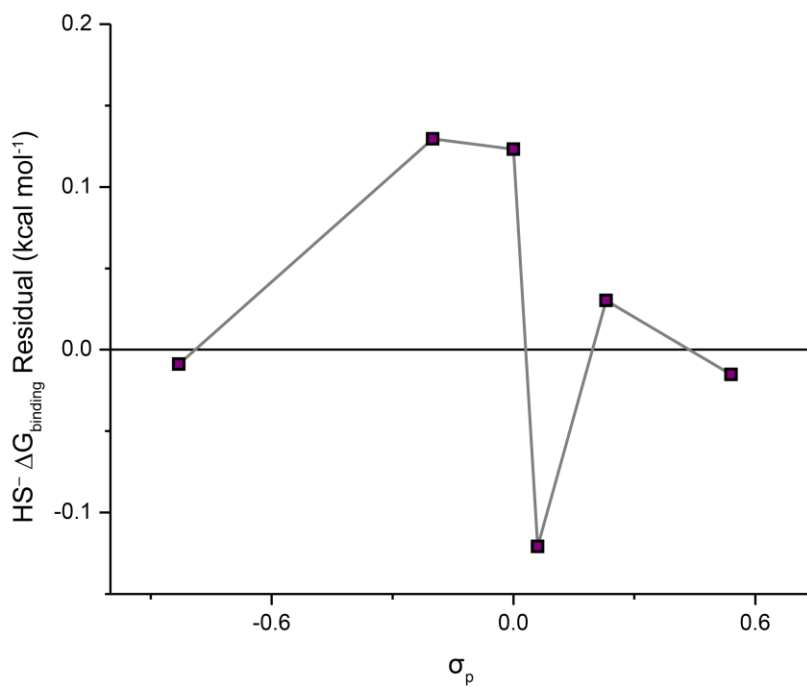


Figure B.29. Linear regression residuals of $\Delta G_{\text{binding}}$ of HS^- and σ_p .

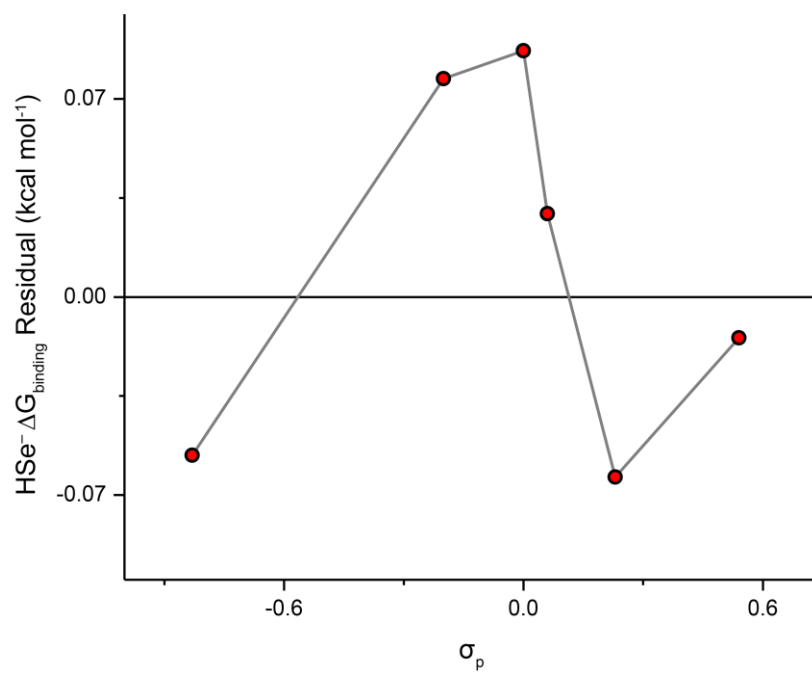


Figure B.30. Linear regression residuals of $\Delta G_{\text{binding}}$ of HSe^- and σ_p .

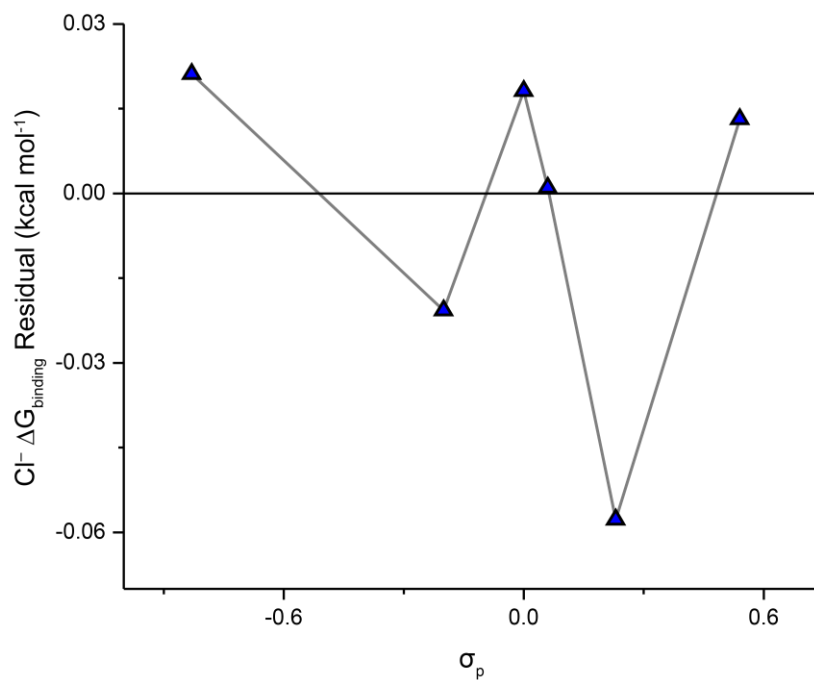


Figure B.31. Linear regression residuals of $\Delta G_{\text{binding}}$ of Cl^- and σ_p .

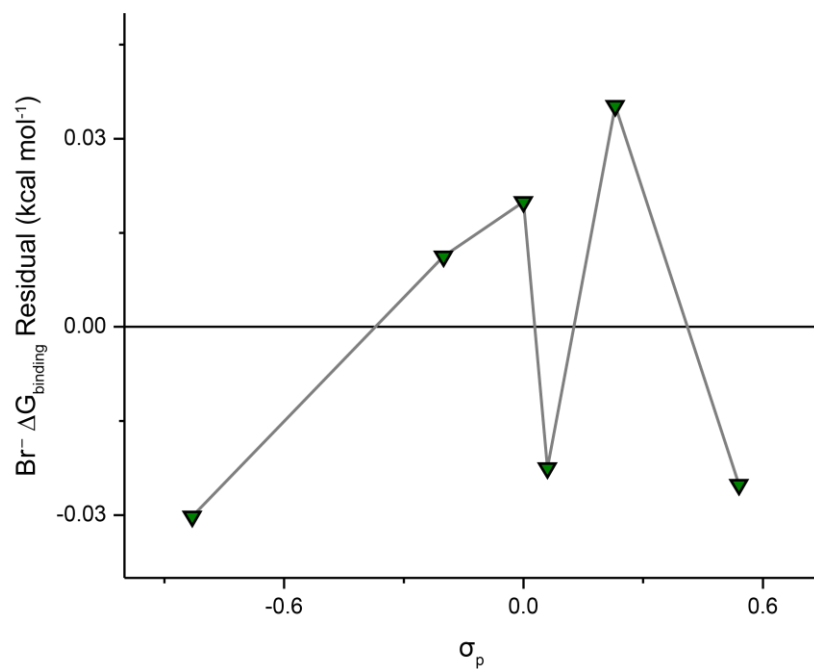


Figure B.32. Linear regression residuals of $\Delta G_{\text{binding}}$ of Br^- and σ_p .

Linear Regression Fitting and Statistics of $\log(K_a^R/K_a^H)$ and σ_p .

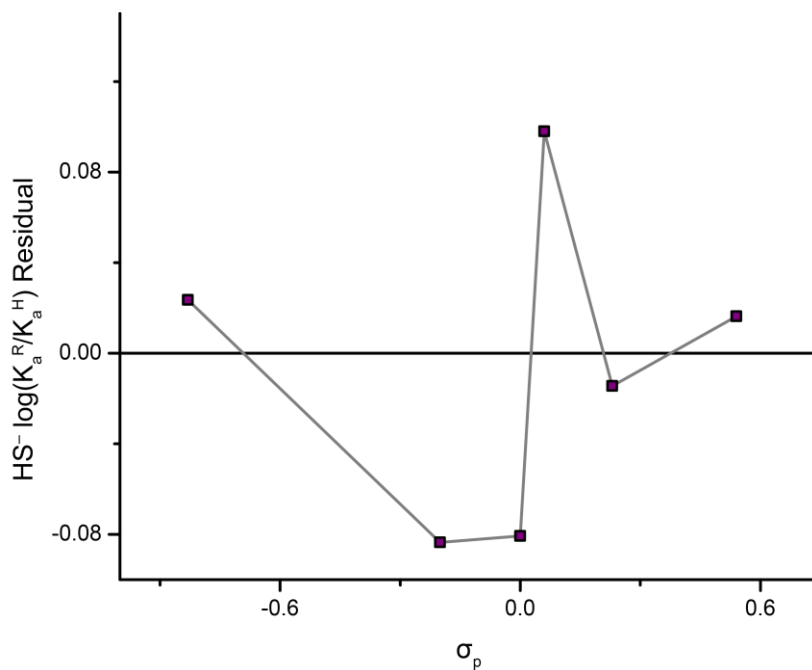


Figure B.33. Linear regression residuals of $\log(K_a^R/K_a^H)$ of HS⁻ and σ_p .

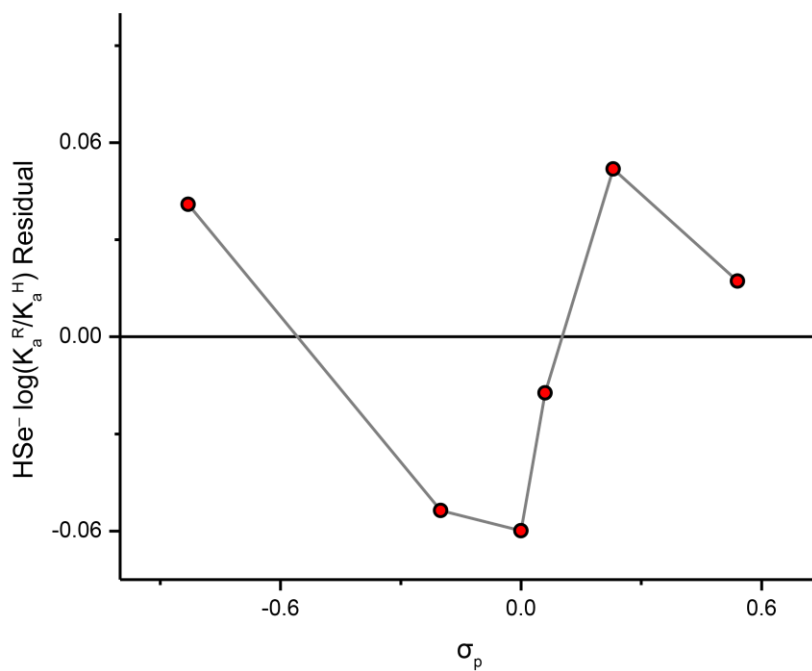


Figure B.34. Linear regression residuals of $\log(K_a^R/K_a^H)$ of HS⁻ and σ_p .

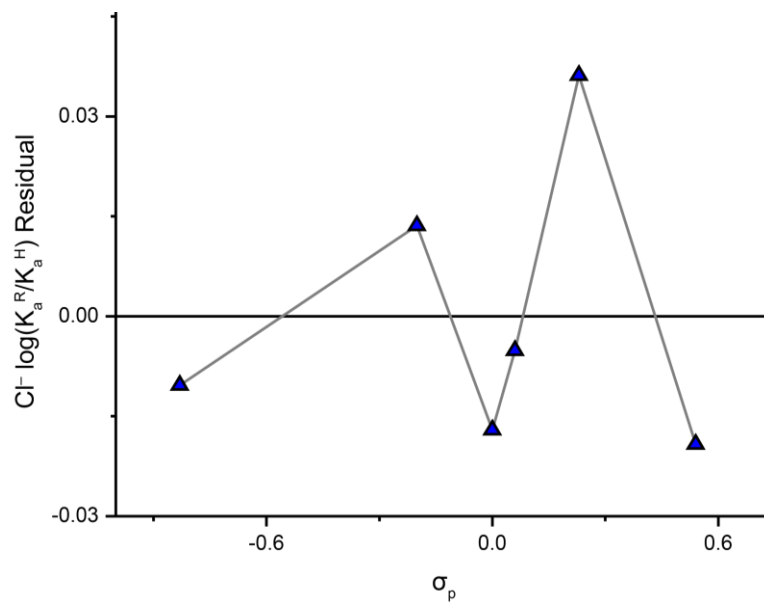


Figure B.35. Linear regression residuals of $\log(K_a^R/K_a^H)$ of Cl^- and σ_p .

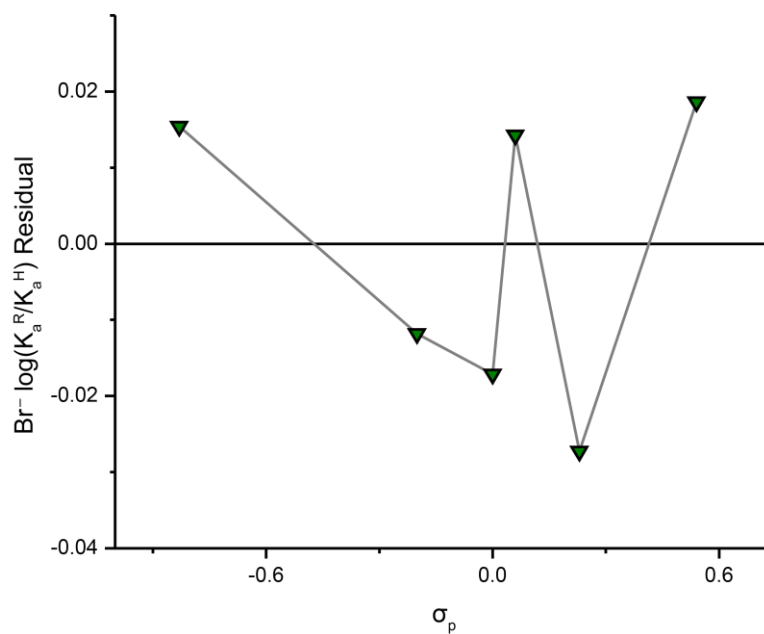


Figure B.36. Linear regression residuals of $\log(K_a^R/K_a^H)$ of Br^- and σ_p .

Table B.20. Results of linear regression of $\log(K_a^R/K_a^H)$ vs. σ_p when the intercept is forced through the origin.

Guest	Slope	p-value		R ²
		Slope	Model	
HS ⁻	0.70 ± 0.10	< 0.01	< 0.01	0.91
HSe ⁻	0.31 ± 0.07	< 0.01	< 0.01	0.80
Cl ⁻	0.25 ± 0.03	< 0.01	< 0.01	0.95
Br ⁻	0.22 ± 0.03	< 0.01	< 0.01	0.94

Analysis of Covariance on Hammett Plots.

Analysis of covariance of the linear regressions obtained for the Hammett plots for each anion was used to determine if the K_a of each anion showed the same response to the changing σ_p of the -R substituent on the receptor. The p-value represents the probability that the linear regressions for two anions would appear to have different slopes when they in fact have the same slope. Any p-value > 0.05 is considered statistically insignificant at the 95% confidence interval, meaning we cannot confidently say that the linear regressions have different slopes.

Table B.21. Results of analysis of covariance on Hammett plots.

	p-value _{different models}
HS ⁻ vs. HSe ⁻	< 0.01
HS ⁻ vs. Cl ⁻	< 0.01
HS ⁻ vs. Br ⁻	< 0.01
HSe ⁻ vs. Cl ⁻	0.28
HSe ⁻ vs. Br ⁻	0.11
Cl ⁻ vs. Br ⁻	0.28

Swain-Lupton Analysis

Table B.22. Results of multivariable linear regression for Swain-Lupton analysis when the intercept is forced through the origin.

Guest	ρ_f	ρ_r	p-value			R^2	$R^2_{adj.}$	%R
			ρ_f	ρ_r	Model			
HS⁻	0.95 ± 0.05	0.63 ± 0.04	> 0.01	> 0.01	> 0.01	0.99	0.99	40 ± 3
HSe⁻	0.49 ± 0.05	0.26 ± 0.04	> 0.01	> 0.01	> 0.01	0.96	0.95	35 ± 6
Cl⁻	0.29 ± 0.04	0.24 ± 0.03	> 0.01	> 0.01	> 0.01	0.96	0.96	45 ± 6
Br⁻	0.26 ± 0.03	0.20 ± 0.02	> 0.01	> 0.01	> 0.01	0.97	0.96	44 ± 6

Alternative Hammett parameters

Table B.23 shows the fitting parameters and statistics the linear fit of the LFERs of the binding energy of HS⁻, HSe⁻, Cl⁻, and Br⁻ with σ_m . The Hammett parameter σ_m was developed for substituents in the *meta* position on benzoic acid. This parameter retains similar field and inductive effects of the *para* parameter while decreasing resonance contributions (the average importance of resonance in the σ_p value for each substituent is 53%, while only 22% in σ_m ⁹⁷). Although none of the resulting R^2 suggest a good fit of binding energies to σ_m ($R^2 < 0.90$), the R^2 for the linear fit of the hydrochalcogenides is higher than that of the halides. This suggests that resonance contribution of the substituent is more important for the halides than the hydrochalcogenides.

Table B.24 shows the fitting parameters and statistics the linear fit of the LFERs of the binding energy of HS⁻, HSe⁻, Cl⁻, and Br⁻ with σ_p^+ . The Hammett parameter σ_p^+ was developed to give weight to substituents that can stabilize a build-up of charge through resonance effects (the average importance of resonance in the σ_p^+ value for each

substituent is 66%⁹⁷). We do not expect σ_p^+ to bind well to our systems since the charged resonance structures in Figure B.37 are informal. However, comparison of R^2 shows that σ_p^+ is a better fit for the halides than the hydrochalcogenides, yielding the same conclusion as for σ_m ; resonance contributions are more important to halide binding than hydrochalcogenide binding.

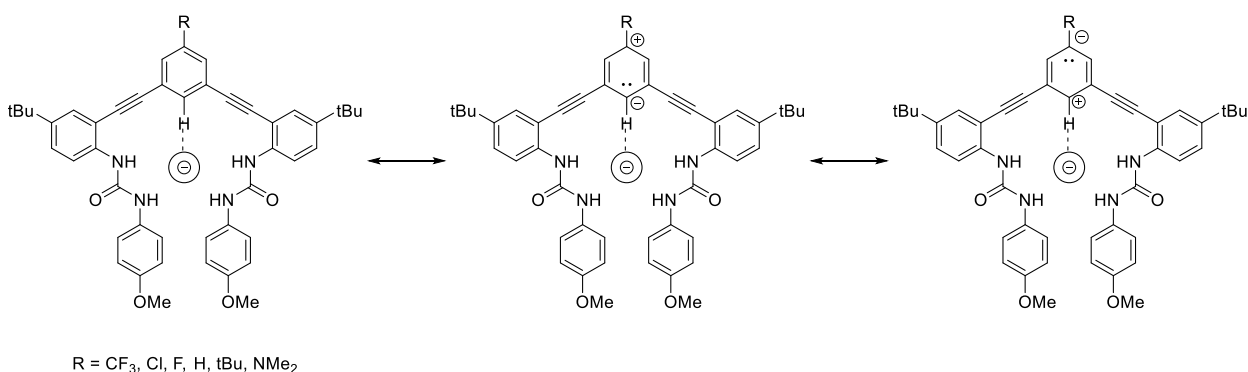


Figure B.37. Informal resonance structures for receptors **3.1^R** that may influence aryl C–H HB donor ability.

Table B.23. Fitting statistics for Hammett plots for all four anions using σ_m .

Guest	ρ	ε	p-value			R^2	$R^2_{\text{adj.}}$
			ρ	ε	Model		
HS⁻	1.20 ± 0.23	-0.13 ± 0.06	< 0.01	0.12	< 0.01	0.87	0.84
HSe⁻	0.55 ± 0.10	-0.04 ± 0.02	< 0.01	0.29	< 0.01	0.88	0.84
Cl⁻	0.39 ± 0.12	-0.05 ± 0.03	0.03	0.21	0.03	0.74	0.67
Br⁻	0.35 ± 0.09	-0.04 ± 0.03	0.02	0.18	0.02	0.78	0.72

Table B.24. Fitting statistics for Hammett plots for all four anions using σ_p^+ .

Guest	ρ	ϵ	p-value			R^2	$R^2_{adj.}$
			ρ	ϵ	Model		
HS⁻	0.40 ± 0.08	0.14 ± 0.06	< 0.01	0.08	< 0.01	0.86	0.83
HSe⁻	0.17 ± 0.05	0.08 ± 0.04	0.02	0.08	0.02	0.76	0.70
Cl⁻	0.15 ± 0.02	0.04 ± 0.02	< 0.01	0.06	< 0.01	0.93	0.91
Br⁻	0.12 ± 0.02	0.04 ± 0.02	< 0.01	0.10	< 0.01	0.89	0.86

Computational Details, Discussion, Geometries, and Energies

We turned to computational investigations to better understand the preference of the C–H HB for HS⁻. All six receptors, four anions, NBu₄⁺ and their respective complexes were optimized in gas phase at the PBE/6-31G* level of theory with final energy refinements at wB97X-D3/def2-TZVPP.²⁴² LFER models correlating σ_p for **3.1^R** to the computed gas phase binding energies agreed with experiments in that more electron-withdrawing *para* substituents favor the host/guest interaction for all four anions. Unlike the experimental data, however, the slopes for all four anions were indistinguishable (average slope = -4), and the receptor was seen to be most selective for Cl⁻ rather than HS⁻.

Exhaustive efforts to refine the energies with solvent corrections were unfruitful. We computed the solvation corrections using SMD²⁴³ at the wB97X-D3/def2-TZVPP level of theory in water, acetonitrile, DMSO, and chloroform. Trends in the binding energies computed in solvent did not match experimental trends. All solvent results showed either no statistically meaningful linear trend ($R^2 < 0.6$ and p-value ~ 0.8), or the

opposite trend in which more electron-donating *para* substituents favor the host-guest interaction.¹⁰⁵ Collectively, these results reveal that the trends observed experimentally are the results of complex solvent-solute interaction or dynamic phenomena and also clearly reveal the limitations of current continuum solvent modeling methods for unique solvent systems as used in this work.

Complete author list of Gaussian 09

Gaussian 09, Revision D.01, Frisch, M. J.; Trucks, G. W.; Schlegel, H. B.; Scuseria, G. E.; Robb, M. A.; Cheeseman, J. R.; Scalmani, G.; Barone, V.; Mennucci, B.; Petersson, G. A.; Nakatsuji, H.; Caricato, M.; Li, X.; Hratchian, H. P.; Izmaylov, A. F.; Bloino, J.; Zheng, G.; Sonnenberg, J. L.; Hada, M.; Ehara, M.; Toyota, K.; Fukuda, R.; Hasegawa, J.; Ishida, M.; Nakajima, T.; Honda, Y.; Kitao, O.; Nakai, H.; Vreven, T.; Montgomery, J. A., Jr.; Peralta, J. E.; Ogliaro, F.; Bearpark, M.; Heyd, J. J.; Brothers, E.; Kudin, K. N.; Staroverov, V. N.; Kobayashi, R.; Normand, J.; Raghavachari, K.; Rendell, A.; Burant, J. C.; Iyengar, S. S.; Tomasi, J.; Cossi, M.; Rega, N.; Millam, J. M.; Klene, M.; Knox, J. E.; Cross, J. B.; Bakken, V.; Adamo, C.; Jaramillo, J.; Gomperts, R.; Stratmann, R. E.; Yazyev, O.; Austin, A. J.; Cammi, R.; Pomelli, C.; Ochterski, J. W.; Martin, R. L.; Morokuma, K.; Zakrzewski, V. G.; Voth, G. A.; Salvador, P.; Dannenberg, J. J.; Dapprich, S.; Daniels, A. D.; Farkas, Ö.; Foresman, J. B.; Ortiz, J. V.; Cioslowski, J.; Fox, D. J. Gaussian, Inc., Wallingford CT, 2009.

Complete author list of ORCA version 4.0

ORCA version 4.0, Neese, F.; Wennmohs, F.; Aravena, D.; Atanasov, M.; Becker, U.; Bykov, D.; Chilkuri, V. G.; Datta, D.; Dutta, A. K.; Ganyushin, D.; Guo, Y.; Hansen, A.; Huntington, L.; Izsak, R.; Kollmar, C.; Kossmann, S.; Krupicka, M.; Lenk, D.; Liakos, D. G.; Manganas, D.; Pantazis, D. A.; Petrenko, T.; Pinski, P.; Reimann, C.; Retegan, M.; Riplinger, C.; Risthaus, T.; Roemelt, M.; Saitow, M.; Sandhofer, B.; Schapiro, I.; Sivalingam, K.; Stoychev, G.; Wezislá, B.; Kallay, M.; Grimme, S.; Valeev, E.; Chan, G.; Pittner, J.; Brehm, M.; Bistoni, G.; Schneider, W. *WIREs: Comp. Mol. Sci.* 8, e1327

D3 corrections in ORCA

S.Grimme, J.Antony, S.Ehrlich and H.Krieg, *J.Chem.Phys.*, **2010**, *132*, 154104

def2-TZVPP

F. Weigend and R. Ahlrichs, *Phys. Chem. Chem. Phys.* **2005**, *7*, 3297

def2/J

F. Weigend, *Phys. Chem. Chem. Phys.* **2006**, *8*, 1057

def2-TZVPP/C

H-La, Hf-Rn : A. Hellweg, C. Hattig, S. Hofener and W. Klopper, *Theor. Chem. Acc.* **2007**, 117, 587

Ce-Lu : J. Chmela and M. E. Harding, *Mol. Phys.* **2018**

General protocol for geometry optimization and energy calculations

Geometry optimizations and single point energy refinements were completed using the Gaussian 09 computational package (see above reference) with the ultrafine integration grid to minimize errors. All pertinent ground state structures were located with geometry optimizations using PBE/6-31G(d). Higher level single point energy refinements were computed in ORCA version 4.0.1 with wB97X-D3/def2-TZVPP in SMD(chloroform). Final corrected energies were the sum of the single point energy refinement and the Gibbs thermal correction factor of the respective optimized structure. All reported computed thermodynamics and barriers are derived from differences in the final corrected energies. All energies are reported as kcal/mol as converted from hartrees (1 Ha = 627.5095 kcal/mol). All 3D structure images were rendered in GaussView visualization software.²⁴³

Figures B.38–B.42. Hammett Value (σ_p) for **3.1^R** vs computed binding energies ($\Delta G_{\text{binding}}$)

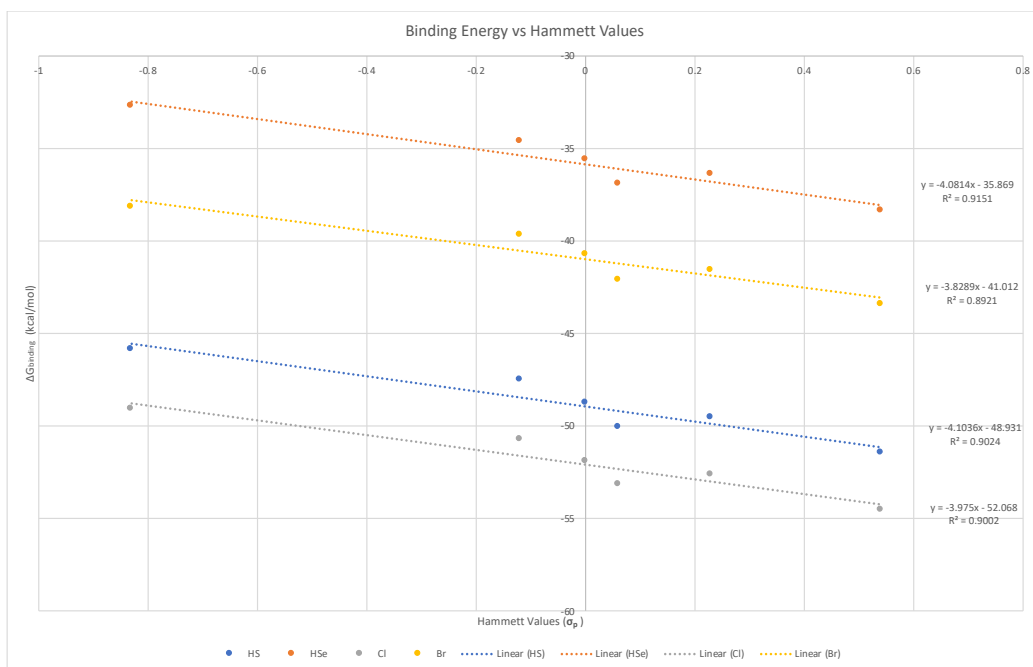


Figure B.38. wb97X-D3/def2-TZVPP//PBE/6-31G(d)/

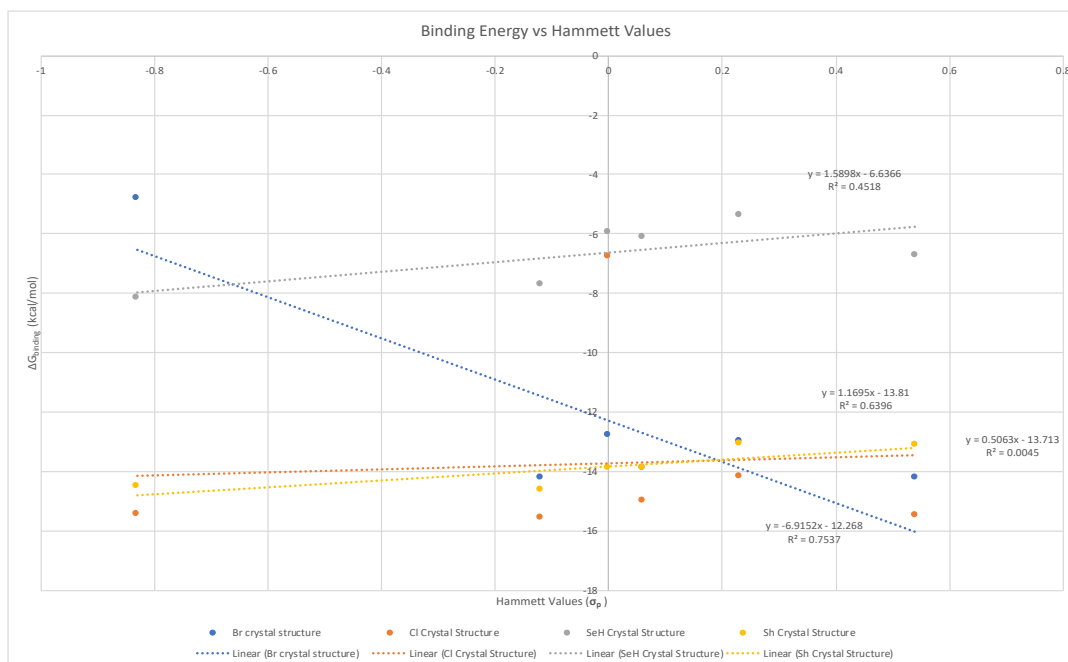


Figure B.39. wb97x/def2-TZVPP/SMD/Chloroform//PBE/6-31G(d)/

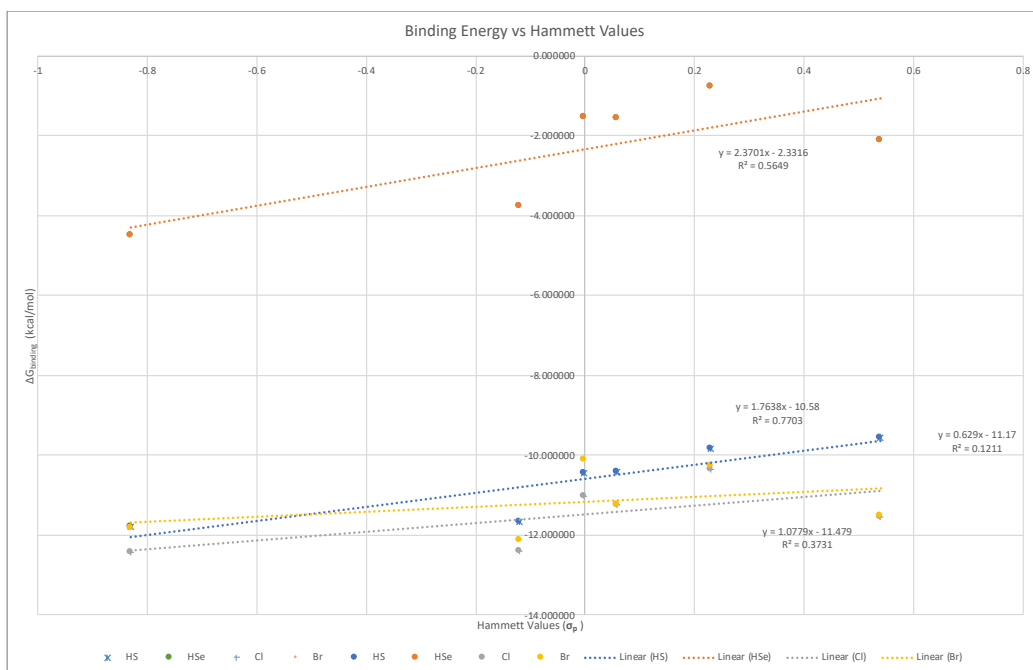


Figure B.40. wb97x/def2-TZVPP/SMD/Acetonitrile//PBE/6-31G(d)

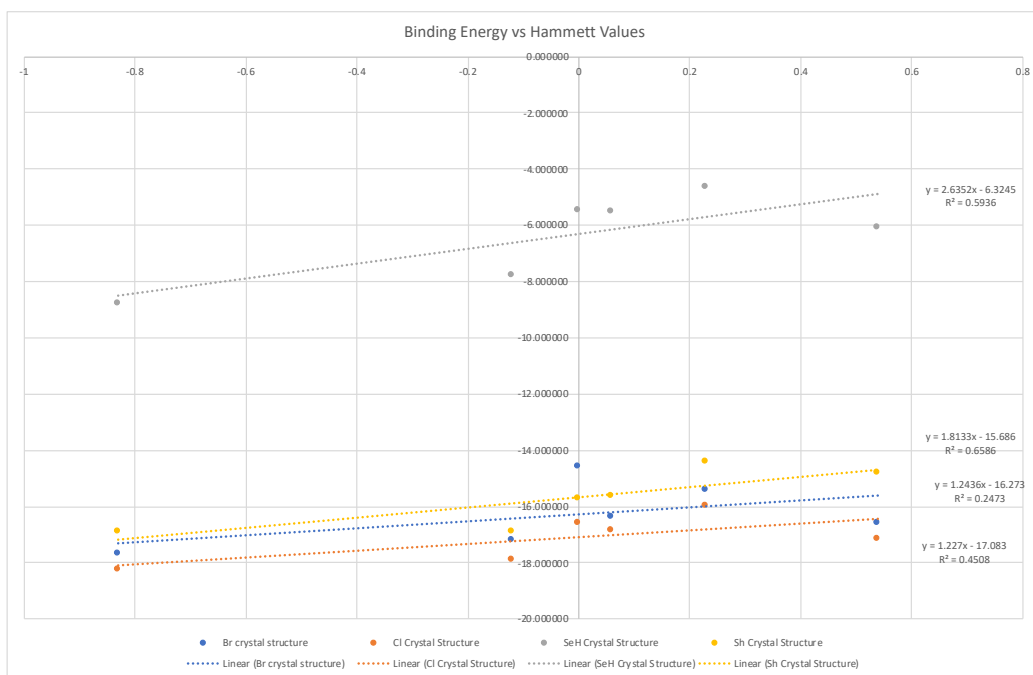


Figure B.41. wb97x/def2-TZVPP/SMD/Water//PBE/6-31G(d)

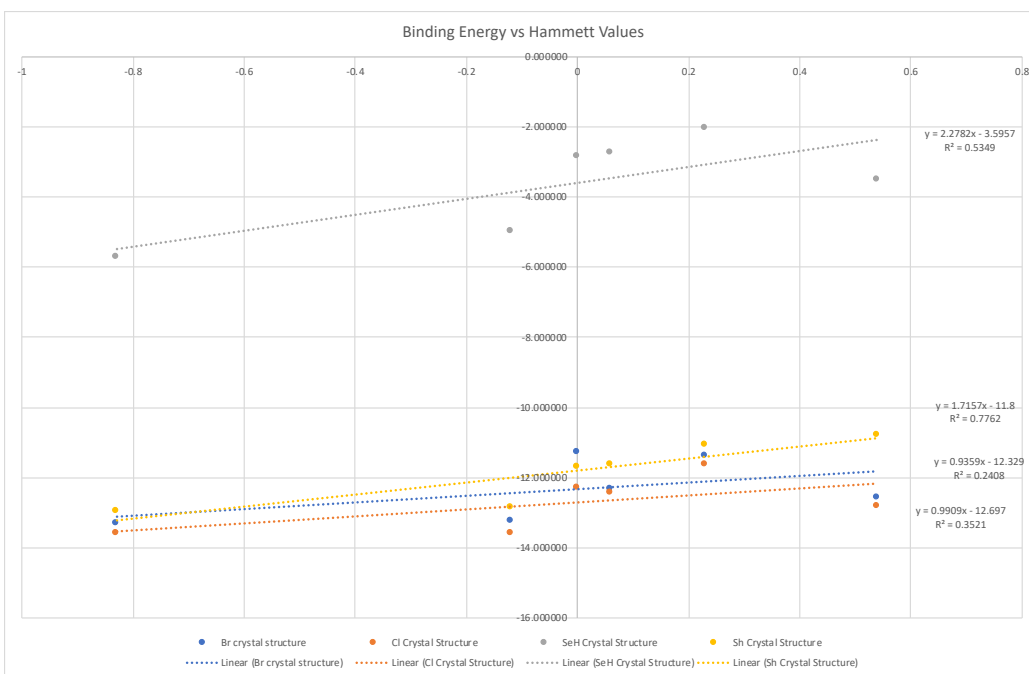


Figure B.42. wb97x/def2-TZVPP/SMD/DMSO//PBE/6-31G(d)

Using Anion pKa, Anion Size, and Hammett Parameters to Fit Experimental ΔG values

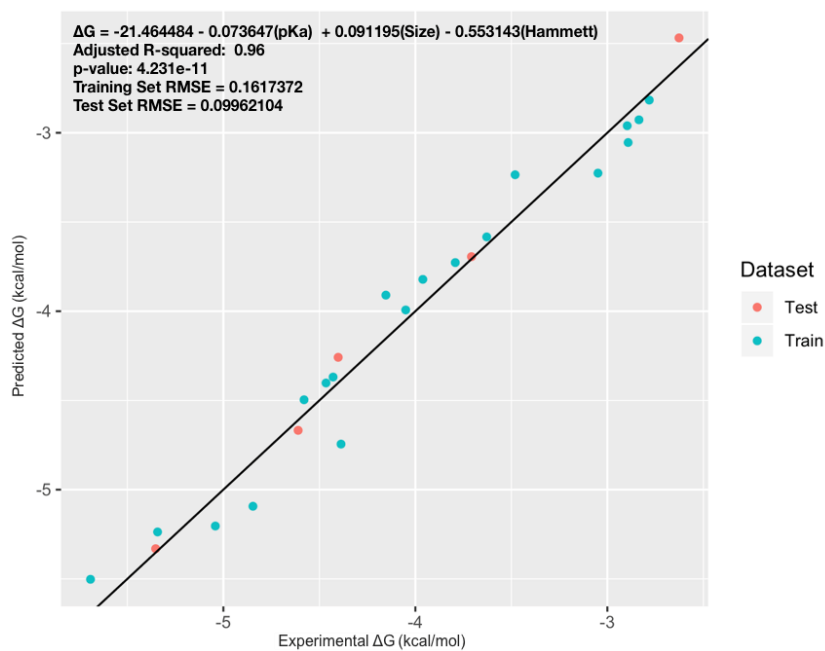


Figure B.43. Experimental vs Predicted ΔG .

Table B.25. Data for fitting ΔG with pKa, Size, and Hammett Values

Anion	-R	pKa	Size (pm)	σ_p	ΔG	Dataset
Br-	NMe2	-9	196	-0.83	-2.6266447	Test
Br-	tBu	-9	196	-0.2	-2.7817043	Train
Br-	H	-9	196	0	-2.8354611	Train
Br-	F	-9	196	0.06	-2.8965979	Train
Br-	Cl	-9	196	0.23	-2.8918604	Train
Br-	CF3	-9	196	0.54	-3.0489736	Test
Cl-	NMe2	-8	181	-0.83	-4.1536742	Train
Cl-	tBu	-8	181	-0.2	-4.4019721	Test
Cl-	H	-8	181	0	-4.4286136	Train
Cl-	F	-8	181	0.06	-4.4654007	Train
Cl-	Cl	-8	181	0.23	-4.579843	Train
Cl-	CF3	-8	181	0.54	-4.6105549	Train
HSe-	NMe2	3.89	198	-0.83	-3.4805005	Train
HSe-	tBu	3.89	198	-0.2	-3.6284077	Train
HSe-	H	3.89	198	0	-3.7078003	Test
HSe-	F	3.89	198	0.06	-3.7921783	Train
HSe-	Cl	3.89	198	0.23	-3.9611945	Train
HSe-	CF3	3.89	198	0.54	-4.050204	Train
HS-	NMe2	7.05	184	-0.83	-4.3872332	Train
HS-	tBu	7.05	184	-0.2	-4.8459966	Train
HS-	H	7.05	184	0	-5.0418164	Train
HS-	F	7.05	184	0.06	-5.3427956	Train
HS-	Cl	7.05	184	0.23	-5.3527232	Test
HS-	CF3	7.05	184	0.54	-5.6921758	Train

Computed Geometries and Energies

For detailed tables of computed geometries and energies for hosts and anion guests, see

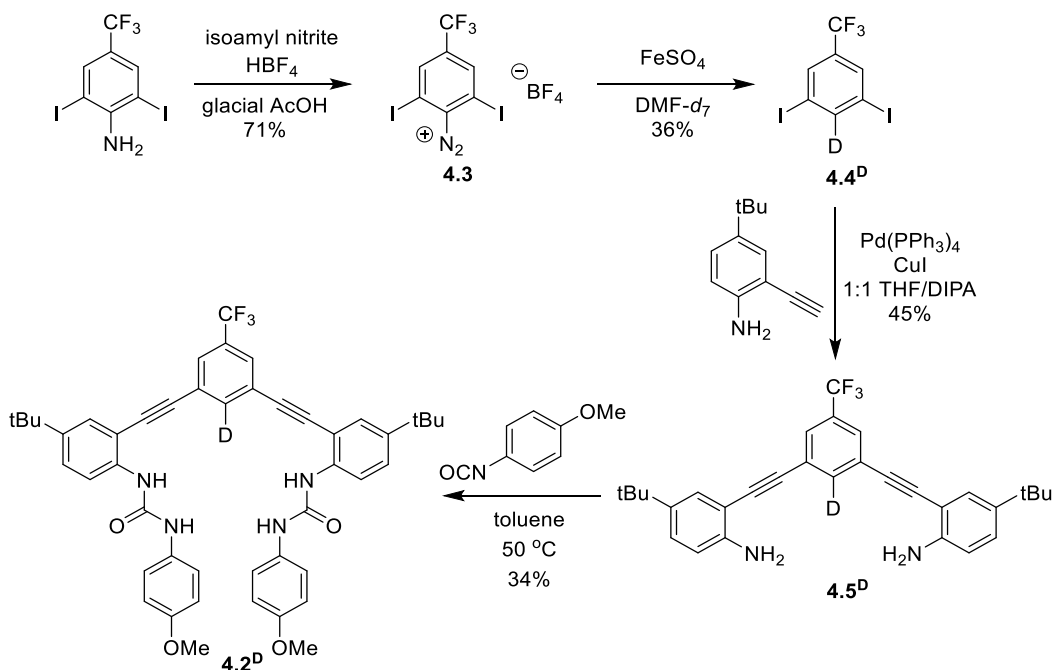
Supporting Information at <https://pubs.acs.org/doi/10.1021/jacs.0c00441>.

APPENDIX C

SUPPLEMENTARY CONTENT FOR CHAPTER IV

Synthesis.

General Methods. All reagents were purchased from commercial sources and used as received, unless otherwise noted. NMR spectra were acquired at room temperature on a Bruker Avance-III-HD 600 MHz (^1H 600 MHz, ^{13}C 151 MHz, ^{19}F 565 MHz, ^2H 76.75 MHz) spectrometer with a Prodigy multinuclear broadband BBO CryoProbe. ^1H and ^{13}C chemical shifts (δ) are reported in ppm relative to residual CHCl_3 (^1H : 7.26 ppm, ^{13}C : 77.16 ppm), CH_3CN (^1H : 1.94 ppm, ^{13}C : 118.26 ppm), or DMSO (^1H : 2.50 ppm, ^{13}C : 39.52 ppm) shifts. ^{19}F chemical shifts are referenced to CFCl_3 ($\delta = 0$ ppm) as an external standard. ^2H chemical shifts are reported in ppm relative to residual CDCl_3 (7.26 ppm), CD_3CN (1.94), or $\text{DMSO-}d_6$ (2.50 ppm). High-resolution mass spectra (HRMS) were recorded on a Waters XEVO G2-SX mass spectrometer. Tetrabutylammonium hydrosulfide (TBASH),⁷⁰ 2,6-diiodo-4-trifluoromethylaniline,¹³⁶ 4-tertbutyl-2-((trimethylsilyl)ethynyl)aniline,¹³⁷ and host **4.2**^{H36} were synthesized according to previous reports. *Note:* Hydrogen sulfide and related salts are highly toxic and should be handled carefully to avoid exposure.



Scheme C.1. Synthetic pathway to the selective deuteration of anion receptor **4.2^D**.

2,6-Diiodo-4-trifluoromethyldiazonium tetrafluoroborate (4.3). This preparation was adapted from previous reports.²⁸ A solution of 2,6-diiodo-4-trifluoromethylaniline¹³⁶ (0.25 g, 0.61 mmol), glacial AcOH (1.0 mL), and 48% HBF₄ (0.18 mL) was stirred at 25 °C. Isoamyl nitrite (0.14 mL) was combined with glacial AcOH (2.0 mL) and added dropwise over 5 min to produce a bright yellow solution. After stirring the reaction mixture at 25 °C for 15 min, diethyl ether (2.0 mL) was slowly added. The resulting liquid was placed in a -20 °C freezer for 16 h, and the solid product was isolated by vacuum filtration and washed with diethyl ether to afford **4.3** (0.25 g, 0.48 mmol, 71%) as a bright yellow solid. *Note:* Caution should be observed when working with isoamyl nitrite or isolating diazonium salts as a solid as these compounds are known to be shock sensitive and explosive.^{244,245} ¹H NMR (600 MHz, CD₃CN) δ: 8.59 (s, 2H). ¹³C NMR

(151 MHz, CD₃CN) δ : 140.2 (q, $J = 34.7$), 139.7 (q, $J = 3.0$), 133.1, 121.4 (q, $J = 274.8$), 102.9. ¹⁹F (565 MHz, CD₃CN) δ : 4.7, -151.8.

1,3-Diiodo-2-deutero-5-trifluoromethylbenzene (4.4^D). This preparation was adapted from previous reports.¹³⁵ A solution of FeSO₄ (0.54 g, 2.0 mmol) and DMF-*d*₇ (10 mL) was allowed to stir for 15 min. A separate solution containing **4.3** (1.0 g, 2.0 mmol) dissolved in DMF-*d*₇ (4 mL) was added dropwise over 10 min to the stirring solution. The solution was allowed to stir for an additional 15 min before adding water to precipitate a solid. The precipitate was isolated by vacuum filtration and washed with water to afford **4.4^D** (0.28 g, 0.71 mmol, 36%) as a tan solid. ¹H NMR (600 MHz, CDCl₃) δ : 7.91 (s, 2H). ¹³C NMR (151 MHz, CDCl₃) δ : 148.3 (t, $J = 27.2$), δ 133.7 (q, $J = 33.7$), δ 133.7 (q, $J = 1.5$), δ 121.9 (q, $J = 273.8$), δ 94.6. ¹⁹F (565 MHz, CDCl₃) δ -63.0. ²H (76.75 MHz, CDCl₃) δ 8.29. HRMS (TOF-MS-ASAP) [M]⁺ calc'd for C₇H₂DF₃I₂ 398.8339, found 398.8317.

Deuterated dianiline intermediate (4.5^D). This preparation was adapted from previous reports.³⁶ A suspension of 4-tertbutyl-2-((trimethylsilyl)ethynyl)aniline¹³⁷ (0.68 g, 2.4 mmol), K₂CO₃ (1.90 g, 13.8 mmol), MeOH (20 mL), and Et₂O (10 mL) was stirred at 25 °C for 3 h. The suspension was diluted with water and extracted with CH₂Cl₂ (15 mL, x3) and washed with brine (15 mL, x2). The organic layer was dried (Na₂SO₄) and concentrated *in vacuo* to afford a dark brown oil. The oil was dissolved in THF (20 mL) and DIPA (20 mL) and purged with N₂ for 40 min. The solution was cannulated into an

N₂-purged solution of **4.4^D** (0.36 g, 0.92 mmol), Pd(PPh₃)₄ (0.032 g, 0.046 mmol), CuI (0.0017 g, 0.0092 mmol), THF (20 mL), and i-PrNH₂ (20 mL). The solution was stirred for 18 h at 50 °C, cooled, and concentrated *in vacuo*. The resulting oil was dissolved in CH₂Cl₂ and filtered through a 3 cm silica plug, which was washed with additional CH₂Cl₂. The filtrate was concentrated *in vacuo* and the resulting brown oil was purified by column chromatography (5:1 hexanes/EtOAc) to afford **5^D** (0.20 g, 0.41 mmol, 45%) as a brown solid. ¹H NMR (600 MHz, CDCl₃) δ: 7.71 (s, 2H), 7.40 (d, *J* = 2.0, 2H), 7.24 (dd, *J* = 8.4, 2H), 6.70 (d, *J* = 8.4, 2H), 4.19 (s, 4H), 1.30 (s, 18H). ¹³C NMR (151 MHz, CDCl₃) δ: 145.8, 141.2, 136.7 (t, *J* = 25.7), 131.5 (q, *J* = 33.2), 129.0, 128.0, 127.4 (q, *J* = 3), 124.9, 124.6 (q, *J* = 273.3), 114.6, 106.6, 92.1, 89.1, 34.1, 31.5. ¹⁹F (565 MHz, CDCl₃) -63.1. ²H (76.75 MHz, CDCl₃) δ: 7.90. HRMS (TOF-MS-ASAP) [M+H]⁺ calc'd for C₃₁H₃₁DN₂F₃ 490.2580, found 490.2549.

Deuterated arylethynyl bisurea host (4.2^D). This preparation was adapted from previous reports.³⁶ All glassware was dried in a 110 °C oven overnight. A round bottom flask was charged with dry toluene (100 mL) and **4.5^D** (0.20 g, 0.41 mmol). 4-Methoxyphenyl isocyanate (0.16 mL, 1.2 mmol) was added dropwise, and the solution was stirred for 46 h at 50 °C. The reaction became cloudy upon completion, and the precipitate was collected by vacuum filtration to afford **4.2^D** (0.11 g, 0.14 mmol, 34%). ¹H NMR (600 MHz, 10% DMSO-*d*₆/CD₃CN) δ: 8.87 (s, 2H), 8.08 (d, *J* = 8.8, 2H), 7.99 (s, 2H), 7.96 (s, 2H), 7.56 (d, *J* = 2.2, 2H), 7.45 (dd, *J* = 8.8, 2H), 7.38 (d, *J* = 8.9, 4H), 6.84 (d, *J* = 8.9, 4H), 3.72 (s, 6H), 1.31 (s, 18H). ¹³C NMR (151 MHz, 10% DMSO-*d*₆/CD₃CN) δ: 156.2, 153.9, 145.9, 139.5, 133.5, 131.8 (q, *J* = 32.2), 129.8, 128.7 (q, *J* =

3.6), 128.3, 125.4, 124.5 (q, $J = 272.8$), 121.8, 120.7, 114.9, 111.6, 93.2, 89.2, 55.9, 34.8, 31.4. ^{19}F (565 MHz, 10% DMSO- d_6 /CD $_3$ CN) δ : -63.2. ^2H (76.75 MHz, 10% DMSO- d_6 /CD $_3$ CN) δ : 8.28. HRMS (TOF-MS-ASAP) $[\text{M}+\text{H}]^+$ calc'd for C $_7$ H $_5$ DN $_4$ O $_4$ F $_3$ 788.3534, found 788.3543.

NMR Spectra.

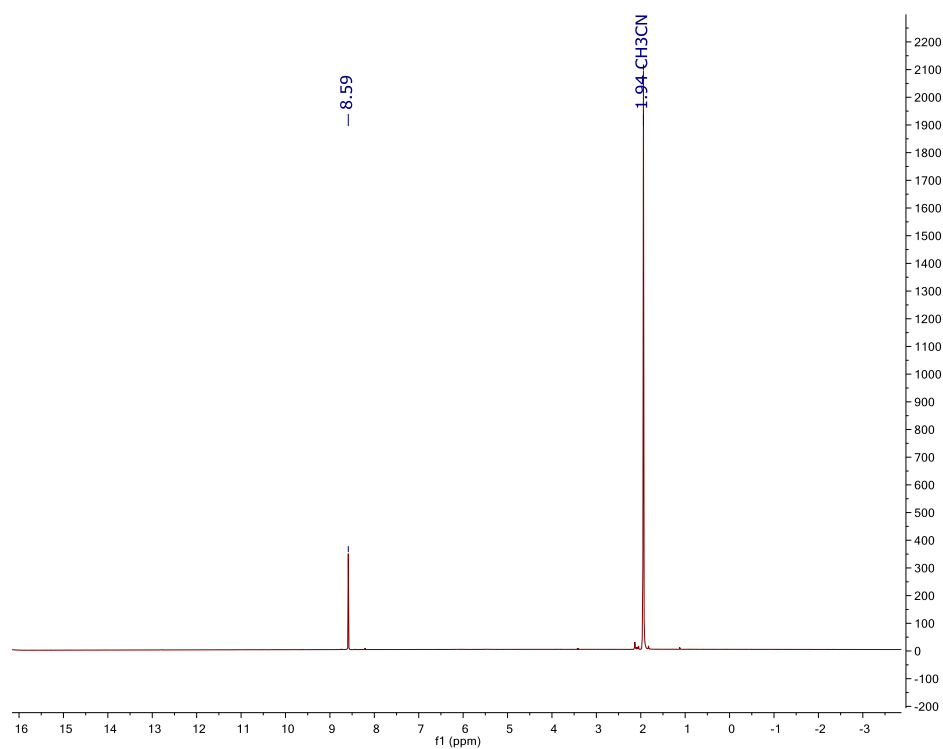


Figure C.1. ^1H NMR spectrum of **4.3** in CD $_3$ CN.

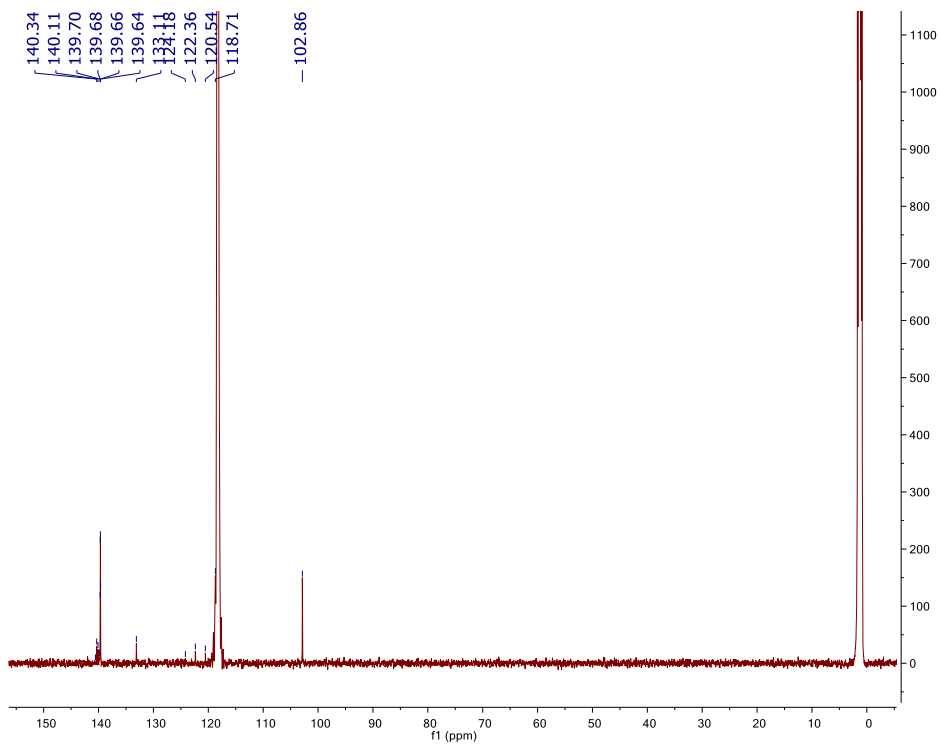


Figure C.2. $^{13}\text{C}\{^1\text{H}\}$ NMR spectrum of 4.3 in CD_3CN .

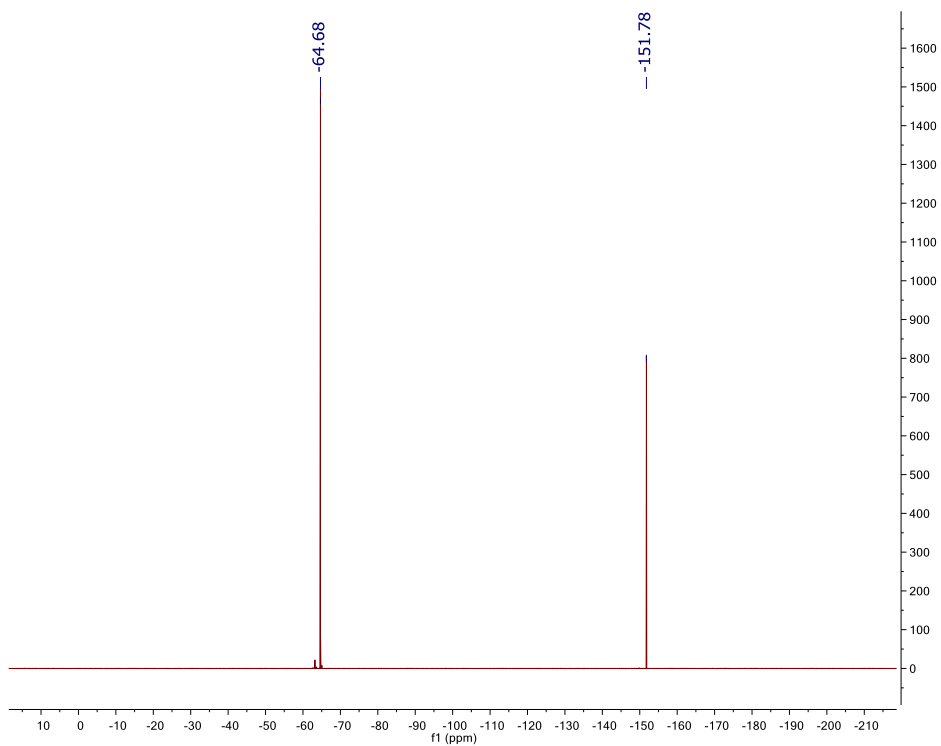


Figure C.3. ^{19}F NMR spectrum of 4.3 in CD_3CN .

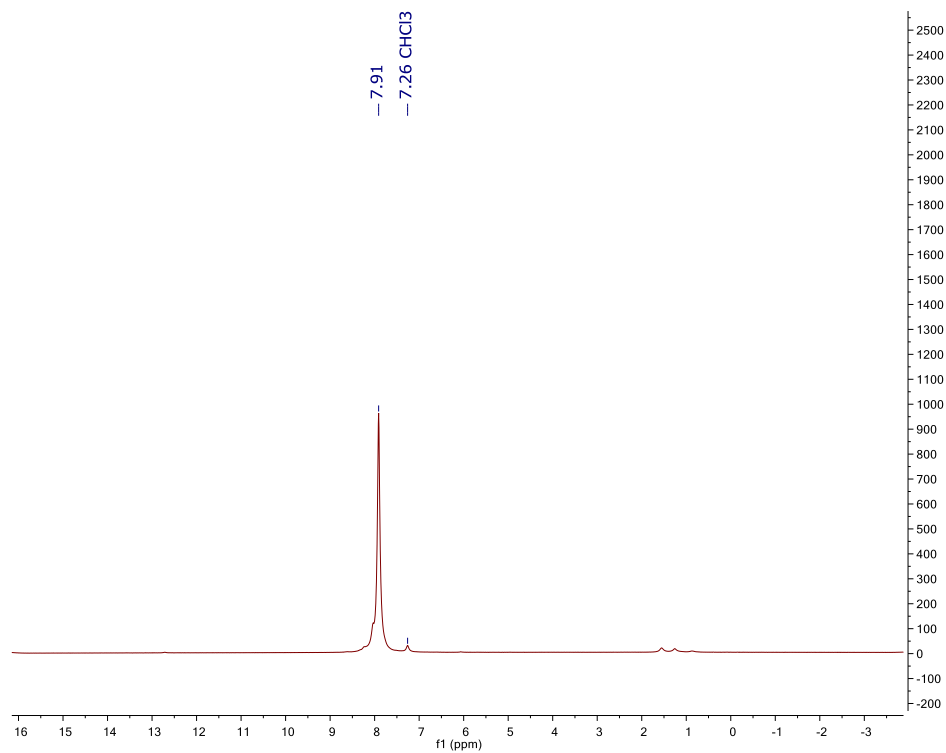


Figure C.4. ^1H NMR spectrum of **4.4^D** in CDCl_3 .

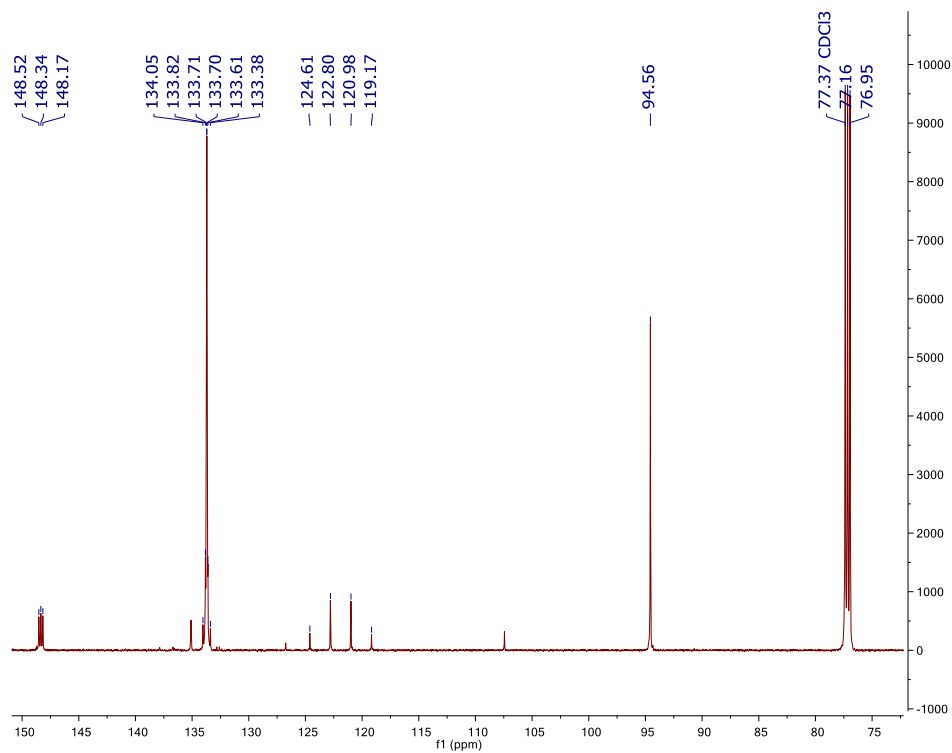


Figure C.5. $^{13}\text{C}\{^1\text{H}\}$ NMR spectrum of **4.4^D** in CDCl_3 .

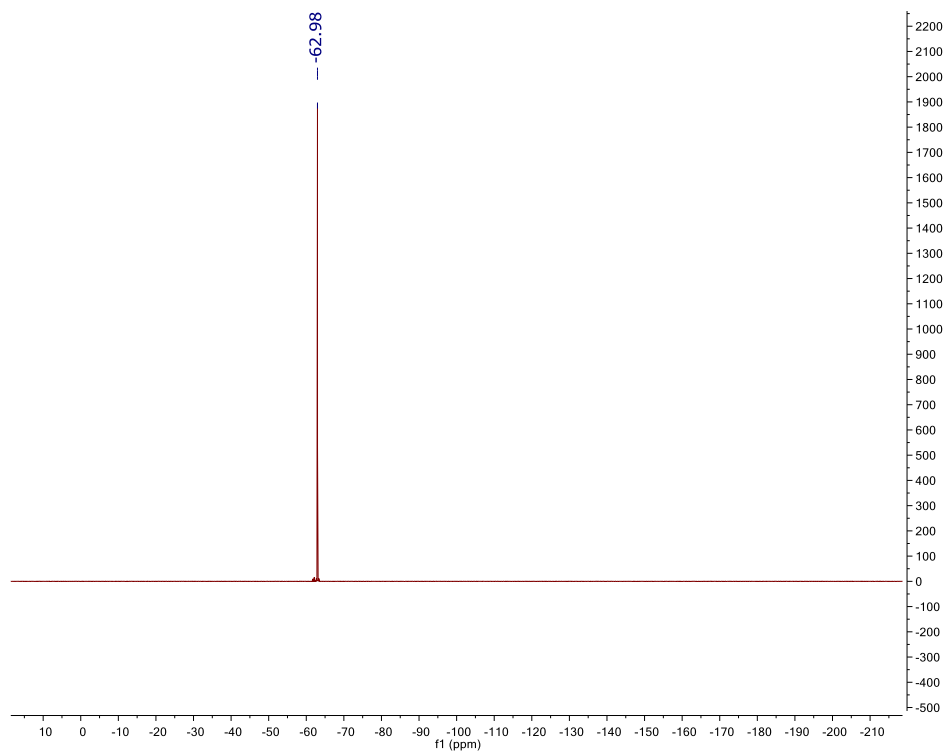


Figure C.6. ^{19}F NMR spectrum of **4.4^D** in CDCl_3 .

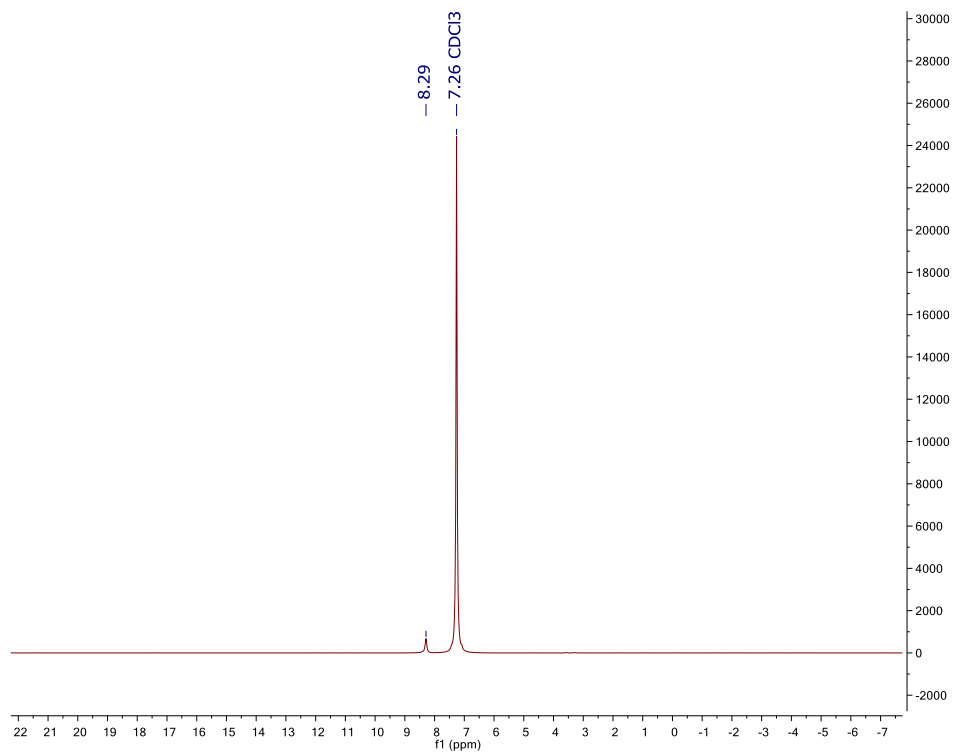


Figure C.7. ^2H NMR spectrum of **4.4^D** in CHCl_3 .

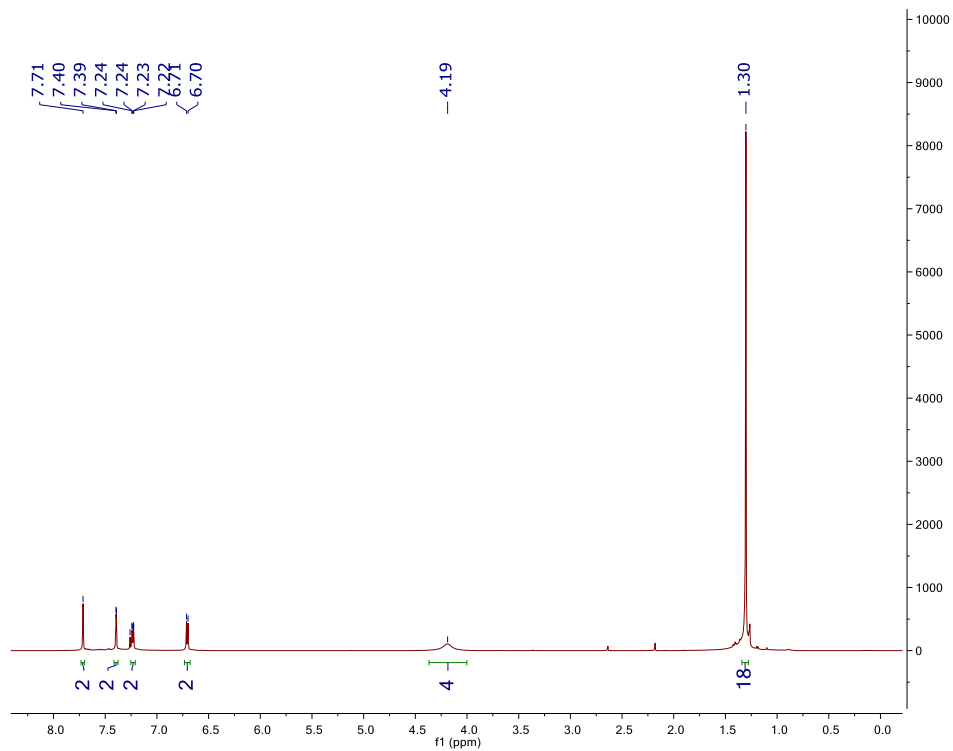


Figure C.8. ^1H NMR spectrum of **4.5^D** in CDCl_3 .

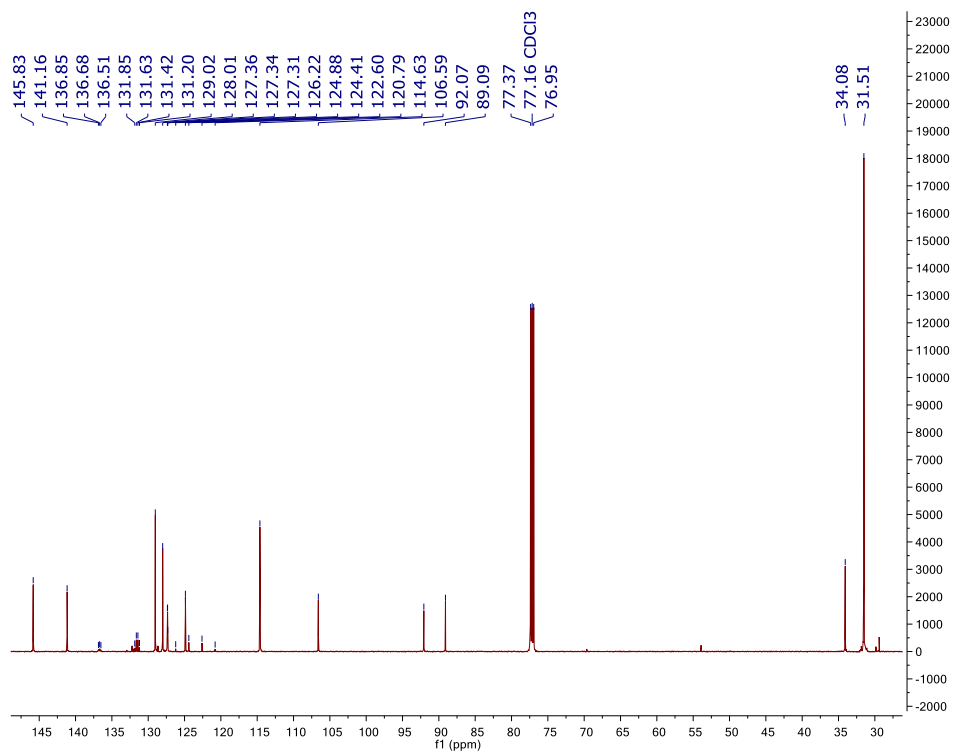


Figure C.9. $^{13}\text{C}\{^1\text{H}\}$ NMR spectrum of **4.5^D** in CDCl_3 .

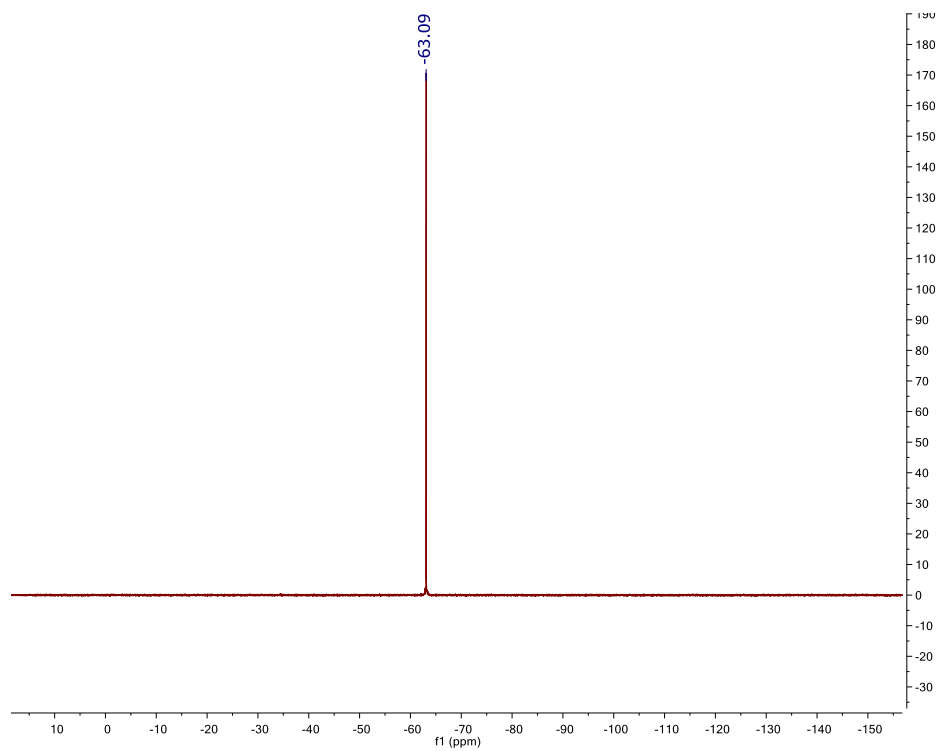


Figure C.10. ^{19}F NMR spectrum of **4.5^D** in CDCl_3 .

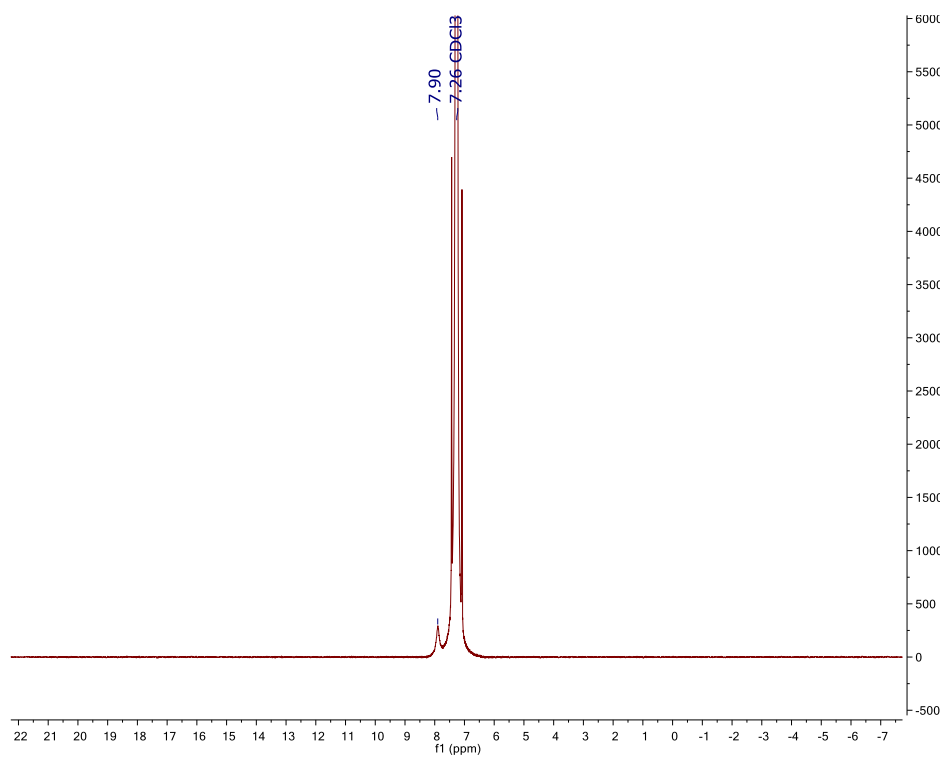


Figure C.11. ^2H NMR spectrum of **4.5^D** in CHCl_3 .

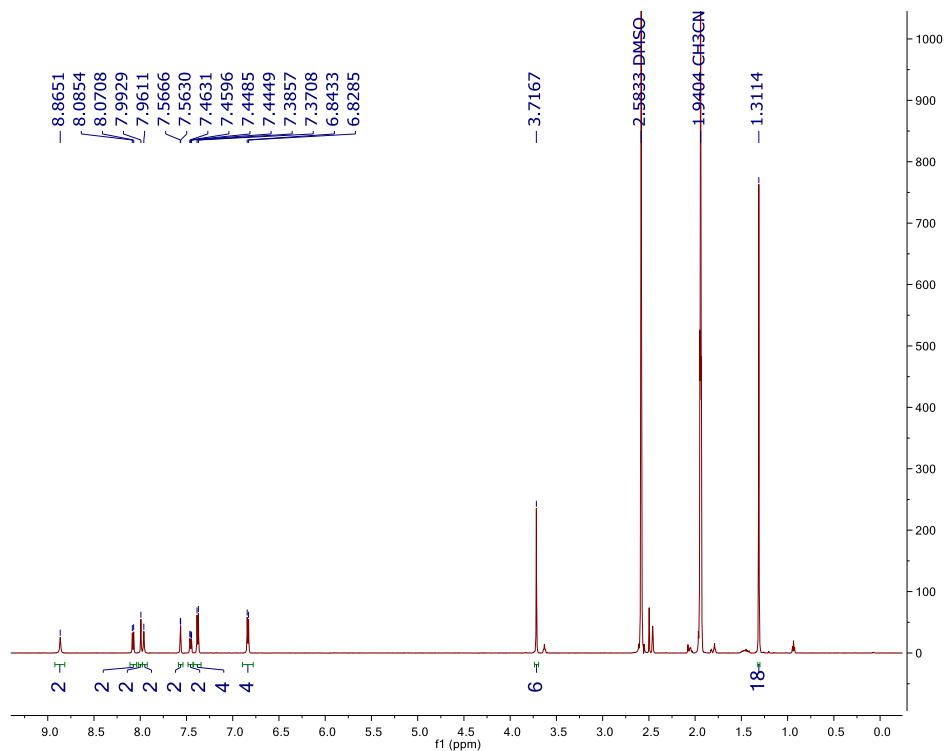


Figure C.12. ^1H NMR spectrum of **4.2^D** in 10% DMSO- d_6 /CD $_3$ CN.

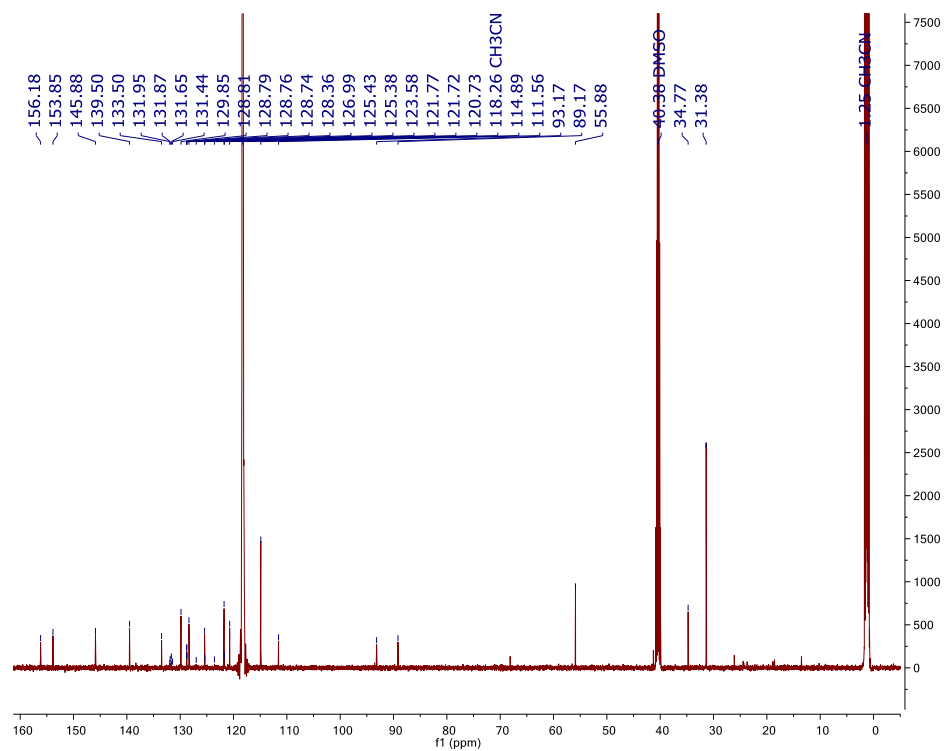


Figure C.13. $^{13}\text{C}\{^1\text{H}\}$ NMR spectrum of **4.2^D** in 10% DMSO- d_6 /CD $_3$ CN.

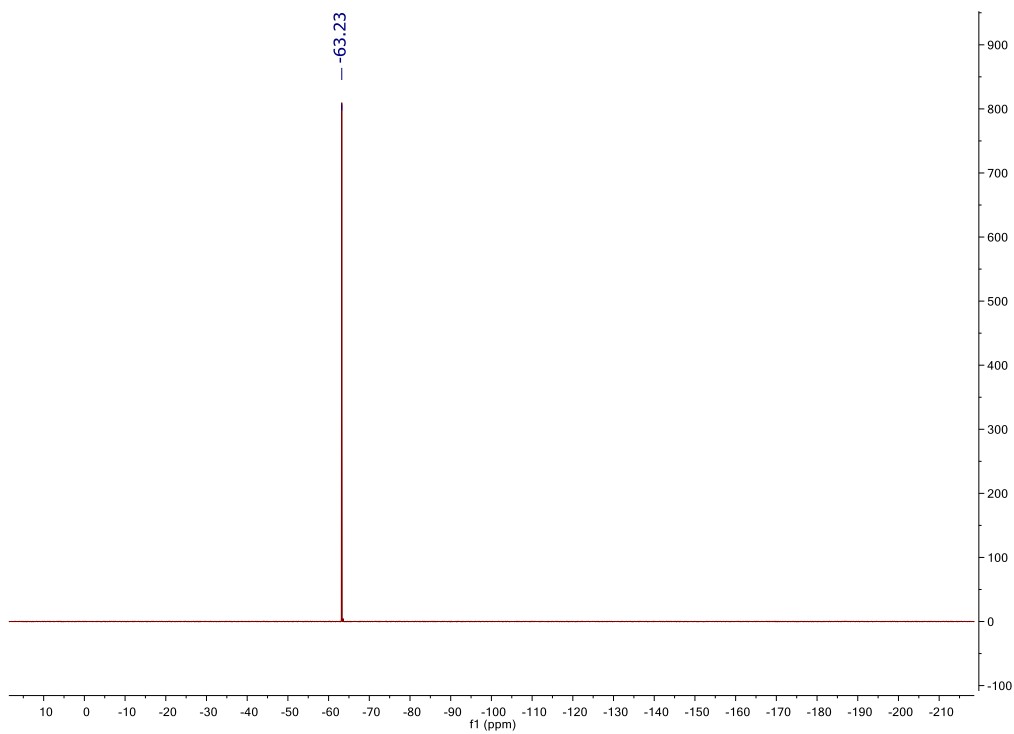


Figure C.14. ^{19}F NMR spectrum of **4.2^D** in 10% $\text{DMSO-}d_6/\text{CD}_3\text{CN}$.

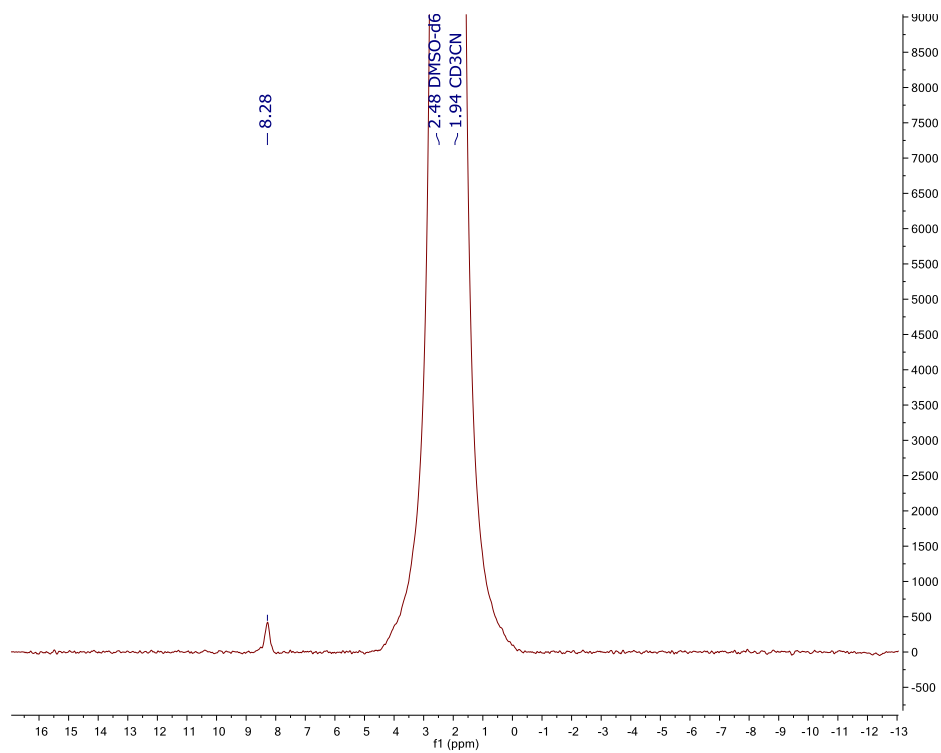


Figure C.15. ^2H NMR spectrum of **4.2^D** in 10% $\text{DMSO}/\text{CH}_3\text{CN}$.

Competitive Titration of **4.2^H** and **4.2^D**.

General Methods. Samples were prepared under an inert atmosphere using an Innovative Atmospheres N₂-filled glovebox. CD₃CN and DMSO-*d*₆ were distilled from calcium hydride under reduced pressure, deoxygenated by purging with N₂ and stored over 4 Å molecular sieves in an inert atmosphere glove box. Tetrabutylammonium chloride (TBACl) and tetrabutylammonium bromide (TBABr) were recrystallized by layering an anhydrous THF solution under anhydrous Et₂O. Tetrabutylammonium hydrosulfide (TBASH) was synthesized according to previous reports.⁷⁰ *Note:* Hydrogen sulfide and related salts are highly toxic and should be handled carefully to avoid exposure.

General Procedure for NMR Titrations.

Method A. A solution of **4.2^H** and **4.2^D** in 10% DMSO-*d*₆/CD₃CN (combined concentration between 5.71 and 13.46 mM) was prepared and 500 μL was added to a septum-sealed NMR tube. A stock solution of guest (TBASH, TBACl, or TBABr) was prepared in 10% DMSO-*d*₆/CD₃CN (54.69 – 223.09 mM). Aliquots of the guest solution were added to the NMR tube using Hamilton gas-tight syringes, and ¹³C NMR spectra were recorded at 25°C after each addition of guest. The Δδ of the C^{ab}, C¹, and C² of **4.2^H** and **4.2^D** were used to follow the progress of the titration, and DEIE were determined using the Perrin method.¹³⁸

Method B. A solution of **4.2^H** and **4.2^D** in 10% DMSO-*d*₆/CD₃CN (combined concentration between 4.65 and 6.04 mM) was prepared and 500 μL aliquots were added to four J-young NMR tubes. A stock solution of TBASH was prepared in CD₃CN (47.18 – 81.29 mM). For each point in the titration, TBASH stock solution and DMSO-*d*₆ were added to a new solution of **2^H** and **2^D** inside an N₂-glovebox shortly before obtaining a ¹³C NMR spectra. The Δδ of the C^{ab}, C¹, and C² of **4.2^H** and **4.2^D** were used to follow the progress of the titration, and DEIE were determined using the Perrin method.¹³⁸

Competitive ^{13}C NMR Titration Representative Data.

Table C.1. Representative competitive titration between **4.2^H** and **4.2^D** with Cl^- in 10% $\text{DMSO-}d_6/\text{CD}_3\text{CN}$ at 25°C .

Entry	V_{Guest} (μL)	[4.2^H] (mM)	[4.2^D] (mM)	[Cl^-] (mM)	$\delta \text{C}^{\text{ab}}$ (4.2^H) (ppm)	$\delta \text{C}^{\text{ab}}$ (4.2^D) (ppm)	δC^1 (4.2^H) (ppm)	δC^1 (4.2^D) (ppm)	δC^2 (4.2^H) (ppm)	δC^2 (4.2^D) (ppm)
1	0	7.4	2.8	0	125.5158	125.4206	93.2006	93.1679	89.1431	89.1625
2	10	7.2	2.7	1.5	125.4586	125.3627	93.2448	93.2117	89.210	89.1440
3	50	6.5	2.5	8.0	125.2459	125.1484	93.4583	93.4213	89.0492	89.0715
4	60	5.8	2.2	14.4	125.1863	125.0894	93.5353	93.4970	89.0370	89.0597
5	200	4.3	1.3	28.4	125.1896	125.0942	93.5570	93.5180	89.0795	89.1019

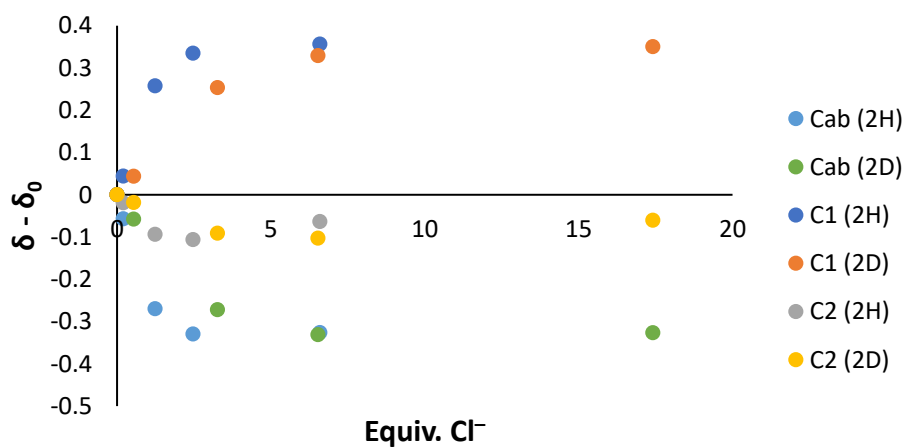


Figure C.16. Binding isotherm for Cl^- binding with a mixture of **4.2^H** and **4.2^D** in 10% $\text{DMSO-}d_6/\text{CD}_3\text{CN}$ at 25°C .

Table C.2. Representative competitive titration between **4.2^H** and **4.2^D** with Br⁻ in 10% DMSO-*d*₆/CD₃CN at 25°C.

Entry	V _{Guest} (μL)	[4.2 ^H] (mM)	[4.2 ^D] (mM)	[Br ⁻] (mM)	δ C ^{ab} (4.2 ^H) (ppm)	δ C ^{ab} (4.2 ^D) (ppm)	δ C ¹ (4.2 ^H) (ppm)	δ C ¹ (4.2 ^D) (ppm)	δ C ² (4.2 ^H) (ppm)	δ C ² (4.2 ^D) (ppm)
1	0	9.4	4.1	0	125.5253	125.4301	93.2145	93.1818	89.1588	89.1780
2	5	9.3	4.0	1.1	125.4977	125.4008	93.2280	93.1959	89.1571	89.1772
3	10	9.1	3.9	3.2	125.4451	125.3496	93.2538	93.2223	89.1546	89.1743
4	60	8.1	3.5	14.1	125.2864	125.1897	93.3491	93.3152	89.1485	89.1692
5	200	5.8	2.5	37.5	125.1987	125.1029	93.4268	93.3909	89.1687	89.1896
6	500	3.5	1.5	62.6	125.1856	125.0898	93.4606	93.4253	89.2015	89.2217

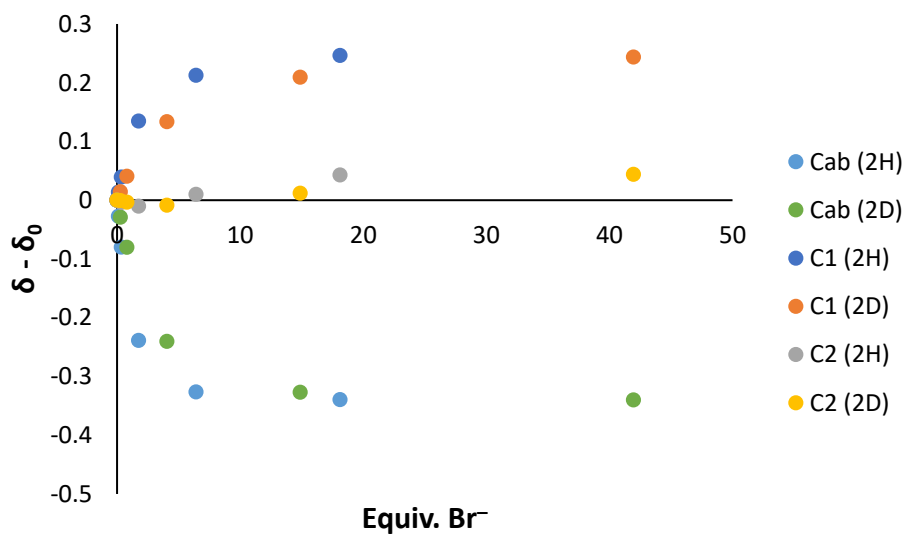


Figure C.17. Binding isotherm for Br⁻ binding with a mixture of **4.2^H** and **2^D** in 10% DMSO-*d*₆/CD₃CN at 25°C.

APPENDIX D

SUPPLEMENTARY CONTENT FOR CHAPTER V

Materials and Methods.

Parameters for Searches.

All non-metal bound HB Acceptor contacts with D–H HB Donors. CCDC Conquest Program was used to identify all D–H···A contacts in crystal structures in the Cambridge Structural Database up to November 2019. D–H···A---NM contacts were identified when A was bound (by any bond order) to 1, 2, and 3 other non-metal (NM) elements. D–H···A---NM contacts in which A did not have a free lone-pair (such as sulfur trioxide) were excluded. Contacts in which A is not bound to any element were determined by searching for all D–H···A contacts and excluding instances when A was bound to another element.

The Draw function of the Conquest program allows the user to restrict contact distances and angles. D···A contacts were defined between 0 and 5 Å. Intramolecular D···A contacts were separated by 4 to 999 bonds. Inter- and intramolecular H···A contacts were defined between 0 and 4 Å. Intramolecular H···A contacts were separated by 4 to 999 bonds. Both D–H···A and NM---A···H angles were defined between and including 90 and 180°. Placing distance and angle restrictions which include H meant that contacts in which the H atom is not located were excluded.

Searches were conducted for each donor and acceptor pair of interest. Both organic and organometallic structures were allowed. No further filters were applied. After the

search was completed, contact distances and angles were downloaded into Microsoft Excel spreadsheets.

S oxidation-state specific searches. S oxidation-state specific searches were performed by searching for C–H···S contacts with specified bond order, charge, and NM elements. To identify C–H···S contacts in which S is in the –2 oxidation state, S could be in the following environments: 1) two single bonds to a less electronegative NM element, 2) one double bond to a less electronegative NM element, 3) one single bond to a less electronegative NM element with a negative charge on the sulfur, or 4) no bonds to another element and with a –2 charge on the sulfur.

To identify C–H···S contacts in which S is in the –1 oxidation state, S could be in the following environments: 1) one single bond to a less electronegative NM element and one single bond to another sulfur, or 2) one single bond to a sulfur and a negative charge on the sulfur.

To identify C–H···S contacts in which S is in the 0 oxidation state, S could be in the following environments: 1) one double bond to a more electronegative NM element and two single bonds to less electronegative NM element, 2) one single bond to a more electronegative NM element, two single bonds to less electronegative NM element, and a positive charge on the sulfur, 3) one double bond to a more electronegative NM element and one double bond to a less electronegative NM element, 4) one single bond to a more electronegative NM element and one single bond to a less electronegative NM element, 5) one double bond to a sulfur, or 6) two single bonds to a sulfur.

Alkyl and aryl C-H HB donor specific searches. Alkyl C–H HB donors were specified by requiring that the C donor formed four single bonds with NM elements. Aryl C–H HB donors were specified by using the benzene ring stamp in the Draw function.

3D Histograms. All weighted and unweighted 3D histograms were plotted in MATLAB using the heatmap function.

Heat Map Figures

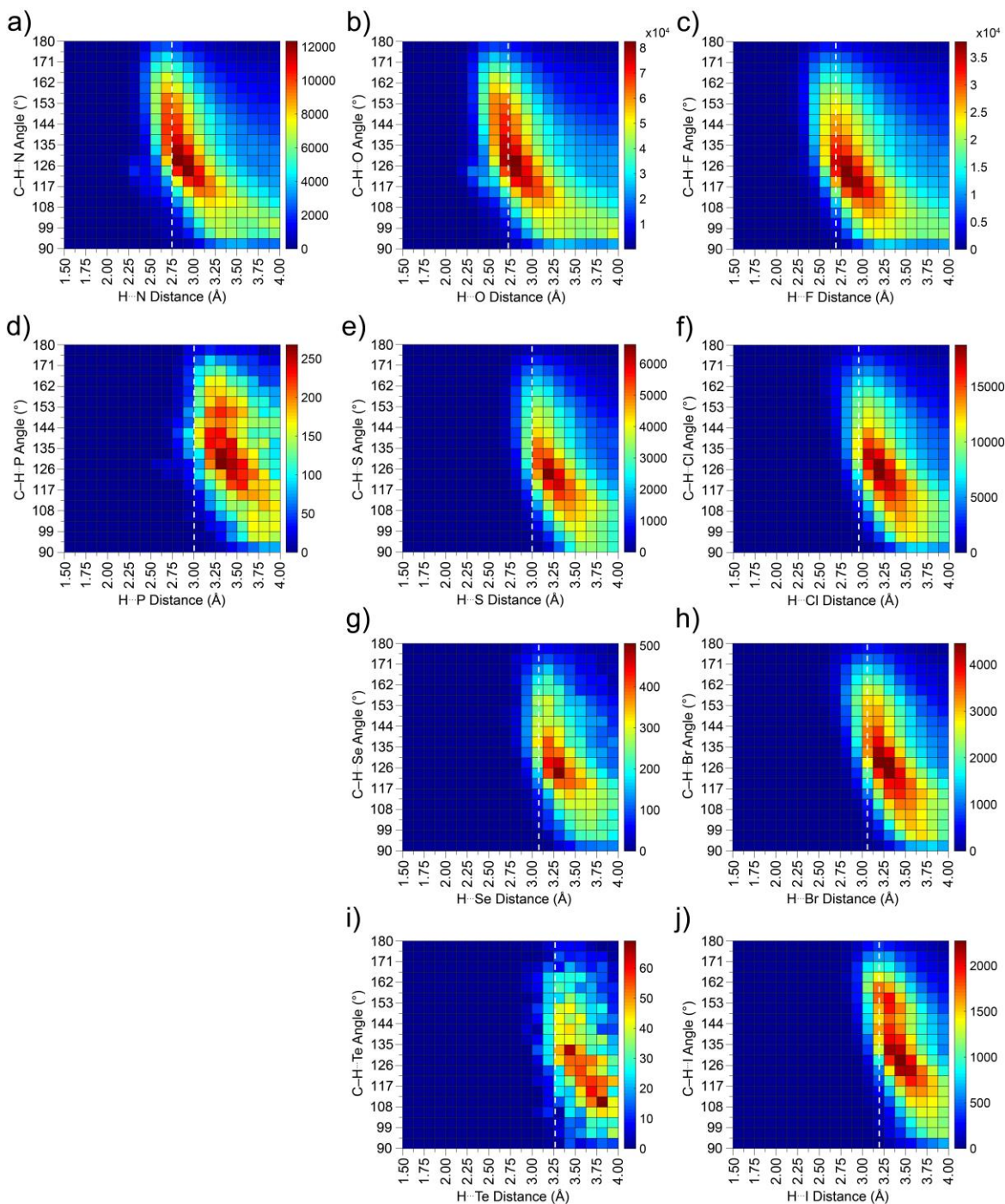


Figure D.1. Unweighted histograms of H...Acceptor distance (Å) vs. C-H...Acceptor contact angle (°). The dashed white line is the sum of the van der Waal radii of C and the Acceptor. C-H...Acceptor contacts with a) N, b) O, c) F, d) P, e) S, f) Cl, g) Se, h) Br, i) Te, j) I.

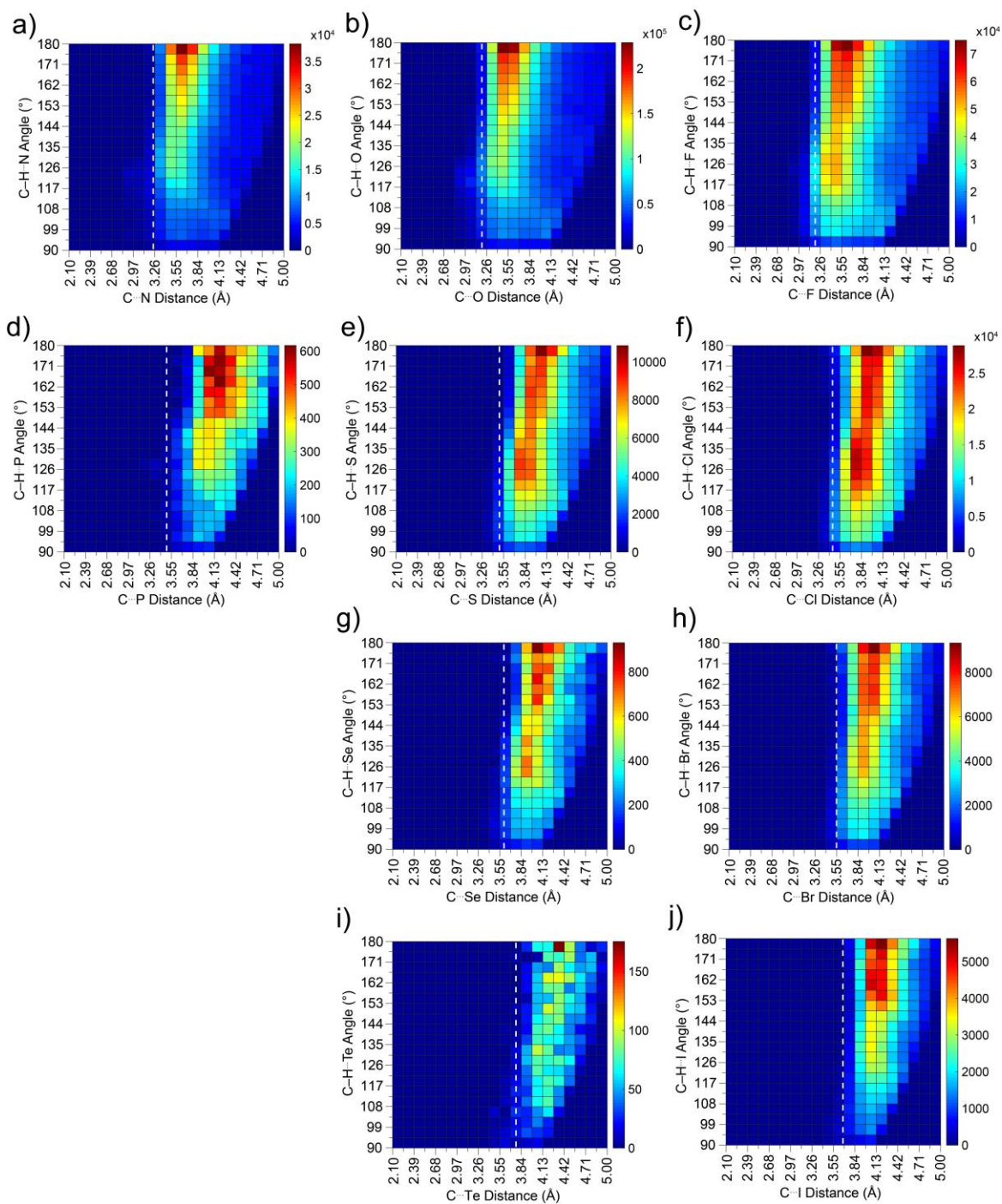


Figure D.2. Cone corrected histograms of C...Acceptor distance (Å) vs. C-H...Acceptor contact angle (°). The dashed white line is the sum of the van der Waal radii of C and the Acceptor. C-H...Acceptor contacts with a) N, b) O, c) F, d) P, e) S, f) Cl, g) Se, h) Br, i) Te, j) I.

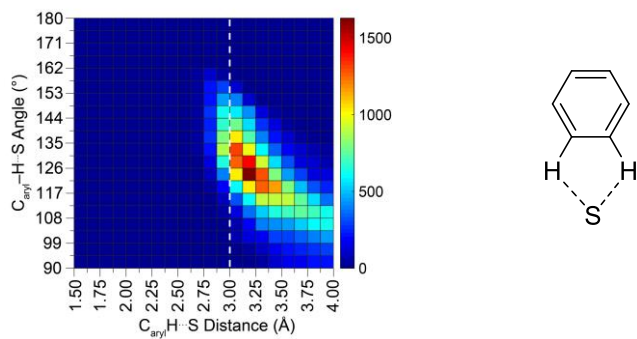


Figure D.3. Cone corrected histograms of C–H···S contacts with S bifurcated between two adjacent aryl C–H HB donors on the same ring.

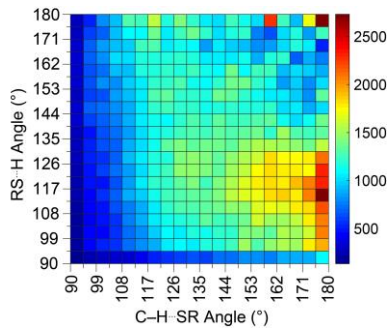


Figure D.4. Bi-weighted 3D histograms of C–H···S contacts when S is bound to only one other non-metal atoms.

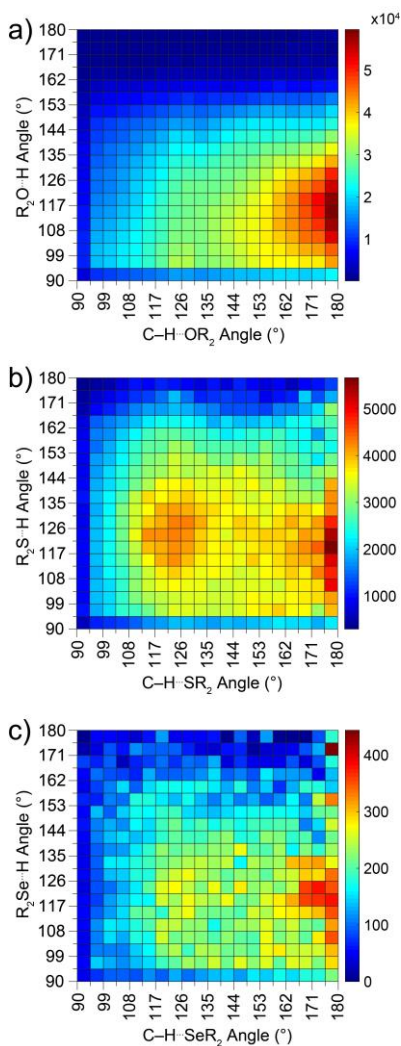


Figure D.5. Bi-weighted 3D histograms of C–H···A contacts when A is bound to two other non-metal atoms for a) O, b) S, and c) Se.

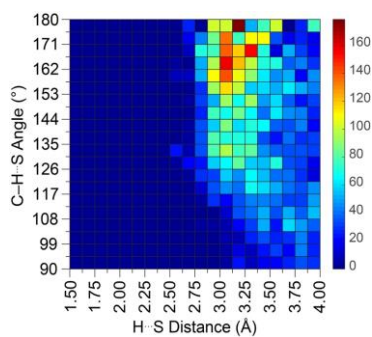


Figure D.6. Cone corrected histograms of C–H···S–M of with group 1 metals of the periodic table.

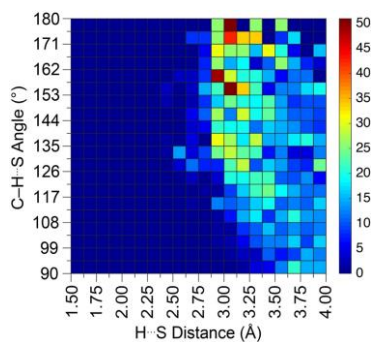


Figure D.7. Cone corrected histograms of C–H···S–M of with group 3 metals of the periodic table.

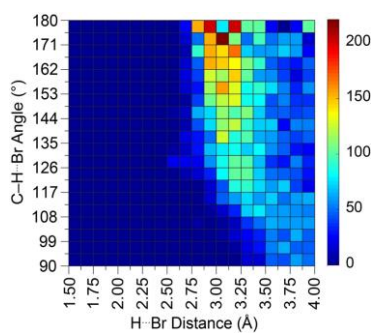


Figure D.8. Cone corrected histograms of C–H···S–M of with group 4 metals of the periodic table.

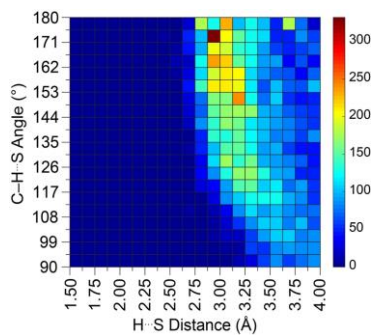


Figure D.9. Cone corrected histograms of C–H···S–M of with group 5 metals of the periodic table.

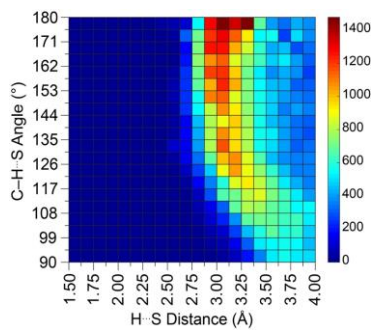


Figure D.10. Cone corrected histograms of C–H···S–M of with group 6 metals of the periodic table.

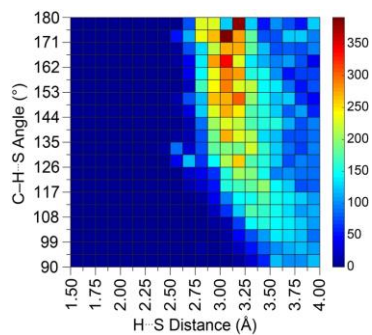


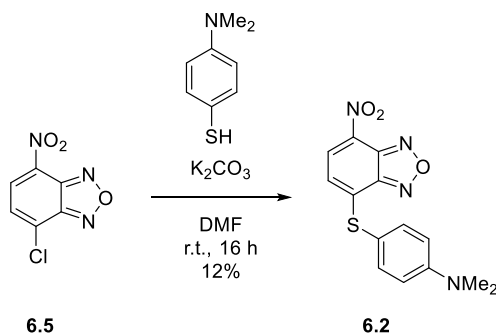
Figure D.11. Cone corrected histograms of C–H···S–M of with group 13 metals (excluding B, a nonmetal) of the periodic table.

APPENDIX E

SUPPLEMENTARY CONTENT FOR CHAPTER VI

Synthesis.

General Procedure. All reagents were purchased from commercial sources and used as received, unless otherwise noted. NMR spectra were acquired at room temperature on a Bruker Avance-III-HD 500 MHz (^1H 500 MHz, ^{13}C 151 MHz) spectrometer with a Prodigy multinuclear broadband BBO CryoProbe. ^1H and ^{13}C chemical shifts (δ) are reported in ppm relative to residual CHCl_3 (^1H : 7.26 ppm, ^{13}C : 77.16 ppm). High-resolution mass spectra (HRMS) were recorded on a Waters XEVO G2-SX mass spectrometer. Tetrabutylammonium hydrosulfide (TBASH)⁷⁰ and host **6.1**³⁶ were synthesized according to previous reports. *Note:* Hydrogen sulfide and related salts are highly toxic and should be handled carefully to avoid exposure.



Scheme E.1. Synthesis of NBD thioether **6.2**.

NBD-thioether 6.2. NBD-Cl (**6.5**, 130 mg, 0.65 mmol) and K_2CO_3 (90 mg, 0.65 mmol) were added to degassed DMF (10 mL). 4-Dimethylaminobenzenethiol (99 mg, 0.65 mmol) was added, and the resultant mixture was stirred at room temperature for 16 h

under nitrogen. The reaction mixture was diluted with saturated LiCl solution (10 mL), and the crude product was extracted with Et₂O (3 × 15 mL) and dried over NaSO₄. The solvent was removed under vacuum. The final product was purified by serial column chromatography on SiO₂ (first 100% DCM, then 1:3:16 EtOAc:DCM:hexanes) and further purified by recrystallization in DCM and hexanes to yield **6.2** (25 mg, 12%) as a dark red powder. ¹H NMR (500 MHz, CDCl₃) δ 8.22 (d, *J* = 8.0 Hz, 1H), 7.46 (d, *J* = 8.8 Hz, 2H), 6.85 (d, *J* = 8.8 Hz, 2H), 6.64 (d, *J* = 8.0 Hz, 1H), 3.08 (s, 6H). ¹³C NMR (151 MHz, CDCl₃) δ 151.9, 148.5, 145.7, 142.7, 137.0, 132.5, 131.0, 121.0, 113.9, 110.2, 40.5. HRMS (TOF-MS-ASAP) [M+H]⁺ calcd for C₁₄H₁₃N₄O₃S 317.0708, found 317.0748.

NMR Spectra.

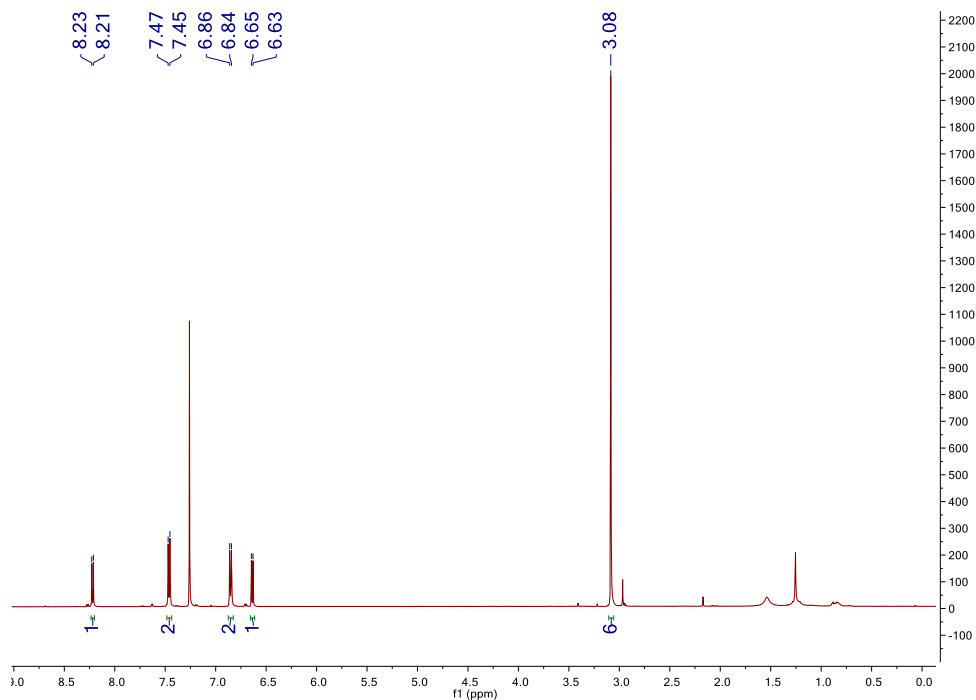


Figure E.1. ¹H NMR spectrum of **6.2** in CDCl₃.

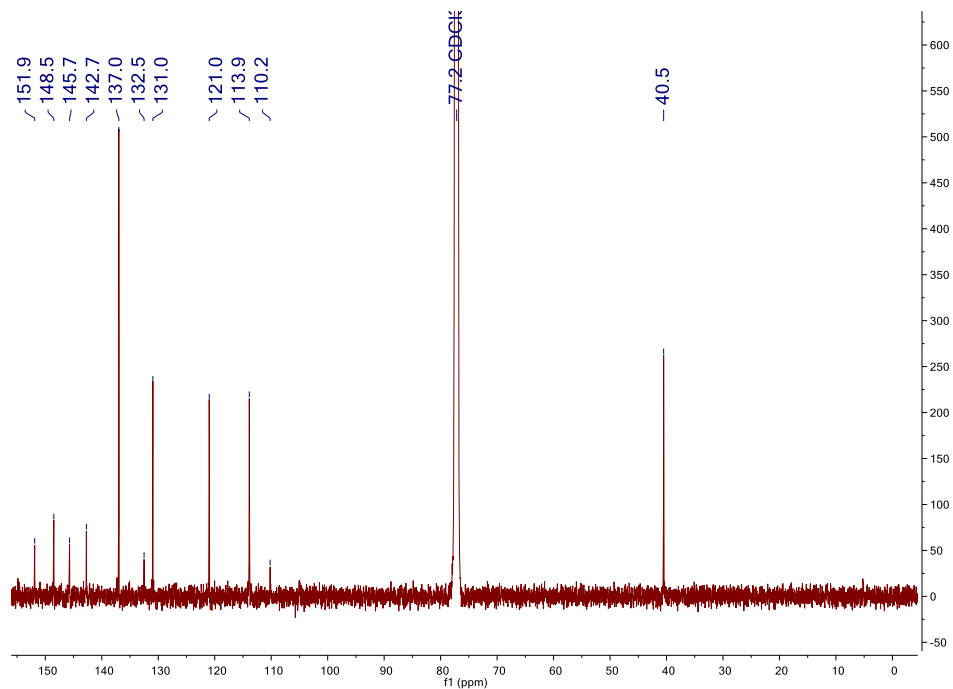


Figure E.2. ^{13}C NMR spectrum of **6.2** in CDCl_3 .

Kinetic Experiments.

General Methods. Samples were prepared under an inert atmosphere using an Innovative Atmospheres N_2 -filled glovebox. Anhydrous and anaerobic MeCN was collected from a solvent still and stored in an N_2 -filled glovebox. Anhydrous and anaerobic DMSO was distilled from calcium hydride under reduced pressure, deoxygenated by purging with N_2 , and stored in an N_2 -filled glovebox. Each kinetic experiment was performed in triplicate.

General Procedure for Kinetic Experiments.

Method A. Reaction in the absence of receptor 6.1. A solution of NBD-thioether **6.2** in 10% DMSO/MeCN (5 mL, 10 μ M) was prepared and 2.5 mL was added to a quartz cuvette with a septum cap and stir bar. A solution of TBASH was prepared in MeCN (5 mL, 5 mM) and added to a septum-capped vial. Prior to each UV-vis experiment, the cuvette was allowed to equilibrate to 25.0 °C for 5 min in the sample holder. After equilibration, the required equiv. TBASH was added to the cuvette by gas-tight Hamilton syringe. The reaction progress was monitored by collection of UV-vis absorption data at the local λ_{max} (570 nm) of the product in 0.9 s intervals.

Method B. Reaction in the presence of receptor 6.1. A 5 mL solution of NBD-thioether **6.2** in 10% DMSO/MeCN (10 μ M, 1 equiv.) and various concentrations of receptor **6.1** in 10% DMSO/MeCN was prepared and 2.5 mL was added to a quartz cuvette with a septum and stir bar. A solution of TBASH was prepared in MeCN (5 mL, 5 mM) and added to a septum-capped vial. Prior to each UV-vis experiment, the cuvette was allowed to equilibrate to 25.0 °C for 5 min in the sample holder. After equilibration, the required equiv. of TBASH was added to the cuvette by gas-tight Hamilton syringe. The reaction progress was monitored by collection of UV-vis absorption data at the local λ_{max} (570 nm) of the product in 0.9 s intervals.

Initial rate of reaction determination. Initial rates were determined from the slope of absorbance at 570 nm over 6.8 ± 0.1 seconds intervals.

Representative Kinetic Data.

Table E.1. Representative UV-vis absorption data at local λ_{\max} (570 nm) for the reaction of 1 equiv. TBASH with 10 μM **6.2**.

Time (s)	Absorbance
0	0.01550293
5	0.12395019
5.9	0.14231665
6.8	0.1529662
7.7	0.16176102
8.6	0.17034186
9.5	0.17605327
10.4	0.18187602
11.3	0.18664622
12.2	0.19040844
13.1	0.19433336
14	0.19663775
14.9	0.2000269
15.8	0.20252961
16.7	0.20460401
17.6	0.20682243
18.5	0.20894596
19.4	0.21076797
20.3	0.21285717
21.2	0.21395658
22.1	0.21547489
23	0.21686134
23.9	0.22567296
24.8	0.2196244
25.7	0.22092912
26.6	0.22243065
27.5	0.22297308
28.4	0.22428685
29.3	0.2251351
30.2	0.22603376
31.1	0.22687277
32	0.22771917
32.9	0.22864383
33.8	0.22953252
34.7	0.2305187
35.6	0.23126289
36.5	0.23163578
37.4	0.23272456
38.3	0.23290217
39.2	0.23358117
40.1	0.2345998
41	0.23523742
41.9	0.23563266
42.8	0.23631662
43.7	0.23720507
44.6	0.23734848
45.5	0.23784542
46.4	0.23784001
47.3	0.23808801

48.2	0.23928988
49.1	0.23936398
50	0.23962288
50.9	0.24041775
51.8	0.24070571
52.7	0.24109302
53.6	0.24158035
54.5	0.24202059
55.4	0.24218857
56.3	0.24256557
57.2	0.2428848
58.1	0.24348243
59	0.24366784
59.9	0.24388348
60.8	0.2442442
61.7	0.24440499
62.6	0.24478716
63.5	0.2450884
64.4	0.24558985
65.3	0.24602255
66.2	0.24615668
67.1	0.24630189
68	0.24671134
68.9	0.24685523
69.8	0.24688083
70.7	0.24721757
71.6	0.24738307
72.5	0.24789099
73.4	0.24812138
74.3	0.24836583
75.2	0.24883914
76.1	0.24935988
77	0.24967577
77.9	0.24969062
78.8	0.24956097
79.7	0.25006583
80.6	0.25013506
81.5	0.25021839
82.4	0.25032926
83.3	0.25020361
84.2	0.25036749
85.1	0.25017947
86	0.25168419
86.9	0.2520943
87.8	0.25205147
88.7	0.25180921
89.6	0.25147447
90.5	0.25181687
91.4	0.25187239
92.3	0.25209019
93.2	0.25216874
94.1	0.25312665
95	0.25333557
95.9	0.25331581
96.8	0.25352377
97.7	0.25348452

98.6	0.25379553
99.5	0.25370833
100.4	0.25403291
101.3	0.25405249
102.2	0.25398976
103.1	0.25419754
104	0.25444239
104.9	0.2547839
105.8	0.25489482
106.7	0.2550317
106.6	0.25505844
108.5	0.25483394
109.4	0.25517386
110.3	0.25532034
111.2	0.25544083
112.1	0.25566223
113	0.25594515
113.9	0.25589833
114.8	0.2562516
115.7	0.2560381
116.6	0.25651938
117.5	0.25654998
118.4	0.25644696
119.3	0.25705493
120.2	0.25697705
121.1	0.25746536
122	0.25752994
122.9	0.25805047
123.8	0.25798202
124.7	0.25782287
125.6	0.25782287
126.5	0.25811735
127.4	0.25795811
128.3	0.258140802
129.2	0.25817415
130.1	0.25791961
131	0.25849944
131.9	0.25853837
132.8	0.25881684
133.7	0.25817114
134.6	0.2587474
135.5	0.25893867
136.4	0.25871059
137.3	0.25906128
138.2	0.25932038
139.1	0.25901785
140	0.25970453
140.9	0.25940821
141.8	0.25952789
142.7	0.2598263
143.6	0.26006603
144.5	0.26039147
145.4	0.25979146
146.3	0.26017535
147.2	0.26032302
148.1	0.2602939

149	0.26011717
149.9	0.26079258
150.8	0.26065892
1517	0.26085958
152.6	0.26114756
153.5	0.26064983
154.4	0.2609778
155.3	0.26162079
156.2	0.26130483
157.1	0.26112309
158	0.26155716
158.9	0.2610842
159.8	0.26152509
160.7	0.26158914
161.6	0.26156348
162.5	0.26197195
163.4	0.26165709
164.3	0.26181424
165.2	0.2622754
166.1	0.26241502
167	0.26214579
167.7	0.26209617
168.8	0.26245567
169.7	0.26221073
170.6	0.262584
171.5	0.26262596
172.4	0.26300791
173.3	0.26291201
174.2	0.26311076
175.1	0.26294881
176	0.26299188
176.9	0.26311284
177.8	0.26318932
178.7	0.26314357
179.6	0.26352811
180.5	0.26344335
181.4	0.26330721
182.3	0.26390359
183.2	0.26351172
184.1	0.26389459

Table E.2. Representative UV-vis absorption data at local λ_{\max} (570 nm) for the reaction of 1 equiv. TBASH with 10 μM **6.2** in the presence of 5 equiv. **6.1**.

Time (s)	Absorbance
0	-0.012978029
5	0.028147
5.9	0.035841
6.8	0.043186
7.7	0.046033
8.6	0.05061
9.5	0.054339968
10.4	0.066763118
11.3	0.061075
12.2	0.063539
13.1	0.065616
14	0.068189
14.9	0.070752
15.8	0.073703
16.7	0.078488514
17.6	0.081005417
18.5	0.080636613
19.4	0.079864
20.3	0.080936
21.2	0.0825
22.1	0.083599
23	0.085222
23.9	0.086394
24.8	0.087682
25.7	0.088811
26.6	0.089566
27.5	0.089779
28.4	0.091106
29.3	0.091636
30.2	0.092682
31.1	0.093735
32	0.094758
32.9	0.095174
33.8	0.096618
34.7	0.097555
35.6	0.09801
36.5	0.098854
37.4	0.100318
38.3	0.101005
39.2	0.101879
40.1	0.101995
41	0.102336
41.9	0.103105
42.8	0.103175
43.7	0.104132
44.6	0.104558
45.5	0.105181
46.4	0.105783
47.3	0.106299
48.2	0.106754
49.1	0.107387
50	0.107797

50.9	0.108159
51.8	0.108598
52.7	0.108824
53.6	0.109275
54.5	0.109586
55.4	0.110083
56.3	0.110115
57.2	0.111101
58.1	0.111443
59	0.111789
59.9	0.112238
60.8	0.112452
61.7	0.113037
62.6	0.11348
63.5	0.114084
64.4	0.114486
65.3	0.114569
66.2	0.115027
67.1	0.115191
68	0.115584
68.9	0.116178
69.8	0.116655
70.7	0.117093
71.6	0.117887
72.5	0.117527
73.4	0.117631
74.3	0.118136
75.2	0.11828
76.1	0.118434
77	0.119135
77.9	0.119137
78.8	0.11957
79.7	0.119447
80.6	0.120263
81.5	0.119897
82.4	0.120244
83.3	0.120499
84.2	0.12098
85.1	0.121037
86	0.121347
86.9	0.121587
87.8	0.121873
88.7	0.122483
89.6	0.123027
90.5	0.123054
91.4	0.123066
92.3	0.123625
93.2	0.123548
94.1	0.124042

Table E.3. Representative UV-vis absorption data at local λ_{\max} (570 nm) for the reaction of 1 equiv. TBASH with 10 μM **6.2** in the presence of 1 equiv. **6.1**.

Time (s)	Absorbance
0	0.01857783
5	0.17583571
5.9	0.18876408
6.8	0.19589932
7.7	0.20465787
8.6	0.211738408
9.5	0.21735308
10.4	0.22300538
11.3	0.22711803
12.2	0.23102577
13.1	0.23436528
14	0.23769514
14.9	0.24082351
15.8	0.24308668
16.7	0.24571204
17.6	0.24850109
18.5	0.25168774
19.4	0.25344294
20.3	0.25391606
21.2	0.25500852
22.1	0.25653836
23	0.25854835
23.9	0.25960714
24.8	0.2611376
25.7	0.26260066
26.6	0.2636269
27.5	0.26478267
28.4	0.26508498
29.3	0.26658493
30.2	0.26806661
31.1	0.26842412
32	0.26968235
32.9	0.27026454
33.8	0.27122444
34.7	0.27214402
35.6	0.27327135
36.5	0.2735624
37.4	0.27414423
38.3	0.27516976
39.2	0.2761381
40.1	0.277201
41	0.27749836
41.9	0.27811816
42.8	0.27883464
43.7	0.27928278
44.6	0.27919877
45.5	0.28042141
46.4	0.28117132
47.3	0.28097665
48.2	0.28166223
49.1	0.28218618
50	0.28337088

50.9	0.28327033
51.8	0.28359637
52.7	0.28389373
53.6	0.28464758
54.5	0.28529614
55.4	0.28543317
56.3	0.28599969
57.2	0.28629801
58.1	0.28655672
59	0.28718439
59.9	0.28781497
60.8	0.28780699
61.7	0.28862748
62.6	0.28899562
63.5	0.2892352
64.4	0.28948557
65.3	0.28973702
66.2	0.29020795
67.1	0.29028285
68	0.29089633
68.9	0.29110503
69.8	0.2915929
70.7	0.29183039
71.6	0.29208523
72.5	0.29231215
73.4	0.29241034
74.3	0.29263377
75.2	0.29345378
76.1	0.29364625
77	0.29386088
77.9	0.29416135
78.8	0.29450291
79.7	0.29469022
80.6	0.29485571
81.5	0.29545265
82.4	0.29551256
83.3	0.2957961
84.2	0.29592487
85.1	0.29606369
86	0.29652941
86.9	0.29692021
87.8	0.29709956
88.7	0.29709426
89.6	0.29787219
90.5	0.29794675
91.4	0.29859284
92.3	0.29843596
93.2	0.2985422
94.1	0.29944566

Table E.4. Representative UV-vis absorption data at local λ_{max} (570 nm) for the reaction of 0.5 equiv. TBASH with 10 μM **6.2**.

Time (s)	Absorbance
0	0.040662743
5	0.082723916
5.9	0.087689571
6.8	0.09055838
7.7	0.094470263
8.6	0.098074362
9.5	0.105915994
10.4	0.109280571
11.3	0.11001239
12.2	0.109949835
13.1	0.112122268
14	0.114668436
14.9	0.117302805
15.8	0.119578421
16.7	0.121920079
17.6	0.124292485
18.5	0.126520798
19.4	0.128055766
20.3	0.12982966
21.2	0.131891117
22.1	0.133973673
23	0.135720119
23.9	0.137886792
24.8	0.139406368
25.7	0.140924946
26.6	0.142315224
27.5	0.144059077
28.4	0.145650864
29.3	0.147155389
30.2	0.148693875
31.1	0.149875745
32	0.151001796
32.9	0.152860522
33.8	0.154232815
34.7	0.155051693
35.6	0.156698316
36.5	0.157879308
37.4	0.158922076
38.3	0.159972489
39.2	0.161110655
40.1	0.161912471
41	0.163182721
41.9	0.164287314
42.8	0.165255964
43.7	0.16696386
44.6	0.167361066
45.5	0.168070242
46.4	0.168891102
47.3	0.169743702
48.2	0.170982018
49.1	0.171741888
50	0.172973543

50.9	0.17402719
51.8	0.174527466
52.7	0.175656378
53.6	0.176387295
54.5	0.177218437
55.4	0.178209513
56.3	0.17883125
57.2	0.17968607
58.1	0.180113941
59	0.180811063
59.9	0.182058707
60.8	0.182902873
61.7	0.183426917
62.6	0.184298754
63.5	0.184594825
64.4	0.185106173
65.3	0.186061427
66.2	0.186852634
67.1	0.187082753
68	0.187667415
68.9	0.188324779
69.8	0.189341232
70.7	0.190107286
71.6	0.190510571
72.5	0.190960735
73.4	0.191740722
74.3	0.192263275
75.2	0.19326824
76.1	0.193875849
77	0.194284052
77.9	0.194512099
78.8	0.195211649
79.7	0.195573658
80.6	0.196102247
81.5	0.196685091
82.4	0.197586551
83.3	0.198454887
84.2	0.198691323
85.1	0.199457586
86	0.199927628
86.9	0.200489953
87.8	0.200884923
88.7	0.201249197
89.6	0.201864943
90.5	0.202436939
91.4	0.203335285
92.3	0.203124374
93.2	0.203509167
94.1	0.203493297
95	0.204673886
95.9	0.205318227
96.8	0.205191284
97.7	0.206195861
98.6	0.206676573
99.5	0.207082346
100.4	0.20744504

101.3	0.207785711
102.2	0.208049268
103.1	0.208857968
104	0.209299743
104.9	0.209957123
105.8	0.210156351
106.7	0.210592285
106.6	0.211409167
108.5	0.21155256
109.4	0.211665288
110.3	0.212210208
111.2	0.211995944
112.1	0.212171763
113	0.212636218
113.9	0.213228881
114.8	0.213496089
115.7	0.213378117
116.6	0.214062139
117.5	0.214180425
118.4	0.215006456
119.3	0.215237811
120.2	0.215696827
121.1	0.216171205
122	0.216103286
122.9	0.216180056
123.8	0.216827825
124.7	0.217036501
125.6	0.217223719
126.5	0.217493027
127.4	0.218104258
128.3	0.218459964
129.2	0.218799874
130.1	0.219202116
131	0.219362274
131.9	0.219517276
132.8	0.220409527
133.7	0.220589131
134.6	0.220761895
135.5	0.221337825
136.4	0.221560672
137.3	0.221558213
138.2	0.221885145
139.1	0.222039938
140	0.222332686
140.9	0.222881943
141.8	0.223262027
142.7	0.224268556
143.6	0.224485442
144.5	0.225319073
145.4	0.224899605
146.3	0.225021705
147.2	0.225339428
148.1	0.225213975
149	0.225488886
149.9	0.225843087
150.8	0.225868598

1517	0.226033881
152.6	0.226195261
153.5	0.22630021
154.4	0.226917028
155.3	0.226648659
156.2	0.227075368
157.1	0.227319002
158	0.227781892
158.9	0.227561951
159.8	0.228055149
160.7	0.228511065
161.6	0.228520617
162.5	0.22856842
163.4	0.22879602
164.3	0.229304448
165.2	0.229606688
166.1	0.229467884
167	0.229702011
167.7	0.229814798
168.8	0.22977002
169.7	0.229846045
170.6	0.230438739
171.5	0.230690658
172.4	0.230791718
173.3	0.230921567
174.2	0.23071602
175.1	0.231408685
176	0.231433034
176.9	0.231419921
177.8	0.231626689
178.7	0.231649548
179.6	0.232044146
180.5	0.232337296
181.4	0.232651755
182.3	0.232757524
183.2	0.23275885
184.1	0.23326008

Table E.5. Representative UV-vis absorption data at local λ_{\max} (570 nm) for the reaction of 2 equiv. TBASH with 10 μM **6.2**.

Time (s)	Absorbance
0	0.042442374
5	0.436351359
5.9	0.469588786
6.8	0.493625224
7.7	0.512905955
8.6	0.512905955
9.5	0.528495967
10.4	0.541837275
11.3	0.56174165
12.2	0.569860816
13.1	0.577571511
14	0.584105969
14.9	0.589415491
15.8	0.595093608
16.7	0.600051999
17.6	0.604568481
18.5	0.60983789
19.4	0.612968624
20.3	0.615731835
21.2	0.619015694
22.1	0.621686339
23	0.624110997
23.9	0.628200352
24.8	0.629559696
25.7	0.631976187
26.6	0.633951187
27.5	0.63623172
28.4	0.637955308
29.3	0.641034603
30.2	0.641942799
31.1	0.64329803
32	0.645370364
32.9	0.645756662
33.8	0.648045898
34.7	0.648665607
35.6	0.651308775
36.5	0.651764095
37.4	0.652747929
38.3	0.654428065
39.2	0.655353725
40.1	0.656938434
41	0.657117128
41.9	0.657929182
42.8	0.659729898
43.7	0.660740972
44.6	0.660475254
45.5	0.661525607
46.4	0.662577331
47.3	0.663590431
48.2	0.663858056
49.1	0.663613141
50	0.665165365

50.9	0.665403128
51.8	0.666760564
52.7	0.666907013
53.6	0.668803513
54.5	0.668807387
55.4	0.669220626
56.3	0.670194507
57.2	0.670579195
58.1	0.670856118
59	0.671714604
59.9	0.672691584
60.8	0.672434568
61.7	0.673205495
62.6	0.673859119
63.5	0.673831821
64.4	0.674048245
65.3	0.67460984
66.2	0.676344752
67.1	0.674993396
68	0.675309777
68.9	0.676924288
69.8	0.677274108
70.7	0.677397907
71.6	0.677988112
72.5	0.677944243
73.4	0.678190768
74.3	0.678650141
75.2	0.678574324
76.1	0.678989768
77	0.679100633
77.9	0.679872572
78.8	0.679673314
79.7	0.680533171
80.6	0.679814816
81.5	0.680388033
82.4	0.68086648
83.3	0.680492997
84.2	0.681759477
85.1	0.681621909
86	0.681435347
86.9	0.68214494
87.8	0.682429254
88.7	0.684416831
89.6	0.682973981
90.5	0.683970451
91.4	0.683242917
92.3	0.683281601
93.2	0.683329642
94.1	0.683836162

APPENDIX F

SUPPLEMENTARY CONTENT FOR CHAPTER VII

Synthesis.

General methods. All reagents were purchased from commercial sources and used as received, unless otherwise noted. All glassware was purified by an overnight acid bath and rinsed with 18 M Ω deionized water. Non-analytical glassware was also purified by overnight base bath. NMR spectra were acquired at room temperature on a Bruker Avance-III-HD 500 MHz (^1H 500 MHz, ^{31}P 202.46 MHz) spectrometer with a Prodigy multinuclear broadband BBO CryoProbe. ^1H chemical shifts (δ) are reported in ppm relative CH₃CN (^1H : 1.94 ppm). ^{31}P chemical shifts are referenced to 85% H₃PO₄ (δ = 0 ppm) as an external standard. **7.1**²⁷ and **7.2**¹⁸ were synthesized according to previous reports.

Tetrabutylphosphonium hydroxide (TBPOH). TBPOH was purchased as 40 wt. % in H₂O. An aliquot of the solution was pumped to dryness and purified in an Innovative Atmospheres N₂-filled drybox through serial recrystallization at 0 °C by layering an anhydrous THF solution under anhydrous Et₂O. ^1H NMR (500 MHz, CD₃CN) δ : 2.03-2.09 (m, 8H), 1.54-1.42 (m, 16H), 0.95 (t, J = 7.1, 12H). ^{31}P NMR (202.46 MHz, CD₃CN) δ : 33.03.

General procedure for tetrabutylphosphonium salt (TBPX) synthesis. 200 μL of a 40 mM aqueous solution of purified TBPOH (8 μmol) was diluted to 3 mL with 18 M Ω deionized water. Excess concentrated acid (5 μL) was added dropwise. TBPX was extracted with HPLC-grade DCM (25 mL, x3). The combined DCM solution was washed with 18 M Ω deionized water (5 mL, x1). The washed DCM solution was concentrated *in vacuo* overnight to afford TBPX as white crystals. *Note:* TBPCl, TBPBr, and TBPNO₃ salts are hygroscopic and will turn into an oil once exposed to air. *Warning:* Tetrabutylphosphonium salts are highly toxic and readily absorbed through nitrile gloves and skin and should be handled carefully to avoid exposure.

Tetrabutylphosphonium chloride (TBPCl). 2.36 mg, 8 μmol , quant. ³¹P NMR (202.46 MHz, CD₃CN) δ : 33.73.

Tetrabutylphosphonium bromide (TBPBr). 2.45 mg, 7.2 μmol , 90%. ³¹P NMR (202.46 MHz, CD₃Cl) δ : 32.84.

Tetrabutylphosphonium iodide (TBPI). 3.09 mg, 8 μmol , quant. ³¹P NMR (202.46 MHz, CD₃Cl) δ : 32.75.

Tetrabutylphosphonium nitrate (TBPNO₃). 2.57 mg, 8 μmol , quant. ³¹P NMR (202.46 MHz, CD₃Cl) δ : 33.08.

NMR spectra.

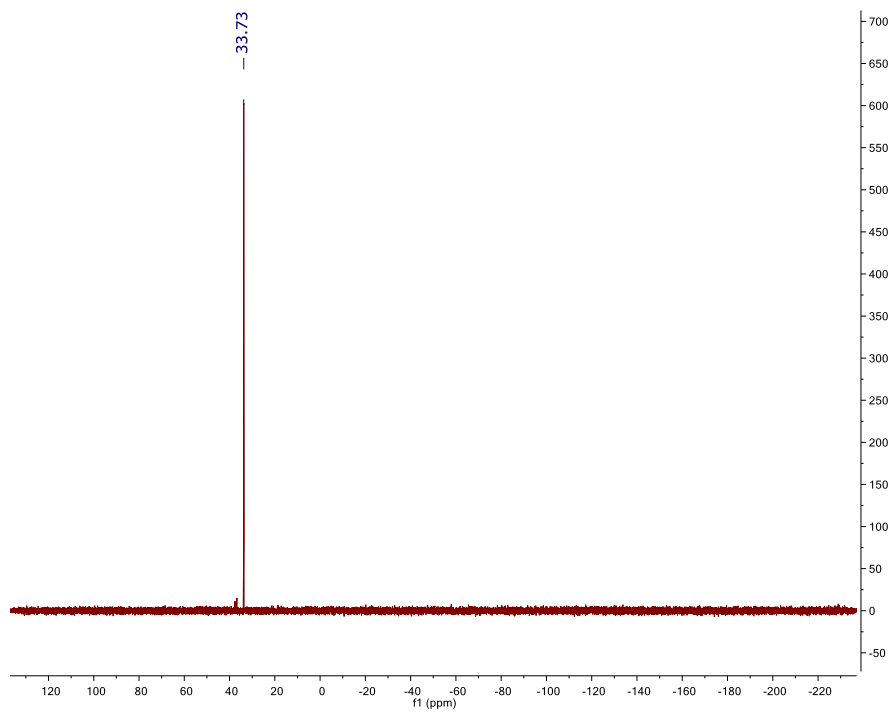


Figure F.1. ^{31}P NMR of TBPOH in CD_3CN .

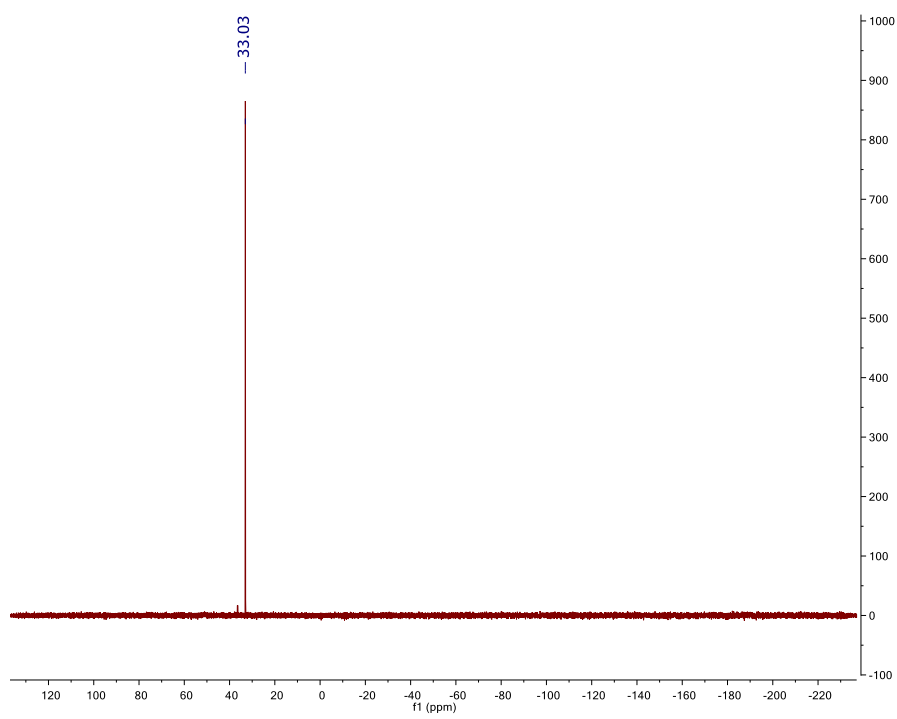


Figure F.2. ^{31}P NMR of TBPCI in CD_3CN .

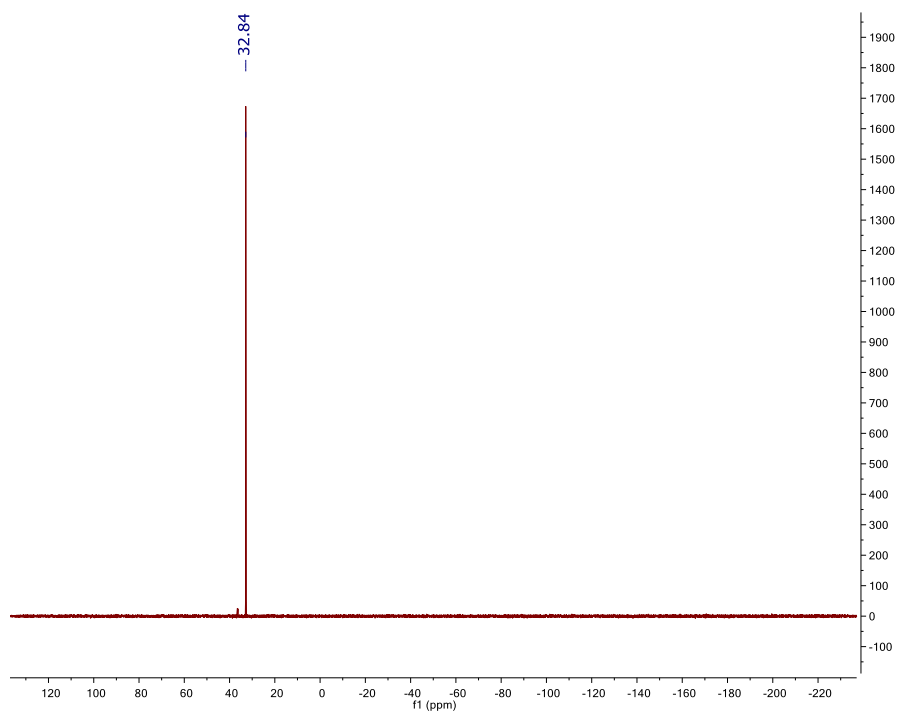


Figure F.3. ^{31}P NMR of TBPBr in CDCl_3 .

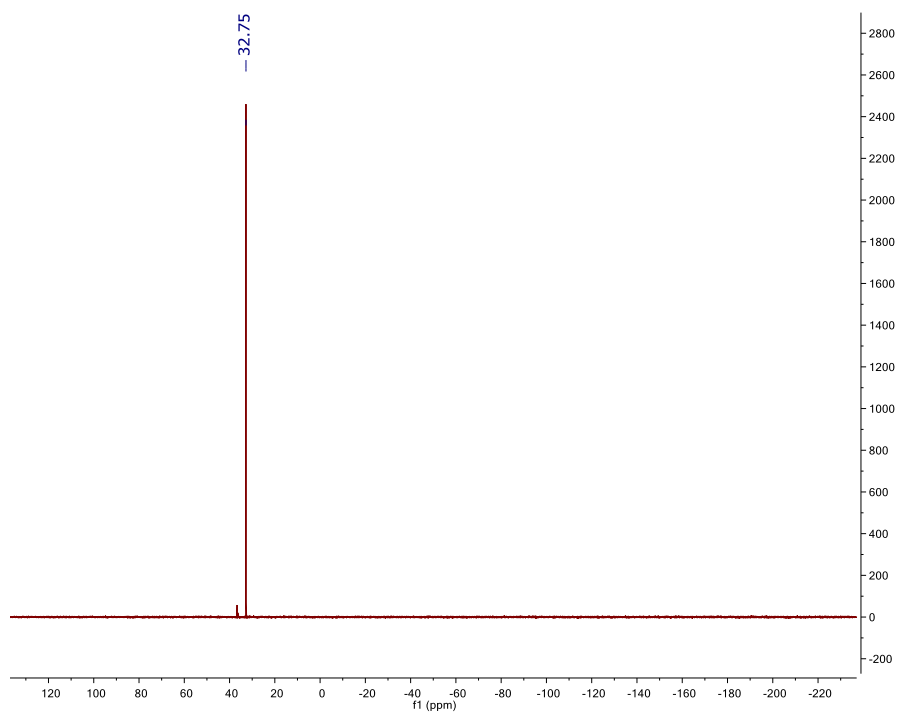


Figure F.4. ^{31}P NMR of TBPI in CDCl_3 .

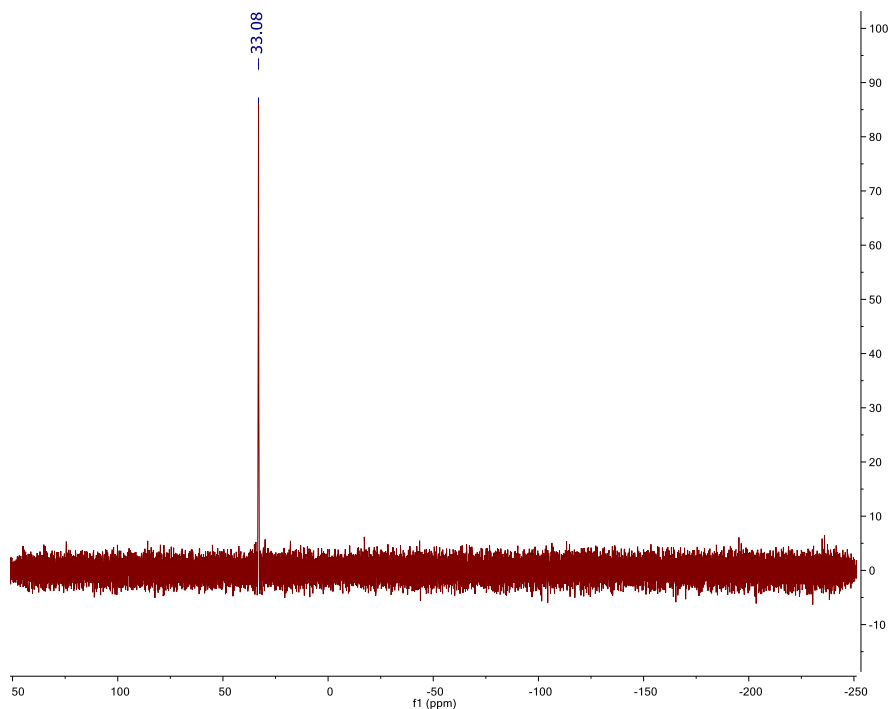


Figure F.5. ^{31}P NMR of TBPNO_3 in CDCl_3 .

Extraction Procedure.

Solvents. Nitrobenzene was purified through previously reported methods.²²⁴ Aqueous solutions of TBPX salts were made in 18 M Ω deionized water. *Note:* Nitrobenzene and tetrabutylphosphonium salts are highly toxic and readily absorbed through nitrile gloves and skin and should be handled carefully to avoid exposure.

Contacting procedure. Batch equilibrium liquid-liquid extractions were performed in polypropylene centrifuge tubes. Equal volumes (0.3 mL) of aqueous and organic phases were contacted for at least 2 h at 25 ± 1 °C by end-over-end rotation at 8 rpm using a laboratory rotator. After rotation, samples were centrifuged at 3000 RCF for 20 min at 25 °C in a refrigerated centrifuge. After centrifugation, 0.2 mL of the aqueous phase was carefully removed by disposable pipette and prepared for analysis by ICP-MS.

Temperature control. Temperature control of contacting experiments was achieved by heating a bead bath beneath the rotator and covering the bead bath, rotator, and headspace with a double layer of aluminum foil. The tip of the temperature controller was held in the headspace to register the temperature. A separate thermometer was also held in the headspace to verify the temperature controller. Figure F.6 shows that temperature at 25 °C remains satisfactorily consistent over 1 h.

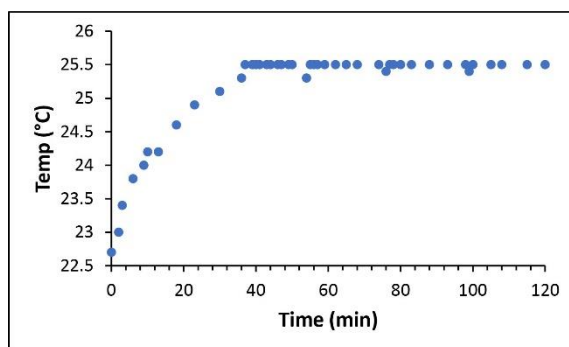


Figure F.6. Temperature of headspace over 2 h using temperature control method described above.

ICP-MS sample preparation. 1000 ppm Y ICP-MS internal standard solution (Y_2O_3 in 2% v/v HNO_3) was purchased from Inorganic Ventures. 0.2 mL of the aqueous phase of the contacting experiments were diluted with 0.8 mL 18 M Ω deionized water. Samples were acidified to 2% v/v HNO_3 with 30.8 μ L concentrated trace metal HNO_3 . 21.4 μ L of 5 ppm Y ICP-MS internal standard solution (0.1 ppm) was added to each sample. Samples which deviated by more than 70% from the Y internal standard concentration determined by ICP-MS were discarded. Extraction experiments were performed in duplicate or triplicate.

ICP-MS P calibration. 1000 ppm P ICP-MS calibration solution (H_2PO_4 in H_2O) was purchased from Inorganic Ventures. 1000 ppm P ICP-MS calibration solution was diluted with 18 M Ω deionized water to make a 1 ppm P ICP-MS calibration solution (15 mL). Further calibration solutions of 0.1, 0.01, 0.001, and 0.0001 ppm P (15 mL) were made through serial dilution with 18 M Ω deionized water starting from the 1 ppm calibration solution. Calibration solutions and a blank solution consisting of 18 M Ω deionized water were acidified up to 2% v/v HNO_3 using concentrated trace metal HNO_3 . 0.1 ppm Y was added to each calibration solution and blank solution from a 5 ppm Y ICP-MS internal standard solution. Exact P and Y concentration for each calibration solution was calculated from the mass and densities of the solutions added or removed.

Representative ICP-MS P calibration and %Y recovery in calibration solutions.

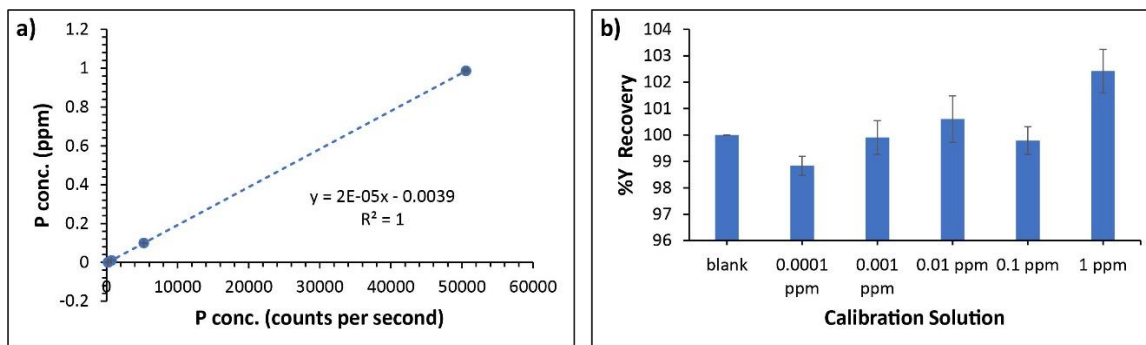


Figure F.7. a) Representative P ICP-MS calibration curve. b) Representative % Y recovery in each calibration solution.

Representative ICP-MS analysis of TBPX extraction.

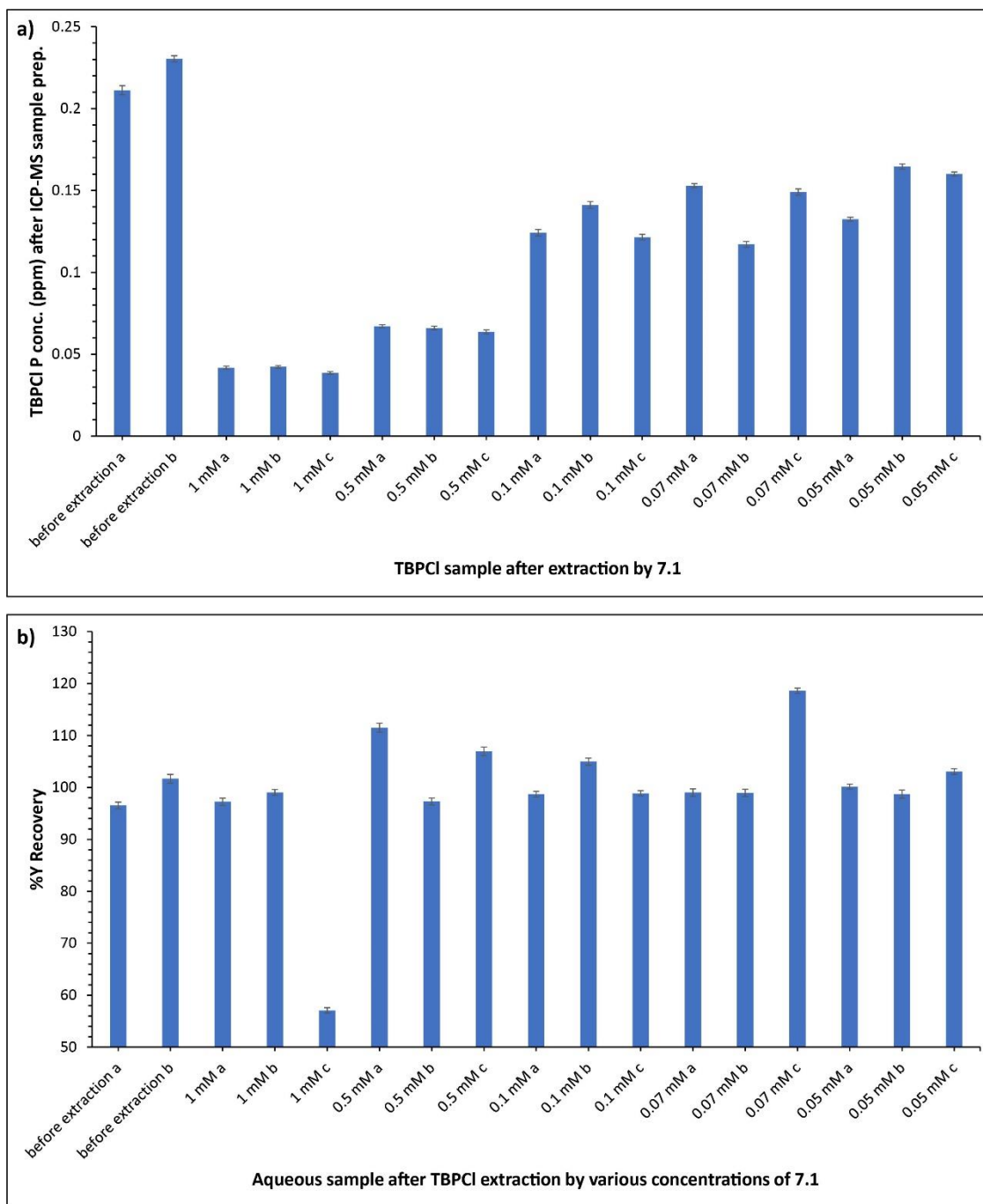


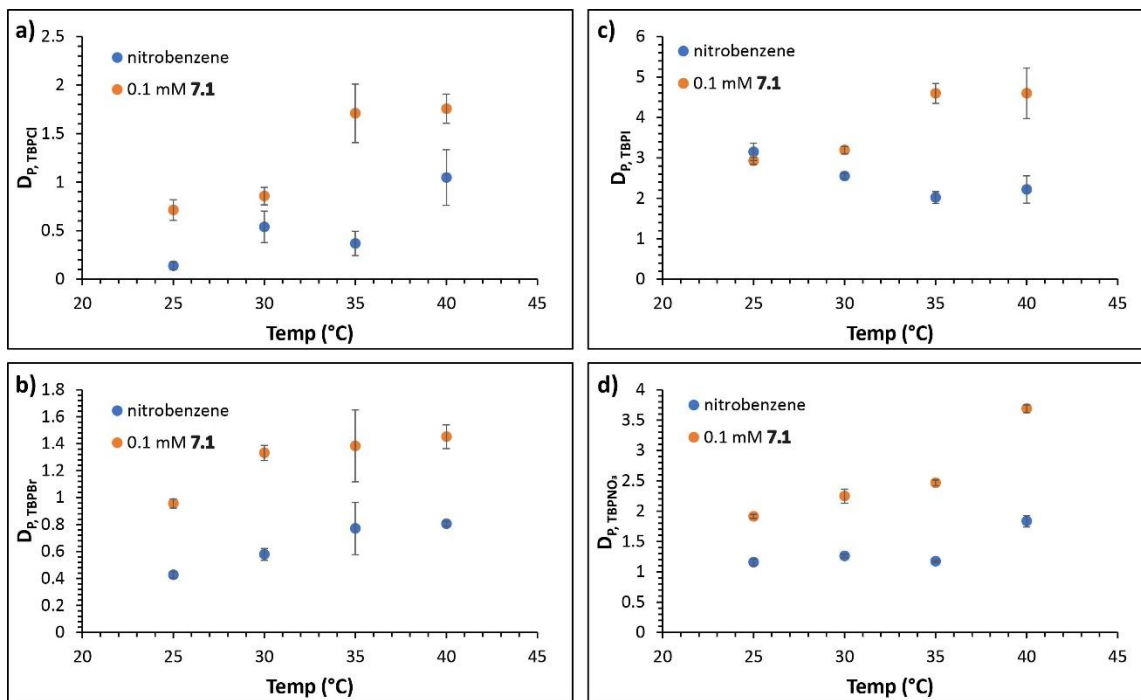
Figure F.8. a) Representative TBPCl concentrations determined through ICP-MS before and after extraction with various concentrations of **7.1**. b) Representative %Y recovery in extraction samples. Samples which had a greater than 30% difference from 100% recovery were discarded (e.g. Sample 1 mM c).

D_P calculation. Because ICP-MS cannot directly determine [TBPX]_{org}, D_P for each sample was calculated by Equation F.1. [TBPX]₀ was determined by subjecting the original TBPX aqueous solution to the same experimental and sample preparation conditions as the contacting experiments, without the presence of an organic phase. Each [TBPX]₀ and [TBPX]_{aq} is an average of values determined from the duplicate or triplicate experiments. Standard error for [TBPX]₀ and [TBPX]_{aq} is the standard deviation of the values determined from the duplicate or triplicate experiments and were propagated appropriately in all following calculations.

$$D_P = \frac{[TBPX]_{org}}{[TBPX]_{aq}} = \frac{[TBPX]_0 - [TBPX]_{aq}}{[TBPX]_{aq}} \quad (\mathbf{F.1})$$

Temperature effect on D_P. Because equilibrium constants in extraction experiments are temperature-dependent and the temperature control method is likely imprecise, a temperature study was performed to determine if small changes in temperature would result in large D_P variation. Extraction was performed with aqueous solutions of TBPCl, TBPBr, TBPI, and TBPNO₃ (0.04 mM) and nitrobenzene or 0.1 mM **7.1** in nitrobenzene at 30, 35, and 40 °C. D_P values determined for each of these experiments were compared with D_P results determined at 25 °C (Figures F.9a-d). Results show that small variation in temperature (1 – 2 °C) are likely not affecting calculated D_P within the precision of this study. While temperature control was not precise enough to determine thermodynamic contribution to extraction, we note that D_P appears to increase with increasing temperature for all experiments with the exception of TBPI (the only lipophilic salt studied) partitioning into nitrobenzene. This is surprising as unpublished isothermal

titration calorimetry of a derivative of **7.1** with TBACl in CHCl₃ suggest that host binding with Cl⁻ in solution is enthalpically driven.



F.9. Temperature effect on D_P for a) TBPCl, b) TBPBr, c) TBPI, and d) TBPNO₃.

REFERENCES CITED

- (1) Hossain, M. F. Arsenic Contamination in Bangladesh—An Overview. *Agric. Ecosyst. Environ.* **2006**, *113*, 1–16.
- (2) Fields, S. Global Nitrogen: Cycling out of Control. *Environ. Health Perspect.* **2004**, *112*, A556–A563.
- (3) U.S. Environmental Protection Agency. Nutrient Pollution: The Issue. <https://www.epa.gov/nutrientpollution/issue> (accessed Jul 01, 2021).
- (4) Power, J. F.; Schepers, J. S. Nitrate Contamination of Groundwater in North America. *Agric. Ecosyst. Environ.* **1989**, *26*, 165–187.
- (5) Wick, K.; Heumesser, C.; Schmid, E. Groundwater Nitrate Contamination: Factors and Indicators. *J. Environ. Manage.* **2012**, *111*, 178–186.
- (6) Mekonnen, M. M.; Hoekstra, A. Y. Global Anthropogenic Phosphorus Loads to Freshwater and Associated Grey Water Footprints and Water Pollution Levels: A High-Resolution Global Study. *Water Resour. Res.* **2018**, *54*, 345–358.
- (7) Moyer, B. A.; Custelcean, R.; Hay, B. P.; Sessler, J. L.; Bowman-James, K.; Day, V. W.; Kang, S.-O. A Case for Molecular Recognition in Nuclear Separations: Sulfate Separation from Nuclear Wastes. *Inorg. Chem.* **2013**, *52*, 3473–3490.
- (8) Gray, M. A.; Winpenny, J. P.; Verdon, B.; McAlroy, H.; Argent, B. E. Chloride Channels and Cystic Fibrosis of the Pancreas. *Biosci. Rep.* **1995**, *15*, 531–541.
- (9) Wang, R. Physiological Implications of Hydrogen Sulfide: A Whiff Exploration That Blossomed. *Physiol. Rev.* **2012**, *92*, 791–896.
- (10) Coates, J. D.; Achenbach, L. A. Microbial Perchlorate Reduction: Rocket-Fueled Metabolism. *Nat. Rev. Microbiol.* **2004**, *2*, 569–580.
- (11) Ojha, L.; Wilhelm, M. B.; Murchie, S. L.; McEwen, A. S.; Wray, J. J.; Hanley, J.; Massé, M.; Chojnacki, M. Spectral Evidence for Hydrated Salts in Recurring Slope Lineae on Mars. *Nat. Geosci.* **2015**, *8*, 829–832.

- (12) Kerr, R. A. Pesky Perchlorates All Over Mars. *Science*. **2013**, *340*, 138–138.
- (13) Molina, P.; Zapata, F.; Caballero, A. Anion Recognition Strategies Based on Combined Noncovalent Interactions. *Chem. Rev.* **2017**, *117*, 9907–9972.
- (14) Sessler, J. L.; Gale, P.; Cho, W.-S. *Anion Receptor Chemistry*; Royal Society of Chemistry: Cambridge, 2006.
- (15) Philip A. Gale; Wim Dehaen. *Anion Recognition in Supramolecular Chemistry*; Springer: Berlin, Heidelberg, 2010.
- (16) Berryman, O. B.; Johnson, C. A.; Zakharov, L. N.; Haley, M. M.; Johnson, D. W. Water and Hydrogen Halides Serve the Same Structural Role in a Series of 2+2 Hydrogen-Bonded Dimers Based on 2,6-Bis(2-Anilinoethynyl)Pyridine Sulfonamide Receptors. *Angew. Chem. Int. Ed.* **2008**, *47*, 117–120.
- (17) Gavette, J. V.; Mills, N. S.; Zakharov, L. N.; Johnson, C. A.; Johnson, D. W.; Haley, M. M. An Anion-Modulated Three-Way Supramolecular Switch That Selectively Binds Dihydrogen Phosphate, H₂PO₄⁻. *Angew. Chem. Int. Ed.* **2013**, *52*, 10270–10274.
- (18) Watt, M. M.; Zakharov, L. N.; Haley, M. M.; Johnson, D. W. Selective Nitrate Binding in Competitive Hydrogen Bonding Solvents: Do Anion- π Interactions Facilitate Nitrate Selectivity? *Angew. Chem. Int. Ed.* **2013**, *52*, 10275–10280.
- (19) Watt, M. M.; Engle, J. M.; Fairley, K. C.; Robitshek, T. E.; Haley, M. M.; Johnson, D. W. “Off-on” Aggregation-Based Fluorescent Sensor for the Detection of Chloride in Water. *Org. Biomol. Chem.* **2015**, *13*, 4266–4270.
- (20) Engle, J. M.; Lakshminarayanan, P. S.; Carroll, C. N.; Zakharov, L. N.; Haley, M. M.; Johnson, D. W. Molecular Self-Assembly: Solvent Guests Tune the Conformation of a Series of 2,6-Bis(2-Anilinoethynyl)Pyridine-Based Ureas. *Cryst. Growth Des.* **2011**, *11*, 5144–5152.
- (21) Gavette, J. V.; Evoniuk, C. J.; Zakharov, L. N.; Carnes, M. E.; Haley, M. M.; Johnson, D. W. Exploring Anion-Induced Conformational Flexibility and Molecular Switching in a Series of Heteroaryl-Urea Receptors. *Chem. Sci.* **2014**, *5*, 2899–2905.

- (22) Johnson II, C. A.; Berryman, O. B.; Sather, A. C.; Zakharov, L. N.; Haley, M. M.; Johnson, D. W. Anion Binding Induces Helicity in a Hydrogen-Bonding Receptor: Crystal Structure of a 2,6-Bis(Anilinoethynyl)Pyridinium Chloride. *Cryst. Growth Des.* **2009**, *9*, 4247–4249.
- (23) Carroll, C. N.; Coombs, B. A.; McClintock, S. P.; Johnson II, C. A.; Berryman, O. B.; Johnson, D. W.; Haley, M. M. Anion-Dependent Fluorescence in Bis(Anilinoethynyl)Pyridine Derivatives: Switchable ON–OFF and OFF–ON Responses. *Chem. Commun.* **2011**, *47*, 5539–5541.
- (24) Engle, J. M.; Carroll, C. N.; Johnson, D. W.; Haley, M. M. Synthesis and Optoelectronic Properties of 2,6-Bis(2-Anilinoethynyl)Pyridine Scaffolds. *Chem. Sci.* **2012**, *3*, 1105–1110.
- (25) Sherbow, T. J.; Fargher, H. A.; Haley, M. M.; Pluth, M. D.; Johnson, D. W. Solvent-Dependent Linear Free-Energy Relationship in a Flexible Host–Guest System. *J. Org. Chem.* **2020**, *85*, 12367–12373.
- (26) Tresca, B. W.; Zakharov, L. N.; Carroll, C. N.; Johnson, D. W.; Haley, M. M. Aryl C–H···Cl– Hydrogen Bonding in a Fluorescent Anion Sensor. *Chem. Commun.* **2013**, *49*, 7240–7242.
- (27) Tresca, B. W.; Hansen, R. J.; Chau, C. V.; Hay, B. P.; Zakharov, L. N.; Haley, M. M.; Johnson, D. W. Substituent Effects in CH Hydrogen Bond Interactions: Linear Free Energy Relationships and Influence of Anions. *J. Am. Chem. Soc.* **2015**, *137*, 14959–14967.
- (28) Tresca, B. W.; Brueckner, A. C.; Haley, M. M.; Cheong, P. H.-Y.; Johnson, D. W. Computational and Experimental Evidence of Emergent Equilibrium Isotope Effects in Anion Receptor Complexes. *J. Am. Chem. Soc.* **2017**, *139*, 3962–3965.
- (29) Hartle, M. D.; Hansen, R. J.; Tresca, B. W.; Praker, S. S.; Zakharov, L. N.; Haley, M. M.; Pluth, M. D.; Johnson, D. W. A Synthetic Supramolecular Receptor for the Hydrosulfide Anion. *Angew. Chem. Int. Ed.* **2016**, *55*, 11480–11484.
- (30) Wang, R. Two’s Company, Three’s a Crowd: Can H₂S Be the Third Endogenous Gaseous Transmitter? *FASEB J.* **2002**, *16*, 1792–1798.
- (31) Lau, N.; Zakharov, L. N.; Pluth, M. D. Modular Tripodal Receptors for the Hydrosulfide (HS[−]) Anion. *Chem. Commun.* **2018**, *54*, 2337–2340.

- (32) Vázquez, J.; Sindelar, V. Supramolecular Binding and Release of Sulfide and Hydrosulfide Anions in Water. *Chem. Commun.* **2018**, *54*, 5859–5862.
- (33) Weekley, C. M.; Harris, H. H. Which Form Is That? The Importance of Selenium Speciation and Metabolism in the Prevention and Treatment of Disease. *Chem. Soc. Rev.* **2013**, *42*, 8870–8894.
- (34) Reich, H. J.; Hondal, R. J. Why Nature Chose Selenium. *ACS Chem. Biol.* **2016**, *11*, 821–841.
- (35) Fargher, H. A.; Lau, N.; Zakharov, L. N.; Haley, M. M.; Johnson, D. W.; Pluth, M. D. Expanding Reversible Chalcogenide Binding: Supramolecular Receptors for the Hydroselenide (HSe⁻) Anion. *Chem. Sci.* **2018**, *10*, 67–72.
- (36) Fargher, H. A.; Lau, N.; Richardson, H. C.; Cheong, P. H.-Y.; Haley, M. M.; Pluth, M. D.; Johnson, D. W. Tuning Supramolecular Selectivity for Hydrosulfide: Linear Free Energy Relationships Reveal Preferential C–H Hydrogen Bond Interactions. *J. Am. Chem. Soc.* **2020**, *142*, 8243–8251.
- (37) Deng, C.-L.; Bard, J. P.; Lohrman, J. A.; Barker, J. E.; Zakharov, L. N.; Johnson, D. W.; Haley, M. M. Exploiting the Hydrogen Bond Donor/Acceptor Properties of PN-Heterocycles: Selective Anion Receptors for Hydrogen Sulfate. *Angew. Chem. Int. Ed.* **2019**, *58*, 3934–3938.
- (38) Kaphan, D. M.; Levin, M. D.; Bergman, R. G.; Raymond, K. N.; Toste, F. D. A Supramolecular Microenvironment Strategy for Transition Metal Catalysis. *Science* **2015**, *350*, 1235–1238.
- (39) Meeuwissen, J.; Reek, J. N. H. Supramolecular Catalysis beyond Enzyme Mimics. *Nat. Chem.* **2010**, *2*, 615–621.
- (40) Morimoto, M.; Bierschenk, S. M.; Xia, K. T.; Bergman, R. G.; Raymond, K. N.; Toste, F. D. Advances in Supramolecular Host-Mediated Reactivity. *Nat. Catal.* **2020**, *3*, 969–984.
- (41) Cram, D. J.; Tanner, M. E.; Thomas, R. The Taming of Cyclobutadiene. *Angew. Chem. Int. Ed.* **1991**, *30*, 1024–1027.
- (42) Mal, P.; Breiner, B.; Rissanen, K.; Nitschke, J. R. White Phosphorus Is Air-Stable Within a Self-Assembled Tetrahedral Capsule. *Science* **2009**, *324*, 1697–1699.

- (43) Hargrove, A. E.; Nieto, S.; Zhang, T.; Sessler, J. L.; Anslyn, E. V. Artificial Receptors for the Recognition of Phosphorylated Molecules. *Chem. Rev.* **2011**, *111*, 6603–6782.
- (44) Gale, P. A.; Caltagirone, C. Anion Sensing by Small Molecules and Molecular Ensembles. *Chem. Soc. Rev.* **2015**, *44*, 4212–4227.
- (45) Gibb, C. L. D.; Oertling, E. E.; Velaga, S.; Gibb, B. C. Thermodynamic Profiles of Salt Effects on a Host–Guest System: New Insight into the Hofmeister Effect. *J. Phys. Chem. B* **2015**, *119*, 5624–5638.
- (46) Beer, P. D.; Gale, P. A. Anion Recognition and Sensing: The State of the Art and Future Perspectives. *Angew. Chem. Int. Ed.* **2001**, *40*, 486–516.
- (47) Pramanik, A.; Powell, D. R.; Wong, B. M.; Hossain, Md. A. Spectroscopic, Structural, and Theoretical Studies of Halide Complexes with a Urea-Based Tripodal Receptor. *Inorg. Chem.* **2012**, *51*, 4274–4284.
- (48) Blondeau, P.; Segura, M.; Pérez-Fernández, R.; de Mendoza, J. Molecular Recognition of Oxoanions Based on Guanidinium Receptors. *Chem. Soc. Rev.* **2007**, *36*, 198–210.
- (49) Sabater, P.; Zapata, F.; Caballero, A.; Fernández, I.; Ramirez de Arellano, C.; Molina, P. 2,4,5-Trimethylimidazolium Scaffold for Anion Recognition Receptors Acting Through Charge-Assisted Aliphatic and Aromatic C–H Interactions. *J. Org. Chem.* **2016**, *81*, 3790–3798.
- (50) Lim, J. Y. C.; Beer, P. D. A Pyrrole-Containing Cleft-Type Halogen Bonding Receptor for Oxoanion Recognition and Sensing in Aqueous Solvent Media. *New J. Chem.* **2018**, *42*, 10472–10475.
- (51) González, L.; Zapata, F.; Caballero, A.; Molina, P.; Ramírez de Arellano, C.; Alkorta, I.; Elguero, J. Host–Guest Chemistry: Oxoanion Recognition Based on Combined Charge-Assisted C–H or Halogen-Bonding Interactions and Anion···Anion Interactions Mediated by Hydrogen Bonds. *Chem. Eur. J.* **2016**, *22*, 7533–7544.
- (52) Lopez, N.; Graham, D. J.; McGuire, R.; Alliger, G. E.; Shao-Horn, Y.; Cummins, C. C.; Nocera, D. G. Reversible Reduction of Oxygen to Peroxide Facilitated by Molecular Recognition. *Science* **2012**, *335*, 450–453.

- (53) Kang, S. O.; Powell, D.; Day, V. W.; Bowman-James, K. Trapped Bifluoride. *Angew. Chem. Int. Ed.* **2006**, *45*, 1921–1925.
- (54) Kang, S. O.; Day, V. W.; Bowman-James, K. Tricyclic Host for Linear Anions. *Inorg. Chem.* **2010**, *49*, 8629–8636.
- (55) Holm, R. H.; Solomon, E. I. Preface: Biomimetic Inorganic Chemistry. *Chem. Rev.* **2004**, *104*, 347–348.
- (56) Hartle, M. D.; Pluth, M. D. A Practical Guide to Working with H₂S at the Interface of Chemistry and Biology. *Chem. Soc. Rev.* **2016**, *45*, 6108–6117.
- (57) Arnold, I. M.; Dufresne, R. M.; Alleyne, B. C.; Stuart, P. J. Health Implication of Occupational Exposures to Hydrogen Sulfide. *J. Occup. Med.* **1985**, *27*, 373–376.
- (58) National Research Council. *Acute Exposure Guideline Levels for Selected Airborne Chemicals: Volume 16*; The National Academies Press: Washington, DC, 2014.
- (59) Zanardo, R. C. O.; Brancalone, V.; Distrutti, E.; Fiorucci, S.; Cirino, G.; Wallace, J. L. Hydrogen Sulfide Is an Endogenous Modulator of Leukocyte-Mediated Inflammation. *FASEB J.* **2006**, *20*, 2118–2120.
- (60) Distrutti, E.; Sediari, L.; Mencarelli, A.; Renga, B.; Orlandi, S.; Russo, G.; Caliendo, G.; Santagada, V.; Cirino, G.; Wallace, J. L.; Fiorucci, S. 5-Amino-2-Hydroxybenzoic Acid 4-(5-Thioxo-5H-[1,2]Dithiol-3yl)-Phenyl Ester (ATB-429), a Hydrogen Sulfide-Releasing Derivative of Mesalamine, Exerts Antinociceptive Effects in a Model of Postinflammatory Hypersensitivity. *J. Pharmacol. Exp. Ther.* **2006**, *319*, 447–458.
- (61) Zhang, Z.; Huang, H.; Liu, P.; Tang, C.; Wang, J. Hydrogen Sulfide Contributes to Cardioprotection during Ischemia-Reperfusion Injury by Opening K ATP Channels. *Can. J. Physiol. Pharmacol.* **2007**, *85*, 1248–1253.
- (62) Veres, Z.; Tsai, L.; Scholz, T. D.; Politino, M.; Balaban, R. S.; Stadtman, T. C. Synthesis of 5-Methylaminomethyl-2-Selenouridine in TRNAs: ³¹P NMR Studies Show the Labile Selenium Donor Synthesized by the SelD Gene Product Contains Selenium Bonded to Phosphorus. *PNAS* **1992**, *89*, 2975–2979.

- (63) Glass, R. S.; Singh, W. P.; Jung, W.; Veres, Z.; Scholz, T. D.; Stadtman, T. Monoselenophosphate: Synthesis, Characterization, and Identity with the Prokaryotic Biological Selenium Donor, Compound SePX. *Biochemistry* **1993**, *32*, 12555–12559.
- (64) Shrimali, R. K.; Irons, R. D.; Carlson, B. A.; Sano, Y.; Gladyshev, V. N.; Park, J. M.; Hatfield, D. L. Selenoproteins Mediate T Cell Immunity through an Antioxidant Mechanism. *J. Biol. Chem.* **2008**, *283*, 20181–20185.
- (65) Hatfield, D. L.; Tsuji, P. A.; Carlson, B. A.; Gladyshev, V. N. Selenium and Selenocysteine: Roles in Cancer, Health, and Development. *Trends Biochem. Sci.* **2014**, *39*, 112–120.
- (66) Weekley, C. M.; Aitken, J. B.; Vogt, S.; Finney, L. A.; Paterson, D. J.; de Jonge, M. D.; Howard, D. L.; Witting, P. K.; Musgrave, I. F.; Harris, H. H. Metabolism of Selenite in Human Lung Cancer Cells: X-Ray Absorption and Fluorescence Studies. *J. Am. Chem. Soc.* **2011**, *133*, 18272–18279.
- (67) Shannon, R. D. Revised Effective Ionic Radii and Systematic Studies of Interatomic Distances in Halides and Chalcogenides. *Acta. Cryst. A* **1976**, *32*, 751–767.
- (68) Dey, S. K.; Das, G. A Selective Fluoride Encapsulated Neutral Tripodal Receptor Capsule: Solvatochromism and Solvatomorphism. *Chem. Commun.* **2011**, *47*, 4983–4985.
- (69) Batchelor, R. J.; Einstein, F. W. B.; Gay, I. D.; Jones, C. H. W.; Sharma, R. D. Syntheses and Solid-State NMR of Tetrabutylammonium Hydrogen Telluride, Tetramethylammonium Hydrogen Selenide and Bis(Tetramethylammonium) Ditelluride and x-Ray Crystal Structures of Me₄NSeH and (Me₄N)₂Te₂. *Inorg. Chem.* **1993**, *32*, 4378–4383.
- (70) Hartle, M. D.; Meininger, D. J.; Zakharov, L. N.; Tonzetich, Z. J.; Pluth, M. D. NBu₄SH Provides a Convenient Source of HS⁻ Soluble in Organic Solution for H₂S and Anion-Binding Research. *Dalton Trans.* **2015**, *44*, 19782–19785.
- (71) Thordarson, P. Determining Association Constants from Titration Experiments in Supramolecular Chemistry. *Chem. Soc. Rev.* **2011**, *40*, 1305–1323.

- (72) Hibbert, D. B.; Thordarson, P. The Death of the Job Plot, Transparency, Open Science and Online Tools, Uncertainty Estimation Methods and Other Developments in Supramolecular Chemistry Data Analysis. *Chem. Commun.* **2016**, 52, 12792–12805.
- (73) Bordwell, F. G. Equilibrium Acidities in Dimethyl Sulfoxide Solution. *Acc. Chem. Res.* **1988**, 21, 456–463.
- (74) Steiner, T. The Hydrogen Bond in the Solid State. *Angew. Chem. Int. Ed.* **2002**, 41, 48–76.
- (75) Shahi, A.; Arunan, E. Why Are Hydrogen Bonds Directional? *J. Chem. Sci.* **2016**, 128, 1571–1577.
- (76) Gale, P. A.; Howe, E. N. W.; Wu, X. Anion Receptor Chemistry. *Chem* **2016**, 1, 351–422.
- (77) Evans, N. H.; Beer, P. D. Advances in Anion Supramolecular Chemistry: From Recognition to Chemical Applications. *Angew. Chem. Int. Ed.* **2014**, 53, 11716–11754.
- (78) Hwang, H. J.; Carey, J. R.; Brower, E. T.; Gengenbach, A. J.; Abramite, J. A.; Lu, Y. Blue Ferrocenium Azurin: An Organometalloprotein with Tunable Redox Properties. *J. Am. Chem. Soc.* **2005**, 127, 15356–15357.
- (79) Lu, Y.; Yeung, N.; Sieracki, N.; Marshall, N. M. Design of Functional Metalloproteins. *Nature* **2009**, 460, 855–862.
- (80) Berry, S. M.; Baker, M. H.; Reardon, N. J. Reduction Potential Variations in Azurin through Secondary Coordination Sphere Phenylalanine Incorporations. *J. Inorg. Biochem.* **2010**, 104, 1071–1078.
- (81) Busschaert, N.; Caltagirone, C.; Van Rossom, W.; Gale, P. A. Applications of Supramolecular Anion Recognition. *Chem. Rev.* **2015**, 115, 8038–8155.
- (82) Gale, P. A.; Davis, J. T.; Quesada, R. Anion Transport and Supramolecular Medicinal Chemistry. *Chem. Soc. Rev.* **2017**, 46, 2497–2519.

- (83) Ko, S.-K.; Kim, S. K.; Share, A.; Lynch, V. M.; Park, J.; Namkung, W.; Van Rossom, W.; Busschaert, N.; Gale, P. A.; Sessler, J. L.; Shin, I. Synthetic Ion Transporters Can Induce Apoptosis by Facilitating Chloride Anion Transport into Cells. *Nat. Chem.* **2014**, *6*, 885–892.
- (84) Reddi, R.; Singarapu, K. K.; Pal, D.; Addlagatta, A. The Unique Functional Role of the C–H···S Hydrogen Bond in the Substrate Specificity and Enzyme Catalysis of Type 1 Methionine Aminopeptidase. *Mol. BioSyst.* **2016**, *12*, 2408–2416.
- (85) Eytel, L. M.; Fargher, H. A.; Haley, M. M.; Johnson, D. W. The Road to Aryl CH···anion Binding Was Paved with Good Intentions: Fundamental Studies, Host Design, and Historical Perspectives in CH Hydrogen Bonding. *Chem. Commun.* **2019**, *55*, 5195–5206.
- (86) Perrin, D. D. *Ionisation Constants of Inorganic Acids and Bases in Aqueous Solution*, 2nd ed.; Elsevier, 1982.
- (87) Vollhardt, P.; Schore, N. *Organic Chemistry: Structure and Function*, 8th ed.; W. H. Freeman and Company: New York, NY, 2018.
- (88) Kelly, C. P.; Cramer, C. J.; Truhlar, D. G. SM6: A Density Functional Theory Continuum Solvation Model for Calculating Aqueous Solvation Free Energies of Neutrals, Ions, and Solute–Water Clusters. *J. Chem. Theory Comput.* **2005**, *1*, 1133–1152.
- (89) Tissandier, M. D.; Cowen, K. A.; Feng, W. Y.; Gundlach, E.; Cohen, M. H.; Earhart, A. D.; Coe, J. V.; Tuttle, T. R. The Proton's Absolute Aqueous Enthalpy and Gibbs Free Energy of Solvation from Cluster-Ion Solvation Data. *J. Phys. Chem. A* **1998**, *102*, 7787–7794.
- (90) Bryantsev, V. S.; Hay, B. P. Influence of Substituents on the Strength of Aryl C–H···Anion Hydrogen Bonds. *Org. Lett.* **2005**, *7*, 5031–5034.
- (91) Nie, L.; Li, Z.; Han, J.; Zhang, X.; Yang, R.; Liu, W.-X.; Wu, F.-Y.; Xie, J.-W.; Zhao, Y.-F.; Jiang, Y.-B. Development of N-Benzamidothioureas as a New Generation of Thiourea-Based Receptors for Anion Recognition and Sensing. *J. Org. Chem.* **2004**, *69*, 6449–6454.

- (92) Wu, F.-Y.; Li, Z.; Guo, L.; Wang, X.; Lin, M.-H.; Zhao, Y.-F.; Jiang, Y.-B. A Unique NH-Spacer for N-Benzamidothiourea Based Anion Sensors. Substituent Effect on Anion Sensing of the ICT Dual Fluorescent N-(p-Dimethylaminobenzamido)-N'-Arylthioureas. *Org. Biomol. Chem.* **2006**, *4*, 624–630.
- (93) Busschaert, N.; Bradberry, S. J.; Wenzel, M.; Haynes, C. J. E.; Hiscock, J. R.; Kirby, I. L.; Karagiannidis, L. E.; Moore, S. J.; Wells, N. J.; Herniman, J.; Langley, G. J.; Horton, P. N.; Light, M. E.; Marques, I.; Costa, P. J.; Félix, V.; Frey, J. G.; Gale, P. A. Towards Predictable Transmembrane Transport: QSAR Analysis of Anion Binding and Transport. *Chem. Sci.* **2013**, *4*, 3036–3045.
- (94) Beer, P. D.; Hazlewood, C.; Heseck, D.; Hodacova, J.; Stokes, S. E. Anion Recognition by Acyclic Redox-Responsive Amide-Linked Cobaltocenium Receptors. *J. Chem. Soc., Dalton Trans.* **1993**, 1327–1332.
- (95) Hammett, L. P. The Effect of Structure upon the Reactions of Organic Compounds. Benzene Derivatives. *J. Am. Chem. Soc.* **1937**, *59*, 96–103.
- (96) McGrath, J. M.; Pluth, M. D. Linear Free Energy Relationships Reveal Structural Changes in Hydrogen-Bonded Host–Guest Interactions. *J. Org. Chem.* **2014**, *79*, 11797–11801.
- (97) Swain, C. G.; Lupton, E. C. Field and Resonance Components of Substituent Effects. *J. Am. Chem. Soc.* **1968**, *90*, 4328–4337.
- (98) Nepal, B.; Scheiner, S. Anionic CH \cdots X $^-$ Hydrogen Bonds: Origin of Their Strength, Geometry, and Other Properties. *Chem. Eur. J.* **2015**, *21*, 1474–1481.
- (99) Jouyban, A.; Soltanpour, S. Prediction of Dielectric Constants of Binary Solvents at Various Temperatures. *J. Chem. Eng. Data* **2010**, *55*, 2951–2963.
- (100) Frisch, M. J. Gaussian 09. **1973**.
- (101) Perdew, J. P.; Burke, K.; Ernzerhof, M. Generalized Gradient Approximation Made Simple. *Phys. Rev. Lett.* **1996**, *77*, 3865–3868.
- (102) Perdew, J. P.; Burke, K.; Ernzerhof, M. Generalized Gradient Approximation Made Simple [Phys. Rev. Lett. 77, 3865 (1996)]. *Phys. Rev. Lett.* **1997**, *78*, 1396–1396.

- (103) Liu, Y.; Sengupta, A.; Raghavachari, K.; Flood, A. H. Anion Binding in Solution: Beyond the Electrostatic Regime. *Chem* **2017**, *3*, 411–427.
- (104) Sengupta, A.; Liu, Y.; Flood, A. H.; Raghavachari, K. Anion-Binding Macrocycles Operate Beyond the Electrostatic Regime: Interaction Distances Matter. *Chem. Eur. J.* **2018**, *24*, 14409–14417.
- (105) Breneman, C. M.; Wiberg, K. B. Determining Atom-Centered Monopoles from Molecular Electrostatic Potentials. The Need for High Sampling Density in Formamide Conformational Analysis. *J. Comput. Chem.* **1990**, *11*, 361–373.
- (106) Lisbjerg, M.; Valkenier, H.; Jessen, B. M.; Al-Kerdi, H.; Davis, A. P.; Pittelkow, M. Biotin[6]Uril Esters: Chloride-Selective Transmembrane Anion Carriers Employing C—H···Anion Interactions. *J. Am. Chem. Soc.* **2015**, *137*, 4948–4951.
- (107) Liu, Y.; Zhao, W.; Chen, C.-H.; Flood, A. H. Chloride Capture Using a C—H Hydrogen-Bonding Cage. *Science* **2019**, *365*, 159–161.
- (108) Lee, S.; Chen, C.-H.; Flood, A. H. A Pentagonal Cyanostar Macrocycle with Cyanostilbene CH Donors Binds Anions and Forms Dialkylphosphate [3]Rotaxanes. *Nat. Chem.* **2013**, *5*, 704–710.
- (109) Ramabhadran, R. O.; Hua, Y.; Li, Y.; Flood, A. H.; Raghavachari, K. From Atomic to Molecular Anions: A Neutral Receptor Captures Cyanide Using Strong C—H Hydrogen Bonds. *Chem. Eur. J.* **2011**, *17*, 9123–9129.
- (110) Sessler, J. L.; Cai, J.; Gong, H.-Y.; Yang, X.; Arambula, J. F.; Hay, B. P. A Pyrrolyl-Based Triazolophane: A Macrocyclic Receptor With CH and NH Donor Groups That Exhibits a Preference for Pyrophosphate Anions. *J. Am. Chem. Soc.* **2010**, *132*, 14058–14060.
- (111) Cai, J.; Hay, B. P.; Young, N. J.; Yang, X.; Sessler, J. L. A Pyrrole-Based Triazolium-Phane with NH and Cationic CH Donor Groups as a Receptor for Tetrahedral Oxyanions That Functions in Polar Media. *Chem. Sci.* **2013**, *4*, 1560–1567.
- (112) Pedzisa, L.; Hay, B. P. Aliphatic C—H···Anion Hydrogen Bonds: Weak Contacts or Strong Interactions? *J. Org. Chem.* **2009**, *74*, 2554–2560.

- (113) Andersen, N. N.; Eriksen, K.; Lisbjerg, M.; Ottesen, M. E.; Milhøj, B. O.; Sauer, S. P. A.; Pittelkow, M. Entropy/Enthalpy Compensation in Anion Binding: Biotin[6]Uril and Biotin-l-Sulfoxide[6]Uril Reveal Strong Solvent Dependency. *J. Org. Chem.* **2019**, *84*, 2577–2584.
- (114) Li, Y.; Flood, A. H. Pure C-H Hydrogen Bonding to Chloride Ions: A Preorganized and Rigid Macrocyclic Receptor. *Angew. Chem. Int. Ed.* **2008**, *47*, 2649–2652.
- (115) Li, Y.; Flood, A. H. Strong, Size-Selective, and Electronically Tunable C-H...Halide Binding with Steric Control over Aggregation from Synthetically Modular, Shape-Persistent [34]Triazolophanes. *J. Am. Chem. Soc.* **2008**, *130*, 12111–12122.
- (116) Cai, J.; Sessler, J. L. Neutral CH and Cationic CH Donor Groups as Anion Receptors. *Chem. Soc. Rev.* **2014**, *43*, 6198–6213.
- (117) Pattawong, O.; Mustard, T. J. L.; Johnston, R. C.; Cheong, P. H.-Y. Mechanism and Stereocontrol: Enantioselective Addition of Pyrrole to Ketenes Using Planar-Chiral Organocatalysts. *Angew. Chem. Int. Ed.* **2013**, *52*, 1420–1423.
- (118) Walden, D. M.; Ogba, O. M.; Johnston, R. C.; Cheong, P. H.-Y. Computational Insights into the Central Role of Nonbonding Interactions in Modern Covalent Organocatalysis. *Acc. Chem. Res.* **2016**, *49*, 1279–1291.
- (119) Quinn, J. R.; Zimmerman, S. C.; Del Bene, J. E.; Shavitt, I. Does the A·T or G·C Base-Pair Possess Enhanced Stability? Quantifying the Effects of CH...O Interactions and Secondary Interactions on Base-Pair Stability Using a Phenomenological Analysis and Ab Initio Calculations. *J. Am. Chem. Soc.* **2007**, *129*, 934–941.
- (120) Derewenda, Z. S.; Lee, L.; Derewenda, U. The Occurrence of C-H...O Hydrogen Bonds in Proteins. *J. Mol. Biol.* **1995**, *252*, 248–262.
- (121) Czyzewski, B. K.; Wang, D.-N. Identification and Characterization of a Bacterial Hydrosulphide Ion Channel. *Nature* **2012**, *483*, 494–497.
- (122) Sippel, D.; Rohde, M.; Netzer, J.; Trncik, C.; Gies, J.; Grunau, K.; Djurdjevic, I.; Decamps, L.; Andrade, S. L. A.; Einsle, O. A Bound Reaction Intermediate Sheds Light on the Mechanism of Nitrogenase. *Science* **2018**, *359*, 1484–1489.

- (123) Schneider, H.-J. Limitations and Extensions of the Lock-and-Key Principle: Differences between Gas State, Solution and Solid State Structures. *Int. J. Mol. Sci.* **2015**, *16*, 6694–6717.
- (124) Antonisse, M. M. G.; Reinhoudt, D. N. Neutral Anion Receptors: Design and Application. *Chem. Commun.* **1998**, 443–448.
- (125) Smulders, M. M. J.; Zarra, S.; Nitschke, J. R. Quantitative Understanding of Guest Binding Enables the Design of Complex Host–Guest Behavior. *J. Am. Chem. Soc.* **2013**, *135*, 7039–7046.
- (126) Świderek, K.; Paneth, P. Binding Isotope Effects. *Chem. Rev.* **2013**, *113*, 7851–7879.
- (127) Laughrey, Z. R.; Upton, T. G.; Gibb, B. C. A Deuterated Deep-Cavity Cavitand Confirms the Importance of C–H···X–R Hydrogen Bonds in Guest Binding. *Chem. Commun.* **2006**, 970–972.
- (128) Rechavi, D.; Scarso, A.; Rebek, J. Isotopomer Encapsulation in a Cylindrical Molecular Capsule: A Probe for Understanding Noncovalent Isotope Effects on a Molecular Level. *J. Am. Chem. Soc.* **2004**, *126*, 7738–7739.
- (129) Zhao, Y.-L.; Houk, K. N.; Rechavi, D.; Scarso, A.; Rebek, J. Equilibrium Isotope Effects as a Probe of Nonbonding Attractions. *J. Am. Chem. Soc.* **2004**, *126*, 11428–11429.
- (130) Haino, T.; Fukuta, K.; Iwamoto, H.; Iwata, S. Noncovalent Isotope Effect for Guest Encapsulation in Self-Assembled Molecular Capsules. *Chem. Eur. J.* **2009**, *15*, 13286–13290.
- (131) Wade, D. Deuterium Isotope Effects on Noncovalent Interactions between Molecules. *Chem.-Biol. Interact.* **1999**, *117*, 191–217.
- (132) Mugridge, J. S.; Bergman, R. G.; Raymond, K. N. Equilibrium Isotope Effects on Noncovalent Interactions in a Supramolecular Host–Guest System. *J. Am. Chem. Soc.* **2012**, *134*, 2057–2066.
- (133) Zhao, C.; Parrish, R. M.; Smith, M. D.; Pellechia, P. J.; Sherrill, C. D.; Shimizu, K. D. Do Deuteriums Form Stronger CH– π Interactions? *J. Am. Chem. Soc.* **2012**, *134*, 14306–14309.

- (134) Paneth, A.; Paneth, P. Isotopic Consequences of Host–Guest Interactions; Noncovalent Chlorine Isotope Effects. *J. Phys. Chem. B* **2021**, *125*, 1874–1880.
- (135) Wassmundt, F. W.; Kiesman, W. F. Efficient Catalysis of Hydrodediazoniations in Dimethylformamide. *J. Org. Chem.* **1995**, *60*, 1713–1719.
- (136) Lindsay, D. M.; Dohle, W.; Jensen, A. E.; Kopp, F.; Knochel, P. Preparation of Polyfunctional Heterocycles Using Highly Functionalized Aminated Arylmagnesium Reagents as Versatile Scaffolds. *Org. Lett.* **2002**, *4*, 1819–1822.
- (137) Carroll, C. N.; Berryman, O. B.; Johnson, C. A.; Zakharov, L. N.; Haley, M. M.; Johnson, D. W. Protonation Activates Anion Binding and Alters Binding Selectivity in New Inherently Fluorescent 2,6-Bis(2-Anilinoethynyl)Pyridine Bisureas. *Chem. Commun.* **2009**, 2520–2522.
- (138) Perrin, C. L.; Fabian, M. A. Multicomponent NMR Titration for Simultaneous Measurement of Relative PKas. *Anal. Chem.* **1996**, *68*, 2127–2134.
- (139) Perrin, C. L.; Karri, P. Position-Specific Secondary Deuterium Isotope Effects on Basicity of Pyridine. *J. Am. Chem. Soc.* **2010**, *132*, 12145–12149.
- (140) Pluth, M. D.; Tonzetich, Z. J. Hydrosulfide Complexes of the Transition Elements: Diverse Roles in Bioinorganic, Cluster, Coordination, and Organometallic Chemistry. *Chem. Soc. Rev.* **2020**, *49*, 4070–4134.
- (141) Pauling, L. C. *The Nature of the Chemical Bond*, 3rd ed.; Cornell University Press: Ithaca, NY, 1960.
- (142) Bruns, C. J.; Stoddart, J. F. Introducing the Mechanical Bond. In *The Nature of the Mechanical Bond: From Molecules to Machines*; John Wiley & Sons, Inc., 2016; pp 1–54.
- (143) Liptrot, D. J.; Power, P. P. London Dispersion Forces in Sterically Crowded Inorganic and Organometallic Molecules. *Nat. Rev. Chem.* **2017**, *1*, 1–12.
- (144) Meyer, E. A.; Castellano, R. K.; Diederich, F. Interactions with Aromatic Rings in Chemical and Biological Recognition. *Angew. Chem. Int. Ed.* **2003**, *42*, 1210–1250.

- (145) Paulini, R.; Müller, K.; Diederich, F. Orthogonal Multipolar Interactions in Structural Chemistry and Biology. *Angew. Chem. Int. Ed.* **2005**, *44*, 1788–1805.
- (146) Beno, B. R.; Yeung, K.-S.; Bartberger, M. D.; Pennington, L. D.; Meanwell, N. A. A Survey of the Role of Noncovalent Sulfur Interactions in Drug Design. *J. Med. Chem.* **2015**, *58*, 4383–4438.
- (147) Arunan, E.; Desiraju, G. R.; Klein, R. A.; Sadlej, J.; Scheiner, S.; Alkorta, I.; Clary, D. C.; Crabtree, R. H.; Dannenberg, J. J.; Hobza, P.; Kjaergaard, H. G.; Legon, A. C.; Mennucci, B.; Nesbitt, D. J. Defining the hydrogen bond: An account (IUPAC Technical Report). *Pure Appl. Chem.* **2011**, *83*, 1619–1636.
- (148) Arunan, E.; Desiraju, G. R.; Klein, R. A.; Sadlej, J.; Scheiner, S.; Alkorta, I.; Clary, D. C.; Crabtree, R. H.; Dannenberg, J. J.; Hobza, P.; Kjaergaard, H. G.; Legon, A. C.; Mennucci, B.; Nesbitt, D. J. Definition of the hydrogen bond (IUPAC Recommendations 2011). *Pure Appl. Chem.* **2011**, *83*, 1637–1641.
- (149) Desiraju, G. R. A Bond by Any Other Name. *Angew. Chem. Int. Ed.* **2011**, *50*, 52–59.
- (150) Lennard-Jones, J. E. Cohesion. *Proc. Phys. Soc.* **1931**, *43*, 461–482.
- (151) June Sutor, D. The C–H...O Hydrogen Bond in Crystals. *Nature* **1962**, *195*, 68–69.
- (152) Dippy, J. F. J. The Dissociation Constants of Monocarboxylic Acids; Their Measurement and Their Significance in Theoretical Organic Chemistry. *Chem. Rev.* **1939**, *25*, 151–211.
- (153) Gu, Y.; Kar, T.; Scheiner, S. Fundamental Properties of the CH...O Interaction: Is It a True Hydrogen Bond? *J. Am. Chem. Soc.* **1999**, *121*, 9411–9422.
- (154) Starikov, E. B.; Steiner, T. Computational Support for the Suggested Contribution of C—H...O=C Interactions to the Stability of Nucleic Acid Base Pairs. *Acta Crystallogr. D* **1997**, *53*, 345–347.
- (155) Corey, E. J.; Barnes-Seeman, D.; Lee, T. W. The Formyl C–H...O Hydrogen Bond as a Key to Transition-State Organization in Enantioselective Allylation, Aldol and Diels-Alder Reactions Catalyzed by Chiral Lewis Acids. *Tetrahedron Lett.* **1997**, *38*, 1699–1702.

- (156) Grayson, M. N.; Yang, Z.; Houk, K. N. Chronology of CH \cdots O Hydrogen Bonding from Molecular Dynamics Studies of the Phosphoric Acid-Catalyzed Allylboration of Benzaldehyde. *J. Am. Chem. Soc.* **2017**, *139*, 7717–7720.
- (157) Johnston, R. C.; Cheong, P. H.-Y. C–H \cdots O Non-Classical Hydrogen Bonding in the Stereomechanics of Organic Transformations: Theory and Recognition. *Org. Biomol. Chem.* **2013**, *11*, 5057–5064.
- (158) Itoh, Y.; Nakashima, Y.; Tsukamoto, S.; Kurohara, T.; Suzuki, M.; Sakae, Y.; Oda, M.; Okamoto, Y.; Suzuki, T. N + -C–H \cdots O Hydrogen Bonds in Protein-Ligand Complexes. *Sci. Rep.* **2019**, *9*, 767.
- (159) Zhou, P.; Tian, F.; Lv, F.; Shang, Z. Geometric Characteristics of Hydrogen Bonds Involving Sulfur Atoms in Proteins. *Proteins* **2009**, *76*, 151–163.
- (160) Mundlapati, V. R.; Ghosh, S.; Bhattacharjee, A.; Tiwari, P.; Biswal, H. S. Critical Assessment of the Strength of Hydrogen Bonds between the Sulfur Atom of Methionine/Cysteine and Backbone Amides in Proteins. *J. Phys. Chem. Lett.* **2015**, *6*, 1385–1389.
- (161) van Bergen, L. A. H.; Alonso, M.; Palló, A.; Nilsson, L.; De Proft, F.; Messens, J. Revisiting Sulfur H-Bonds in Proteins: The Example of Peroxiredoxin AhpE. *Sci. Rep.* **2016**, *6*, 30369.
- (162) Juanes, M.; Saragi, R. T.; Pinacho, R.; Rubio, J. E.; Lesarri, A. Sulfur Hydrogen Bonding and Internal Dynamics in the Monohydrates of Thenyl Mercaptan and Thenyl Alcohol. *Phys. Chem. Chem. Phys.* **2020**, *22*, 12412–12421.
- (163) Sherbow, T. J.; Zakharov, L. N.; Johnson, D. W.; Pluth, M. D. Hydrosulfide Oxidation at a Molybdenum Tetrasulfido Complex. *Inorg. Chem.* **2020**, *59*, 15574–15578.
- (164) Ghosh, S.; Chopra, P.; Wategaonkar, S. C–H \cdots S Interaction Exhibits All the Characteristics of Conventional Hydrogen Bonds. *Phys. Chem. Chem. Phys.* **2020**, *22*, 17482–17493.
- (165) Hwang, J.; Li, P.; Smith, M. D.; Warden, C. E.; Sirianni, D. A.; Vik, E. C.; Maier, J. M.; Yehl, C. J.; Sherrill, C. D.; Shimizu, K. D. Tipping the Balance between S- π and O- π Interactions. *J. Am. Chem. Soc.* **2018**, *140*, 13301–13307.

- (166) Mondal, P.; Solel, E.; Fridman, N.; Keinan, E.; Reany, O. Intramolecular van Der Waals Interactions Challenge Anion Binding in Perthio-Bambusurils. *Chem. Eur. J.* **2019**, *25*, 13336–13343.
- (167) Kroon, J.; Kanters, J. A. Non-Linearity of Hydrogen Bonds in Molecular Crystals. *Nature* **1974**, *248*, 667–669.
- (168) Steiner, T.; Desiraju, G. R. Distinction between the Weak Hydrogen Bond and the van Der Waals Interaction. *Chem. Commun.* **1998**, 891–892.
- (169) van den Berg, J.-A.; Seddon, K. R. Critical Evaluation of C–H···X Hydrogen Bonding in the Crystalline State. *Cryst. Growth Des.* **2003**, *3*, 643–661.
- (170) Collins, M. S.; Carnes, M. E.; Nell, B. P.; Zakharov, L. N.; Johnson, D. W. A Facile Route to Old and New Cyclophanes via Self-Assembly and Capture. *Nat. Commun.* **2016**, *7*, 11052.
- (171) Jeffrey, G. A. *An Introduction to Hydrogen Bonding*; Oxford University Press, 1997.
- (172) Laursen, J. S.; Engel-Andreasen, J.; Fristrup, P.; Harris, P.; Olsen, C. A. Cis–Trans Amide Bond Rotamers in β -Peptoids and Peptoids: Evaluation of Stereoelectronic Effects in Backbone and Side Chains. *J. Am. Chem. Soc.* **2013**, *135*, 2835–2844.
- (173) Raghuvanshi, A.; Jha, A. K.; Sharma, A.; Umar, S.; Mishra, S.; Kant, R.; Goel, A. A Nonarchetypal 5,6-Dihydro-2H-Pyrano[3,2-g]Indolizine-Based Solution-Solid Dual Emissive AIEgen with Multicolor Tunability. *Chem. Eur. J.* **2017**, *23*, 4527–4531.
- (174) Viglianti, L.; Leung, N. L. C.; Xie, N.; Gu, X.; Sung, H. H. Y.; Miao, Q.; Williams, I. D.; Licandro, E.; Tang, B. Z. Aggregation-Induced Emission: Mechanistic Study of the Clusteroluminescence of Tetrathienylethene. *Chem. Sci.* **2017**, *8*, 2629–2639.
- (175) Ghosh, M.; Panwaria, P.; Tothadi, S.; Das, A.; Khan, S. Bis(Silanetellurone) with C–H···Te Interaction. *Inorg. Chem.* **2020**, *59*, 17811–17821.
- (176) Steiner, T. Chloroform Molecules Donate Hydrogen Bonds to S, Se, and Te Acceptors: Evidence from a Published Series of Terminal Chalcogenido Complexes. *J. Mol. Struct.* **1998**, *447*, 39–42.

- (177) Lau, N.; Pluth, M. D. Reactive Sulfur Species (RSS): Persulfides, Polysulfides, Potential, and Problems. *Curr. Opin. Chem. Biol.* **2019**, *49*, 1–8.
- (178) Hisaki, I.; Sakamoto, Y.; Shigemitsu, H.; Tohnai, N.; Miyata, M.; Seki, S.; Saeki, A.; Tagawa, S. Superstructure-Dependent Optical and Electrical Properties of an Unusual Face-to-Face, π -Stacked, One-Dimensional Assembly of Dehydrobenzo[12]Annulene in the Crystalline State. *Chem. Eur. J.* **2008**, *14*, 4178–4187.
- (179) Roche, C.; Luo, Q.; Gil-Ramírez, G.; Jiang, H.-W.; Kohn, D. R.; Xiong, Y.; Thompson, A. L.; Anderson, H. L. Unexpected Interactions between Alkyl Straps and Pyridine Ligands in Sulfur-Strapped Porphyrin Nanorings. *J. Org. Chem.* **2017**, *82*, 7446–7462.
- (180) Chiou, S.-J.; Riordan, C. G.; Rheingold, A. L. Synthetic Modeling of Zinc Thiolates: Quantitative Assessment of Hydrogen Bonding in Modulating Sulfur Alkylation Rates. *PNAS* **2003**, *100*, 3695–3700.
- (181) Sessler, C. D.; Rahm, M.; Becker, S.; Goldberg, J. M.; Wang, F.; Lippard, S. J. CF₂H, a Hydrogen Bond Donor. *J. Am. Chem. Soc.* **2017**, *139*, 9325–9332.
- (182) Shanahan, J. P.; Mullis, D. M.; Zeller, M.; Szymczak, N. K. Reductively Stable Hydrogen-Bonding Ligands Featuring Appended CF₂-H Units. *J. Am. Chem. Soc.* **2020**, *142*, 8809–8817.
- (183) Batsanov, S. S. Van Der Waals Radii of Elements. *Inorg. Mater.* **2001**, *37*, 871–885.
- (184) Vitvitsky, V.; Yadav, P. K.; Kurthen, A.; Banerjee, R. Sulfide Oxidation by a Noncanonical Pathway in Red Blood Cells Generates Thiosulfate and Polysulfides. *J. Biol. Chem.* **2015**, *290*, 8310–8320.
- (185) Bostelaar, T.; Vitvitsky, V.; Kumutima, J.; Lewis, B. E.; Yadav, P. K.; Brunold, T. C.; Filipovic, M.; Lehnert, N.; Stemmler, T. L.; Banerjee, R. Hydrogen Sulfide Oxidation by Myoglobin. *J. Am. Chem. Soc.* **2016**, *138*, 8476–8488.
- (186) Vitvitsky, V.; Yadav, P. K.; An, S.; Seravalli, J.; Cho, U.-S.; Banerjee, R. Structural and Mechanistic Insights into Hemoglobin-Catalyzed Hydrogen Sulfide Oxidation and the Fate of Polysulfide Products. *J. Biol. Chem.* **2017**, *292*, 5584–5592.

- (187) Filipovic, M. R.; Zivanovic, J.; Alvarez, B.; Banerjee, R. Chemical Biology of H₂S Signaling through Persulfidation. *Chem. Rev.* **2018**, *118*, 1253–1337.
- (188) Rizzi, M.; Wittenberg, J. B.; Coda, A.; Ascenzi, P.; Bolognesi, M. Structural Bases for Sulfide Recognition in *Lucina Pectinata* Hemoglobin I. *J. Mol. Biol.* **1996**, *258*, 1–5.
- (189) Vitvitsky, V.; Yadav, P. K.; An, S.; Seravalli, J.; Cho, U.-S.; Banerjee, R. Structural and Mechanistic Insights into Hemoglobin-Catalyzed Hydrogen Sulfide Oxidation and the Fate of Polysulfide Products. *J. Biol. Chem.* **2017**, *292*, 5584–5592.
- (190) Pietri, R.; Lewis, A.; León, R. G.; Casabona, G.; Kiger, L.; Yeh, S.-R.; Fernandez-Alberti, S.; Marden, M. C.; Cadilla, C. L.; López-Garriga, J. Factors Controlling the Reactivity of Hydrogen Sulfide with Hemeproteins. *Biochemistry* **2009**, *48*, 4881–4894.
- (191) Galardon, E.; Tomas, A.; Selkti, M.; Roussel, P.; Artaud, I. Synthesis, Characterization, and Reactivity of Alkyldisulfanido Zinc Complexes. *Inorg. Chem.* **2009**, *48*, 5921–5927.
- (192) Galardon, E.; Tomas, A.; Roussel, P.; Artaud, I. Synthesis, Stability, and Reactivity of [(TPA)Zn(SH)]⁺ in Aqueous and Organic Solutions. *Eur. J. Inorg. Chem.* **2011**, *2011*, 3797–3801.
- (193) Kang, J.; Rebek, J. Acceleration of a Diels–Alder Reaction by a Self-Assembled Molecular Capsule. *Nature* **1997**, *385*, 50–52.
- (194) Zhang, Q.; Tiefenbacher, K. Terpene Cyclization Catalysed inside a Self-Assembled Cavity. *Nat. Chem.* **2015**, *7*, 197–202.
- (195) Hart-Cooper, W. M.; Clary, K. N.; Toste, F. D.; Bergman, R. G.; Raymond, K. N. Selective Monoterpene-like Cyclization Reactions Achieved by Water Exclusion from Reactive Intermediates in a Supramolecular Catalyst. *J. Am. Chem. Soc.* **2012**, *134*, 17873–17876.
- (196) Hastings, C. J.; Pluth, M. D.; Bergman, R. G.; Raymond, K. N. Enzymelike Catalysis of the Nazarov Cyclization by Supramolecular Encapsulation. *J. Am. Chem. Soc.* **2010**, *132*, 6938–6940.

- (197) Yoshizawa, M.; Tamura, M.; Fujita, M. Diels-Alder in Aqueous Molecular Hosts: Unusual Regioselectivity and Efficient Catalysis. *Science* **2006**, *312*, 251–254.
- (198) Yoshizawa, M.; Takeyama, Y.; Okano, T.; Fujita, M. Cavity-Directed Synthesis within a Self-Assembled Coordination Cage: Highly Selective [2 + 2] Cross-Photodimerization of Olefins. *J. Am. Chem. Soc.* **2003**, *125*, 3243–3247.
- (199) Kuil, M.; Soltner, T.; van Leeuwen, P. W. N. M.; Reek, J. N. H. High-Precision Catalysts: Regioselective Hydroformylation of Internal Alkenes by Encapsulated Rhodium Complexes. *J. Am. Chem. Soc.* **2006**, *128*, 11344–11345.
- (200) Dong, V. M.; Fiedler, D.; Carl, B.; Bergman, R. G.; Raymond, K. N. Molecular Recognition and Stabilization of Iminium Ions in Water. *J. Am. Chem. Soc.* **2006**, *128*, 14464–14465.
- (201) Trembleau, L.; Rebek, J. Helical Conformation of Alkanes in a Hydrophobic Cavitand. *Science* **2003**, *301*, 1219–1220.
- (202) Pluth, M. D.; Bergman, R. G.; Raymond, K. N. Acid Catalysis in Basic Solution: A Supramolecular Host Promotes Orthoformate Hydrolysis. *Science* **2007**, *316*, 85–88.
- (203) Iwasawa, T.; Hooley, R. J.; Rebek, J. Stabilization of Labile Carbonyl Addition Intermediates by a Synthetic Receptor. *Science* **2007**, *317*, 493–496.
- (204) Warmuth, R. O-Benzynes: Strained Alkyne or Cumulene?—NMR Characterization in a Molecular Container. *Angew. Chem. Int. Ed.* **1997**, *36*, 1347–1350.
- (205) Warmuth, R.; Marvel, M. A. 1,2,4,6-Cycloheptatetraene: Room-Temperature Stabilization inside a Hemicarcerand. *Angew. Chem. Int. Ed.* **2000**, *39*, 1117–1119.
- (206) Montoya, L. A.; Pearce, T. F.; Hansen, R. J.; Zakharov, L. N.; Pluth, M. D. Development of Selective Colorimetric Probes for Hydrogen Sulfide Based on Nucleophilic Aromatic Substitution. *J. Org. Chem.* **2013**, *78*, 6550–6557.
- (207) Izatt, S. R.; Bruening, R. L.; Izatt, N. E. Metal Separations and Recovery in the Mining Industry. *J. Miner. Met. Mater. Soc.* **2012**, *64*, 1279–1284.
- (208) Xie, F.; Zhang, T. A.; Dreisinger, D.; Doyle, F. A Critical Review on Solvent Extraction of Rare Earths from Aqueous Solutions. *Miner. Eng.* **2014**, *56*, 10–28.

- (209) Ranjan, D.; Talat, M.; Hasan, S. H. Biosorption of Arsenic from Aqueous Solution Using Agricultural Residue ‘Rice Polish.’ *J. Hazard. Mater.* **2009**, *166*, 1050–1059.
- (210) Moss, B. Water Pollution by Agriculture. *Philos. Trans. R. Soc. Lond., B, Biol. Sci.* **2008**, *363*, 659–666.
- (211) Wägli, P.; Chang, Y.-C.; Homsy, A.; Hvozدارa, L.; Herzig, H. P.; de Rooij, N. F. Microfluidic Droplet-Based Liquid–Liquid Extraction and On-Chip IR Spectroscopy Detection of Cocaine in Human Saliva. *Anal. Chem.* **2013**, *85*, 7558–7565.
- (212) Forsberg, C. W. Rethinking High-Level Waste Disposal: Separate Disposal of High-Heat Radionuclides (90Sr and 137Cs). *Nucl. Technol.* **2000**, *131*, 252–268.
- (213) McHenry, R. E.; Posey, J. C. Separation of Strontium-90 from Calcium by Solvent Extraction. *Ind. Eng. Chem.* **1961**, *53*, 647–650.
- (214) Moyer, B. A.; Bonnesen, P. V.; Custelcean, R.; Delmau, L. H.; Hay, B. P. Strategies for Using Host-Guest Chemistry in the Extractive Separations of Ionic Guests. *Kem. Ind.* **2005**, *54*, 65–87.
- (215) Li, A.; Zhai, H.; Li, J.; He, Q. Practical Applications of Supramolecular Extraction with Macrocycles. *Chem. Lett.* **2020**, *49*, 1125–1135.
- (216) Vargas-Zúñiga, G. I.; He, Q.; Sessler, J. L. Liquid–Liquid Separation by Supramolecular Systems. In *Ion Exchange and Solvent Extraction: Volume 23*; CRC Press, 2019.
- (217) Haverlock, T. J.; Bonnesen, P. V.; Sachleben, R. A.; Moyer, B. A. Analysis of Equilibria in the Extraction of Cesium Nitrate by Calix[4]Arene-Bis(t-Octylbenzo-Crown-6) in 1,2-Dichloroethane. *J. Incl. Phenom.* **2000**, *36*, 21–37.
- (218) Bhattacharyya, A.; Egberink, R. J. M.; Mohapatra, P. K.; Verma, P. K.; Kanekar, A. S.; Yadav, A. K.; Jha, S. N.; Bhattacharyya, D.; Huskens, J.; Verboom, W. Remarkable Enhancement in Extraction of Trivalent F-Block Elements Using a Macrocyclic Ligand with Four Diglycolamide Arms: Synthesis, Extraction, and Spectroscopic and Density Functional Theory Studies. *Inorg. Chem.* **2019**, *58*, 14885–14899.

- (219) Frensdorff, H. K. Salt Complexes of Cyclic Polyethers. Distribution Equilibriums. *J. Am. Chem. Soc.* **1971**, *93*, 4684–4688.
- (220) Kim, S. K.; Sessler, J. L.; Gross, D. E.; Lee, C.-H.; Kim, J. S.; Lynch, V. M.; Delmau, L. H.; Hay, B. P. A Calix[4]Arene Strapped Calix[4]Pyrrole: An Ion-Pair Receptor Displaying Three Different Cesium Cation Recognition Modes. *J. Am. Chem. Soc.* **2010**, *132*, 5827–5836.
- (221) Kim, S. K.; Sessler, J. L. Ion Pair Receptors. *Chem. Soc. Rev.* **2010**, *39*, 3784–3809.
- (222) Levitskaia, T. G.; Maya, L.; Van Berkel, G. J.; Moyer, B. A. Anion Partitioning and Ion-Pairing Behavior of Anions in the Extraction of Cesium Salts by 4,5'-Bis(Tert-Octylbenzo)Dibenzo-24-Crown-8 in 1,2-Dichloroethane. *Inorg. Chem.* **2007**, *46*, 261–272.
- (223) J. Williams, N.; Roy, S.; O. Reynolds, C.; Custelcean, R.; S. Bryantsev, V.; A. Moyer, B. Enhancing Selectivity of Cation Exchange with Anion Receptors. *Chem. Commun.* **2019**, *55*, 3590–3593.
- (224) Wintergerst, M. P.; Levitskaia, T. G.; Moyer, B. A.; Sessler, J. L.; Delmau, L. H. Calix[4]Pyrrole: A New Ion-Pair Receptor As Demonstrated by Liquid–Liquid Extraction. *J. Am. Chem. Soc.* **2008**, *130*, 4129–4139.
- (225) Marcus, Y. *Ion Properties*; Marcel Dekker: New York, 1997.
- (226) Saha, S.; Prakash, V.; Halder, S.; Chakraborty, K.; Krishnan, Y. A PH-Independent DNA Nanodevice for Quantifying Chloride Transport in Organelles of Living Cells. *Nat. Nanotechnol.* **2015**, *10*, 645–651.
- (227) Bao, X.; Wu, X.; Berry, S. N.; Howe, E. N. W.; Chang, Y.-T.; Gale, P. A. Fluorescent Squaramides as Anion Receptors and Transmembrane Anion Transporters. *Chem. Commun.* **2018**, *54*, 1363–1366.
- (228) Vallejos, S.; Hernando, E.; Trigo, M.; C. García, F.; García-Valverde, M.; Iturbe, D.; Jesús Cabero, M.; Quesada, R.; M. García, J. Polymeric Chemosensor for the Detection and Quantification of Chloride in Human Sweat. Application to the Diagnosis of Cystic Fibrosis. *J. Mater. Chem. B* **2018**, *6*, 3735–3741.

- (229) Zhao, C.; Sojda, C. A.; Myint, W.; Seidel, D. Reductive Etherification via Anion-Binding Catalysis. *J. Am. Chem. Soc.* **2017**, *139*, 10224–10227.
- (230) Zhang, Z.; R. Schreiner, P. (Thio)Urea Organocatalysis—What Can Be Learnt from Anion Recognition? *Chem. Soc. Rev.* **2009**, *38*, 1187–1198.
- (231) Sherbow, T. J.; Kuhl, G. M.; Lindquist, G. A.; Levine, J. D.; Pluth, M. D.; Johnson, D. W.; Fontenot, S. A. Hydrosulfide-Selective ChemFETs for Aqueous H₂S/HS⁻ Measurement. *Sens. Bio-Sens. Res.* **2021**, *31*, 100394.
- (232) Li, L.; Du, P.; Zhang, Y.; Duan, Y.; Li, Y.; Qian, Y.; Zhang, P.; Guo, Q. Deploying Hydrogen Bond Donor/Acceptor on Arylethynyl Scaffold I: PN-Heterocycles and Urea Based Cleft Ionophores for Hydrosulfide/Hydrosulfate Selective Electrodes. *Sens. Actuators B Chem.* **2021**, *345*, 130413.
- (233) Mibu, N.; Yokomizo, K.; Uchida, W.; Takemura, S.; Zhou, J.; Aki, H.; Miyata, T.; Sumoto, K. Molecular Symmetry and Biological Activities of New Symmetrical Tris(2-Aminoethyl)Amine Derivatives. *Chem. Pharm. Bull.* **2012**, *60*, 408–414.
- (234) G. M. Sheldrick. *Bruker/Siemens Area Detector Absorption Correction Program, Bruker AXS*; Madison, WI, 1998.
- (235) van der Sluis, P.; Spek, A. L. BYPASS: An Effective Method for the Refinement of Crystal Structures Containing Disordered Solvent Regions. *Acta. Crystallogr. A* **1990**, *46*, 194–201.
- (236) Sheldrick, G. M. A Short History of SHELX. *Acta. Crystallogr. A* **2008**, *64*, 112–122.
- (237) Rajca, A.; Rajca, S.; Wongsriratanakul, J.; Ross II, C. R. 4,6-Bis(Trifluoromethyl)-N,N'-Di-Tert-Butyl-1,3-Phenylenebis(Aminoxyl) and Its Bis(Hexafluoroacetylacetonato)Manganese(II) Complex: Synthesis, X-Ray Crystallography, and Magnetism. *Polyhedron* **2001**, *20*, 1669–1675.
- (238) Asmus, S.; Beckendorf, S.; Zurro, M.; Mück-Lichtenfeld, C.; Fröhlich, R.; García Mancheño, O. Influence of the Substitution and Conformation of C–H-Bond-Based Bis-Triazole Acceptors in Anion-Binding Catalysis. *Asian J. Chem.* **2014**, *9*, 2178–2186.

- (239) Kimball, D. B.; Weakley, T. J. R.; Haley, M. M. Cyclization of 1-(2-Alkynylphenyl)-3,3-Dialkyltriazenes: A Convenient, High-Yield Synthesis of Substituted Cinnolines and Isoindazoles. *J. Org. Chem.* **2002**, *67*, 6395–6405.
- (240) Rajca, A.; Rajca, S.; Wongsriratanakul, J.; Ross, C. R. 4,6-Bis(Trifluoromethyl)-N,N'-Di-Tert-Butyl-1,3-Phenylenebis(Aminoxyl) and Its Bis(Hexafluoroacetylacetonato)Manganese(II) Complex: Synthesis, X-Ray Crystallography, and Magnetism. *Polyhedron* **2001**, *20*, 1669–1675.
- (241) Asmus, S.; Beckendorf, S.; Zurro, M.; Mück-Lichtenfeld, C.; Fröhlich, R.; García Mancheño, O. Influence of the Substitution and Conformation of C–H-Bond-Based Bis-Triazole Acceptors in Anion-Binding Catalysis. *Asian J. Chem.* **2014**, *9*, 2178–2186.
- (242) Neese, F. Software Update: The ORCA Program System, Version 4.0. *Wiley Interdiscip. Rev. Comput. Mol. Sci.* **2018**, *8*, e1327.
- (243) Marenich, A. V.; Cramer, C. J.; Truhlar, D. G. Universal Solvation Model Based on Solute Electron Density and on a Continuum Model of the Solvent Defined by the Bulk Dielectric Constant and Atomic Surface Tensions. *J. Phys. Chem. B* **2009**, *113*, 6378–6396.
- (244) Bernard, M. K. Isoamyl Nitrite Can Cause Serious Explosions. *J. Chem. Educ.* **2010**, *87*, 583–583.
- (245) Firth, J. D.; Fairlamb, I. J. S. A Need for Caution in the Preparation and Application of Synthetically Versatile Aryl Diazonium Tetrafluoroborate Salts. *Org. Lett.* **2020**, *22*, 7057–7059.